

Understanding astrocyte-derived extracellular vesicles in health and disease

By Katherine White, MSc

A thesis submission for the qualification of
doctor in philosophy (PhD)

School of Life Sciences,
University of Nottingham

September 2024

Acknowledgments

What a rollercoaster ride this PhD has been! Firstly, I would like to thank my long-suffering supervisors Rob, Dan and most of all, Sébastien. Without your unwavering support and enthusiasm, this work would not have been possible. You have been amazing PIs through everything and have given me the confidence and support to keep pursuing my passion (as well as the beautiful astrocytes of course...). Thank you for always listening and putting up with my stubbornness.

I would also like to say a big thank you to all of my fellow lab members, particularly my D61 people, both past and present who have made me laugh every day during this PhD. Whether it be a bit of juicy gossip or some fun science ideas, I know my day will always get better when I come and chat with you all. You are all truly fantastic people. In particular, I would like to thank Alex, Barry and Raquel for all of your help and advice throughout my work. I would also like to particularly thank Hannah for all of your help, particularly with our paper, and for being a fantastic lab partner. I feel very lucky to have found such a friendly and supportive lab environment.

Finally, I would like to thank all of my friends and family outside of the QMC who have supported me unconditionally over the past 5 years. Most of all my soon-to-be husband, Bradley, who has managed to put up with all my rantings and random science thoughts over the years. Thank you, I could not have finished this without all of your continuing love and support.

Publications

The work in this thesis had been published in:

*White, K.E., Bailey, H.L., Shaw, B.S., Geiszler, P.C., Mesquita-Ribeiro, R., Scott, D., Layfield, R. and Serres, S., 2024. A convenient model of serum-induced reactivity of human astrocytes to investigate astrocyte-derived extracellular vesicles. *Frontiers in Cellular Neuroscience*, 18, p.1414142.*

Abstract

Astrocytes are glial cells within the brain responsible for maintaining healthy brain function. They also have the ability to react to harmful stimuli by changing into a reactive phenotype in order to protect the brain alongside microglia. Extracellular vesicles (EVs) are released from all cell types within the central nervous system (CNS) and are thought to represent the phenotype of the cell at the time of release. Therefore astrocyte-derived EVs (ADEVs) were hypothesised to change to represent the reactive state of the astrocytes, making them useful tools to monitor brain health. The aim of this thesis was to better understand ADEVs from both quiescent and reactive astrocytes, as well as how they may change in disease.

Characterisation of serum-free and serum-grown human primary astrocytes was completed through morphological analysis as well as RNA-sequencing and mass spectrometry analysis using a multi-omics approach, which found large differences in gene expression despite few differences in protein expression. Serum-free characterisation identified a quiescent phenotype which contrasted with serum-grown cultures which mimicked a reactive phenotype. ADEVs were then isolated using ultrafiltration of conditioned media followed by size exclusion chromatography (SEC). Serum-grown ADEVs were identified as smaller using nanoparticle tracking analysis (NTA) yet displayed a similar morphology to serum-free ADEVs. Mass spectrometry produced a detailed ADEV dataset for both models for future investigation. Tissue-derived EVs (BDEVs) were also isolated from frontal lobe tissue of Alzheimer's disease (AD) and amyotrophic lateral sclerosis (ALS) patients as well as age and sex-matched controls to investigate how EVs are altered in disease. Mass spectrometry was completed on the BDEVs producing a second dataset that was compared to the ADEVs. Finally, ADEV functionality was explored by treating quiescent, serum-free astrocytes with reactive, serum-grown ADEVs and exploring gene expression changes. ATP concentrations within cells were also explored to investigate whether EVs had the potential for glycolytic activity, however, glycolysis was not discovered during this work.

In conclusion, serum elicits a reactive response in quiescent, serum-free astrocytes leading to morphological and transcriptional changes. These changes are reflected in the astrocyte secretome and their ADEVs suggesting astrocyte health can be monitored using ADEVs. Protein datasets were produced for ADEVs and BDEVs for future comparisons creating a foundation for future ADEV and BDEV research using the models characterised in this work.

Contents

Chapter 1:	Introduction	23
1.1	Astrocytes: key players in the mammalian brain	23
1.1.1	Astrocyte functions.....	24
1.1.2	Astrocyte response to injury: the reactive astrocyte	28
1.1.3	Astrocyte models	31
1.1.4	The importance of modelling astrocyte communication	33
1.2	Extracellular vesicles.....	33
1.2.1	What are extracellular vesicles?	33
1.2.2	EVs in intercellular communication	35
1.2.3	Are exosomes a form of secretory autophagy?.....	36
1.2.4	Difficulties with EV research.....	39
1.2.5	Future applications: Why the interest in EVs?	39
1.3	Astrocyte-derived extracellular vesicles.....	40
1.3.1	Functionality of ADEVs.....	41
1.3.2	ADEVs from reactive astrocytes	42
1.3.3	ADEVs in disease	43
1.4	Aims of the PhD	47
1.4.1	To create physiologically relevant models of astrocytes.....	48
1.4.2	To characterise ADEVs from serum-free (quiescent) and serum-cultured (reactive) astrocytes.....	48
1.4.3	To investigate functionality of ADEVs.....	48
Chapter 2:	Materials and methods.....	49
2.1	Cell culture	49
2.1.1	Cell models.....	49
2.1.2	Media compositions	49
2.1.3	Cell maintenance	50
2.1.4	Seeding densities	51
2.1.5	Cryostorage of cells	51
2.1.6	Brightfield microscopy	51
2.1.7	Cytokines.....	52
2.2	Immunofluorescence	52
2.2.1	Immunocytochemistry (ICC)	52
2.2.2	Immunohistochemistry.....	53

2.2.3	Imaging and analysis.....	54
2.3	Gene expression measurements	55
2.3.1	RNA extraction.....	55
2.3.2	cDNA synthesis by reverse transcription	55
2.3.3	Real-time quantitative polymerase chain reaction (RT-qPCR)	55
2.3.4	RNA sequencing.....	57
2.4	Protein expression measurements.....	58
2.4.1	Cell lysis.....	58
2.4.2	Protein quantification.....	59
2.4.3	Immunoblotting.....	60
2.4.4	Mass spectrometry	62
2.5	Extracellular vesicle isolation.....	64
2.5.1	Isolation from tissue	64
2.5.2	Media collection for EV isolation	65
2.5.3	Ultrafiltration	65
2.5.4	Size exclusion chromatography	66
2.6	Extracellular vesicle characterisation	66
2.6.1	Transmission electron microscopy (TEM).....	66
2.6.2	Zetaview® (Nanoparticle tracking analysis).....	66
2.6.3	Direct stochastic optical reconstruction microscopy (dSTORM)	67
2.7	Functional studies.....	68
2.7.1	Metabolic assays.....	68
2.8	EVs for treatment	69
2.9	Statistical analysis.....	69
Chapter 3:	Developing an accessible serum-free culture of human primary astrocytes	70
3.1	Introduction	70
3.1.1	Importance of <i>in vitro</i> models of human astrocytes	70
3.1.2	Limitations of commonly used astrocyte culture models	70
3.1.3	The impact of serum on astrocyte culture	71
3.1.4	Established serum-free models for astrocyte culture	72
3.1.5	Aims of this chapter.....	72
3.2	Developing serum-free conditions for human primary astrocyte culture ..	73
3.2.1	Testing serum-free media compositions	73
3.3	The effects of serum on cultured human primary astrocytes.....	75
3.3.1	Morphology changes when human astrocytes are cultured in FBS	75

3.3.2	Quantification of astrocyte reactive morphology	76
3.3.3	Serum exposure causes an irreversible morphological change in cultured human primary astrocytes	78
3.3.4	Comparison of <i>in vitro</i> and <i>ex vivo</i> human and rat primary astrocyte morphologies.....	79
3.4	Stability of serum-cultured human primary astrocytes over time	81
3.4.1	Astrocyte morphology changes with increasing passage number in serum-cultures.....	81
3.4.2	GFAP expression reduces in serum-cultured human primary astrocytes with increasing passage number	82
3.5	Expression of astrocyte markers in serum-free and serum-cultured human primary astrocytes	84
3.5.1	GFAP expression is lower in serum-cultured human primary astrocytes compared to serum-free astrocytes	84
3.5.2	S100 β expression in serum-free and serum-cultured human primary astrocytes.....	86
3.5.3	EAAT2 expression in serum-free and serum-cultured human primary astrocytes.....	88
3.6	Other markers of astrocyte reactivity	89
3.7	Reactivity of serum-free human primary astrocytes in response to different stimuli	90
3.7.1	Changes in morphology of serum-free human primary astrocytes after acute (24 h) cytokine or FBS treatment.....	90
3.7.2	Serum concentration affects reactive human primary astrocyte morphology.....	94
3.7.3	Serum concentration does not affect the expression of astrocyte markers	95
3.7.4	Cytokines produced by astrocytes change in the presence of serum .	96
3.8	Discussion	98
3.8.1	Summary.....	98
3.8.2	Optimisation of a suitable serum-free medium for quiescent human primary astrocyte culture	98
3.8.3	Morphological analysis identifies distinct phenotypes in serum-free and serum-cultured human primary astrocytes.....	99
3.8.4	Serum causes changes in proliferation and nuclear size of human primary astrocytes	100
3.8.5	Cytokine treatment did not elicit a clear reactive response in serum-free human primary astrocytes	100
3.8.6	Serum-free human primary astrocytes have a dose-dependent response to FBS	101

3.8.7	Transcriptional differences between serum-free and serum-cultured human primary astrocytes.....	101
3.8.8	Overall limitations of the work	102
3.8.9	Conclusions	102
Chapter 4:	Effects of serum exposure on the transcriptome and proteome of human primary astrocytes.....	104
4.1	Introduction	104
4.1.1	The importance of multi-omics analysis	104
4.1.2	RNA-sequencing.....	104
4.1.3	Mass spectrometry	105
4.1.4	Aims of the chapter	105
4.2	RNA-sequencing analysis of serum-free and serum-cultured human primary astrocytes.....	106
4.2.1	Overall distribution of the samples	106
4.2.2	Differentially expressed genes in serum-free and serum-cultured human primary astrocytes.....	109
4.2.3	Pathway analysis of differentially expressed genes in serum-free and serum-cultured human primary astrocytes.....	111
4.2.4	Comparison of serum-free and serum-cultured astrocyte phenotypes to published 'A1' and 'A2' astrocyte phenotypes.....	112
4.3	Proteomic analysis by LC-MS/MS analysis.....	114
4.3.1	Protein identification in serum-free and serum-cultured human primary astrocyte whole-cell lysates	115
4.3.2	Pathway analysis of human primary astrocyte proteomes	116
4.3.3	Limitations of LC-MS/MS analysis.....	116
4.4	Sequential Window Acquisition of all Theoretical Mass Spectra (SWATH-MS)	117
4.4.1	SWATH analysis pipeline.....	117
4.4.2	Measuring similarity between the proteomic samples	118
4.4.3	Qualitative analysis of serum-free and serum-cultured astrocyte proteomes	120
4.4.4	Differentially expressed proteins.....	121
4.4.5	Comparison of conventional LC-MS/MS and SWATH-MS to describe the astrocyte proteome.....	123
4.5	Comparison of RNA sequencing and Mass spectrometry techniques to describe astrocyte phenotype	124
4.6	Discussion	125
4.6.1	Summary.....	125

4.6.2	Consistency between biological replicates.....	126
4.6.3	RNA sequencing analysis	127
4.6.4	Conventional LC-MS/MS vs SWATH analysis when comparing the proteome of serum-free and serum-cultured astrocytes	128
4.6.5	Importance of a multi-omics analysis.....	128
4.6.6	Other limitations of the work within this chapter	129
4.6.7	Conclusions.....	129
Chapter 5:	Investigating the characteristics and functions of human astrocyte-derived extracellular vesicles.....	130
5.1	Introduction	130
5.1.1	The importance of understanding extracellular vesicles.....	130
5.1.2	Current knowledge of ADEVs.....	131
5.1.3	A multi-targeted approach is required for the study of EVs	132
5.1.4	Aims of this chapter	132
5.2	Isolation and visual confirmation of EVs from cultured astrocytes and human tissues.....	133
5.2.1	Optimisation of ADEV isolation from serum-free and serum-cultured astrocytes.....	133
5.2.2	Isolation of tissue-derived BDEVs	134
5.2.3	TEM analysis of ADEV and BDEV fractions confirms the presence of extracellular vesicles.....	134
5.3	Analysis of EV size and concentration	136
5.3.1	Direct stochastic optical reconstruction microscopy (dSTORM) analysis of ADEVs	136
5.3.2	Zetaview analysis of ADEVs	137
5.3.3	Comparison of dSTORM and Zetaview techniques for analysing ADEV size and concentration.....	139
5.3.4	ADEVs were isolating in earlier fractions than expected using generation 2 IZON columns	142
5.3.5	The effect of freezing on ADEV size and concentration	143
5.3.6	Zetaview analysis of control and disease BDEVs	145
5.3.7	Comparison of particle size and concentration between ADEVs and BDEVs	146
5.4	Detection of EV-associated markers in ADEV and BDEVs.....	147
5.4.1	Western blotting of EV markers within ADEVs.....	147
5.4.2	Identification of EV protein markers in ADEVs.....	148
5.4.3	EV markers within BDEVs.....	151
5.5	SWATH analysis of ADEVs to understand the ADEV proteome.....	152

5.5.1	Comparing similarity between the proteomes of serum-free and serum-cultured ADEV biological replicates	153
5.5.2	Qualitative analysis of the ADEV proteome	155
5.5.3	Differentially expressed proteins between serum-free and serum-cultured human primary ADEVs	161
5.6	SWATH-MS analysis of BDEVs.....	163
5.6.1	Principal component analysis of control and disease BDEVs analysed using SWATH-MS	163
5.6.2	Qualitative analysis of BDEV proteomes from control and disease frontal lobe tissue by SWATH-MS.....	164
5.6.3	Differentially expressed proteins between healthy and disease BDEVs identified by SWATH-MS	169
5.6.4	Cell-specific markers within BDEVs that could be used to isolate cell-specific BDEVs.....	171
5.7	Comparison of ADEVs and BDEV proteomes by SWATH-MS	175
5.8	Investigating ADEV functionality beyond cargo transport	175
5.8.1	The induction of astrocyte reactivity in serum-free astrocytes by serum-cultured ADEVs.....	175
5.9	Glycolysis within EVs: Are EVs metabolically active?	179
5.10	Discussion	182
5.10.1	Summary.....	182
5.10.2	Successful EV isolation from human primary astrocytes.....	183
5.10.3	Importance of comprehensive EV characterisation	184
5.10.4	Size differences between serum-free and serum-cultured ADEVs from human primary astrocytes.....	185
5.10.5	Comparison between ADEVs and BDEVs.....	185
5.10.6	Cell-specific proteins found on BDEVs could be used to isolate populations of EVs	186
5.10.7	Functionality of EVs	186
5.10.8	Limitations of EV characterisation	187
5.10.9	Conclusions	188
Chapter 6:	General discussion	189
6.1	Background of the work	189
6.1.1	Understanding reactivity in astrocytes.....	189
6.1.2	Current knowledge of human ADEVs	190
6.2	Summary of work.....	190
6.2.1	Establishing quiescent and reactive human primary astrocyte cultures.	190

6.2.2	Isolation and characterisation of ADEVs.....	191
6.2.3	Comparing ADEVs to tissue-derived BDEVs to investigate the translatability of ADEV findings	192
6.2.4	Functionality of ADEVs.....	193
6.3	Maintaining a quiescent, serum-free human astrocyte culture.....	194
6.4	The effect of serum on astrocytes.....	195
6.5	Multi-omics analysis of human primary astrocytes.....	196
6.6	Isolation of human ADEVs and BDEVs	197
6.7	Future analysis of ADEVs to be completed.....	198
6.8	ADEV functionality beyond cargo delivery?	198
6.9	Overall Limitations.....	199
6.9.1	Limitations of the astrocyte models	199
6.9.2	Limitations of the mass spectrometry analyses	200
6.10	Concluding remarks	200
Chapter 7:	References	201
Chapter 8:	Appendix.....	240

Table of Figures

Figure 1-1 - The major functions of astrocytes.....	24
Figure 1-2 - The lactate shuttle hypothesis (taken from Deitmer et al., 2017).	26
Figure 1-3 – Glutamate/GABA recycling.....	27
Figure 1-4 - Reactive astrocyte phenotypes	29
Figure 1-5 - The creation of iPSC-derived astrocytes.....	32
Figure 1-6 - Exosome biogenesis and release.....	34
Figure 1-7 - Secretory autophagy	37
Figure 1-8 - Prion theory.	44
Figure 2-1 - mRNA sequencing pipeline completed by Novogene (Image created by Novogene).....	57
Figure 2-2 - Example standard curve created using BCA standards to calculate unknown protein concentrations of samples.....	59
Figure 2-3 - Graphical representation of extracellular vesicle isolation from (A) tissue and (B) cell culture.....	65
Figure 3-1 - Human primary astrocytes show a ‘quiescent’ morphology when cultured in different serum-free media and change morphology in response to FBS treatment.....	74
Figure 3-2 – Qualitative analysis of human primary astrocytes cultured with and without serum show distinct morphological differences typically associated with reactive and non-reactive phenotypes, respectively.....	76
Figure 3-3 - Human primary astrocyte morphology analysis using the ‘Simple neurite tracer’ plug-in.....	77

<i>Figure 3-4 - Quantitative analysis of human primary astrocytes cultured with or without serum shows significant morphological differences.....</i>	<i>78</i>
<i>Figure 3-5 – Morphological changes in serum-cultured human primary astrocytes are irreversible.....</i>	<i>79</i>
<i>Figure 3-6 – Comparison of both human and rat GFAP expression between serum-free and serum-cultured primary astrocytes and ex vivo tissue.....</i>	<i>80</i>
<i>Figure 3-7 – The morphology of serum-cultured human primary astrocytes changes between P1 and P9 in comparison to serum-free astrocytes which remain the same after 4 weeks in culture.....</i>	<i>81</i>
<i>Figure 3-8 - Serum-cultured human primary astrocytes have increased hypertrophy with increasing passage number.....</i>	<i>82</i>
<i>Figure 3-9 - GFAP expression reduces in serum-cultured human primary astrocytes with increasing passage number.....</i>	<i>83</i>
<i>Figure 3-10 - GFAP expression is lower in serum-cultured human primary astrocytes compared to serum-free astrocytes.....</i>	<i>85</i>
<i>Figure 3-11 – The percentage of GFAP-positive cells is higher in serum-free human primary astrocytes compared to serum-cultures.....</i>	<i>86</i>
<i>Figure 3-12 - S100β and GFAP co-expression in serum-free and serum-cultured human primary astrocytes.....</i>	<i>87</i>
<i>Figure 3-13 - EAAT2 expression in serum-free and serum-cultured human primary astrocytes.....</i>	<i>88</i>
<i>Figure 3-14 – Gene expression comparisons between serum-free and serum-cultured human primary astrocytes.....</i>	<i>89</i>
<i>Figure 3-15 – Serum-free human primary astrocytes display changes in morphology but not GFAP expression after treatment with either a cytokine cocktail or 2% FBS for 24 h.....</i>	<i>91</i>
<i>Figure 3-16 - Raw Ct values of GAPDH, Actin and B2M to determine suitability as housekeeping genes for RT-qPCR of human primary astrocytes treated for 24 h with cytokines or 2% FBS.....</i>	<i>92</i>
<i>Figure 3-17 - RT-qPCR analysis of astrocyte markers and inflammatory cytokines in serum-free astrocytes treated with either 2% FBS or cytokines for 24 h.....</i>	<i>93</i>
<i>Figure 3-18 – 24 h treatment with higher concentrations of FBS (10%) cause a greater morphological change in serum-free human primary astrocytes than 2% FBS.....</i>	<i>94</i>
<i>Figure 3-19 – Raw Ct values of GAPDH, B2M and 18s to determine suitability as housekeeping genes for RT-qPCR of human primary astrocytes treated for 24 h with 2% or 10% FBS.....</i>	<i>95</i>
<i>Figure 3-20 – No transcriptional differences in astrocyte markers and pro-inflammatory cytokines in serum-free human primary astrocytes after treatment with either 2% or 10% FBS for 24 h.....</i>	<i>96</i>
<i>Figure 3-21 - Serum-free astrocytes have a more diverse secretome than serum-cultured astrocytes.....</i>	<i>97</i>
<i>Figure 4-1 - Principal component analysis shows clear separation in mRNA expression between serum-free and serum-cultured astrocyte replicates.....</i>	<i>107</i>
<i>Figure 4-2 – Partial least squares discriminant analysis identified the most 20 influential genes on the separation of serum-free and serum-cultured astrocyte transcriptomes.....</i>	<i>107</i>
<i>Figure 4-3 - The majority of protein-coding mRNAs were identified in all 4 replicates of serum-free and serum-cultured human primary astrocytes.....</i>	<i>108</i>
<i>Figure 4-4 - The majority of protein-coding mRNAs were identified in both serum-free and serum-cultured astrocytes.</i>	<i>107</i>
<i>Figure 4-5 - Differential expression of protein-coding genes in serum-free and serum-cultured astrocytes.....</i>	<i>108</i>

Figure 4-6 – KEGG pathway analysis of serum-free and serum-cultured human primary astrocytes suggests pathway differences in quiescent and reactive phenotypes, respectively.....	112
Figure 4-7 - Serum-cultured astrocyte transcriptome resembles both ‘A1’ and ‘A2’ reactive astrocyte phenotypes defined by Liddelow et al (2017).....	114
Figure 4-8 - More proteins were identified in all three replicates from the proteomic analysis of serum-free astrocytes compared to the serum-cultured astrocytes.	115
Figure 4-9 - Proteins identified in serum-free and serum-cultured astrocytes by LC-MS/MS.	116
Figure 4-10 - Analysis pipeline completed to analyse the SWATH-MS data from human primary astrocytes.	118
Figure 4-11 - Principal component analysis of proteins identified in serum-free and serum-cultured astrocytes.....	119
Figure 4-12 - More proteins were identified in all three biological replicates in the proteomic analysis of serum-cultured astrocytes compared to the serum-free astrocytes.....	119
Figure 4-13 – Many unique proteins were identified in serum-free and serum-cultured astrocytes through SWATH analysis.....	120
Figure 4-14 – The top 15 enriched KEGG pathways identified in uniquely identified proteins in serum-cultured astrocytes after SWATH analysis.	121
Figure 4-15 – 26 differentially expressed proteins were identified between serum-free and serum-cultured astrocytes.	123
Figure 5-1 - Serum-removal does not change reactive astrocyte morphology, with astrocytes surviving for up to 5 days without serum (repeat of Figure 3-5).	134
Figure 5-2 - ADEVs were visible in EV fractions after isolation from both serum-free and serum-cultured human primary astrocyte conditioned media.	135
Figure 5-3 - Brain-derived EVs were successfully isolated from frontal lobe tissue of control, AD and ALS patients.....	135
Figure 5-4 - DSTORM analysis identified a difference in particle concentration between serum-free and serum-cultured ADEVs, but not average size	137
Figure 5-5 - NTA analysis of ADEV fractions from serum-free and serum-cultured human primary astrocytes.	138
Figure 5-6 - Size distribution of particles identified a shift in serum-cultured ADEV fractions compared to serum-free ADEV fractions.....	139
Figure 5-7 – Using generation 2 IZON columns, EVs were eluting earlier than expected from the columns with many particles identified within the final void fraction.....	142
Figure 5-8 – Freezing human primary ADEVs at -80 °C does not affect particle concentration	143
Figure 5-9 – Storage of astrocyte conditioned media at either 4 °C or -80 °C does not effect ADEV concentration and is preferable to freeze-thawing isolated EVs.....	144
Figure 5-10 - NTA analysis of BDEVs isolated from human control, Alzheimer's disease and ALS tissue shows no difference between conditions	146
Figure 5-11 - Immunoblotting identifies some EV-associated markers in serum-free and serum-cultured ADEVs.....	148
Figure 5-12 – Relative abundance of EV-associated proteins (category 1 and 2) and cell-associated proteins (category 3-5) identified within human ADEV and their parent astrocyte lysate samples using SWATH-MS.....	150
Figure 5-13- Relative abundance of EV-associated proteins (category 1 and 2) and cell-associated proteins (category 3-5) identified within healthy and disease BDEVs using SWATH-MS.	152
Figure 5-14 - PCA of ADEV proteins indicates no distinct difference between serum-free and serum-cultured ADEV proteomes.....	153

<i>Figure 5-15 – High variation between biological replicates by SWATH-MS, with the majority of proteins only identified in either 1 or 2 biological replicates for both serum-free and serum-cultured ADEVs.....</i>	154
<i>Figure 5-16 - Fewer proteins were identified by SWATH-MS in serum-free and serum-cultured ADEVs compared to their parent cell lysates.....</i>	154
<i>Figure 5-17 - The 15 most significantly upregulated KEGG pathways in ADEV proteins identified exclusively in serum-free cultures.....</i>	156
<i>Figure 5-18 - Top 10 KEGG pathways upregulated in serum-free and serum-cultured human primary ADEV proteins.....</i>	156
<i>Figure 5-19 – The majority of Serum-free and serum-cultured ADEV proteins were also present within the Vesiclepedia database.....</i>	157
<i>Figure 5-20 - Qualitative differences in human primary ADEV and their parent cell lysate proteomes by SWATH-MS.....</i>	158
<i>Figure 5-21 - Differentially expressed proteins identified in serum-free and serum-cultured ADEVs by SWATH-MS.....</i>	162
<i>Figure 5-22 - Principal component analysis of BDEVs shows no clear differences in the proteomes between control and disease conditions as well as between ALS and Alzheimer’s BDEVs by SWATH-MS.....</i>	164
<i>Figure 5-23 – The number of proteins identified by SWATH-MS in multiple biological replicates across different BDEV conditions.....</i>	165
<i>Figure 5-24 - Comparison of BDEV proteins identified by SWATH-MS in four or more replicates for each condition.....</i>	166
<i>Figure 5-25 – The majority of BDEV proteins were identified within the Vesiclepedia database.....</i>	167
<i>Figure 5-26 - Proteins identified in BDEVs by SWATH-MS that were not found within the Vesiclepedia database are enriched in neurodegenerative disease pathways.....</i>	164
<i>Figure 5-27 - 12 differentially expressed proteins were identified when comparing ALS BDEVs and Alz BDEVs by SWATH-MS.....</i>	171
<i>Figure 5-28 – Many astrocyte markers were identified within control and disease BDEVs by SWATH-MS.....</i>	172
<i>Figure 5-29 - Neuronal markers were also identified within BDEVs.....</i>	173
<i>Figure 5-30 - Microglial and oligodendrocyte markers identified within BDEVs.....</i>	174
<i>Figure 5-31 – No morphological differences were observed after 72 h of reactive ADEV treatment in human primary serum-free astrocytes.....</i>	176
<i>Figure 5-32 – B2M and Actin are suitable housekeeping genes when comparing gene expression changes in EV-treated serum-free astrocytes.....</i>	178
<i>Figure 5-33 - Transcriptional changes in serum-free human primary astrocytes after treatment with purified ADEVs from serum-cultured cells.....</i>	179
<i>Figure 5-34 - ATP concentration is similar in serum-free and serum-cultured human primary ADEVs.....</i>	180
<i>Figure 5-35 - ATP production via glycolysis was not identified within N2A EVs after treatment with glycolytic substrates.....</i>	182

Table of Tables

<i>Table 1-1 - Common astrocyte markers.....</i>	41
<i>Table 2-1 - Media compositions used for cell culture.....</i>	50
<i>Table 2-2 - Antibodies and their dilutions used for immunocytochemistry.....</i>	53

Table 2-3 - Antibodies used in immunohistochemistry with the dilutions used	54
Table 2-4 - qPCR master mix for one sample	55
Table 2-5 - Forward and reverse primer sequences used for RT-qPCR	57
Table 2-6 - Urea lysis buffer recipe	58
Table 2-7 - RIPA lysis buffer recipe	58
Table 2-8 - Gradient gel composition for SDS-PAGE	61
Table 2-9 - Antibodies used in immunoblotting	61
Table 2-10 – Description of fractions collected using qEVoriginal 70 nm columns	66
Table 3-1 (repeated) - Media compositions used for cell culture	73
Table 4-1 - Expression of astrocyte and inflammatory markers in serum-free and serum-cultured astrocytes in comparison to RT-qPCR data from Prah et al. (2019) and RT-qPCR analysis completed in Chapter 3	119
Table 4-2 - Differentially expressed proteins in serum-free and serum-cultured astrocytes identified using Limma analysis with different NA and CV criteria	122
Table 4-3 – High similarity in the proteins identified by LC-MS/MS and SWATH analysis after manual filtering	123
Table 4-4 – High similarity between protein-coding RNA and corresponding protein identified during RNA-SEQ and SWATH mass spectrometry, respectively	125
Table 4-5 - Comparison of differentially expressed proteins identified in SWATH analysis, with the corresponding mRNA identified in RNA-SEQ analysis	125
Table 5-1 - Comparison of size and concentration of EV fraction 2 using NTA and dSTORM analysis	140
Table 5-2 - Comparison summary between dSTORM and NTA techniques for the quantification of EV concentration and size	141
Table 5-3 - Comparison of the size and concentration of ADEVs and BDEVs using NTA (Zetaview®)	147
Table 5-4 – 16 proteins were identified within serum-free and serum-cultured ADEVs but not their parent cell lysates	155
Table 5-5 - Protein sub-types identified in the ADEVs and their parent cells using online databases	160
Table 5-6 - Glycolytic enzymes were identified within ADEVs and their parent cell lysates	161
Table 5-7 - Lowering the threshold for variance increased the number of differentially expressed proteins between serum-free and serum-cultured ADEVs identified by SWATH-MS	162
Table 5-8 - All enzymes required for glycolysis were identified by SWATH- within the BDEVs with no differences observed between conditions	169
Table 5-9 - Comparison of ADEV proteins and BDEV proteins identified by SWATH-MS indicates high similarity between the EV proteomes	175

Abbreviations

Full name	Abbreviation
18s ribosomal RNA	18s
2-Deoxy-D-glucose	2-DG
Alpha-1B-glycoprotein	A1BG
Alpha-2-macroglobulin	A2M
4-Aminobutyrate aminotransferase (mitochondrial)	ABAT
ATP-binding cassette sub-family B member 1	ABCB1
ATP-binding cassette sub-family B member 6	ABCB6
ATP-binding cassette sub-family G member 2	ABCG2
Alpha-actinin-1	ACTN1
Alzheimer's disease	AD/Alz
Disintegrin and metalloproteinase domain-containing protein 10	ADAM10
Astrocyte-derived extracellular vesicle	ADEVs
Adenosine diphosphate	ADP
Astrocyte growth supplement	AGS
Albumin	ALB
CD166 antigen	ALCAM
Aldehyde dehydrogenase 1 family member L1	ALDH1L1
Fructose-bisphosphate aldolase A/B/C	ALDOA/B/C
Programmed cell death 6-interacting protein	ALIX
Alkaline phosphatase, tissue-nonspecific isozyme	ALPL
Amyotrophic lateral sclerosis	ALS
Analysis of variance	ANOVA
Annexin A1	ANXA1
Apolipoprotein A-I	APOA1
Apolipoprotein B100	APOB
Apolipoprotein D	APOD
Apolipoprotein E	APOE
Ammonium persulfate	APS
Aquaporin 4	AQP4
ADP-ribosylation factor 6	ARF6
Adenosine triphosphate	ATP
ATPase Na ⁺ /K ⁺ transporting subunit beta 2	ATP1B2
ATP synthase subunit gamma mitochondrial	ATP5F1C
ATP synthase subunit d mitochondrial	ATP5PD
Beta-amyloid 1-42	A β ₁₋₄₂
Beta-2-microglobulin	B2M
Blood-brain barrier	BBB
Bicinchoninic acid assay	BCA
Brain-derived extracellular vesicles	BDEVs
Brain-derived neurotrophic factor	BDNF
Bovine serum Albumin	BSA

Chromosome 1 open reading frame 61	C1orf61
Complement component 1q	C1q
Guanine nucleotide exchange factor C9orf72	C9orf72
Voltage-dependent calcium channel subunit alpha-2/delta-3	CACNA2D3
Calnexin	CANX
Calpain-1 catalytic subunit	CAPN1
Caspase-14	CASP14
Cellular communication network factor 2	CCN2
Integrin alpha-M	CD11b
Scavenger receptor cysteine-rich type 1 protein M130	CD163
Tumour necrosis factor receptor superfamily member 5	CD40
Cluster of differentiation 44	CD44
Receptor-type tyrosine-protein phosphatase C	CD45
Integrin alpha 6	CD49f/ITGA6
CD63 antigen	CD63
High affinity immunoglobulin gamma Fc receptor I	CD64
Macrosialin	CD68
CD81 antigen	CD81
CD9 antigen	CD9
complementary DNA	cDNA
Compliment factor I	CFI
Protein c-Fos	C-FOS
Cell adhesion molecule L1 like	CHL1
Creutzfeldt-Jakob disease	CJD
Casein kinase 1	CK1
Cell lysate	CL
2',3' cyclic-nucleotidase 3'-phosphodiesterase	CNP
CB1 cannabinoid receptor-interacting protein 1	CNRIP1
Central nervous system	CNS
Contactin-2	CNTN2
Ciliary neurotrophic factor	CNTF
Carbon dioxide	CO ₂
Collagen alpha-2(I) chain	COL1A2
Coronin-1C	CORO1C
Ceruloplasmin	CP
Cerebral spinal fluid	CSF
Cycle threshold	Ct
Catenin beta-1	CTNNB1
Coefficient of variation	CV
CX3C chemokine receptor 1	CX3CR1
CXC motif chemokine 10	CXCL10
Gap junction alpha-1 protein	CXN-43
Disease associated astrocyte	DAA
Disease associated microglia	DAM
4',6-diamidino-2-phenylindole	DAPI

Neuronal migration protein doublecortin	DCX
Double distilled water	ddH ₂ O
Parkinson disease protein 7	DJ-1
Disks large homolog 4	DLG4
Dulbecco's Modified Eagle medium	DMEM
Dimethyl sulphoxide	DMSO
Deoxynucleoside triphosphates	dNTP
Dihydropyrimidinase-related protein 5	DPYSL5
Desmoplakin	DSP
Direct stochastic optical reconstruction microscopy	dSTORM
Dithiothreitol	DTT
Excitatory amino acid transporter	EAAT
Enhanced chemiluminescence	ECL
Ethylenediamine tetraacetic acid	EDTA
Epidermal growth factor	EGF
Alpha/Gamma/Beta enolase	ENO1/2/3
Endosomal sorting complex required for transport	ESCRTs
Extracellular vesicle	EV
Protein eva-1 homolog A	EVA1A
EGF-like module-containing mucin-like hormone receptor-like 1	F4/80
Foetal bovine serum	FBS
False discovery rate	FDR
Fibroblast growth factor	FGF
Flotillin-1	FLOT1
Fibronectin	FN1
Fragment per kilobase per million mapped fragments	FPKM
Fused in Sarcoma	FUS
Gel application buffer	GAB
γ -aminobutyric acid	GABA
Glutamate decarboxylase	GAD
Neuromodulin	GAP43
Glyceraldehyde-3-phosphate dehydrogenase	GAPDH
Vitamin D-binding protein	GC
Glutamate cysteine ligase modifier	GCLM
Growth/differentiation factor 15	GDF-15
NAD-specific glutamate dehydrogenase	GDH2
Glial derived neurotrophic factor	GDNF
Glial fibrillary acidic protein	GFAP
Gap junction alpha-1 protein	GJA1
Glutamate–aspartate transporter	GLAST
Glutamate synthase	GLT-1
Glutamate transporter	GLUT
Guanine nucleotide-binding protein G(i) subunit alpha-3	GNAI3
Guanine nucleotide-binding protein G(i)/G(s)/G(T) subunit beta-2	GNB2

Gene ontology	GO
Golgin subfamily A member 3	GOLGA3
Glucose-6-phosphate isomerase	GPI
Retinoic acid-induced protein 3	GPRC5A
Glutamate Ionotrphic receptor Kainate type subunit 3	GRIK3
Glutamine synthetase	GS/GLUL
Glutathione S-transferase mu 2	GSTM2
Histone H2A type 2-B	H2AC21
Histone H4	H4C1
Heparin-binding EGF-like growth factor	HB-EGF
Hyaluronan and proteoglycan link protein 1/3	HAPLN1/3
Hydrochloric acid	HCL
Human immunodeficiency virus	HIV
Hexokinase-1/2/3	HK1/2/3
HLA class II histocompatibility antigen, DR alpha chain	HLA-DRA
Heterogeneous nuclear ribonucleoproteins A2/B1	hnRNPA2B1
Heterogeneous nuclear ribonucleoprotein M	HNRNPM
Hypochlorous acids	HOCl
Hippocalcin-like protein 4	HPCAL4
Horseradish peroxidase	HRP
Heat shock protein beta-1	HSPB1
Allograft inflammatory factor 1	IBA1
Immunocytochemistry	ICC
Insulin-like growth factor 1	IGF1
Insulin like growth factor binding protein 1/2	IGFBP1/2
Immunoglobulin heavy constant gamma 4	IGHG4
Immunoglobulin superfamily member 8	IGSF8
Immunohistochemistry	IHC
Interleukin-6	IL-6
Interleukin-10	IL-10
Interleukin-1 alpha	IL-1a
Interleukin-1 beta	IL-1β
MICOS complex subunit MIC60	IMMT
Induced neural stem cells	iNSCs
Induced pluripotent stem cells	iPSCs
International society of extracellular vesicles	ISEV
Integrin alpha 1	ITGA1
Integrin alpha 2	ITGA2
Inter-alpha-trypsin inhibitor heavy chain H1/3/4	ITIH1/3/4
Immunoglobulin J chain	JCHAIN
Junction plakoglobin	JUP
Potassium / Sodium/ Chlorine ions	K ⁺ / Na ⁺ / Cl ⁻
Kilodalton	kDa
Kyoto Encyclopedia of Genes and Genomes	KEGG

Keratin 19	KRT19
Neural cell adhesion molecule L1	L1CAM
Lysosome-associated membrane glycoprotein 1	LAMP1
Microtubule-associated protein 1A/1B light chain 3	LC3
Liquid chromatography tandem mass spectrometry	LC-MS/MS
Lipocalin-2	LCN2
Lactate dehydrogenase	LDH
L-Lactate dehydrogenase A/B chain	LDHA/B
Galectin-3-binding protein	LGALS3BP
Prelamin-A/C	LMNA
LIM-domain only	LMO
Lipopolysaccharide	LPS
Leucine-rich repeat kinase 2	LRRK2
Lactotransferrin	LTF
Lysosome C-2	LYZ
Microtubule-associated protein 2	MAP2
Amine oxidase B	MAOB
Microtubule-associated protein tau	MAPT
Myelin basic protein	MBP
Monocyte Chemoattractant protein-1	MCP-1
Monocarboxylate transporters	MCT
Microglial-derived extracellular vesicles	MDEV
Micro RNAs	miRNA
Minimal information for studies of extracellular vesicles	MISEV
Modulator of VRAC current 1	MLC1
Matrix metalloproteinase	MMP
Myelin-oligodendrocyte glycoprotein	MOG
Myeloperoxidase	MPO
Messenger RNA	mRNA
Multiple sclerosis	MS
Cytochrome C oxidase subunit 2	MT-CO2
3-(4,5-dimethylthiazolyl-2)-2, 5-diphenyltetrazolium bromide	MTT
Multivesicular body	MVB
Molecular weight cut-off	MWCO
Neuro2A	N2A
Sodium chloride	NaCl
Nicotinamide-adenine dinucleotide	NAD
Nicotinamide adenine dinucleotide + hydrogen	NADH
Sodium hydroxide	NaOH
Neurobasal medium	NB
Neighbour of BRCA1 gene 1	NBR1
Neural cell adhesion molecule 1	NCAM
Neuronal-derived extracellular vesicles	NDEVs
N-Myc Downstream-Regulated Gene 2	NDRG2

Neurofilament light polypeptide	NEFL
Nuclear factor kappa B	NF-kB
Ammonia	NH ₃
NTPase KAP family P-loop domain-containing protein 1	Nkpd1
Neuronal cell adhesion molecule	NRCAM
Neutral sphingomyelinase II	nSMase2
Nanoparticle tracking analysis	NTA
Nottingham trent university	NTU
Oligodendrocyte transcription factor 1/2/3	OLIG1/2/3
Oligodendrocyte progenitor cells	OPCs
Claudin-11	OSP
Sequestosome 1	p62
Adjusted P value	Padj
Phosphate-activated glutaminase	PAG
Photoactivated localisation microscopy	PALM
Parkinsonism associated deglycase	PARK7
Phosphate buffered Saline	PBS
Pyruvate carboxylase	PC
Principal component 1/2	PC1/2
Principal component analysis	PCA
Parkinson's disease	PD
Platelet-derived growth factor	PDGF
Penicillin and streptomycin	Pen/strep
Positron emission tomography	PET
Paraformaldehyde	PFA
Profilin-1	PFN1
ATP-dependent 6-phosphofructokinase muscle type	PFKM
ATP-dependent 6-phosphofructokinase liver type	PFKL
ATP-dependent 6-phosphofructokinase platelet type	PFKP
Phosphoglycerate kinase 1	PGK1
Phosphoglucomutase-1/2/3	PGM1/2/3
Pyruvate kinase	PKM
Plasminogen	PLG
Poly L-lysine	PLL
Myelin-proteolipid protein	PLP1
Partial least squares discriminant analysis	PLS-DA
Myelin P2 protein	PMP2
Inorganic polyphosphate	PolyP
Palmitoyl-protein thioesterase 1	PPT1
Cellular prion	PrP ^C
Protease-resistant prion	PrP ^{sc}
Protein tyrosine phosphatase receptor Type Z1	PTPRZ1
Glutamine-rich protein 2	QRICH2
RNA-binding protein 3	RBM3

RNA binding proteins	RBPs
Ras homolog family member A	RhoA
RNA integrity number	RIN
Radioimmunoprecipitation assay	RIPA
Ribonucleic acid	RNA
Reactive nitrogen species	RNS
Reactive oxygen species	ROS
Robust regression and Outlier removal	ROUT
Ras-related protein R-RAS	RRAS
Ribonucleotide reductase regulatory TP53 inducible subunit M2B	RRM2B
Reticulon-3	RTN3
Real-time quantitative polymerase chain reaction	RT-qPCR
S100 calcium binding Protein B	S100 β
Sphingosine 1-phosphate receptor 3	S1PR3
Serum-cultured	SC
Serum-free	SF
Secretoglobin family 1D member 1	SCGB1D1
Syndecan-1	SDC1
Sodium Dodecyl sulphate	SDS
Size exclusion chromatography	SEC
Alpha-1-antichymotrypsin	SERPINA3
Antithrombin-III	SERPINC1
Serpin family E member 1	SERPIN-E1
Solute carrier proteins	SLC
Sodium-dependent phosphate transporter 2	SLC20A2
Large neutral amino acids transporter small subunit 1	SLC7A5
Synaptosomal associated protein 25	SNAP25
Simple neurite tracer	SNT
Superoxide dismutase 1	SOD1
Sortillin Related VPS10 domain containing receptor 1	SORCS1
Transcription factor SOX-10	SOX10
SPARC like 1	SPARCL1
Spectrin beta, non-erythrocytic 1	SPTBN1
Serglycin	SRGN
Soluble scavenger receptor cysteine-rich domain-containing protein	SSC5D
Metalloreductase STEAP4	STEAP4
Sequential window acquisition of theoretical mass	SWATH
SWATH-mass spectrometry	SWATH-MS
Synaptotagmin-binding, cytoplasmic RNA-interacting protein	SYNCRIP
Synaptophysin	SYP
Tris-buffered saline	TBS
Tris-buffered saline with Tween	TBS-T
Tricarboxylic acid	TCA
TAR DNA-binding protein 43	TDP-43

Triethylammonium bicarbonate	TEAB
Transmission electron microscopy	TEM
Tetramethylethylenediamine	TEMED
Transforming growth factor beta-1 proprotein	TGFβ1
Thy-1 membrane glycoprotein	THY1
Total internal reflection microscopy	TIRF
Toll-like receptor 7	TLR7
Opalin	TMEM10
Transmembrane protein 119	TMEM119
1,3,5-trinitrobenzene	TNB
Tumour necrosis factor alpha	TNFα
Mitochondrial import receptor subunit TOM20 homolog	TOMM20
Triosephosphate isomerase	TPI1
Trisaminomethane	Tris
Transfer RNA	tRNA
Transient receptor potential cation channel Subfamily C member 6	TRPC6
Transmissible spongiform encephalopathies	TSEs
Tumour susceptibility gene 101 protein	TSG101
Tetraspanin-4	TSPAN4
Translocator protein	TSPO
Tubulin alpha-4A chain	TUBA4A
Tubulin beta-3 chain	TUBB3
Vimentin	VIM
Protein KPLCE	XP32

Chapter 1: Introduction

1.1 Astrocytes: key players in the mammalian brain

Astrocytes are a type of glial cell within the central nervous system (CNS) which support neurons and ensure healthy brain function. Astrocytes form a large proportion of the CNS (20-40%) and perform numerous roles including metabolic support for neurons, ion buffering, neurotransmitter recycling, maintaining the blood-brain barrier (BBB) and participating in the brain immune response (Figure 1-1; Khakh and Sofroniew, 2015). In fact, new roles are still being discovered demonstrating the need for continued research into the functions of healthy astrocytes (Delepine et al., 2023). Whilst studied as a homogenous group, the term 'astrocyte' encompasses a heterogenous population of cells, which are specialised for particular aspects of astrocyte function (Zhang and Barres, 2010; Pestana et al., 2020).

There is increasing evidence suggesting that astrocytes play an active role in neurodegenerative disease, and not only because they fail to support neurons. Neurons are often the focus of neurodegeneration research as they are the most vulnerable brain cell, and also display the clearest pathology. However, evidence indicates astrocytes have a role in the spread of disease, as well as exacerbating disease through the secretion of toxic compounds leading to neuronal death (Gu et al., 2010; Liddel et al., 2017; Silverman et al., 2019). In this thesis, we seek to understand the importance of astrocyte communication through secretion of extracellular vesicles (EVs) and how this process may be altered in neurodegeneration.

Astrocytes were initially characterised by their typical stellate morphology, but were later found to be heterogenous in nature reflecting their varied functions within the CNS. Kimelberg details well-established criteria for defining astrocytes, which covers their wide array of functions and abilities (Kimelberg, 2010). In brief, astrocytes are non-excitabile cells containing the intermediate filament, glial fibrillary acidic protein (GFAP), and glycogen granules. They uptake synaptically released glutamate and γ -aminobutyric acid (GABA) through astrocyte-specific transporters and are connected to other astrocytes through connexin gap junctions (Kimelberg, 2010). Astrocytes have many long processes, some of which surround blood vessels and others around neuronal synapses. Whilst this characterisation encompasses a 'general' astrocytic phenotype, there are different sub-types of astrocytes based upon their morphology and neuroanatomical positioning, with varied functionality and specialist purpose (Vasile et al., 2017). Throughout this thesis, the astrocytes described will refer to this general description of an astrocyte rather than any specialised sub-types of astrocytes.

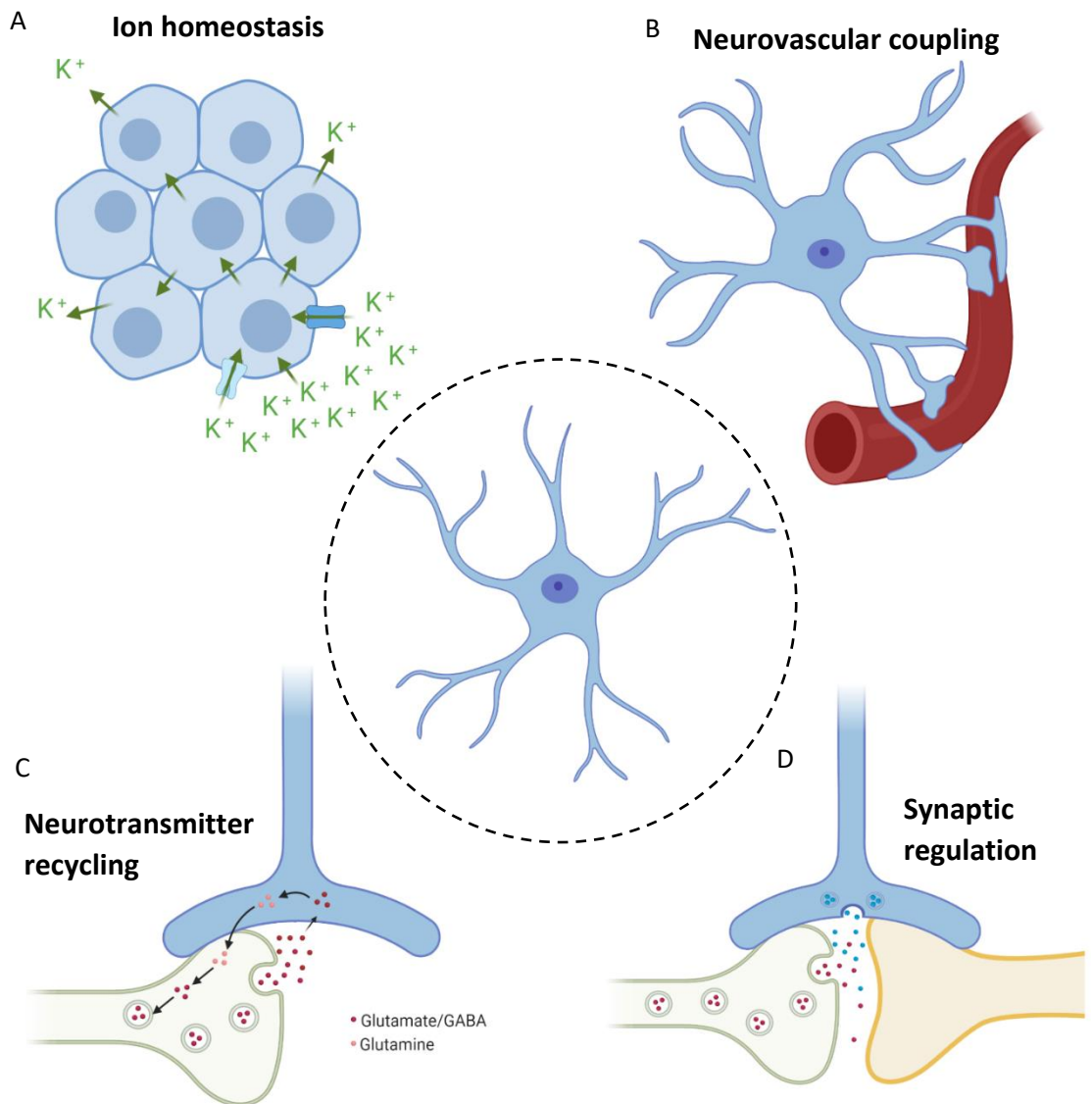


Figure 1-1 - The major functions of astrocytes. Astrocytes perform an array of functions within the CNS, particularly using their many end-feet processes that are characteristic of astrocytes and give the astrocyte their 'star-like' appearance. (A) During neuronal activity, astrocytes are responsible for ion homeostasis by dispersing potassium concentrations in the extracellular space as well as (B) providing metabolic support due to their proximity to blood vessels, with their end-feet involved in maintaining the BBB. (C) Astrocytes can also regulate synaptic activity by clearing and recycling glutamate and GABA to be transported to the neuron safely as glutamine. (D) They also release gliotransmitters in response to neuronal activity which alters the response of the neurons. Image created by the author through BioRender.com.

1.1.1 Astrocyte functions

1.1.1.1 Potassium buffering

Astrocytes provide ion homeostasis for neurons to maintain membrane potential, allowing neuronal activity to occur (Figure 1-1A). Astrocytes do this through potassium ion (K^+) buffering (Somjen, 1979; Müller and Somjen, 2000; Bellot-Saez et al., 2017). During neuronal activation, sodium ions (Na^+) flood into the cell causing an increase in membrane potential. This results in a positive membrane potential to open voltage-gated K^+ channels, allowing K^+ to diffuse out of the neuron into the extracellular space, repolarising the membrane potential of neurons. To rebalance

the ion concentration and maintain the resting potential, Na⁺/K⁺-ATPase pumps actively transport K⁺ into both neurons and astrocytes. The active removal of K⁺ from the extracellular space explains how extracellular K⁺ concentration only increases by <1 mM despite the flood of ions diffusing out of the neuron during neuronal activity (Somjen, 1979).

Astrocytes are the key mediators of K⁺ clearance from the extracellular space with two clearance mechanisms described – net K⁺ uptake and K⁺ spatial buffering (see review: Bellot-Saez et al., 2017). Net K⁺ uptake utilises two protein transporters to actively transport K⁺ into the cell in exchange for other ions - Na⁺/K⁺-ATPase and Na⁺/K⁺/Cl⁻ cotransporter (Larsen et al., 2016). In contrast, K⁺ spatial buffering utilises connexin gap junctions formed between astrocytes to move K⁺ from areas of high extracellular concentration to areas of low concentration using changes in membrane potential that occur through depolarisation, dispersing the change in concentration and minimising impact (Orkand et al., 1966; Bellot-Saez et al., 2017). Gap junctions allow the spread of membrane depolarisation through the astrocyte syncytium to maintain a negative membrane potential at areas of high extracellular K⁺ whilst increasing K⁺ outflux at areas where the equilibrium potential of K⁺ remains more negative (low extracellular K⁺ concentration) than the astrocyte membrane potential (Ma et al., 2016).

1.1.1.2 Neurovascular coupling and metabolic demand

Astrocytes are found in close proximity to blood vessels and ensheath most of the blood vessel with their processes (end-feet) allowing them to regulate cerebral blood flow, maintain the BBB and transport nutrients to neurons (Abbott et al., 2006; Attwell et al., 2010; Mathiisen et al., 2010; Lia et al., 2023; Figure 1-1B). Astrocytes can regulate the constriction and dilation of adjacent blood vessels upon neuronal activity to ensure neurons within areas of high activity receive enough nutrients (Macvicar and Newman, 2015; Nortley and Attwell, 2017).

The BBB tightly regulates the interaction between neural cells and the blood to create the perfect environment. The BBB is composed of (i) endothelial cells, that form the walls of the blood vessels which are held together by tight junctions, (ii) Mural cells including vascular smooth muscle cells on large vessels and pericytes, which incompletely cover small vessels and are embedded in the vascular basement membrane, and (iii) astrocytic end-feet (Abbott et al., 2006; Daneman and Prat, 2015). The BBB restricts ionic substances and molecules through endothelial tight junctions as well as using specific ion transporters, often preventing drugs from accessing the brain (Wong et al., 2013; Daneman and Prat, 2015). Astrocytic end-feet participate in BBB homeostasis by regulating water and ion concentration using high concentrations of receptors on their end-feet such as aquaporin 4 (AQP4) and potassium channels (Abbott et al., 2006). Astrocytes can also regulate and maintain the BBB through the release of molecules such as basic fibroblast growth factor (FGF) and glial derived-neurotrophic factor (GDNF) which has been shown to induce a BBB phenotype in endothelial cells *in vivo* (Abbott, 2002).

Given their close proximity with blood vessels, astrocytes are ideally situated to take up glucose from the blood through surface glucose transporters (e.g., GLUT1-4) for

immediate use but also for long-term storage as glycogen (Figure 1-2; Maher, 1995). Astrocytes are the only cells within the adult brain with the ability to convert glucose into glycogen for storage, which can then be converted to lactate when needed as an energy substrate for neurons (Brown and Ransom, 2007). The lactate shuttle hypothesis was formulated to explain astrocytic involvement in neuronal energy supply and has received both support and criticism since its creation (Pellerin and Magistretti, 1994; Tang, 2018; Cali et al., 2019). This hypothesis describes how neuronal activity triggers astrocyte glycolysis, through the release of glutamate by neurons and subsequent metabolism by astrocytes, which in turn causes astrocytes to release excess lactate for neurons during high neuronal activity (Pellerin et al., 2007).

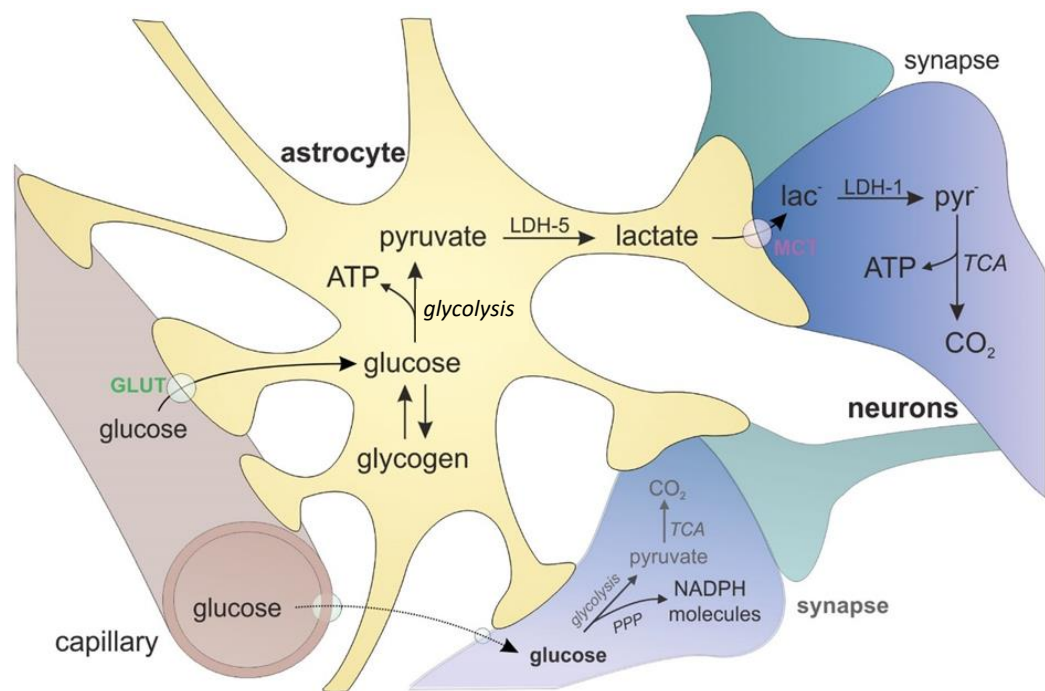


Figure 1-2 - The lactate shuttle hypothesis (taken from Deitmer et al., 2017). Astrocytes are hypothesised to support neurons through the delivery of lactate during high neuronal activity. Astrocytes are found in close proximity to blood vessels where they can uptake glucose through GLUT1 transporters. Neurons can also directly take up glucose from blood vessels through GLUT3 receptors. Astrocytes can convert the glucose to glycogen for storage or it can be metabolised to lactate through glycolysis. Lactate can then be transported via monocarboxylate transporters (MCT) to the neuron where it can be used as oxidative substrate for energy metabolism. When there is high neuronal activity, more glutamate will be released which is taken up and metabolised by astrocytes leading to more lactate production and release.

1.1.1.3 Neurotransmitter recycling

After neurotransmitter release, it is important to clear the synaptic cleft to prevent prolonged stimulation and to recycle valuable resources. The glutamate/GABA-glutamine cycle demonstrates clear metabolic compartmentalisation in the brain with cell-specific elements of this cycle found in astrocytes and neurons, highlighting the effective communication that occurs between these cells (Rae et al., 2003; Andersen and Schousboe, 2022, 2023; Figure 1-1C).

Astrocytes are responsible for clearing the majority of excitatory glutamate and inhibitory GABA neurotransmitters after neuronal activation and metabolising these molecules back to their precursor, glutamine (Figure 1-3; Schousboe, 2019). Astrocytes take up the majority of the glutamate through astrocyte-specific excitatory amino acid transporters (EAATs), EAAT1 and EAAT2 with neurons also taking up some glutamate through EAAT3 to a lesser extent (Schousboe et al., 2004). Astrocytes can convert glutamate to glutamine through astrocyte-specific glutamine synthetase (GS) before releasing back into the extracellular space to be taken up by neurons (Norenberg and Martinez-Hernandez, 1979). To convert GABA into glutamine, GABA enters the tricarboxylic acid (TCA) cycle in the astrocytes where it is converted into succinate before conversion to glutamate (Bak et al., 2006). This molecule of glutamate is then processed in the same pathway as extracellular glutamate.

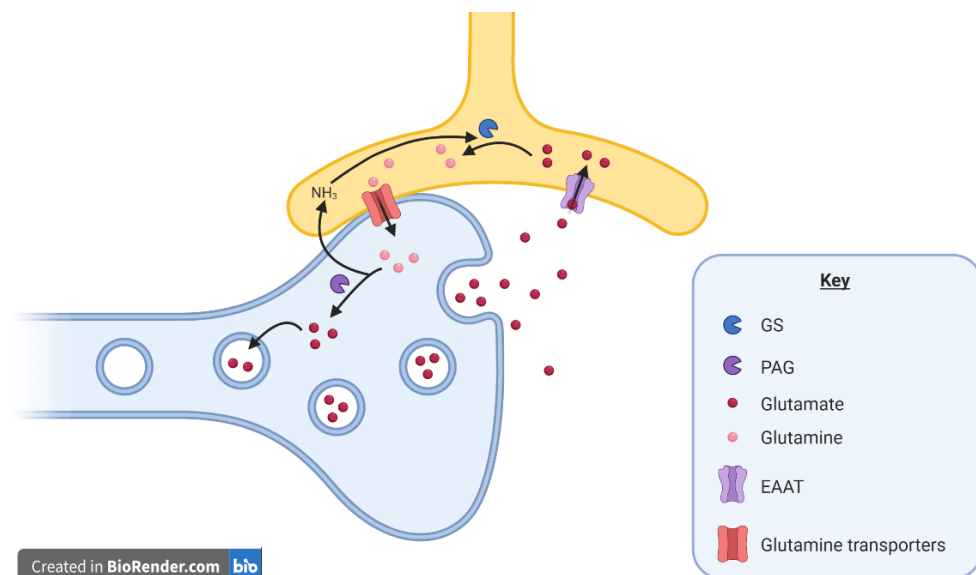


Figure 1-3 – Glutamate/GABA recycling. Astrocytes are responsible for clearing the synaptic cleft of neurotransmitters and recycling them for future use by neurons. Glutamate is an excitatory neurotransmitter which can cause hyperexcitability if allowed to reach high concentrations. Astrocytes actively take up glutamate through EAATs before converting the glutamate into its precursor, glutamine. This occurs through the enzyme glutamine synthetase (GS) using ammonia (NH_3). Glutamine is then transported back to neurons where it is converted back to glutamate through phosphate-activated glutaminase (PAG). This reaction creates ammonia which is transported back to adjacent astrocytes for use in the conversion of glutamate to glutamine. The glutamate can then be packaged into vesicles by neurons for release upon depolarisation. GABA is also recycled in this pathway but requires extra steps to convert GABA to glutamate through the astrocyte TCA cycle and to convert glutamate into GABA through glutamate decarboxylase (GAD) in neurons. Images created by the author through BioRender.com.

After glutamine is taken up by the neurons, it can be converted back to glutamate through phosphate-activated glutaminase (PAG; Akiyama et al., 1990). Whilst this process is thought to mostly occur in neurons, PAG has been identified in astrocytes suggesting they can also perform this process (Kvamme et al., 2001, 2008). Astrocytes also can generate glutamate through the TCA cycle using pyruvate carboxylase (PC) unlike neurons suggesting a role in replenishing gliotransmitter stores (Shank et al., 1985). Glutamate can then be further converted into GABA through glutamate decarboxylase (GAD; Ueno, 2000). During this cycle, ammonia is

created in the neurons through the conversion of glutamine to glutamate and required in astrocytes for the reverse reaction providing ammonia homeostasis, adding a second homeostatic aspect to the glutamate/GABA-glutamine cycle whilst preventing a toxic accumulation of ammonia (Waagepetersen et al., 2002). However, how this transfer occurs is not fully understood. As well as clearing the synaptic cleft after neuronal activity, astrocytes can also modify neuronal signalling using gliotransmitters (glia-based neurotransmitters).

1.1.1.4 The tripartite synapse and gliotransmission

Alongside recycling neurotransmitters, astrocytes form the 'tripartite synapse' with neurons to participate in synaptic communication between adjacent neurons (Araque et al., 1999; Figure 1-1D). Astrocyte processes surround the pre-synaptic and post-synaptic terminals of neurons and actively participate in synaptic transmission. Neurotransmitters (e.g., glutamate), released by neurons during neuronal activation, bind to receptors on the astrocyte cell surface to trigger a transient surge in intracellular calcium in proportion to the intensity of neuronal activity, which can propagate between astrocytes through connexin gap junctions (Cornell-Bell et al., 1990; Charles et al., 1991). This initiates 'gliotransmitter' release from the astrocyte to regulate the synaptic activity (Halassa et al., 2007; Bazargani and Attwell, 2016). Whilst this simplifies the tripartite synapse to one unit, a single astrocyte is estimated to form connections with over 100,000 synapses as well as forming gap junctions with adjacent astrocytes (Giaume and Venance, 1998; Bushong et al., 2002). Calcium waves can propagate to many adjacent astrocytes; therefore a single signal can activate many cells (Goldberg et al., 2010).

1.1.2 Astrocyte response to injury: the reactive astrocyte

The activities above describe basic astrocyte functions which occur in healthy, quiescent astrocytes. However, these same functions are altered or compromised under physiological stress or pathological conditions. Astrocytes have the ability to change phenotype and become reactive in response to injury or disease. These reactive astrocytes display hypertrophy, proliferate, and undergo transcriptional, proteomic, metabolic and morphological changes (Pekny and Pekna, 2014; Escartin et al., 2019, 2021). Whilst neglecting the quiescent functions described above, reactive astrocytes develop new abilities, allowing them to play an important role in the immune system of the brain. Although reactive astrocytes are important for healthy brain function, this phenotype also has harmful consequences with chronic activation associated with neurodegeneration, and therefore it has been a focus of intensive research (Chun and Lee, 2018; Escartin et al., 2007, 2006; Liddel and Sofroniew, 2019; Pekny et al., 2016; Ponath et al., 2018; Yamanaka and Komine, 2018).

1.1.2.1 Terminology

Due to their similar involvement in the immune system, reactive astrocyte phenotypes have been described based upon microglial/macrophage nomenclature

(Liddelow and Barres, 2017; Liddelow et al., 2017). Microglial nomenclature describes ‘M1’ microglia, associated with a pro-inflammatory response, and ‘M2’ microglia which are associated with an anti-inflammatory response (Tang and Le, 2016). Whilst there is controversy about the appropriateness of this nomenclature, it is still often used to describe microglial phenotypic states and has formed the basis for astrocyte nomenclature (Cherry et al., 2014).

Much like microglia, astrocytes activate upon detection of harmful stimuli/tissue damage. Two reactive phenotypes were originally described by Liddelow and Barres, (2017) – inflammatory ‘A1’ and anti-inflammatory ‘A2’ astrocytes, as an attempt to explain the range of responses astrocytes can produce (Figure 1-4). Different stimuli can elicit these phenotypes, with inflammation and toxic insult preferentially activating A1 astrocytes, and ischemia preferentially activating A2 astrocytes (Zamanian et al., 2012). Whilst this terminology is still popular, astrocyte reactivity is better described as a spectrum between these two opposing phenotypes with both phenotypes observed in healthy responses (Anderson et al., 2014).

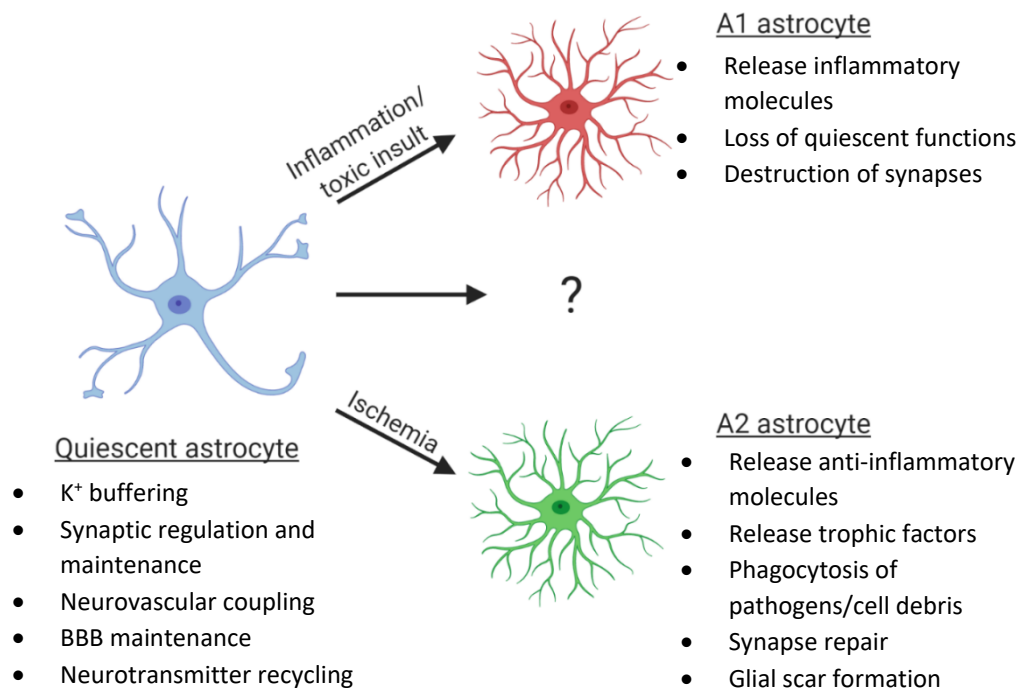


Figure 1-4 - Reactive astrocyte phenotypes. Astrocytes change phenotype upon interaction with harmful stimuli either in the form of pathogens or molecules released from injured/dying cells. An A1 phenotype is associated with inflammation or toxic insult and is primarily described with detrimental functions. The A2 phenotype is associated with ischemia and is described with more beneficial functions. It is unclear whether these phenotypes represent all reactive phenotypes or whether there are other unknown phenotypes which have not been identified at present. It is argued that these phenotypes represent the extremes of a reactive spectrum with single astrocytes displaying aspects of both A1 and A2 phenotypes. A third distinct disease phenotype has been described in the context of Alzheimer’s disease suggesting the possibility of a chronic, disease-associated phenotype. Image was created by the author through BioRender.com.

1.1.2.2 Acquired functions

Reactive astrocytes have both beneficial and detrimental functions which have been tentatively assigned to A1/A2 astrocytes based upon their distinct gene expression

(Figure 1-4; Liddelw and Barres, 2017). However, individual astrocytes can perform both beneficial and detrimental functions. A1 astrocytes are often described with detrimental functions through the release of inflammatory molecules and the destruction of synapses. A1 astrocytes can be activated by M1 microglia, which causes a loss of basic astrocyte functions and leads to the production of an inflammatory secretome released into the local environment, exacerbating inflammation. By preventing A1 activation, neurons have been protected from cell death demonstrating the destructive nature of this phenotype (Yun et al., 2018). However, this destructive nature is needed when dealing with invading pathogens to prevent damage in the brain. Inflammation is a key response of the immune system and therefore, despite the perceived detrimental functions attributed to A1 astrocytes, they are necessary for a healthy immune response.

A2 astrocytes on the other hand, are associated with 'healing' functions with release of anti-inflammatory molecules and neurotrophic factors to promote neuronal survival and synapse repair. These astrocytes have also been shown to phagocytose cell debris after ischemia alongside microglia (Morizawa et al., 2017). Whilst this phenotype is seen as 'protective', the glial scar that is formed upon nerve damage prevents nerve repair and regeneration (Bradbury and Burnside, 2019). But by producing this scar, the damaged tissue is isolated from healthy tissue and prevents any further damage. Extensive research is still needed to fully understand the reactive astrocyte and how this can be better manipulated to help treat disease and injury. For instance, it is unclear if other reactive phenotypes exist and how they act in different situations.

1.1.2.3 Disease phenotypes

To better understand astrocyte reactivity, a clear differentiation should be made between healthy, reactive astrocytes and those seen in pathology (Escartin et al., 2021). A third reactive phenotype has been described in Alzheimer's disease (AD) that have a distinct gene expression from both A1 and A2 astrocytes, described as a disease-associated astrocyte (DAA; Habib et al., 2020). Disease-associated microglia (DAM) have also been described, further demonstrating a similarity between microglia and astrocyte phenotypes (Keren-Shaul et al., 2017; Deczkowska et al., 2018). Astrocytes in disease have been shown to produce a toxic secretome that leads to the death of neurons; however, research is still ongoing to identify the exact cause(s) of this toxicity (Liddelw et al., 2017; Guttenplan et al., 2021; Kushwaha et al., 2021; Arredondo et al., 2022). Together, these results highlight the lack of knowledge surrounding different reactive astrocytic phenotypes. Due to the difficulty in separating astrocytic phenotypes, research often does not distinguish between reactive astrocyte phenotypes. If it does, it has focused on the 'A1/inflammatory astrocyte' due to the perceived negative effects it produces and its presence in neurological disease. A prominent, recent publication has suggested a global term for physiological reactivity to be described as 'astrocyte activation', with disease associated reactivity to be described as a 'reactive astrocyte' (Escartin et al., 2021). But for these terms to be used, a clearer distinction between physiological reactivity and disease needs to be established. For simplicity, in this work, reactive astrocytes will refer to a general, reactive phenotype that describes any changes from the

quiescent, homeostatic phenotype. This is because it is unclear whether the reactivity observed better models pathological or physiological reactivity.

1.1.3 Astrocyte models

The lack of knowledge surrounding the different astrocytic phenotypes is largely due to the difficulty in modelling reactive and quiescent astrocytes. Most astrocyte research generally takes place *in vitro* with the addition of foetal bovine serum (FBS) to support growth and proliferation of the astrocytes. However, with the addition of FBS, the astrocytes appear to change to a more reactive phenotype (increased GFAP and hypertrophy) rather than acting as a 'normal, healthy' astrocyte (Prah et al., 2019). New methods are being published to grow astrocytes without FBS to produce a more realistic, quiescent astrocyte model *in vitro*, but to truly advance astrocyte research, a more established, universally accepted model needs to be adopted (Zhang et al., 2016; Liddelow et al., 2017; Prah et al., 2019).

1.1.3.1 Issues with rodent models

Rodent models are often used to investigate astrocyte function *in vivo* to overcome some of the issues with *in vitro* modelling and to allow better manipulation. However, human astrocytes are far more complex than rodent astrocytes and vary in their functional ability (Oberheim et al., 2009; Zhang et al., 2016). Particular sub-types of astrocytes have been described that are unique to primate brains such as interlaminar and polarized astrocytes which cannot be modelled by rodent models (Colombo et al., 1995; Colombo and Reisin, 2004; Oberheim et al., 2006). But even those astrocytes that are shared between rodents and humans vary drastically with human protoplasmic astrocytes being 2.6-fold larger in diameter with 10-fold more GFAP⁺ processes (Oberheim et al., 2006). As well as unique sub-types, human astrocytes also have a greater capacity for glutamine synthesis with a unique enzyme, GDH2, identified that is not present in rodents (Andersen and Schousboe, 2023). Inducing expression of GDH2 in mice elevates glutamate uptake and oxidation capacity in astrocytes (Nissen et al., 2017). By transplanting human glial progenitor cells into rodent brains and allowing human astrocytes to mature and integrate with rodent astrocytes, the rodents displayed improved synaptic transmission and performed better than their littermates in behavioural tests (Han et al., 2013). By using rodent models, a level of human complexity is ignored and therefore results are less relatable. Many diseases also cannot be replicated in rodents, so treatments developed in rodent models often do not translate well in clinical trials (Pound and Ritskes-Hoitinga, 2018). With new technologies emerging, research should move towards human *in vitro* models which can still be manipulated but are far more relevant to human disease.

1.1.3.2 Current human models

Post-mortem human brain tissue can be used to investigate disease pathology and to better understand the origin of proteins of interest in brain cells. However, access to human tissue is limited due to the inaccessibility of the brain and within the available

tissue, there are shortages of healthy tissue with many donations often displaying age-related or neurodegenerative disease pathology, preventing the study of healthy, quiescent astrocytes. Nevertheless, imaging techniques have enabled the visualisation of reactive astrocytes in living subjects using compounds such as TSPO, but this approach is very expensive and is not specific to astrocytes (O'Brien et al., 2014; Jamadar et al., 2020; Pannell et al., 2020).

Induced pluripotent stem cells (iPSCs) have provided neuroscience research with a new *in vitro* model which better represents human astrocytes in both health and disease (Figure 1-5). iPSCs can be generated from human somatic cells to produce embryonic-like stem cells that can differentiate into any cell type, including neurons and astrocytes (Takahashi and Yamanaka, 2006; Takahashi et al., 2007; Yu et al., 2007; Karumbayaram et al., 2009; TCW et al., 2017; Solomon et al., 2021). More importantly, somatic cells can be taken from patients with disease and reprogrammed into neural cells while retaining the genome of the person and features of the disease (Dimos et al., 2008; Park et al., 2008; Ebert et al., 2009; Juopperi et al., 2012). Whilst this is revolutionising *in vitro* modelling of disease, it also has huge potential in drug discovery and treatment of disease through personalised medicine (Shi et al., 2017). Given that iPSCs are generated from the patient's own cells, there is no immune rejection of the cells when used in transplantation (Wernig et al., 2008; Oki et al., 2012). In fact, a number of clinical studies are investigating the use of iPSC-derived cells in transplantation to replace cells lost due to disease or injury (Barker et al., 2017; Forostyak et al., 2020; Sugai et al., 2021; Miura et al., 2022) .

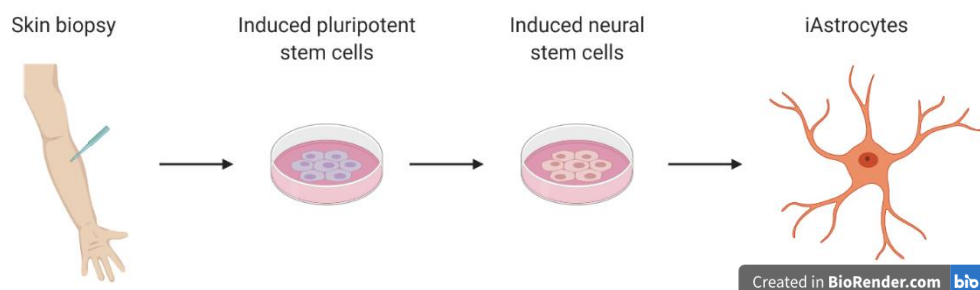


Figure 1-5 - The creation of iPSC-derived astrocytes. A skin biopsy can be taken from a subject to harvest fibroblast cells. These cells are then reprogrammed to produce iPSCs which can differentiate into any cell type in the body. iPSCs can then be differentiated into induced neural stem cells (iNSCs) which can produce neuronal and glial cell types. Cells can be maintained as iPSCs or iNSCs providing a stock solution of cells which can then be differentiated a final time to produce the cell of interest. These cells maintain the genotype of the subject and therefore are a valuable resource in investigating inherited disease and designing personal medicine for patients. Image created by the author through BioRender.com.

An issue with iPSC models is that they are expensive and time-consuming, and there are still questions regarding the accuracy of the model compared to *in vivo* models. This method produces foetal phenotypes due to the conversion back to stem cells and therefore techniques are needed to 'age' these cells to study the ageing cells seen in neurodegenerative disease (Doss and Sachinidis, 2019). *In vitro* cultures also often only use one or two cell types and therefore do not fully encompass the

complexity of cell-cell interactions. Attempts have been made to better model age-related disease using organoids made up of a variety of different cell types (Chen et al., 2021; Szebényi et al., 2021). One study has used human serum on iPSC-derived AD organoids to model BBB dysfunction resulting in enhanced levels of A β and phosphorylated tau (Chen et al., 2021). By using multiple cell types, models become more relevant, and the importance of cell-cell communication can be investigated.

1.1.4 The importance of modelling astrocyte communication

Many astrocyte functions rely on communication between astrocytes, and with other cell types such as neurons and microglia. For example, astrocytes communicate with microglia to survey the local environment, forming the immune response of the brain. Activated microglia have been shown to induce a neurotoxic phenotype in astrocytes by secreting inflammatory cytokines such as interleukins and complement factors (Liddel et al., 2017; Joshi et al., 2019). In particular, IL-1 α , TNF α and C1q have been shown to produce a reactive, inflammatory phenotype with this method now commonly used for generating reactive astrocytes *in vitro* (Liddel et al., 2017; Clarke et al., 2018; Barbar et al., 2020; Leng et al., 2022). In addition to secreted proteins, recent advances in extracellular vesicle research have shown that EVs are key players in cell-to-cell communication and likely perform a key role in astrocyte communication (You et al., 2020; Pivoriūnas and Verkhratsky, 2021).

1.2 Extracellular vesicles

1.2.1 What are extracellular vesicles?

The international society of Extracellular vesicles (ISEV) define EVs as a heterogeneous population of non-replicating molecules delimited by a lipid bilayer, that are released naturally from cells (Théry et al., 2018). They contain proteins, RNAs, and metabolite cargo which can be taken up by recipient cells, exerting their effect within the recipient cell as a form of intercellular communication. Two key sub-types (exosomes and microvesicles) have been defined based upon their origin and release mechanism. However, in practice, it is difficult to distinguish between them due to a lack of specific markers for each group. Other criteria such as physical properties (size), biochemical composition (presence of particular markers) or cell of origin (e.g., astrocyte-derived EVs) are therefore advised to describe EVs in research where it is not possible to identify how the EVs were released.

1.2.1.1 Exosomes

Exosomes are defined as EVs with an endosomal origin and range between 30 – 200 nm in diameter (Pegtel and Gould, 2019; Kalluri and LeBleu, 2020; Krylova and Feng, 2023). Vesicles are formed through the inward budding of the endosomal membrane with the endosome forming a multivesicular body (MVB). This fuses either with lysosomes for degradation, or with the plasma membrane to secrete their contents of exosomes into the extracellular space (Figure 1-6). Due to their origin, exosomes are thought to be more homologous than other EV types and carry endosomal proteins such as ALIX and a variety of tetraspanins (Kalluri and LeBleu, 2020).

However, current issues with separation techniques make studying exosomes in isolation very difficult, even with more specific markers.

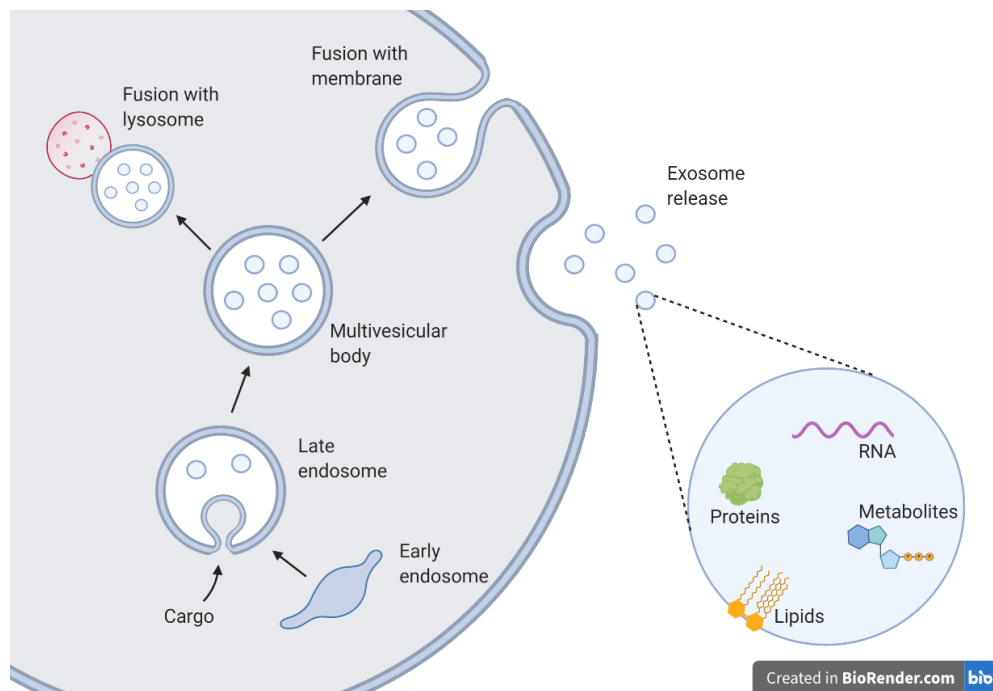


Figure 1-6 - Exosome biogenesis and release. Exosomes are formed through the inward budding of the endosome creating a multivesicular body (MVB). The MVB can either fuse with lysosomes and be degraded and then recycled (autophagy), or it can fuse with the plasma membrane and release the vesicles into the extracellular space. Cargo appears to be selectively loaded into these exosomes during exosome formation, but the exact mechanisms of cargo loading are not fully understood. Exosomes cargo contains proteins, metabolites and various forms of RNA surrounded by a lipid bilayer. Image created by the author through BioRender.com

Whilst the exact mechanism of exosome formation and release is not fully understood, endosomal sorting complex required for transports (ESCRTs) are thought to be involved alongside other associated proteins such as ALIX and syntenin (Baietti et al., 2012; Colombo et al., 2013; Choi et al., 2015; Xie et al., 2022). ESCRT-independent mechanisms also exist, with depletion of ESCRT machinery not entirely preventing exosome formation (Stuffers et al., 2009; Colombo et al., 2013; Kenific et al., 2021; Wei et al., 2021). Evidence highlights the importance of ceramide in the vesicle budding process. Neutral sphingomyelinase II (nSMase2) converts sphingomyelin into ceramide, with ceramide thought to create inward membrane curvature through its cone-like structure to form the vesicles in the MVB (Trajkovic et al., 2008). Raft microdomains found in lipid membranes, are enriched in lipids such as sphingomyelin and ceramide with inhibition of nSMase2 leading to a reduction in exosome release (Trajkovic et al., 2008; Elsherbini et al., 2021; Crivelli et al., 2022). Interestingly, altered ceramide has been associated with brain dysfunction (Fan et al., 2021; Kurzawa-Akanbi et al., 2021; Fonseca-Ferrer et al., 2022). Rab GTPase proteins, such as RAB11 and RAB35, regulate vesicular trafficking in the cell and have been associated with MVB biogenesis and fusion with the cell membrane (Ostrowski et al., 2010; Blanc and Vidal, 2018; Wei et al., 2021).

It is likely there are multiple mechanisms for exosome formation based upon the role of the individual MVB due to the heterogenous population of exosomes that is created. Whilst there is still limited understanding of exosome mechanics, there is even less understanding about the mechanism of release for the other key EV sub-type: the microvesicle.

1.2.1.2 *Microvesicles*

Microvesicles (also known as ectosomes or microparticles) are larger EVs ranging between 150 – 1000 nm in diameter which arise directly from the budding of the plasma membrane into the extracellular space (Sedgwick and D'Souza-Schorey, 2018; Clancy et al., 2021). Whilst released under normal conditions, microvesicles are also released upon stimulation or physical stress (Cocucci et al., 2007; Turola et al., 2012). An example of this is that astrocyte-derived ATP can stimulate microvesicle release in microglia, not only demonstrating communication between different cells but also how astrocyte reactivity can cause changes in adjacent cells (Bianco et al., 2005).

Like exosomes, ESCRTs and ceramide have been implicated in microvesicle formation suggesting a common mechanism between the two vesicle sub-types (Cocucci and Meldolesi, 2015; Sedgwick and D'Souza-Schorey, 2018). However other proteins have been indicated as key proteins in microvesicle shedding such as RhoA and ARF6 (Muralidharan-Chari et al., 2009; Li et al., 2012; Sedgwick and D'Souza-Schorey, 2018). Cholesterol depletion reduces microvesicle formation suggesting cholesterol-rich lipid rafts are involved in microvesicle shedding (Del Conde et al., 2005).

1.2.2 EVs in intercellular communication

When first discovered, EVs were initially thought to be cellular artefacts or part of the cell's waste disposal mechanism and therefore were largely ignored. However, after the discovery of their role in intercellular communication, a surge of research has moved these nanoparticles into the forefront of biological research, especially in the neuroscience field (Couch et al., 2021). Due to the nature of working across a range of disciplines and with such a range of techniques, the EV community has produced a set of guidelines to improve the quality of the work produced in the field and to better standardise protocols. These are known as the MISEV guidelines which are based upon the overall consensus from researchers in the field which are updated every four years to encompass advances in research (Théry et al., 2018). Alongside these guidelines, other tools such as EVTRACK (online scoring/checklist for publications) have been produced to improve the quality of research in the community (Van Deun et al., 2017).

Vesiclepedia and Exocarta are two databases that have been created to catalogue EV cargo based upon their parent cell type (Kalra et al., 2012; Simpson et al., 2012; Pathan et al., 2019). Both resources have great value with Exocarta focusing on cargo reported from exosome studies, and Vesiclepedia encompassing all types of EV cargo. One major issue with these databases at present is a lack of results for all cell

types with no detailed database for astrocytes or neuronal cells. By identifying cell-specific cargo, a range of diagnostic possibilities arise.

With EVs involved in cell-cell communication and responsible for non-cell autonomous control of cell fate, there must be mechanisms for selecting specific cargo to be loaded in EVs. If there was non-selective cargo loading, it would be expected that EVs perfectly reflect the composition of the cell, however this is not the case with certain cargo being enriched in EVs compared to the cell (Chen et al., 2021; Dixon et al., 2023; Jovičić and Gitler, 2017; Nolte' T Hoen et al., 2012). Similar loading mechanisms have been described for EVs and autophagy suggesting the pathways are closely related (Leidal and Debnath, 2021).

1.2.3 Are exosomes a form of secretory autophagy?

Autophagy has originally been considered as a waste-disposal pathway in cells to remove damaged proteins/organelles and to recycle nutrients at times of cellular-starvation (Rabinowitz and White, 2010). Selective autophagy requires cargo to be ubiquitinated before being sequestered into the autophagosome through autophagy adaptor proteins such as p62 and NBR1 which then interact with LC3 to connect cargo with the emerging autophagosome (Figure 1-7; Lamark et al., 2009; Pankiv et al., 2007). The autophagosome will then fuse to lysosomes for degradation and the components recycled. It is thought a similar process occurs in the formation of exosomes, described as 'Secretory autophagy' in which instead of fusing with the lysosome, the vesicles can fuse with MVBs to form exosomes upon secretion (Baixauli et al., 2014; Ponpuak et al., 2015; Buratta et al., 2020; Solvik et al., 2022). It appears a fine balance between traditional autophagy and exosome generation exists to provide homeostasis within the cell. When conditions stimulate increased autophagy, exosome release is inhibited with MVBs being targeted for lysosome recycling rather than excretion (Fader et al., 2008; Leidal et al., 2020; Solvik et al., 2022). In fact, the reverse has also been demonstrated in pathology where autophagy inhibition led to the increase of pathological α -synuclein secretion in EVs (Minakaki et al., 2018).

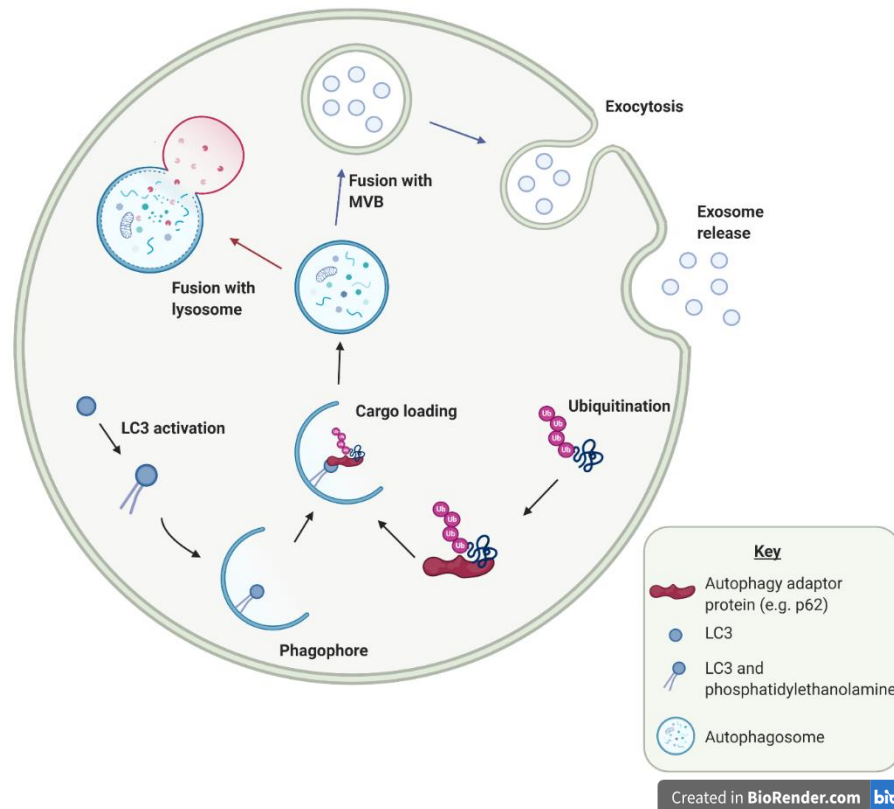


Figure 1-7 - Secretory autophagy. Secretory autophagy shares a common pathway with traditional, selective autophagy. LC3 is activated through the interaction with phosphatidylethanolamine and binds with a developing phagophore. Autophagy adapter proteins then sequester ubiquitinated cargo into the phagophore by binding to LC3. Recent evidence suggests that RNA can be loaded into autophagosomes in the same way as ubiquitinated proteins with RNA-binding proteins acting as adaptors (Leidal et al., 2020). Once the phagophore has matured into an autophagosome, it can then fuse with a lysosome and be degraded (selective autophagy). However, the autophagosome can instead fuse with the MVB and secrete its content as exosomes (secretory autophagy). Secretory autophagy is also thought to involve microvesicles as well, however the mechanism is less understood. By inhibiting either selective or secretory autophagy, the opposing pathway is increased.

1.2.3.1 Protein loading

Similar selective protein loading mechanisms further highlight the similarity between traditional autophagy and exosome release. ESCRTs are responsible for transporting ubiquitinated proteins into vesicles which either go on to fuse with lysosomes or to be released as EVs (Villarroya-Beltri et al., 2014). Through ubiquitination, specific proteins can be selected and transported into the vesicle. Secretory autophagy begins to explain the presence of potentially pathological protein aggregates in EVs such as TDP-43, α -synuclein and prions (Lööv et al., 2016; Liu et al., 2017; Sproviero et al., 2018). These proteins would likely be targeted for degradation but instead are released in EVs. Why the cell would want to release proteins destined for degradation remains a mystery with this mechanism potentially causing the spread of neurological disease. ESCRT-independent mechanisms have also been described for protein cargo loading through tetraspanins and lipid-dependent mechanisms which likely reflects the heterogeneity of proteins within EVs (Villarroya-Beltri et al., 2014).

1.2.3.2 RNA loading

The joint autophagy and EV loading mechanisms are also evident when considering RNA loading. Within extracellular vesicles, protein-coding messenger RNAs (mRNAs) are found alongside many types of non-coding RNAs such as micro RNAs (miRNAs) and transfer RNAs (tRNAs; Blandford et al., 2018; Kim et al., 2017; Mesquita-Ribeiro et al., 2021; Valadi et al., 2007). MiRNAs target mRNAs for cleavage or translational repression inhibiting the translation of the targeted mRNA (Huntzinger and Izaurralde, 2011). Therefore, an increase in miRNA expression would lead to a decrease in protein expression in the recipient cell. A single miRNA can target many different mRNAs and a single mRNA can be repressed by multiple different miRNAs. MiRNAs are protected from degradation by the cell through binding with RNA binding proteins (RBPs) or being sequestered into EVs and have been shown to exert their effect in recipient cells making these molecules an intriguing target for biomarkers and treatments (Mittelbrunn et al., 2011; Lafourcade et al., 2016; Luarte et al., 2017; Varcianna et al., 2019).

A role for LC3 machinery in selectively loading RBPs and small non-coding RNA into EVs has been explored (Leidal et al., 2020). Certain RBPs such as hnRNPA2B1, SYNCRIP and FUS has been shown to select miRNAs for EV loading (Villarroya-Beltri et al., 2013; Santangelo et al., 2016; Garcia-Martin et al., 2021). In particular, it appears that certain sequences in the miRNAs leads to the preferred selection or retention of the RNA by the cell for secretion in extracellular vesicles (Garcia-Martin et al., 2021). More research needs to be completed to understand this mechanism for miRNA selection and what these sequences are in order for EVs to be manipulated to deliver therapeutic miRNAs.

RBPs and RNA metabolism proteins are enriched in EVs indicating EVs as key transport mechanisms for RNAs between cells. Whilst it is clear that miRNAs are commonly present in EVs, it is debated how many miRNA molecules are present in a single vesicle and whether they are found in every EV or in RNA-specific EVs (Chevillet et al., 2014; Li et al., 2014). It is suggested there may be less than one miRNA per vesicle with estimates ranging from one miRNA in every ten EVs to one in every 120 EVs (Janas et al., 2015). Current methods are not sensitive enough to examine the contents of a single EV, so it is difficult to understand whether all EVs carry RNA cargo or whether there are subsets of EVs that preferentially carry RNA cargo.

1.2.3.3 Metabolites in EVs

A metabolite is considered any biologically relevant molecule smaller than 2 kDa so this term encompasses a wide range of molecules involved in most cellular processes. Despite this, less is known about metabolites in EVs compared to protein and RNA cargo, but some studies have begun to investigate their purpose and potential use in diagnostics (Huang-Doran et al., 2017; Puhka et al., 2017; Harmati et al., 2021). EVs have been shown to carry metabolic enzymes and may produce metabolites such as ATP whilst acting as independent units (Iraci et al., 2017; Göran Ronquist and Ronquist, 2019). If shown to act as metabolically active units, it would suggest a more important role for EVs rather than simply acting as an intercellular delivery system.

Far more research needs to be conducted before we can begin to elucidate the role of metabolites in EVs and to what extent EVs can act as independent, functional units. It is clear that EVs are not simply cellular waste and instead, contain varied cargo that is used in intercellular communication. With future advances in methodology, the cargo of these EVs can be manipulated and utilised to mediate intercellular communication to benefit patients. This is important for neurodegenerative disease due to the inaccessibility of the brain which at present results in a lack of treatments and diagnostic tests.

1.2.4 Difficulties with EV research

Whilst MISEV guidelines have helped establish more common methodologies regarding EV research, there is still a huge amount of variation in the isolation of EVs resulting in differences in EV sample compositions (Palviainen et al., 2019; Brennan et al., 2020; Dudzik et al., 2021; Nigro et al., 2021; Wallis et al., 2021). This ultimately affects cargo analysis and therefore it is difficult to collate work from different research groups. This has limited EV cargo research but with improved techniques and clearer publication of methodology (EV-TRACK), there is hope for more reproducible results that can be used for biomarker identification.

1.2.5 Future applications: Why the interest in EVs?

1.2.5.1 Biomarker potential

One of the most intriguing aspects of EVs is they are thought to reflect the state of the cell at the time of release and change their cargo in response to stress and disease (de Jong et al., 2012). It is incredibly difficult to monitor the state of the brain at a cellular level in living humans and therefore EV cargo provides a valuable insight. EVs contain cell-specific molecules which allows the isolation of specific cell-derived EVs from biological fluid such as cerebral spinal fluid (CSF) and blood plasma (Mustapic et al., 2017; Willis et al., 2017; Eren et al., 2022). EVs have also been shown to cross the BBB allowing CNS-derived EVs to be found in the blood as well as in the CSF (Goetzl et al., 2016, 2019; Dickens et al., 2017; Nogueras-Ortiz et al., 2020). By identifying disease molecules within EVs from specific cells, there is the potential to use EVs as a biomarker for neurodegeneration and as a marker of general brain health without invasive techniques. Diagnostic tests for neurodegenerative disease are currently lacking in living patients. Many disease diagnoses rely on excluding other measurable criteria and then predicting the most likely form of the disease from symptom/disease progression. The exclusion of other diseases can take a long time and patients often cannot start treatment until diagnosed. For many with neurodegeneration, these early stages of disease are precious with cognitive and physical deterioration progressing quickly.

1.2.5.2 Potential treatments

With much more research into the uptake mechanism of these EVs, it may be possible to manipulate EVs from an individual to deliver therapeutic drugs or use naturally-derived EVs that have therapeutic effects such as mesenchymal stem cell-

derived EVs (Chulpanova et al., 2018; Agrahari et al., 2019; Baek et al., 2019; Hou et al., 2021; Soares Martins et al., 2021). If taken from patients, the advantage of using EVs is that they can be utilised to deliver treatment without eliciting an immune response against the host. For neurological treatments, an even greater advantage is the potential to deliver drugs non-invasively across the BBB which is currently very difficult. If it is possible to target a specific cell type with the EVs, it would also reduce side effects. Far more research needs to be conducted before either diagnostics or treatments can be designed but with this potential recognised, there is much hope across biological and medical research for these nanoparticles.

1.3 Astrocyte-derived extracellular vesicles

The rest of this chapter will begin to explore the current knowledge of ADEVs and how ADEV cargo changes in neurodegenerative disease. As previously discussed, astrocytes change phenotype in response to harmful stimuli or disease and therefore it is expected this will be reflected in ADEVs. Neurodegenerative disease research has often taken a very neuronal-centric view but in recent years, the role of astrocytes in disease has become apparent (Liddelow and Sofroniew, 2019; Acioglu et al., 2021; Lee et al., 2022; Brandebura et al., 2023). What is becoming clear is that the astrocytic role in disease often includes abnormal secretions from reactive astrocyte.

At present, there is no detailed description of ADEV contents on EV databases with no description found on Exocarta and only 1 protein (Nkpd1) identified in the Vesiclepedia database. This is not due to a lack of research with many studies undertaking proteomic and transcriptomic analysis in various astrocyte models (Dickens et al., 2017; Willis et al., 2017; Chaudhuri et al., 2018, 2020; You et al., 2020). What is lacking is a detailed group analysis of this data which can be used as a reference for further studies. Common astrocyte markers, GFAP and GLAST (known as EAAT1 in humans), are found within ADEVs and have been utilised to isolate ADEVs in biological fluid (Goetzl et al., 2016; Willis et al., 2017; Winston et al., 2019).

GFAP is an intermediate filament found in the cytoplasm of astrocytes and is commonly used to assess astrocyte morphology and reactivity. However, whilst GFAP is described as an astrocytic marker, it is present in other cell types such as radial glial cells and does not encompass all astrocytes (Casper and McCarthy, 2006; Jurga et al., 2021). With GFAP expression increasing in disease due to the induction of reactive astrocytes, an increase in GFAP expression in ADEVs may be a useful marker of disease if used in a panel of other disease-associated markers. By completing a detailed analysis of quiescent and reactive astrocytes and their ADEVs, more astrocyte-specific or astrocyte-enriched markers can be identified which will allow better isolation of ADEVs in biological fluids for diagnostics (Table 1-1).

Table 1-1 - Common astrocyte markers. A list of common astrocyte markers and the issues with each of these markers (Garwood et al., 2017; Preston et al., 2019; Escartin et al., 2021; Jurga et al., 2021). Many of these markers are either found in other cell types or do not stain all astrocytes due to their heterogeneity. GFAP is the most used astrocyte marker however this also does not stain all astrocytes. CD49f is a newly identified marker of both quiescent and reactive astrocytes however it has not yet been thoroughly tested by other research groups and is found in endothelial cells (Barbar et al., 2020). All of these markers have been detected in EVs except AQP4 suggesting their potential as ADEV markers (Vesiclepedia database). *AQP4 may be present in ADEVs because astrocytes have not yet been profiled in the Vesiclepedia database and AQP4 is astrocyte specific.

Astrocyte marker	Function of molecule	Problems with marker
GFAP	Intermediate filament	<ul style="list-style-type: none"> Does not stain all astrocytes and can vary throughout the brain Stains other cells such as radial glia
S100 β	Calcium, copper and zinc-binding protein	<ul style="list-style-type: none"> Not specific to astrocytes (NG2 cells, neurons, neonatal oligodendrocytes) Does not label all astrocytes
ALDH1L1	Enzyme in folate metabolism	<ul style="list-style-type: none"> Labels more astrocytes than GFAP but also oligodendrocytes and radial glia
EAAT1/2 (Rodents: GLUT1/ GLAST)	Glutamate transporters	<ul style="list-style-type: none"> Not specific to astrocytes (all CNS cells at low levels)
Glutamine synthetase (GS)	Enzyme in glutamate cycle	<ul style="list-style-type: none"> Not specific to astrocytes (Found in the liver, lungs and adipose tissue)
CD44	Hyaluronic acid receptor and adhesion molecule	<ul style="list-style-type: none"> Stains processes but not much cytoplasm
NDRG2	Tumour suppressor	<ul style="list-style-type: none"> Downregulated in reactive astrocytes Varies in expression with anatomical localisation
CD49f	An integrin	<ul style="list-style-type: none"> Newly identified marker so it has not been rigorously tested Also found endothelial cells
AQP4*	Water channel	<ul style="list-style-type: none"> Astrocyte-specific but preferentially stains processes that are in contact with blood vessel
Connexin 30/43	Gap junctions	<ul style="list-style-type: none"> Cx30 is only in grey matter astrocytes Cx43 also seen in endothelial and ependymal cells
Vimentin	Intermediate filament	<ul style="list-style-type: none"> Not specific to astrocytes (Bergmann glia, radial glia and ependymal cells)

1.3.1 Functionality of ADEVs

Whilst ADEVs may be important in disease and therefore research has primarily focused on this, it is also important to understand their role in the healthy brain and how they are used to influence functional changes in adjacent cells. Without an understanding of healthy ADEVs, it is difficult to identify exact changes in pathological ADEVs. This is an area of research which needs to be explored as current knowledge is limited.

1.3.1.1 The effect of ADEVs on neurons

Astrocytes are known for their supportive and neuroprotective effects on neurons, especially in oxidative stress (Fujita et al., 2009; Pitt et al., 2017; Teh et al., 2017). This is reflected in ADEVs, with trophic factors found within the EVs such as Apolipoprotein D (APOD) and insulin-like growth factor 1 (IGF1) which protect neurons under stress (Ranjit et al., 2018; Pascua-Maestro et al., 2019; Zhang et al.,

2021). Prion proteins have been suggested as critical for neuroprotection by astrocytes in oxidative stress (Bertuchi et al., 2012; Guitart et al., 2015, 2016; Kabani et al., 2020). Prions in ADEVs released during oxidative stress are taken up by neurons, facilitating astrocytic neuroprotection for the neuron (Guitart et al., 2016). ADEVs have even been shown to contain glutamate transporters which suggests they may partake in glutamate clearance (Gosselin et al., 2013). Whilst protecting neurons under stress is a key function for astrocytes, ADEVs can also promote synapse formation and neurite growth (Patel and Weaver, 2021; Sun et al., 2022).

1.3.1.2 The effect of ADEVs on glia

ADEVs can also influence other cell types in the CNS such as microglia and oligodendrocytes. ADEVs from young, healthy astrocytes induce the maturation of oligodendrocyte progenitor cells (OPCs) into oligodendrocytes with this ability diminishing with age and during inflammation (Willis et al., 2020). Oligodendrocytes are vital for efficient neuronal transmission because they increase the conduction rate of neuronal activity by insulating the neuronal axon with myelin (Goldman and Kuypers, 2015).

Astrocytes also work closely with microglia to form the immune system of the brain and often form positive feedback loops when harmful stimuli are detected. Microglia are the CNS's resident macrophage and are essential for protecting the brain against invading pathogens and damage with an ability to phagocytose. Once activated themselves, microglia release factors such as TNF α and IL1 β to activate astrocyte reactivity, however, this communication is bidirectional with ADEVs also effecting microglia (Bianco et al., 2005; Pascual et al., 2012; Liddelow et al., 2017; Joshi et al., 2019). ADEVs have been shown to modulate microglial activation by activating Toll-like receptor 7 (TLR7) after treatment with morphine leading to a reduction of microglial phagocytosis (Hu et al., 2018).

1.3.2 ADEVs from reactive astrocytes

Far more research has been conducted on ADEVs in disease and the changes that occur within ADEV cargo upon astrocyte activation. ADEV composition changes in reactive astrocytes so ADEV contents reflect the current state of the cell at the point of release (Chaudhuri et al., 2018, 2020; You et al., 2020). Reactive ADEVs have been shown to cross the BBB to activate a peripheral immune response and promote leukocyte migration to the brain (Dickens et al., 2017). With reactive astrocytes present in neurodegenerative disease and the ability of ADEVs to cross into the blood, a change in ADEV cargo could be utilised to detect neurodegeneration through a non-invasive blood test. With more detailed analysis, it may even be possible to detect disease-specific cargo within the ADEVs to diagnose specific neurodegenerative disease.

Astrocytes incubated with pro-inflammatory molecules (e.g., IL-1 β) recapitulate the astrocyte reaction to an inflammatory environment. These pro-inflammatory molecules are primarily produced by microglia when exposed to an inflammatory stimuli/environment and is commonly used as an inducer of the reactive astrocyte

phenotype. Dr You and colleagues demonstrated the loss of normal astrocyte function in a pro-inflammatory environment with clear changes to the cargo of ADEVs from these cells leading to negative consequences in the recipient neurons (You et al., 2020). Reactive ADEVs were more readily taken up by neurons compared to control ADEVs and an enrichment in proteins involved in the signalling of pathogenic molecules were found. This would suggest that reactive ADEVs would influence neurons to a greater extent in pathological conditions and would provide the ideal vehicle to transmit pathology. In fact, IL-1 β has been shown to enhance EV release as well as alter cargo in other studies with different models (Dickens et al., 2017; Chaudhuri et al., 2018, 2020). Changes in ADEV cargo is not limited to a pro-inflammatory environment with EV cargo composition also effected by anti-inflammatory stimuli such as interleukin-10 (IL-10; Chaudhuri et al., 2020).

One difficulty with astrocyte models is to produce a control, quiescent phenotype with current models displaying some levels of reactivity even in controls. There is also no current standard to categorise phenotypes with many studies deciding phenotype based on morphology, levels of GFAP expression (present in all phenotypes but increased in a reactive phenotype), perceived functions and gene expression if completed. Markers for the individual phenotypes are desperately needed. With astrocytes often grown in FBS, researchers may be altering the ADEV cargo towards a reactive phenotype and therefore may miss changes between quiescent ADEVs and reactive ADEVs. This needs to be explored further to determine if there are differences between ADEVs when parent cells are cultured in FBS and those cultured in serum-free conditions. By completing a comprehensive basis for healthy astrocyte phenotypes and their ADEVs, changes in disease can be more easily distinguished.

1.3.3 ADEVs in disease

Reactive astrocytes and inflammation are found in neurological disease and therefore the changes described above, would also be expected in neurodegenerative disease models. EVs have a role in neurodegenerative disease, however the extent of their role is only beginning to be explored (Hill, 2019; Yuan et al., 2020). Many neurodegenerative diseases display characteristic protein pathology with protein aggregates found in and around neurons, leading to cell death. Interestingly, these protein aggregates such as beta-amyloid (A β ₁₋₄₂), α -synuclein, TDP-43, SOD1 and prions, have all been discovered in neuronal and ADEVs. This suggests EVs are involved in disease transmission within the brain with a suggestion that these protein aggregates are 'infectious' in a similar way as the prion protein.

1.3.3.1 Prion diseases

Creutzfeldt-Jakob disease (CJD) is the most common human form of a group of conditions known as transmissible spongiform encephalopathies (TSEs) or prion diseases (Chen and Dong, 2016). Whilst CJD can arise sporadically or be inherited, TSEs are also infectious diseases that can be spread through the digestion or transplantation of infected nervous tissue either from the same species (human \rightarrow human; Kuru) or between species (cattle \rightarrow human; variant CJD). The transmissible

nature of this rare neurodegenerative disease has interested many biologists due to the potential commonality for the transmission mechanism in other diseases.

Prion proteins were the first infectious proteins identified that could cause protein misfolding in healthy proteins upon interaction with an infected protein, described as 'prion theory' (Prusiner, 1982; Aguzzi and Weissmann, 1997). Prion theory describes the existence of two forms of the prion protein, the normal cellular form (PrP^{C}) and the protease-resistant form (PrP^{Sc}), where interaction of PrP^{C} with PrP^{Sc} leads to a conformational change in the PrP^{C} to form PrP^{Sc} (Figure 1-8). The infectious PrP^{Sc} is more prone to aggregation with an increased stability from β -sheets, leading to the formation of amyloid plaques, resulting in cell death and neurodegeneration (Pan et al., 1993). More recently, prion proteins have been identified in EVs suggesting a mechanism of disease spread between cells via EV cargo (Fevrier et al., 2004; Saá et al., 2014; Liu et al., 2017). Prion theory and the involvement of EVs in disease transmission is now being investigated in other, non-infectious neurodegenerative diseases that have characteristic protein aggregates (Grad et al., 2014; Stopschinski and Diamond, 2017; Takashima et al., 2021; Gosset et al., 2022).

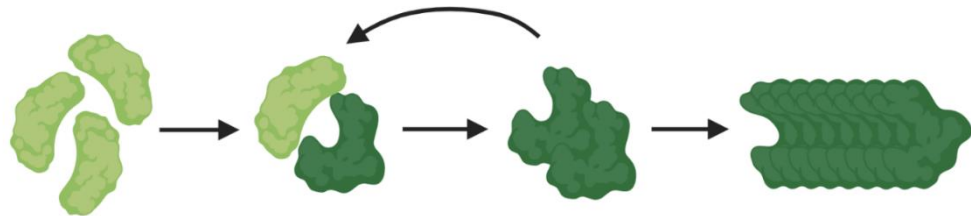


Figure 1-8 - Prion theory. Prion theory explains the conversion of healthy proteins into misfolded, pathological proteins that cause disease. Prions can exist in two forms – the normal cellular protein (light green; PrP^{C}) and the protease resistant form (dark green; PrP^{Sc}) which is responsible for the disease. Interaction with PrP^{Sc} can cause a conformational change in the PrP^{C} to transform into PrP^{Sc} . This molecule can then go onto to alter other healthy PrP^{C} leading to an increase in toxic PrP^{Sc} and a decrease in healthy proteins. The toxic PrP^{Sc} is more stable due to more β -pleated sheets and cannot be broken down by proteases, leading to aggregation of the proteins. These aggregations form amyloid plaques which lead to neuronal death. With prions detected within EVs, it is hypothesised that mutated proteins can spread between cells causing widespread disease within the brain. It is hypothesised that this mechanism is not unique to prion proteins and may occur in other diseases such as ALS (Grad et al., 2014; Stopschinski and Diamond, 2017).

Prion-infected astrocytes have been shown to be toxic to neurons through non-cell autonomous mechanisms with infected astrocytes demonstrating a pro-inflammatory, neurotoxic phenotype (Kushwaha et al., 2021). In this study, astrocyte conditioned medium from infected astrocytes caused a detrimental effect on neuronal survivability and impaired synapse integrity. Further work should investigate the role of EVs directly in this toxicity given the presence of the infected prion protein in ADEVs. Whilst research has generally focused on the role of infectious prions in disease, new work is beginning to establish the role of healthy, cellular prion protein in the brain (Guitart et al., 2015, 2016; Wulf et al., 2017; Brenna et al., 2020). One study has shown prion proteins and their receptor to be involved in the movement of ADEVs along the neuronal surface to reach preferential interaction sites (D'Arrigo et al., 2021). With other neurodegenerative diseases being more prevalent, more research has been done on the role of ADEVs in disease.

1.3.3.2 *Alzheimer's disease*

AD is the most common neurodegenerative disease in the world and the leading cause of dementia (Niu et al., 2017; Alzheimer's Association, 2018; Scheltens et al., 2021). Two altered proteins have been identified as the cause of protein pathology in AD - hyperphosphorylated tau protein and $A\beta_{1-42}$, leading to neurofibrillary tangles and amyloid plaque deposits throughout the brain (Ballatore et al., 2007; Ittner and Götz, 2011; Selkoe and Hardy, 2016). Much like the prion protein, these proteins have been identified within EVs suggesting EVs as a mechanism of disease spread (Rajendran et al., 2006; Saman et al., 2012; Wang et al., 2017; Sardar Sinha et al., 2018; Ruan et al., 2021; Fowler et al., 2023).

Reactive astrocytes have been shown to be important contributors in AD with both beneficial and detrimental functions (Garwood et al., 2017; Chun and Lee, 2018; Nanclares et al., 2021). In particular, reactive astrocytes have been shown to migrate towards $A\beta_{1-42}$ deposits and degrade toxic $A\beta_{1-42}$, removing it from the extracellular space (Wyss-Coray et al., 2003). It has been suggested that there is a failure of this degradation in AD, leading to the accumulation of toxic $A\beta_{1-42}$ (Mawuenyega et al., 2010; Wildsmith et al., 2013). A failure to clear $A\beta_{1-42}$ through autophagy leads to the release of $A\beta_{1-42}$ within ADEVs, enhancing disease transmission and causing neuronal cell death (Dinkins et al., 2014; Söllvander et al., 2016; Beretta et al., 2020). As well as the inclusion of toxic AD proteins, $A\beta_{1-42}$ production machinery is enriched in ADEVs from AD patients compared to controls and neuron-derived EVs (Goetzl et al., 2016; Nikitidou et al., 2017; Pérez-González et al., 2020). In fact, astrocytes stimulated with IL-1 β actively encourage $A\beta_{1-42}$ production in neurons through the delivery of the protein CK1 in their extracellular vesicles (Li et al., 2020). This suggests a possible mechanism where reactive astrocytes are involved in the very early stages of AD where they can cause a positive feedback loop ($A\beta_{1-42}$ causes neuronal death and a reactive response in astrocytes, leading to release of inflammatory ADEVs and increasing $A\beta_{1-42}$ production in neurons). Inflammatory complement proteins have been identified within ADEVs in AD indicating a harmful inflammatory phenotype of the reactive astrocytes, resulting in more neuroinflammation (Goetzl et al., 2018; Winston et al., 2019). These changes in ADEV cargo when released from an inflammatory astrocyte implies a detrimental role for astrocytes and their EVs in AD. However, ablation of reactive astrocytes has been shown to exacerbate pathology demonstrating the complex role of reactive astrocytes in AD (Katsouri et al., 2020).

1.3.3.3 *Parkinson's disease*

Parkinson's disease (PD) is a progressive motor disorder caused by the death of dopaminergic neurons in the substantia nigra. This death can be associated with abnormal misfolding and aggregation of α -synuclein, found within Lewy-bodies in PD (Baba et al., 1998; Ingelsson, 2016). α -synuclein has been identified within EVs and has been shown to be readily taken-up by neurons resulting in neuronal death (Emmanouilidou et al., 2010; Danzer et al., 2012; Gustafsson et al., 2018; Guo et al., 2020; Stüendl et al., 2021). Dysfunctional autophagy is implicated in Parkinson's disease with many causal genes involved in the autophagy pathway (Michiorri et al., 2010; Schöndorf et al., 2014; Karabiyik et al., 2017; Pitcairn et al., 2019). With the connection between autophagy and EV secretion becoming clearer, it is no surprise

that inhibition of autophagy leads to the increased release of α -synuclein in EVs. This would explain how dysfunctional autophagy can lead to the spread of neurodegenerative disease (Poehler et al., 2014; Minakaki et al., 2018). By inhibiting EV release, it is possible to reduce α -synuclein pathology (Zhu et al., 2021).

Understanding and eliminating disease spread is particularly important in PD due to excitement around potential stem cell replacement therapies with the use of tissue transplantation currently in clinical trials for the disease. Foetal or iPSC neurons have been transplanted into PD patients in the hope of replacing the lost dopaminergic neurons; increasing patient survival and relieving symptoms (Barker et al., 2017; Sonntag et al., 2018). Studies have also begun to attempt conversion of astrocytes into neurons to replace neuronal death in PD (Wei and Shetty, 2021). However, disease pathology has been observed in the grafted neurons demonstrating host-graft disease transmission (Kordower et al., 2008; Li et al., 2008). A likely pathway for this is EV transmission from the diseased host cells.

Whilst PD may appear to only affect a select group of dopaminergic neurons, astrocytes have been implicated in the disease with many causal genes associated with PD affecting key astrocyte functions (Booth et al., 2017). PARK7, a PD causal gene encoding DJ-1, causes alterations in lipid-raft endocytosis, impaired glutamate uptake through altered EAAT2 expression, an altered neuroinflammatory response and reduced neuroprotective properties (Mullett et al., 2013; Ashley et al., 2016; Kim et al., 2016). Another common PD causal gene, LRRK2, has been shown to reduce α -synuclein clearance by astrocytes, leading to accumulation of the protein (Streubel-Gallasch et al., 2021). Similarly in other neurodegenerative diseases, reactive astrocytes are present in PD leading to neuroinflammation and directly causing neuronal death (Koprach et al., 2008; Gu et al., 2010; Yun et al., 2018). Whilst little research has taken place on ADEVs in PD, reactive ADEVs have been shown to enhance the vulnerability of dopaminergic neurons to toxins through miR-34a (Mao et al., 2015). However, ADEVs also appear to have neuroprotective properties but the protection varies depending on the brain region where the astrocytes were derived (Leggio et al., 2022). With limited understanding into the contribution of astrocytes in PD, it is clear more research needs to be conducted to find out about the role of reactive astrocytes and ADEVs in PD.

1.3.3.4 Amyotrophic lateral sclerosis

Amyotrophic lateral sclerosis (ALS) is also a progressive motor disorder which is caused by the death of motor neurons leading to paralysis and eventually death, often within 3 years of diagnosis. Many altered proteins have been identified in ALS and the specific pathology is reflected by the genetics of the patient (Blokhuis et al., 2013). For example, SOD1 mutations which account for 15-20% of familial ALS cases and 5% of sporadic ALS cases, demonstrate mutant SOD1 protein but not TDP-43 aggregation, which is characteristic in other forms of ALS (Rosen et al., 1993; Mackenzie et al., 2007; Tan et al., 2007). C9orf72 repeat expansion mutations are the most common genetic cause of ALS (20-25%) and cause the production of different dipeptide repeat proteins and as well as TDP-43 pathology (DeJesus-Hernandez et al., 2011; Renton et al., 2011).

Many ALS-associated proteins have been identified in EVs and are transferred between cells causing pathology in recipient cells (Grad et al., 2014; Ding et al., 2015; Silverman et al., 2016, 2019; Westergard et al., 2016; Sproviero et al., 2018). Autophagy dysfunction has been strongly implicated as a disease mechanism in ALS with common genetic mutations often occurring in autophagy-related proteins (Wong and Holzbaur, 2014; Goode et al., 2016; Sullivan et al., 2016; Oakes et al., 2017; Rudnick et al., 2017). With so many autophagy related genes effected in ALS and the abundance of protein pathology found within EVs, it is likely ALS is caused by a defect in this combined mechanism.

Whilst motor neurons are the most affected cell type in ALS, the importance of astrocytes in the disease is becoming clearer (Yamanaka et al., 2008; Yamanaka and Komine, 2018). ALS astrocytes are toxic to motor neurons and responsible for neuronal death and not simply due to a loss of support, but also by secreting toxic factors (Marchetto et al., 2008; Haidet-Phillips et al., 2011; Liddelw et al., 2017; Madill et al., 2017; Tripathi et al., 2017; Zhao et al., 2020; Guttenplan et al., 2021; Arredondo et al., 2022). Interestingly, this toxicity also has an effect on wild-type motor neurons demonstrating the direct toxicity of the ALS astrocyte (Nagai et al., 2007; Fritz et al., 2013; Rojas et al., 2014; Kia et al., 2018; Birger et al., 2019). In fact, the knock-out of reactive-inducing factors such as TNF α in astrocytes slows disease progression in ALS mouse models, highlighting reactive astrocytes as a potential target for new treatments (Guttenplan et al., 2020). Whilst many of these studies demonstrate the toxic effects of ALS astrocyte conditioned media, it is important to identify these toxic factors and whether they are found within ADEVs, or if they are secreted freely into the external environment. One study demonstrated that ADEVs caused toxicity, even when trophic factors are added suggesting the toxicity is found within EVs (Varcianna et al., 2019). This study then found miRNA changes in ALS ADEVs highlighting possible causes of the toxicity in motor neurons. Whilst the exact cause of the toxicity remains a focus in ALS research, ADEVs have also been implicated in the spread of disease by transmission of the protein aggregates (Basso et al., 2013; Silverman et al., 2019). With improved isolation and analysis techniques within the EV field, the role of ADEVs in ALS will become more apparent.

1.4 Aims of the PhD

The overall aim of this thesis is to establish a human serum-free astrocyte culture that maintains primary astrocytes in a quiescent state to study the morphology, function and protein cargoes of ADEVs. By thoroughly characterising healthy human astrocytes and their vesicles, we can establish a baseline that can be used to investigate changes in disease. To do this, a reproducible model of healthy, quiescent astrocytes needs to be developed that can be easily replicated by other groups. A complimentary reactive model also needs to be thoroughly characterised to better model general disease. Then their EVs can be characterised to identify changes between the quiescent and reactive astrocytes that can be further investigated as to their potential to be biomarkers for human disease. Finally, it is still unclear whether these vesicles are simply 'packages' or whether they have functional roles that have not been uncovered. This thesis aims to address these issues by fully characterising both quiescent, serum-free human primary astrocytes and those grown in serum to

produce a reactive model. Their extracellular vesicles will then be isolated and compared to identify any changes in the reactive phenotype. Then they will be used to assess any functionality that they may possess based upon the detailed characterisation.

1.4.1 To create physiologically relevant models of astrocytes

To date, there is no standard model of astrocytes and in particular, no real consensus on how to generate reactive astrocytes. Here human primary astrocytes (SC1800) will be utilised with different culture conditions to create reproducible, quiescent and reactive astrocytes. The use of serum in culture will be thoroughly investigated to determine whether this is a relevant model for reactive astrocytes. A multi-omic approach (RNA-SEQ and mass spectrometry) will be used to fully investigate any changes observed between the models to determine if this model can be used as a general model of disease.

1.4.2 To characterise ADEVs from serum-free (quiescent) and serum-cultured (reactive) astrocytes

EVs will be isolated from the models characterised above using ultrafiltration and size-exclusion chromatography. ADEVs will be characterised using nanoparticle tracking analysis (NTA), transmission electron microscopy (TEM) and mass spectrometry to create a detailed picture of EVs released from quiescent and reactive astrocytes. This data will be compared to extracellular vesicles derived from healthy and diseased human brain tissue to attribute any changes in reactive ADEVs to CNS pathology.

1.4.3 To investigate functionality of ADEVs

Once thoroughly characterised, ADEVs can then be investigated for any possible functionality. Any proteins that could highlight EV functionality will be further investigated using novel techniques that have not previously been used for EV work. The effect of adding ADEVs to cells will be measured to determine whether they have the ability to elicit a change in astrocyte phenotype and whether this could be a method of cell co-ordination in the immune response of the brain.

Chapter 2: Materials and methods

Chemicals were purchased from Merck Sigma-Aldrich, UK unless otherwise stated.

2.1 Cell culture

All cell culture work was completed under aseptic conditions in a cell culture hood, and cells were incubated at 37 °C in 5% CO₂ until needed.

2.1.1 Cell models

Human primary astrocytes (SC1800s) were purchased from ScienCell (cat# 1800; distributed by Caltag Medsystems, UK) and kept frozen in liquid nitrogen upon arrival. SC1800s were isolated by ScienCell from human cerebral cortex and cryopreserved before delivery.

Rat primary cortical astrocytes were used to compare with human astrocytes. After isolation from neonatal pups (postnatal 1-2 days; Serres et al, unpublished protocol), rat primary astrocytes were thawed from liquid nitrogen and cultured in the same way as the human SC1800 astrocytes.

Neuro2A (N2A) cells were purchased from ATCC (UK) and used to measure glycolysis due to their high production of EVs compared to the human primary astrocytes (see section 5.9.1.2).

2.1.2 Media compositions

A variety of media were trialled to determine the best astrocyte media to grow serum-free astrocytes (Table 2-1, see section 3.2.1 for results). After deciding on the best serum-free medium, astrocytes were either cultured in astrocyte medium for serum-cultured astrocytes, or G5 serum-free medium for serum-free astrocytes (for G5 composition, see Supplementary figure 1). N2A cells were grown in Dulbecco's Modified Eagle medium (DMEM) using 10% FBS. Due to the presence of EVs in FBS, FBS-free media was required for experiments involving EV collection and therefore, FBS-free astrocyte medium and FBS-free DMEM medium were used when required for serum-cultured astrocytes and N2A cells respectively. All FBS used within this work was purchased from ScienCell.

Table 2-1 - Media compositions used for cell culture. *Later experiments moved to Advanced DMEM due to supply issues. FBS = Foetal bovine serum, AGS = astrocyte growth serum, Pen/Strep = Penicillin and Streptomycin, HB-EGF = Heparin-binding EGF-like growth factor.

Media type	Components
Astrocyte medium	Astrocyte medium, 1% Pen/Strep, 1% AGS, 2% FBS
FBS-Free astrocyte medium (AGS AM)	Astrocyte medium, 1% Pen/Strep, 1% AGS
DMEM medium	DMEM with Glutamax, 1% Pen/Strep, 10% FBS
FBS-Free DMEM medium	DMEM with Glutamax, 1% Pen/Strep
G5 serum-free medium (DMEM G5)	DMEM/F12*, 1% Pen/Strep, 1% G5 supplement, 1% L-glutamine
<i>Neurobasal serum-free medium (NB-27)</i>	<i>(50% Neurobasal media, 50% DMEM/F12), 1% Pen/Step, 2% B27 supplement, 1% L-glutamine, 0.025% HB-EGF</i>
<i>B27 serum-free medium (DMEM B27)</i>	<i>DMEM/F12, 1% Pen/Strep, 2% B27 supplement, 1% L-glutamine, 0.025% HB-EGF</i>
<i>DMEM AGS medium</i>	<i>DMEM/F12, 1% Pen/Strep, 1% AGS, 1% L-glutamine</i>
<i>B27 + G5 serum-free medium (DMEM B27 G5)</i>	<i>DMEM/F12, 1% Pen/Strep, 1% G5 supplement, 2% B27 supplement, 1% L-glutamine</i>

2.1.3 Cell maintenance

2.1.3.1 Passaging cells

When cells grew above 70% confluency, media was removed, and the cells washed in Dulbecco's Phosphate buffered saline (PBS) without calcium chloride and magnesium chloride. Trypsin/EDTA was added to the cells and incubated at 37 °C for 5 min to detach cells. Trypsin/EDTA was quenched in media containing FBS. Cells were either counted and seeded for experiments (see section 2.1.4) or were split into an appropriate number of flasks for further culturing depending on proliferation rate of the cells. Astrocytes grown in serum-free media did not require subculturing due to a lack of proliferation without FBS.

To begin SC1800 culture from the original ScienCell vial, astrocytes were seeded onto 2x T75 flasks in astrocyte medium and left to proliferate until above 70% confluency. Cells were then passaged once at a ratio of 1:6 into 12x T75 flasks, and again cultured until above 70% confluency. Cells were then cryopreserved at a ratio of 1 T75 flask to 2 cryovials as described in section 2.1.5 for future use.

2.1.3.2 Cell maintenance

Serum-cultured cells were passaged regularly so media changes were not required for cell maintenance. However, due to a lack of proliferation, serum-free astrocytes were not passaged and instead maintained for a minimum of 7 days to allow processes to develop and to collect enough media for EV isolation. During this time, serum-free media was changed every 3 - 4 days to ensure healthy growth. For all experiments, serum-cultured astrocytes were maintained in FBS for a minimum of 5 days before use to ensure a chronic phenotype. Serum-free astrocytes were cultured for a minimum of 5 days before use to ensure the astrocytes had settled into culture and did not present with a reactive phenotype.

2.1.3.3 Coating

For early experiments, coating was completed to increase cell adhesion to cell culture surfaces as advised by ScienCell (USA). Poly-L-Lysine was used at 0.01% and left for a minimum of 1 h at 37 °C to coat plates before excess was washed away with PBS. Coating was found to be unnecessary during optimisation, so was not completed for experiments completed after serum-free optimisation (section 3.2). This also helped in reducing variation between plates.

2.1.4 Seeding densities

To ensure the same number of cells were seeded for each experiment, a 1:1 ratio of cell solution and trypan blue solution were mixed and added to a dual-chamber cell counting slide (Bio-Rad, UK). The number of cells was then calculated using a TC 20 automated cell counter (Bio-Rad, UK) to ensure consistency in plating.

Serum-free astrocytes were initially seeded into a 6-well plate from each frozen vial of serum-cultured astrocytes (frozen at passage 2) with a cell density of 100,000 – 150,000 cells/well. Due to a lack of proliferation, no further passaging was required. When serum-free astrocytes were needed for immunocytochemistry (section 2.2.1), cells were seeded directly onto 13 mm glass coverslips at a density of 10,000 cells/coverslip from the frozen vial.

2.1.5 Cryostorage of cells

All cells used in this work were cryopreserved in 900 µl FBS and 100 µl dimethyl sulphoxide (DMSO) using a Mr Frosty™ Freezing Container (Nalgene, UK) at -80 °C for no more than a week before cryopreservation in liquid nitrogen. Cells were carefully rethawed in warm water (~37 °C) and immediately placed into appropriate media. If cells were used for serum-based culture, the cells were plated immediately in the correct culture media. For cells used in serum-free experiments, the cells were centrifuged at 300 g for 5 min with 5 ml of DMEM to pellet the cells before removing the supernatant. The cells were then resuspended in the correct culture media and plated. To ensure residual FBS and DMSO were fully removed from the cells, a media change was completed after 24 hrs for all cell conditions.

2.1.6 Brightfield microscopy

Live cell imaging was performed using an inverted microscope (AXIO Vert A.1, Zeiss microscopy) with a 10x lens (Zeiss microscopy) to assess cell morphology. Morphology measurements were initially attempted using the simple neurite tracer (SNT) plug-in but due to issues with the contrast of brightfield microscopy was not suitable. Instead, area and perimeter of the cells were measured by manually tracing the cells in at least 5 images per replicate. Then an area/perimeter ratio was calculated to account for variations in process length.

2.1.7 Cytokines

An inflammatory cytokine cocktail containing TNF α , IL1 α and C1q was made based upon findings published in (Liddelow et al., 2017). Human cytokines TNF α and IL1 α were purchased from Peprotech (UK) and human C1q from Merck Sigma-Aldrich (UK). TNF α and IL1 α were reconstituted using 5% Trehalose to create stock solutions of 100 μ g/ml (IL1 α) and 500 μ g/ml (TNF α). C1q did not require reconstitution and arrived at a concentration of 1.1 mg/ml. TNF α was used at a final concentration of 30 ng/ml, IL1 α at 3 ng/ml and C1q at 400 ng/ml.

2.2 Immunofluorescence

2.2.1 Immunocytochemistry (ICC)

2.2.1.1 Staining

13 mm coverslips were autoclaved and stored in sterile conditions before use. Coverslips were added to a 24-well plate before cells were seeded at a low density of approximately 10,000-15,000 cells per coverslip (see 2.1.4). Cells were incubated for at least 24 hrs in standard cell culture conditions to allow cells to adhere. Cells were then washed in PBS before being fixed in 4% Paraformaldehyde (PFA) for 10 min. 3x 5 min PBS washes were used to remove remaining PFA before 0.1% Triton-x100 was added to permeabilise the cells for 10 min. This was followed by 3x 5 min washes with PBS. Non-specific binding was blocked using 1% bovine serum albumin (BSA) in PBS for 1 h at room temperature. Primary antibodies were diluted to the appropriate concentration in 1% BSA (see Table 2-2) and incubated with the cells overnight at 4 °C. The next day, cells were washed 3x for 5 min in PBS to remove any unbound antibody before the cells were incubated with secondary antibody diluted in 1% BSA (1:500 dilution) for 45 min at room temperature, protected from light. Cells were washed 3x for 5 min in PBS to remove unbound secondary antibody. The coverslips were mounted onto glass microscope slides with 4 μ l of VectorShield mounting media (Vector laboratories, UK) and left to dry before imaging. For most experiments, the mounting media contained 4',6-diamidino-2-phenylindole (DAPI). However, when DAPI was not required, a VectorShield mounting media which did not contain DAPI (Vector laboratories, UK) was used. The slides were stored at 4 °C until imaged.

2.2.1.2 Antibodies

Some experiments used phalloidin conjugated to Rhodamine to stain for F-actin filament, which was added at the secondary antibody stage. Anti-S100 β was already diluted to an unknown concentration when purchased so for S100 β staining, no dilution in 1% BSA was needed. Any antibody co-staining with S100 β was added to the S100 β solution directly.

Table 2-2 - Antibodies and their dilutions used for immunocytochemistry. Antibodies were diluted in 1% BSA with the exception of anti-S100 β which was purchased in a ready-to-use form. When co-staining with anti-S100 β , other antibodies were diluted in this solution.

Antibody	Dilution	Primary/Secondary	Species	Details
Anti-GFAP	1:500	Primary	Rabbit	Dako (ZO334)
Anti-GFAP	1:500	Primary	Mouse	Abcam (ab4648)
Anti-S100 β	N/A	Primary	Rabbit	Dako (GA504)
Anti-rabbit Alexa Fluor 488	1:500	Secondary	Goat	Invitrogen (A11008)
Anti-rabbit Alexa Fluor 568	1:500	Secondary	Goat	Invitrogen (A11011)
Anti-mouse Alexa Fluor 488	1:500	Secondary	Goat	Invitrogen (A11001)
Anti-mouse Alexa Fluor 568	1:500	Secondary	Donkey	Invitrogen (A10037)
Rhodamine Phalloidin (TRITC)	1:500	Both	N/A	Invitrogen (R415)

2.2.2 Immunohistochemistry

2.2.2.1 Slide preparation

6 μ m thick paraffin-embedded sections mounted on gelatin-coated glass slides were used to stain adult human brain tissue, whilst 10-20 μ m thick frozen sections were used to stain adult female rat brain tissue (tissue from 6-12 week old BD-IX rats). Both tissues were obtained from Dr Serres' lab.

2.2.2.2 Fluorescence staining

Paraffin-embedded slides were baked at 60 °C for at least 30 min to increase adherence to the gelatin-coated glass slides and prevent the tissue lifting. The sections were then rehydrated in xylene for 10 min followed by 3x 10 min washes of decreasing concentrations of ethanol (100%, 90% then 75%). Then the sections were washed in ddH₂O for 10 min followed by 5 min in PBS. Frozen tissue was left to thaw at room temperature for 20 min before a 5 min wash in PBS. No rehydration was needed.

For antigen retrieval, slides were submerged in citrate buffer (section 0) and heated in the microwave for 2x 5 min at 750 W. The slides were cooled for 20 min on ice before they were washed in PBS for 5 min. The slides were quenched using 0.3% hydrogen peroxide in PBS for 20 min. The slides were washed in PBS followed by PBS-tween (0.05%) and another PBS wash, each time for 5 min. The tissue was blocked in TNB blocking buffer (section 0) for 1 h at room temperature before the slides were washed for 5 min in PBS. Primary antibody was made up to the appropriate dilution in TNB buffer before incubating with the tissue overnight at 4 °C (Table 2-3).

The next day, the slides were warmed to room temperature for 30 min before 3x 5 min washes in PBS. The slides were incubated with appropriate secondary antibody

(made in TNB buffer, 1:200 dilution) for 1 h at room temperature, protected from light. The slides were washed twice in PBS before they were cover-slipped using 4 μ l of Vectorshield mounting media with DAPI (Vector Laboratories, UK).

Table 2-3 - Antibodies used in immunohistochemistry with the dilutions used. Antibodies were diluted in TNB buffer with the exception of anti-S100 β which was purchased in a ready-to-use form. When co-staining with anti-S100 β , other antibodies were diluted in this solution.

Antibody	Dilution	Primary/Secondary	Species	Details
Anti-GFAP	1:500	Primary	Rabbit	Dako (ZO334)
Anti-GFAP	1:500	Primary	Mouse	Abcam (ab4648)
Anti-S100 β	N/A	Primary	Rabbit	Dako (GA504)
Alexa Fluor 488 Anti-mouse	1:200	Secondary	Goat	Invitrogen (A11001)
Alexa Fluor 488 Anti-rabbit	1:200	Secondary	Goat	Invitrogen (A11008)
Alexa Fluor 568 Anti-rabbit	1:200	Secondary	Goat	Invitrogen (A11011)

2.2.2.3 Buffers

Citrate buffer: 2.94 g of trisodium citrate was dissolved in 1 L of ddH₂O and adjusted to pH 6.0. Tween20 was then added to reach a 0.05% concentration.

TNB Blocking reagent: 0.5% TSA blocking reagent (Perkin Elmer, FP1012) was added to TNB buffer (0.1 M Tris-HCl, 0.15 M NaCl, pH 7.5) and heated gradually to 55 °C until dissolved. The solution was then cooled to room temperature before use or stored at -20 °C for long term storage.

2.2.3 Imaging and analysis

Immunofluorescent images were acquired using an inverted confocal microscope equipped with a Camera AxioCam 305 monodigital (Axio Vert A1, Zeiss microscopy). Detection ranges were set to eliminate crosstalk between fluorophores: 385-425 nm for DAPI, 469-514 nm for Alexa Fluor 488 and 555-632 nm for Alexa Fluor 568.

All image analysis was completed using FIJI software (Image J). Images for each channel of the same section/cell were merged to produce a colour composite image, and a scale bar was added, if necessary, at this stage. To calculate protein expression (i.e for GFAP, S100 β and EAAT2), multiple measurements of the fluorescent signal outside of the cell (i.e., background signal) and within the cells were taken and averaged for each image. Cell measurements were normalised to background signal and for each condition, multiple images were used. The area of the nucleus was measured by manually drawing around the nucleus (detected using DAPI). For IHC slides, a confocal laser scanning microscope (LSM880, Zeiss microscopy) was used for Z-stack imaging of the brain tissue. The same process as above was applied to form composite images. Scale bars were added using FIJI software.

2.3 Gene expression measurements

2.3.1 RNA extraction

Cells were seeded at high density (100,000-200,000 cells per well of a 6-well plate or 500,000 cells per 10 cm diameter dish) and incubated in cell culture conditions. At the end of the experiment, media was removed and 1 ml of TRIzol® reagent was added per condition and left for 5 min before the cells were scraped with a sterile cell-scraper and put into an Eppendorf (for a 6-well plate, 2 wells were combined per condition). 200 µl of chloroform was added before centrifugation at 12,000 x g for 15 min at 4 °C. The top aqueous phase was carefully removed and added to 500 µl of isopropanol before incubation at room temperature for 10 min to precipitate RNA. The solution was then centrifuged at 12,000 x g for 15 min at 4 °C to pellet RNA. The supernatant was removed and 800 µl of 70% ethanol was added before centrifugation at 12,000 x g for 5 min at 4 °C. All ethanol was removed, and the pellet left to partially dry. Once colourless, the RNA pellet was dissolved in a minimum of 10 µl of RNase-free water (Invitrogen, UK). To identify the concentration and purity of the sample, the sample was analysed using the 2000c UV/IV Spectrophotometer (Nanodrop; ThermoFisher scientific, UK) before storage at -80 °C or used immediately to synthesise complementary DNA (cDNA).

2.3.2 cDNA synthesis by reverse transcription

Each RNA sample was diluted to 2 µg in 11.375 µl of RNase-free water, and 0.625 µl of random hexamers (Qiagen, UK) with 1 µl of 10 mM deoxynucleoside triphosphate mix (dNTP; Promega, UK) was added to each sample before heating at 65 °C for 5 min. The samples were then cooled. To each sample, 4 µl of 5x first strand buffer, 1 µl of 0.1 M dithiothreitol (DTT), 1 µl of RNaseOUT® recombinant RNase inhibitor and 1 µl of Superscript III reverse transcriptase, was added (all from ThermoFisher, UK). The samples were then heated to 25 °C for 5 min, 50 °C for 60 min followed by 70 °C for 15 min in a 96-well thermal cycler (Sensoquest, UK). The samples were diluted 1:10 in RNase-free water and aliquoted before being analysed on the Nanodrop 2000c. cDNA was stored at -20 °C until needed.

2.3.3 Real-time quantitative polymerase chain reaction (RT-qPCR)

All samples were plated in duplicate with the results averaged between two wells. For each gene of interest, a master mix was created based upon the number of samples (Table 2-4). 16 µl of master mix was added to 4 µl of sample cDNA per well in a MicroAmp® Fast 96-well reaction plate (Applied Biosystems, UK). The plate was then sealed using PCR sealing foil and centrifuged at 1500 x g for 1 min to remove bubbles.

Table 2-4 - qPCR master mix for one sample

Master mix component	Per sample
Forward primer (10 µM)	1 µl
Reverse primer (10 µM)	1 µl
RNase-free water	4 µl
SYBR Green qPCR master mix power up (Applied Biosystems™, UK)	10 µl

Most RT-qPCR experiments were run on a StepOne Real time PCR system (Applied Biosystems, UK) using the standard SYBR green power up protocol:

Stage 1: Initial increase to 95 °C (10 min)

Stage 2: 40 cycles of (95 °C for 15 s, 60 °C for 20 s, 72 °C for 35 s)

Stage 3: Melt curve creation

Later experiments (section 5.8.1) were measured on the QuantStudio5 (ThermoFisher scientific, UK) using the Fast SYBR green power up protocol:

Stage 1: Initial increase to 95 °C (2 min)

Stage 2: 40 cycles of (95 °C for 15 s, 60 °C for 20 s, 72 °C for 35 s)

Stage 3: Melt curve creation

2.3.3.1 Analysis

Results were either analysed using the StepOne software v2.3 (Applied biosystems) or QuantStudio design and analysis software (ThermoFisher, UK). Melting point curves were created to confirm the absence of primer dimers and ensure the results collected were due to the presence of target mRNA in the sample. Data was analysed by the $2^{-\Delta\Delta Ct}$ method (Livak and Schmittgen, 2001; see equation below). Ct values were normalised to suitable housekeeping genes and a fold change was calculated for each sample compared to the untreated or earliest timepoint.

$$2^{-\Delta\Delta Ct}, \text{ where } \Delta\Delta Ct = \Delta Ct (\text{target sample}) - \Delta Ct (\text{reference sample})$$

2.3.3.2 Design of primers

Genes of interest were chosen, and primers designed for these gene products before they were synthesised by Sigma-Aldrich (see Table 2-5). Where possible, primer sequences were used from original peer-reviewed papers. Other primer sequences were used from previous successful *in-house* RT-qPCR. If primer sequences were not available from either source, primers were designed using Primer-BLAST. The primers were designed to span exon-exon junctions to avoid amplifying genomic DNA and tested to check specificity. To initially test the functionality of the primers, serial dilutions of a single sample underwent RT-qPCR (see above). A 4-fold serial dilution was completed with a final dilution of 1:1024. Once plotted on a graph (Ct vs dilution), the R^2 value was calculated, and the primer was deemed successful if $R^2 > 0.9$ and slope > -3.3 .

Table 2-5 - Forward and reverse primer sequences used for RT-qPCR.

Gene of interest	Forward primer (5'→ 3')	Reverse primer (5'→ 3')
18s	CGCGGTTCTATTTTGTGGT	AGTCGGCATCGTTTATGGTC
B2M	AAGTGGGATCGAGACATGTAAG	GGAATTCATCCAATCCAATGCG
Caspase-1	TTTCCGCAAGGTTGATTTC	GGCATCTGCGCTCTACCATC
CD49F	CTCCTGTCCCGGCTCG	CCCACGAGCAACAGCC
EAAT2	CAGGGAAAGCAACTAATC	CAAGGTTCTTCTCAACA
GAPDH	AGCCACATCGCTCAGACAC	GCCCAATACGACCAATCC
GFAP	GTGGTGAAGACCGTGGAGAT	GTCCTGCCTCACATCACATC
GS	GGAGGATCCCCGCTGGTC	CAAATGTTGCTTCCCCCTTA
IL10	GACTTTAAGGGTTACCTGGGTTG	GACTTTAAGGGTTACCTGGGTTG
IL1β	AGCTACGAATCTCCGACCAC	CGTTATCCCATGTGTGGAAGAA
NDRG2	GAGATATGCTCTTAACCACCG	GCTGCCAATCCATCCAA
S100β	ATGTCTGAGCTGGAGAAGGC	TTCAAAGAACTGGAGAAGGC
SOCS3	ATCCTGGTGACATGCTCCTC	CAAATGTTGCTTCCCCCTTA
TNFα	GACAAGCCTGTAGCCCATGT	TCTCAGCTCCACGCCATT
Vimentin	TGTCAAATCGATGTGGATGTTTC	TTGTACCATTCTTCTGCCTCCTG
β-Actin	ATTGGCAATGAGCGTTC	GGATGCCACAGGACTCCA

2.3.4 RNA sequencing

2.3.4.1 Sample preparation

RNA was harvested as described in section 2.3.1. For improved accuracy of the purity and concentration of the RNA, samples were assigned RNA integrity numbers (RIN) using the Agilent technologies TapeStation as a stringent indicator of RNA quality (University of Nottingham, Deep-Seq). Samples were prepared to ensure >500 ng of RNA was sent to Novogene for mRNA analysis (Figure 2-1). During mRNA analysis, an RNA library is constructed before sequencing the samples. Then bioinformatic analysis can take place.

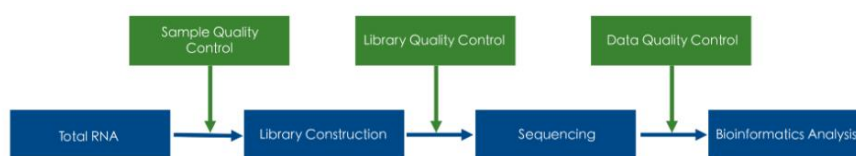


Figure 2-1 - mRNA sequencing pipeline completed by Novogene (Image created by Novogene).

2.3.4.2 Analysis

Once sequenced, the data was mapped to the reference genome (*Homo sapiens*) before gene expression quantification was completed to obtain FPKM values (Fragment Per Kilobase per Million mapped fragments; completed by Novogene). To complete a principal component analysis (PCA) which determines the similarity between samples, FPKM values were log transformed with a threshold of -15 applied before normalisation to the median, ensuring compatibility between groups. Then transformed zFPKM values were calculated from the normalised data using a threshold of zFPKM > -3 to select expressed genes only (Hart et al., 2013). The 16830 most expressed genes were used to run the PCA using SIMCA v.18 (Satorius stedim Data analysis, Sweden). zFPKM data was mean-centred before PCA analysis. Partial least squares discriminant analysis (PLS-DA) was also completed using the mean-

centred zFPKM values to reveal which genes were responsible for the differences observed between conditions.

Differential expression analysis was completed by calculating the log₂ (fold change) between the average of each condition (serum-cultured vs serum-free). Multiple t-test analysis was used to calculate a p-value for each gene and corrected using a two-stage step-up method to obtain false discovery rate values due to the high volume of genes identified in the samples (Benjamini et al., 2006). A false discovery rate <1% and a fold change >2 was used to identify differentially expressed genes. For pathway analysis, ClusterProfiler software was utilised for KEGG enrichment analysis.

2.4 Protein expression measurements

2.4.1 Cell lysis

Cells were harvested once above 70% confluency unless otherwise stated. Early LC-MS/MS experiments used urea buffer to lyse the cells (Table 2-6). Prior to cell harvesting, 10 µl of 0.1 M DTT, 1 µl protease inhibitor (P8340) and 1 µl phosphatase inhibitor cocktails (P0044) were added to 1 ml aliquots of urea lysis buffer (Table 2-6). Cell media was removed, and the cells washed in cold PBS before they were harvested in 60 µl urea lysis buffer using a cell scraper. The cell lysate solution was broken down by passing through a 25-gauge needle for a minimum of 10 passes before centrifuging for 10 min at 10,000 x g at 4 °C. The supernatant was collected for downstream processing.

Table 2-6 - Urea lysis buffer recipe. HCl = hydrochloric acid, SDS = sodium dodecyl sulphate.

Component of urea lysis buffer	Final concentration
Glycerol	10%
1 M Tris-HCl, pH 6.8	10 mM
10% SDS	0.1%
8 M urea solution	6.28 M

The majority of experiments used RIPA buffer (Table 2-7) to harvest cell lysates instead of Urea buffer. Cell media was removed, and the cells washed with cold PBS. The cells were then harvested in ice-cold PBS using a cell scraper and the solution centrifuged at 4000 rpm at 4 °C for 10 min to pellet the cells. The supernatant was removed, and the pellet resuspended in RIPA buffer with 0.1% protease and 0.1% phosphatase inhibitors. The cells in RIPA buffer were then sonicated for 20 s and then centrifuged at 13,000 rpm for 15 min at 4 °C. The supernatant was collected and used for downstream processing.

Table 2-7 - RIPA lysis buffer recipe. EDTA = Ethylenediamine tetra-acetic acid, SDS = sodium dodecyl sulphate

RIPA buffer component	Final concentration
5 M NaCl	150 mM
0.5 M EDTA (pH 8.0)	5 mM
1 M Tris (pH 8.0)	50 mM
NP40	1%
10% Sodium deoxycholate	0.5%
10% SDS	0.1%

2.4.2 Protein quantification

Protein quantification was completed using either a Bradford assay in earlier experiments (with Urea buffer) or a bicinchoninic acid (BCA) assay in later experiments (with RIPA buffer).

2.4.2.1 Bradford assay

Protein standards were made using BSA with 10% Urea buffer (Table 2-6) diluted in ddH₂O (1:2 serial dilution, 4000 - 15 µg/ml). 10% Urea buffer was used as a blank measurement. Samples were also diluted 10-fold in ddH₂O. 10 µl of each standard/sample were plated in triplicate in a clear 96 well plate and 250 µl Bradford reagent was added. The plate was incubated at room temperature for 10 min before protein absorbance was measured using a MultiSkan FC microplate spectrophotometer (ThermoFisher, UK) at 595 nm absorbance.

2.4.2.2 BCA assay

Protein standards were made up using BSA in 10% RIPA buffer (Table 2-7) diluted in ddH₂O (1:2 serial dilution, 2000 - 15 µg/ml) with 10% RIPA buffer used as a blank measurement. Samples were also diluted 10-fold in ddH₂O and 25 µl of sample/standard plated in triplicate in a clear 96-well plate. The Pierce® BCA protein assay (ThermoFisher, UK) mixture was created by adding 200 µl buffer A to 4 µl buffer B per well (e.g., for five wells, 1000 µl buffer A was mixed with 20 µl buffer B), before 200 µl of the BCA mixture was added to each well. The plate was incubated at 37 °C for 30 min before protein absorbance was read on the SPECTROstar Nano microplate spectrophotometer (BMG Labtech, UK) at 562 nm.

2.4.2.3 Analysis

The average absorbance of each standard was plotted on a graph to create a standard curve (Figure 2-2). Protein concentration in unknown samples (µg/ml) were calculated using a simple linear regression equation. The final concentration was multiplied by the dilution factor (1:10). The corresponding amount of protein was then calculated to load 20 µg of protein for immunoblotting and 5 µg for mass spectrometry, respectively.

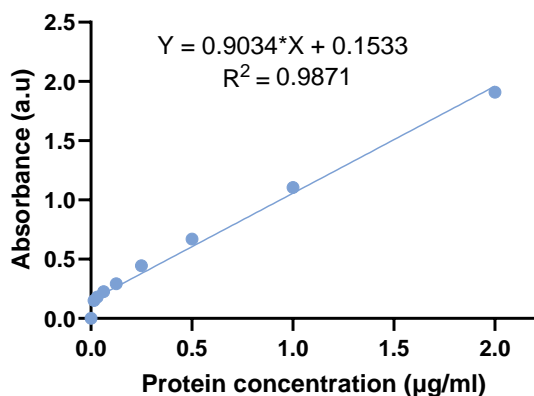


Figure 2-2 - Example standard curve created using BCA standards to calculate unknown protein concentrations of samples. Known protein standards were plotted alongside absorbance. Unknown sample concentrations were calculated using the simple linear regression equation calculated from the standards. The R-squared value demonstrates how well the equation fits to the known standards.

2.4.3 Immunoblotting

2.4.3.1 Cytokine array

Cytokines were measured using the Proteome profiler Human XL cytokine array kit (ARY022B; RnD systems, UK) according to the manufacturer's instructions. The nitrocellulose membranes containing 105 different capture antibodies were blocked in array buffer 6 for 1 h at room temperature. 1.5 ml of astrocyte conditioned media (both serum-free and serum-cultured) were incubated with the membranes overnight at 4 °C. The membranes were then washed 3x in 1x wash buffer for 10 min each. Detection antibody cocktail was incubated with the membranes for 1 h at room temperature. The membranes were then washed again 3x in 1x wash buffer for 10 min each. Streptavidin-HRP was then incubated with the membrane for 30 min at room temperature. The membrane was washed 3x in 1x wash buffer for 10 min each. Enhanced chemiluminescence (ECL) reagents (Perkin Elmer, UK) were added to the membrane for 1 min before being exposed to Amersham Hyperfilm® ECL (Scientific laboratory supplies, UK). Different exposure times were completed to avoid overexposure (ranging from 30 s – 10 min).

The mean intensity of each dot was measured using FIJI software and an average calculated for each cytokine. The dots were then traced back to the original map of cytokines to identify the cytokine of interest. Due to most cytokines only being present in one of the samples, statistics were not completed.

2.4.3.2 SDS-PAGE

After the protein concentrations were calculated (section 2.4.2), the appropriate amount of gel application buffer (GAB; 0.15 M Tris, 8 M Urea, 2.5% SDS (w/v), 20% Glycerol (v/v), 10% 2-mercaptoethanol (v/v), 3% DTT (w/v) and 0.1% Bromophenol blue (w/v)) was added to 20 µg of cell lysate to achieve a 1:2 ratio for sample to GAB. For purified EV samples, protein concentration was not detectable with protein assays, so samples were concentrated using ultrafiltration (see section 2.5.4.1) and 45 µl of concentrate was mixed with 15 µl GAB. Samples were then heated to 95 °C for 5 min to lyse the EVs and denature proteins.

5-20% gradient acrylamide SDS-PAGE gels were used for all SDS-PAGE gels (see Table 2-8). Equal amounts of the 5% and 20% solution were combined in a gradient mixer and poured into a glass cassette (1 mm thickness). The gel was left to set before stacking solution was poured on top and a 14-well comb added to create wells for the samples. Alongside the protein samples, 3 µl of BLUeye prestained protein ladder (MERCK, Sigma Aldrich, UK) was also added as a protein molecular weight marker. The gels were run in 1x Electrode buffer (25 mM Tris, 187 mM Glycine, 0.1% SDS (w/v)) at 45 mA per gel and 500 V until the samples had migrated to the bottom of the gel.

Table 2-8 - Gradient gel composition for SDS-PAGE. Gradient gels were made using a 5% and a 20% acrylamide solution to ensure better separation of proteins. Stacking solution was added to the top of the gels to create the wells needed to load each sample and ensure proteins entered the resolving gel at the same time. APS = Ammonium persulfate, TEMED = Tetramethylethylenediamine, Buffer A (1.1 M Tris, 0.1% (w/v) SDS, 30% (w/v) glycerol, pH 8.8), Buffer B (1.1 M Tris, 0.1% (w/v) SDS, pH 8.8), Stacking buffer (0.14 M Tris, 0.1% (w/v) SDS, pH 6.8).

Components	5%	20%	Stacking solution
Buffer A	-	3.33 ml	-
Buffer B	3.33 ml	-	-
Stacking buffer	-	-	5 ml
ddH ₂ O	5 ml	-	-
30% Acrylamide-bisacrylamide	1.67 ml	6.67 ml	1 ml
10% SDS	100 µl	100 µl	-
10% APS	100 µl	100 µl	100 µl
TEMED	10 µl	10 µl	10 µl

2.4.3.3 Western blotting

Once SDS-PAGE was complete, the gel was sandwiched between filter paper and a nitrocellulose membrane (Amersham™ Protran® western blotting membrane, 0.45 µm pore). Then the gel was placed into a transfer tank containing 1x Transfer buffer (25 mM Tris, 192 mM glycine and 20% (v/v) methanol) and transferred overnight at 40 mA and 500 V. The next day, the membrane was washed 3x in Tris-buffered saline (TBS; 20 mM Tris, 150 mM NaCl, pH 7.5) with 0.05% Tween (TBS-T) before blocking in 5% milk-TBS-T (5% Marvel milk powder in TBS-T) for 1 h at room temperature. The membrane was then incubated with primary antibody diluted in 5% milk-TBS-T overnight at 4°C (Table 2-9). The membrane was washed a further 3x in TBS-T before incubation with secondary antibody diluted in 5% milk-TBS-T for 1 hr.

Table 2-9 - Antibodies used in immunoblotting. All antibodies were made up in 5% milk-TBS-T. Primary antibodies are represented by a 1, and secondary antibodies by a 2.

Antibody	Dilution	MW	1° or 2°	Species	Details
Anti-FLOT-1	1:1000	49kDa	1	Mouse	BDSciences (AB_398139)
Anti-ALIX	1:1000	80, 100kDa	1	Rabbit	Abcam (ab186429)
Anti-GFAP	1:10000	50kDa	1	Mouse	Abcam (ab4648)
Anti-Calnexin	1:1000	90kDa	1	Goat	SICGEN (AB3747-200)
Anti-EAAT2	1:500	62kDa	1	Mouse	Santa Cruz biotechnologies (365634)
Anti-mouse HRP	1:3000	-	2	Rabbit	Dako (PO260)
Anti-rabbit HRP	1:3000	-	2	Swine	Dako (PO399)
Anti-Goat HRP	1:5000	-	2	Rabbit	Sigma (A5420)

2.4.3.4 Enhanced chemiluminescence (ECL)

The nitrocellulose membrane described above (section 2.4.3.3) was washed 3x in TBS-T before incubation in ECL solution for 30 s and then was protected from light. Amersham Hyperfilm® ECL film was placed on the membrane and exposed for an

appropriate time to capture protein signal from the ECL. In most experiments, a range of exposure times were completed to ensure the best image. The film was then placed into Ilford PQ universal (Ilford photos, UK) until the signal was observed before washing with water and fixing in Ilford Hypam fixer (Ilford photos, UK).

2.4.4 Mass spectrometry

2.4.4.1 LC-MS/MS

Protein samples were run into an SDS-PAGE gel so they could migrate through the stacking gel and reach approximately 1 cm into the resolving gel (section 2.4.3.2). The gel was then stopped and stained with Coomassie dye (50% methanol (v/v), 20% glacial acetic acid (v/v), 1.12% Coomassie Brilliant Blue (w/v)) for 1.5 h to visualise the proteins before incubation with destain solution (10% methanol (v/v), 10% glacial acetic acid (v/v)) overnight to remove excess staining. Once the gel was de-stained, a scalpel blade was used to cut around the protein band. These gel samples were then sent to the Cambridge Proteomics Centre for a 1 h LC-MS/MS mass spectrometry run. For cell lysate samples, 20 µg of protein were sent for analysis. EV fraction 2 was sent for analysis as this fraction showed the highest protein content through western blotting. Due to the low amount of protein present in EV samples, the protein concentration was not possible to identify through standard BCA/Bradford assays.

2.4.4.2 Sequential Window Acquisition of all Theoretical Mass Spectra (SWATH)

5 µg of cell lysate samples were stored in RIPA lysis buffer after BCA protein quantification (section 2.4.2.2). For purified EV samples, the content of all EV-enriched fractions were pooled and concentrated (section 2.5.4.1). Samples were delivered to Dr. Clare Coveney at Nottingham Trent University for LC-MS/MS followed by SWATH analysis.

To digest the proteins for mass spectrometry, samples underwent S-trap™ Micro spin column digestion. Due to the EV samples having a starting volume higher than the required volume (25 µl) for S-trap™ digestion, EV samples were dried at 60 °C in a vacuum concentrator (Eppendorf™ concentrator plus). All samples were then made up to a final volume of 25 µl in 5% SDS lysis buffer (SDS/100 mM triethylammonium bicarbonate (TEAB) pH 7.55). Samples were then reduced using 1 µl of DTT and incubated for 20 min at 56 °C in a shaking thermomixer. Samples were then cooled before 2 µl of 0.5 M iodoacetamide was added to alkylate cysteines. The samples were then incubated for 15 min at room temperature, protected from light. 12% phosphoric acid was added at a 1:10 ratio for a final concentration of 1.2% phosphoric acid to alter the pH for protein trapping.

185 µl of S-Trap buffer (90% aqueous methanol and 100 mM TEAB, adjusted to pH 7.1) was added to the acidified samples and mixed before the solution was transferred to a 1.7 ml tube containing an S-Trap micro column. The column was then centrifuged at 4000 x g until all solution had passed through the column. Protein was trapped within the protein-trapping matrix of the S-Trap spin column. Captured protein was washed by adding 150 µl S-Trap buffer and the centrifuge repeated. Three washes were completed on the samples before the column was transferred to a clean 1.7 ml Eppendorf™ protein lo-bind sample tube for digestion.

Digestion buffer was prepared by adding 50 mM TEAB at pH 7.5-8.0 to 20 µg of trypsin/EDTA. 25 µl of digestion buffer containing protease (trypsin/EDTA) at a 1:10 ratio was added to the top of the micro column to digest the trapped protein for 1.5 h at 47 °C. The resulting peptides were eluted by centrifugation at 4000 x g with 40 µl of 50 mM TEAB and then 0.2% aqueous formic acid. Hydrophobic peptides were recovered by centrifuging with 35 µl of 50% acetonitrile containing 0.2% formic acid. The peptide elutions were pooled before drying at 60 °C in a vacuum concentrator. The dried samples were then resuspended in 5% acetonitrile acid with 0.2% formic acid. For EV and 5 µg cell lysates, samples were resuspended in 30 µl of solution before 2 µl was injected into the SCIEX TripleTOF® 6600 mass spectrometer for SWATH analysis.

2.4.4.3 Proteomic analysis

For LC-MS/MS analysis, samples were compared using the presence/absence of proteins in the samples. Proteins required a minimum of 2 peptides with a peptide threshold of over 95% to be identified with a protein threshold of over 99%. Proteins were identified using the Uniprot database and the proteins analysed using Scaffold 4 (proteome software) and Microsoft Excel. As a more stringent analysis, proteins had to be present in at least two of the three samples to be confirmed as present during the specific mass spectrometry run, with protein showing *Bos Taurus* origin omitted due to contamination from FBS. This was to reduce type 1 errors.

For SWATH datasets, data was normalised by overlaying overall traces as well as the initial normalisation of using 5µg. The relative abundance of protein across samples was calculated, providing a quantitative approach to measure protein expression. To process the data, peptide hits which were attributed to more than one protein (E.g. 'PMM1;PMM2' may share identical peptides) were removed because it was unclear which protein the values are attributed to.

To generate a PCA to determine the similarity between samples, protein values were log transformed with a threshold of -15 applied before normalisation to the median, ensuring compatibility between groups. The PCA was completed using SIMCA v.18 (Satorius stedim Data analysis, Sweden). Protein values were mean-centred before PCAs were completed. PLS-DA was not required for any proteomic analysis due to a lack of separation seen in the PCAs.

The biological repeats for two conditions after initial processing (e.g., Serum ADEVs vs serum-free ADEVs) were entered into an excel file and uploaded to StatsPro software (<https://www.omicsolution.com/wukong/StatsPro/>). Different values were trialled for the missing values as well as the coefficient of variance to best identify significant values (see sections 4.4.4 and 5.5.3). A linear model for microarray data (Limma) test was completed to calculate the p-values for any differentially expressed proteins between samples (Ritchie et al., 2015). A Benjamini-Hochberg procedure was applied to calculate the adjusted p-values due to the number of proteins analysed, in order to reduce type 1 errors. The P-value was set at 0.05 with a log2FC of > ±0.3 for significant differentially expressed proteins (all completed in StatsPro software).

STRING analysis was completed on specific protein groups during both qualitative and quantitative analysis to identify a list of enriched KEGG pathways as well as any GO pathways and localisation.

2.5 Extracellular vesicle isolation

2.5.1 Isolation from tissue

Frozen human frontal lobe samples were obtained from both approved Bristol Brain bank (AD tissue; SWDBB 0029) and Oxford Brain bank (ALS tissue; OBB634). Control tissue was age and sex-matched to each disease tissue cohort (see Supplementary table 3-6 for sample details).

Brain tissue was finely sliced using a sterile scalpel blade and added to 75 U/ml collagenase-3 (Worthington biochemical corporation, supplied through Lorne laboratories, UK) in HibernateTM-E buffer (Gibco, UK) at a ratio of 800 µl per 100 mg tissue (Figure 2-3A). The solution was incubated at 37 °C for 15 min (mouse tissue) or 20 min (human tissue). Samples were then immediately incubated on ice, and PhosStopTM and cOmpleteTM protease inhibitor (Roche, UK) was added for a 1x concentration. The samples were then centrifuged at 300 x g for 10 min at 4 °C to pellet the tissue. The supernatant was collected and further centrifuged at 2000 x g for 15 min at 4 °C. The supernatant was slowly filtered through a 0.22 µm filter and centrifuged for a final time at 10,000 x g for 30 min at 4 °C. The supernatant was concentrated using 3k MWCO concentrators (ThermoFisher Scientific, UK) to 500 µl for size exclusion chromatography (SEC; see section 2.5.4).

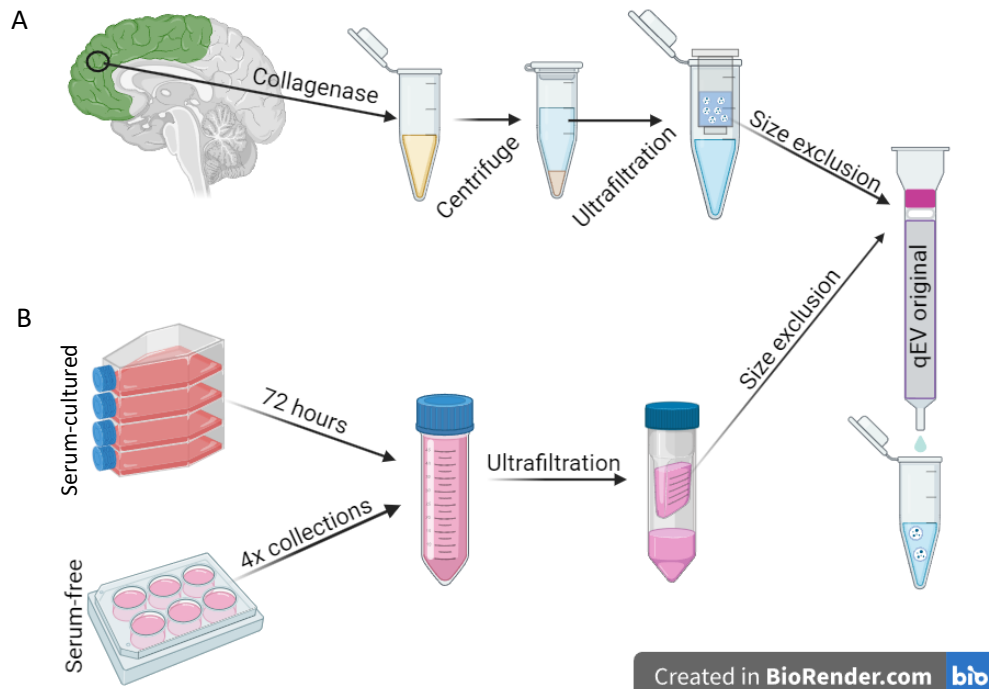


Figure 2-3 - Graphical representation of extracellular vesicle isolation from (A) tissue and (B) cell culture. Extracellular vesicles were isolated using ultrafiltration followed by size exclusion chromatography (SEC) using qEV original columns (Izon, France). Image was created by the user through BioRender.com.

2.5.2 Media collection for EV isolation

2.5.2.1 Serum-cultured cells

Cells were initially cultured in FBS-containing media for 24 h and then washed in PBS. Cells were then cultured in FBS-free astrocyte media for a further 72 h (SC1800 astrocytes) or FBS-free DMEM media for 24 h (N2A cells). At this time point, the conditioned media was collected and centrifuged at 300 x g for 5 min to remove cell debris. The media was stored at 4 °C if used within 5 days or frozen at -80 °C for future use. For SC1800 cells, four T75 flasks were required to collect enough media for a successful EV isolation (Figure 2-3B). For N2A cells, only one T75 flask was required.

2.5.2.2 Serum-free cells

For serum-free cultures, conditioned media was collected when the media was refreshed as part of cell maintenance (every 3 - 4 days) and centrifuged at 300 x g for 5 min to remove cell debris. The media was then stored at -80 °C until enough media was collected for isolation (>40 ml). Generally, each 6-well plate of serum-free cells were cultured for two weeks so 4x media collections could take place to ensure collection of over 40 ml (Figure 2-3B).

2.5.3 Ultrafiltration

To concentrate the >40 ml conditioned media for use in SEC (section 2.5.4), the media was centrifuged in a 10 kDa MWCO protein concentrator (ThermoFisher Scientific) at 3600 x g until 500 µl of concentrated media remained (Figure 2-3). Media flow-through was also collected for immunoblotting of ADEVs.

2.5.4 Size exclusion chromatography

SEC was completed using qEVOoriginal 70 nm columns (IZON, France) in the automated fraction collector (IZON, France; Figure 2-3). The column was initially washed with 17 ml of PBS (>2 column volumes) before addition of the 500 μ l concentrated media. Fractions were then collected according to the manufacturer's guidance (Table 2-10). The column was then washed with 0.5 M sodium hydroxide (NaOH) and PBS between samples. Each column was used for a maximum of five samples. Fractions were stored at 4 °C for up to a week or were frozen at -80 °C for future use.

*Table 2-10 – Description of fractions collected using qEVOoriginal 70 nm columns. *Later gen 2 columns recommended 2.9 ml void across 3 fractions and to collect 400 μ l per fraction due to the improved resin.*

Fraction number	Quantity per fraction	Total volume	Classification
1-3	1 ml*	3 ml*	Void (PBS)
4-6	500 μ l*	1.5 ml*	EV-enriched
7-9	1 ml	3 ml*	Protein

2.5.4.1 Further ultrafiltration

The concentration of EVs after SEC was often too low for downstream processes such as immunoblotting or mass spectrometry, so EV fractions were concentrated 10-fold using Vivaspin500, 3 kDa MWCO concentrators (Merck, UK).

2.6 Extracellular vesicle characterisation

2.6.1 Transmission electron microscopy (TEM)

2.6.1.1 Fixation and creation of grids

EV-enriched fractions were fixed in 3% glutaraldehyde in 0.1 M Cacodylate buffer for 30 min in a 1:1 ratio. The fixed EV solution was then added onto copper carbon-coated, 200-mesh electron microscopy grids (EM resolutions, UK) for 30 min to allow the EVs to settle. Samples were washed twice in MilliQ water before staining with 2% Uranyl acetate for a further 30 min. The grids were then left to dry before imaging using Tecnai biotwin T12 electron microscope.

2.6.2 Zetaview® (Nanoparticle tracking analysis)

Before each use, the Zetaview® (Analytik, UK) was calibrated using polystyrene beads of known size and concentration. Samples were then diluted appropriately based on predicted EV concentration (for SC1800 samples, 1:50 - 1:100, for N2A, 1:500 - 1:1000 and for tissue, 1:1000 - 1:2000). The samples were injected into the Zetaview® where the software was programmed to image 11 positions using the 488 nm laser set to scatter. Two cycles were completed for each measurement to improve accuracy of measurements, and two technical replicates were completed per sample.

2.6.2.1 Analysis

The size of the particles was analysed during measurements as well as the concentration of particles in the sample. To combine the size distribution of each repeat, raw values for each technical repeat were averaged within each sample. To calculate the size distribution for the whole sample, values were added together from each of the three EV-enriched fractions to produce a cumulative size distribution.

2.6.3 Direct stochastic optical reconstruction microscopy (dSTORM)

2.6.3.1 Sample processing

Vybrant™ DiD cell-labelling solution (ThermoFisher scientific, UK) was required for d-STORM imaging to stain phospholipids in the EV membrane, with wash steps required to remove any unbound dye. For this reason, 1 mM dye was added to the 500 µl concentrate obtained after ultrafiltration (section 2.5.3) during EV isolation to create a final 5 µM solution. The concentrate was incubated for 15 min at 37 °C to allow the dye to bind to the EV membrane. The concentrate was then used for SEC as normal (section 2.5.4). Once the EVs were isolated, 15 µl were added inside a Secure-Seal™ 13 mm spacer (0.12 mm depth; ThermoFisher Scientific, UK) attached to a glass microscope slide. A coverslip was then placed on top to seal the chamber and the sample imaged immediately.

2.6.3.2 Measurements

Imaging was completed on the Zeiss ElyraPS1 super resolution microscope using an α -Plan Apo 100 \times /1.46 oil immersion objective in TIRF (Total internal reflection microscopy) mode. Zeiss™ Immersol™ 518F immersion oil (Zeiss Microscopy) was used to allow imaging at high magnification. LP655 filter and TIRF were used to visualise the EVs with automatic focusing maintaining the desired focus throughout the experiment. Both the 405 nm and 642 nm lasers were used to illuminate the Vybrant™ DiD dye bound to the EVs. 405 nm power remained at 1% throughout the experiment. A widefield image was taken using 16 averaging at 0.5% 642 laser power in TIRF mode to produce an overview of the field before STORM imaging began. For the dSTORM experiment, laser power was then increased to 25%, recording 5000 frames with 25 ms exposure and 200 gain.

Initial image processing was completed using the photoactivated localisation microscopy (PALM) module of the Zeiss Zen Black software, as described previously (Nizamudeen et al., 2018). Briefly, the images were set to account for overlap of particles followed by application of model-based drift correction to account for particle movement during the experiment. Outliers were set as <5 hits within 300 nm radius and then removed to exclude background artifacts (particles should have more than 5 hits within a very small radius). The experiment was then converted to an image to allow analysis in FIJI software (5000 frames converted into one image).

2.6.3.3 Analysis

A previously developed ImageJ macro was adjusted to analyse the vesicles in the dSTORM files after processing in Zen black software (Supplementary figure 1; Nizamudeen et al., 2018). Within the macro, a gaussian blur filter was set to 3 in order to smooth the edges of the vesicle, the scale was set to 5 nm per pixel, and the threshold set to Li white (default method) to distinguish vesicles from the background. The macro then analysed the particles to generate the size (width and height) and general shape of the vesicles (e.g. area, circularity, perimeter). The results were then exported to a text file which could be processed further in Microsoft Excel.

From the results produced by the ImageJ macro, median size and the size distribution can be generated from each image. Particles with a circularity of less than 0.5 are unlikely to be EVs so were removed from the analysis. The concentration of the particles was calculated by dividing the area of the spacer by the area of the image to produce the multiplication factor for the spacer. This multiplication factor was then multiplied by the number of particles found in the images to calculate the number of EVs in the 15 μ l. This value was then used to estimate the number of particles per ml. Fraction EV2 was used in dSTORM analysis as this fraction was expected to have the highest EV concentration.

2.7 Functional studies

2.7.1 Metabolic assays

2.7.1.1 ATP assay

The luminescent ATP detection kit (ab113849; Abcam, UK) was used to measure ATP concentrations in cell lysates and extracellular vesicles. The assay was completed according to the manufacturer's instructions with the exception that 100 μ l EV or cell lysate samples were added to wells during the assay instead of cultured cells. ATP standards were made in PBS to produce a standard concentration gradient between 0.01 nM and 10 μ M. PBS was used as a blank. 50 μ l of detergent was added to 100 μ l of sample in each well and the plate shaken on an orbital shaker at 700 rpm for 5 min to lyse the samples. 50 μ l of substrate solution was then added and the plate shaken for a further 5 min. The plate was then protected from light for 10 min before reading on a GloMax[®] Navigator microplate luminometer (Promega, UK).

Analysis was completed using the same methodology as section 2.4.2.3 with a standard curve generated from the ATP standards (see Figure 2-2 for an example). This was then used to calculate the concentration of ATP based upon the luminescence values. All values were normalised to a PBS blank control. For ADEVs, all EV fractions were combined and concentrated to 400 μ l (amount required for assay). For N2A EVs, EV fractions were combined but not diluted due to the higher concentration of EVs within the samples. Cell lysate samples were used at a concentration of 50 μ g/ml.

2.7.1.2 Measuring glycolytic energy production

Glycolytic substrates were reconstituted using ddH₂O to create stock solutions of 50 mM glucose, 50 mM 2-Deoxy-D-glucose (2-DG), 10 mM ATP, 10 mM ADP and 20 mM NAD⁺. Substrates were then diluted appropriately to achieve a final concentration of 500 μM glucose or 2-DG, 10 μM ATP and ADP and 2 mM NAD⁺. NAD⁺ was added to all samples, and PBS used for inorganic phosphate presence in samples. Substrates were added to EV samples on ice to prevent enzymatic reaction whilst preparing the samples. The samples were then plated and measured using the luminescent ATP detection kit (Abcam; section 2.7.1.1).

2.8 EVs for treatment

After Zetaview[®] analysis (section 2.6.2), ADEV fractions isolated from serum-cultured astrocytes were combined before treating serum-free astrocytes for 72 h (for concentrations used, see Table 5-11). Brightfield imaging was completed throughout at 90 min and 3, 6, 24, 48 and 72 h. The treated astrocytes were harvested for RNA extraction after 72 h and gene expression quantified using RT-qPCR (section 2.3).

2.9 Statistical analysis

All statistical analysis was completed using GraphPad prism 10 software unless otherwise stated. A normality test was used to determine whether data was drawn from a normally distributed population. Data were then analysed using student t-tests when two variables were compared, or ANOVAs when three or more variables were compared. When analysing large datasets such as the RNA sequencing or proteomic data, adjusted p-values were calculated using an appropriate test (described in analysis) to reduce type 1 errors. ROUT outlier analysis was used to identify potential outliers. Statistical significance was set as $P < 0.05$ (identified as * on graphs). Asterisks show the level of significance identified by the statistical tests with $P < 0.01$ (**), $P < 0.001$ (***) and $P < 0.0001$ (****). Power calculations were determined using GPower 3.1 software. Mean values and standard deviations from a minimum of 3 repeats were used to calculate the number of repeats needed for statistical significance.

Chapter 3: Developing an accessible serum-free culture of human primary astrocytes

3.1 Introduction

3.1.1 Importance of *in vitro* models of human astrocytes

The importance of physiologically relevant mammalian cell culture approaches, including for cells of the nervous systems such as astrocytes, cannot be overstated, with such cellular models underpinning basic research into disease mechanisms as well as drug discovery programmes. Cell models permit pharmacological and genetic manipulation of candidate biochemical pathways more easily than *in vivo* animal models and allow drug screening and disease biomarker identification.

Notably, up to 50% of potential new drug therapies fail due to a lack of efficacy when moving into Phase 1 clinical trials, despite positive results in preclinical testing using animal models (Sun et al., 2022). Improving *in vitro* cellular models at the start of translational pipelines is one potential route to better clinical outcomes.

3.1.2 Limitations of commonly used astrocyte culture models

Currently *in vitro* astrocyte culture models often rely on primary cells extracted from rodents, in part due to the accessibility of genetically modified animals used to model human disease. However, rodent astrocytes are less complex than human astrocytes (see section 1.1.3.1) and therefore these cells are likely missing relevant human/primate features (Oberheim et al., 2006, 2009). Although *postmortem* human tissue may be available as a source of primary astrocytes in some instances, accessibility is limited and certainly for adult tissue, lack of proliferative ability makes cell expansion a challenge.

Cancer and transformed cells have been used *in vitro* as a model of astrocytes (e.g. C6 and SVGA cells to mimic rat and human astrocytes, respectively) but these cells often lack key characteristics of astrocytes (e.g. GFAP expression) and do not behave like healthy astrocytes (e.g. showing reduced cellular communication and glutamate uptake; Galland et al., 2019). iPSC reprogramming has allowed the differentiation of human skin cells into cells of the CNS including astrocytes, leading to more relevant human models, but this approach is expensive and time-consuming (section 1.1.3.2). There can also be significant variations between different iPSC-derived cell lines, resulting in studies requiring multiple lines and appropriate controls to ensure reproducible phenotypes are observed.

As an alternative, primary human astrocytes from foetal tissue can be obtained, which are more physiologically relevant than age-matched rodent cells, and do not require the time or expense of human iPSC cultures. Such cells are commercially available, and although they represent foetal astrocytes and therefore aging-related

changes cannot be easily modelled, present as an accessible alternative to primary rodent astrocytes or human iPSC-derived astrocytes that allow fundamental processes to be interrogated. Further, as they can be induced from quiescent to reactive phenotypes *in vitro* using a variety of stimuli, they can be used to study pathological processes regardless of genetic influence. Human primary astrocytes are the main *in vitro* cellular culture system used in this thesis to investigate healthy human astrocytes, astrocyte reactivity, and ultimately astrocyte-derived extracellular vesicles (ADEVs).

3.1.3 The impact of serum on astrocyte culture

Mammalian cells are routinely cultured in the presence of serum (e.g. FBS) to stimulate proliferation and support growth. In the case of human iPSC-derived astrocytes, serum is commonly added to culture medium to promote differentiation of the iPSCs (TCW et al., 2017; Soubannier et al., 2020; Leng et al., 2022; Stoklund Dittlau et al., 2023). However, the use of serum for long-term culture of astrocytes presents caveats, given that it can have pronounced impact on cellular phenotype and pathology. Astrocytes help to form the blood-brain barrier (BBB) which prevents serum proteins from entering the brain. Astrocytes filter important molecules from the blood, such as glucose, and help maintain the appropriate environment for brain function. When the BBB is damaged due to disease or injury, serum proteins may enter the brain environment and disrupt normal functions, promoting a reactive astrocyte phenotype (Michinaga and Koyama, 2019; Heithoff et al., 2021; Kim et al., 2022). In fact, histological markers of serum proteins, iron, and erythrocyte extravasation, have been used to detect increased permeability of the BBB in the *postmortem* tissue of Alzheimer's (AD) and Parkinson's disease (PD) patients (Gray and Woulfe, 2015). Therefore, the inclusion of serum as a component of *in vitro* astrocyte culture medium may be effectively mimicking a diseased or injured brain environment, rather than quiescent astrocyte biology.

In response to serum exposure *in vivo*, quiescent astrocytes will react by assuming a reactive phenotype (see section 1.1.2) to minimise damage to the rest of the brain. It is reasonable to assume that the use of serum in astrocyte culture *in vitro* will recapitulate astrocyte reactivity in the brain, seen in response to trauma or disease when the BBB is leaking. Previous studies using cultured primary rodent astrocytes have begun to investigate the effects of FBS, with serum-free cultures displaying more efficient energy metabolism, lower GFAP expression and comparable cellular morphology to *in vivo* astrocytes when compared to astrocytes grown in 10% FBS, which appeared to display a more reactive phenotype (Prah et al., 2019). However more work needs to be done to thoroughly investigate the effect of FBS in astrocytes and in particular, knowledge gaps remain related to its impact on human primary astrocyte culture.

FBS is the most common form of growth supplement used in mammalian cell culture, which is obtained from the blood of foetal bovines, containing a wide variety of growth factors, hormones, amino acids and vitamin. Due to the nature of FBS collection, there may be geographical and seasonal variations between batches, and it can be contaminated with endotoxins such as lipopolysaccharide (LPS) which will alter the growth of cultured cells (Kirikae et al., 1997; Gstraunthaler et al., 2013).

With such a range of components, it can be difficult to replace FBS for more controlled, synthetic supplements that will equally support the growth of cells. However, with more defined supplements, cultures should be less variable and more reproducible leading to better overall scientific practice.

Of particular interest for EV research, a focus of this thesis, FBS contains endogenous EVs which can contaminate cellular-derived EV preparations when used as a culture medium supplement. Where FBS is essential to culture particular cell types, groups have attempted to deplete EVs from FBS through ultracentrifugation (Kornilov et al., 2018). However, studies have shown that EV contaminants can persist even after depletion (Aswad et al., 2016; Lehrich et al., 2018). Lehrich et al (2018) reported reduced proliferation and viability in rodent primary astrocytes cultured with EV-depleted FBS, further emphasising the need for serum-free cultures rather than using EV-depleted serum when investigating ADEVs.

3.1.4 Established serum-free models for astrocyte culture

Despite many studies continuing to report astrocyte culture including FBS, more recent work has begun to move towards serum-free cultures, particularly for primary astrocytes. The application of FGF has had some success in maintaining quiescent astrocytes in serum-free culture, with FGF thought to cause astrocyte maturation and increased glutamate clearance (Roybon et al., 2013; Prah et al., 2019; Savchenko et al., 2019). FGF has also been shown to increase the expression and release of trophic factors enhancing survival for both neurones and astrocytes. Other groups have used similar medium compositions with minor differences to culture serum-free astrocytes, such as the combination of DMEM and Neurobasal medium alongside supplements such as EGF (epidermal growth factor; Foo et al., 2011; Jia et al., 2018; Prah et al., 2019; Barbar et al., 2020). Serum-free supplements such as N2 and B27 are commercially available which are intended to replace FBS with key growth factors required for cell growth. G5 supplement has been described as an astrocyte growth supplement with EGF and FGF forming key components of the supplement. We reason that by creating a standardised simple, inexpensive, serum-free medium that consistently maintains quiescent human astrocytes, there can be a marked improvement in the quality of astrocyte research.

3.1.5 Aims of this chapter

This chapter aims to optimise methods for the serum-free culture of commercially available human primary astrocytes and compare their molecular and cellular phenotypes with FBS-cultured equivalents, allowing mechanisms of astrocyte activation to be interrogated *in vitro*. Morphological analysis of both serum-free and serum-cultured human astrocytes will be complemented with gene and protein expression analyses, alongside ICC, immunoblotting and RT-qPCR methods. Further morphological comparisons will be made with rodent primary astrocytes cultured in the same serum-free conditions. Establishing a standardised serum-free culture method of human primary astrocytes is essential for subsequent studies of astrocyte EV biology (Chapter 5).

3.2 Developing serum-free conditions for human primary astrocyte culture

3.2.1 Testing serum-free media compositions

To ultimately investigate the effect of serum (FBS) on human astrocytes and their EVs, quiescent astrocyte cultures were required as a baseline condition. Based on manual literature searches of publications describing serum-free astrocyte cultures, five commonly used culture medium compositions were trialled on human primary astrocytes to establish which components were essential to maintain a quiescent phenotype (SC1800 cells; see Table 2-1-1 for medium compositions, repeated below with the five serum-free medium highlighted in red). Initially, all astrocytes were cultured on poly-L-lysine (PLL) coated plates as suggested by ScienCell, the commercial supplier of the human foetal astrocytes. Morphological analysis of astrocytes was performed using brightfield microscopy (10x magnification) after 1 and 4 weeks in culture after thawing (Figure 3-1, columns 1 and 2). Visual inspection was used to identify differences in morphology during these initial analyses, however subsequent quantitative morphological analysis was completed after optimisation stages of culture were complete (see section 3.3.2).

Table 3-1 (repeated) - Media compositions used for cell culture. FBS = Foetal bovine serum, AGS = astrocyte growth serum, Pen/Strep = Penicillin and Streptomycin, HB-EGF = Heparin-binding EGF-like growth factor. Medium highlighted in blue were used for serum-free optimisation experiments. For G5 composition, see Supplementary figure 1)

Media type	Components
Astrocyte medium	Astrocyte medium, 1% Pen/Strep, 1% AGS, 2% FBS
FBS-Free astrocyte medium (AGS AM)	Astrocyte medium, 1% Pen/Strep, 1% AGS
DMEM medium	DMEM with Glutamax, 1% Pen/Strep, 10% FBS
FBS-Free DMEM medium	DMEM with Glutamax, 1% Pen/Strep
G5 serum-free medium (DMEM G5)	DMEM/F12*, 1% Pen/Strep, 1% G5 supplement, 1% L-glutamine
Neurobasal serum-free medium (NB-27)	(50% Neurobasal media, 50% DMEM/F12), 1% Pen/Step, 2% B27 supplement, 1% L-glutamine, 0.025% HB-EGF
B27 serum-free medium (DMEM B27)	DMEM/F12, 1% Pen/Strep, 2% B27 supplement, 1% L-glutamine, 0.025% HB-EGF
DMEM AGS medium	DMEM/F12, 1% Pen/Strep, 1% AGS, 1% L-glutamine
B27 + G5 serum-free medium (DMEM B27 G5)	DMEM/F12, 1% Pen/Strep, 1% G5 supplement, 2% B27 supplement, 1% L-glutamine

From visual inspection, serum-free astrocytes did not obviously proliferate as a similar number of cells were present over a 4-week period in all media tested. Thus, these cells did not require passaging throughout. Likewise, astrocyte morphology remained consistent across the five different serum-free media conditions with small cell bodies and long thin processes typically observed, resembling descriptions of quiescent astrocyte morphology (Figure 3-1). An initial test was performed to determine whether the serum-free astrocyte cultures retained the ability to react to stimuli such as FBS. After four weeks of culture, serum-free astrocytes were subsequently treated with 2% FBS for 24 hours, with any visible changes in

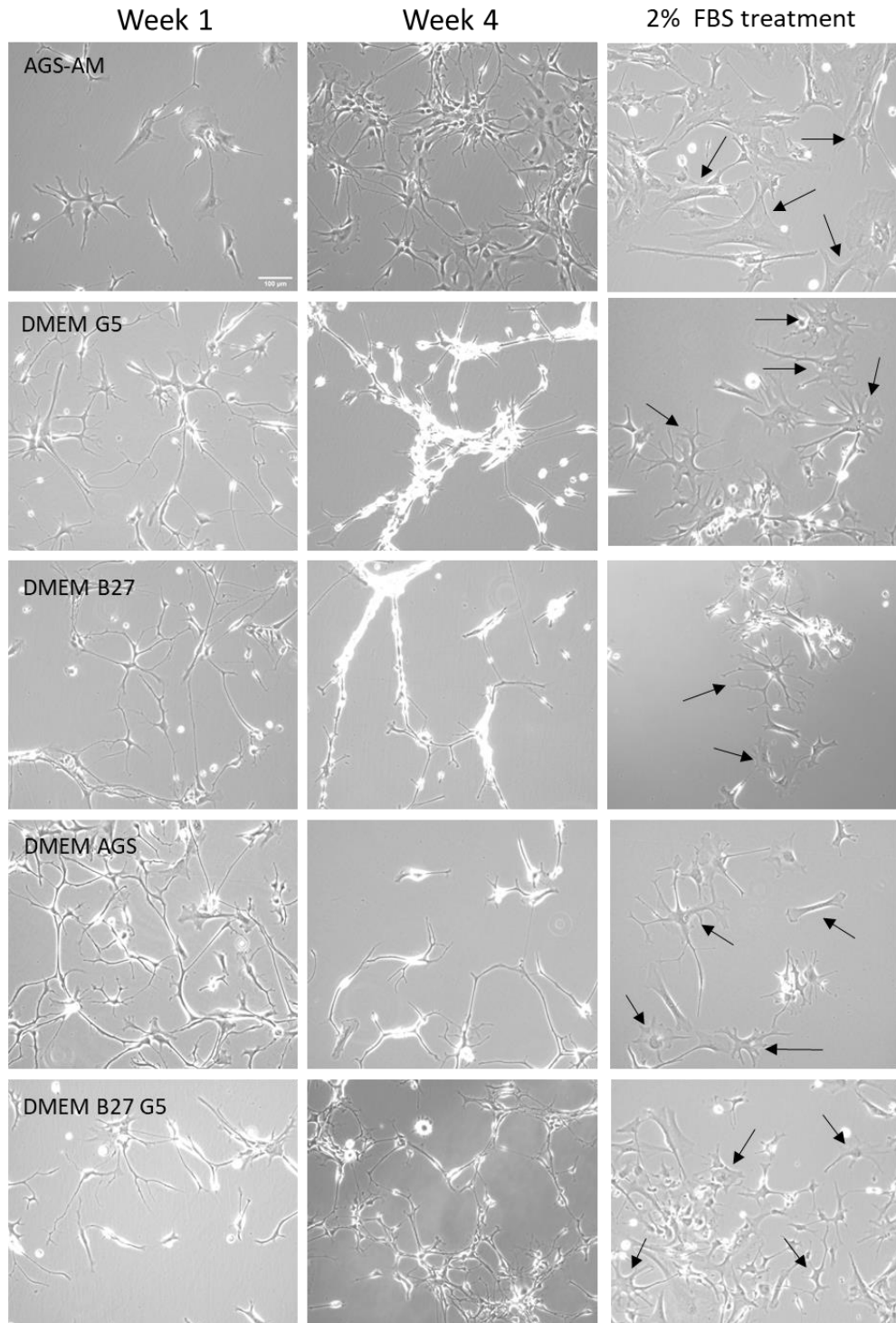


Figure 3-1 – Human primary astrocytes show a ‘quiescent’ morphology when cultured in different serum-free media and change morphology in response to FBS treatment. Visual inspection of SC1800 human astrocytes indicate a similar ‘quiescent’ morphology (multiple, long processes and small cell bodies) after 1 and 4 weeks regardless of the serum-free media composition used. Changes in morphology were observed when week 4 serum-free astrocytes were subsequently treated with 2% FBS for 24 h resulting in a more reactive phenotype (hypertrophic cell bodies, smaller processes; black arrows). Images were taken at 10x magnification whilst cells remained in culture. The five astrocyte cultures were generated using the same original vial of astrocytes on a single occasion, however three conditions (DMEM G5, DMEM B27 and DMEM B27 G5) were completed a second time to confirm reproducibility (data not shown). Scale bar represents 100 μ m. Media compositions used to culture the astrocytes are described in [Table 2-1-1](#) (reproduced in text above).

morphology taken as indication of ability to become reactive. Clear morphological changes for all serum-free media were observed after FBS treatment (Figure 3-1; arrows). Cell bodies became hypertrophic with shorter processes which is previously described in reactivity morphology (Escartin et al., 2021). This observation supported further quantitative investigation into the effect of serum on astrocyte phenotypes (section 3.3.2).

The DMEM medium with G5 supplement (DMEM G5) was judged to provide the optimum condition for quiescent astrocyte culture with high viability (few dead cells floating in medium) and no signs of reactive morphology (Figure 3-1, second row). DMEM G5, DMEM B27 and DMEM B27 G5 conditions were all trialled a second time to ensure reproducibility of observations (not shown). As noted earlier, in DMEM G5 medium quiescent astrocytes retained the ability to react to FBS by changing to a reactive morphology. There was no noticeable difference in astrocyte phenotypes with the addition of B27 supplement to the DMEM medium containing G5 supplement (DMEM B27 G5). Therefore, due to G5 supplement being designed for astrocyte culture (unlike B27, a neuronal based supplement), and G5 supplement having a published composition (unlike AGS; astrocyte growth supplement, supplied by ScienCell), we opted to use G5 serum-free medium (DMEM G5) for the routine culture of serum-free astrocytes for the duration of the project (see Supplementary figure 1 for G5 composition).

3.3 The effects of serum on cultured human primary astrocytes

3.3.1 Morphology changes when human astrocytes are cultured in FBS

After establishing the preferred condition for serum-free astrocyte culture (i.e. DMEM G5 medium), human astrocytes were also cultured using the suppliers' recommended astrocyte medium that includes FBS (astrocyte medium supplemented with 2% FBS and 1% AGS). Both serum-free and serum-cultured astrocytes were compared at passage 3 (P3), where the latter had been exposed to FBS throughout the astrocyte culture (minimum culture time was 5 days). This is the only passage number available for serum-free cultured astrocytes due to their lack of proliferation and having been cryopreserved at passage 2, were therefore revived (and remained) at passage 3. Consistent with observations in Figure 3-1, visual inspection of brightfield images revealed a clear difference in the morphology of the astrocytes when cultured with the suppliers' recommended medium containing FBS. Serum-cultured astrocytes showed hypertrophic cell bodies and less defined processes compared to the serum-free astrocytes (Figure 3-2). This morphology is typically associated with a reactive phenotype supporting the hypothesis that FBS is inducing reactivity (Escartin et al., 2021). In contrast to serum-free astrocytes, serum-cultured cells rapidly proliferated with two passages per week required. Cellular proliferation is known to be a feature of reactive astrocytes (Sofroniew and Vinters, 2010).

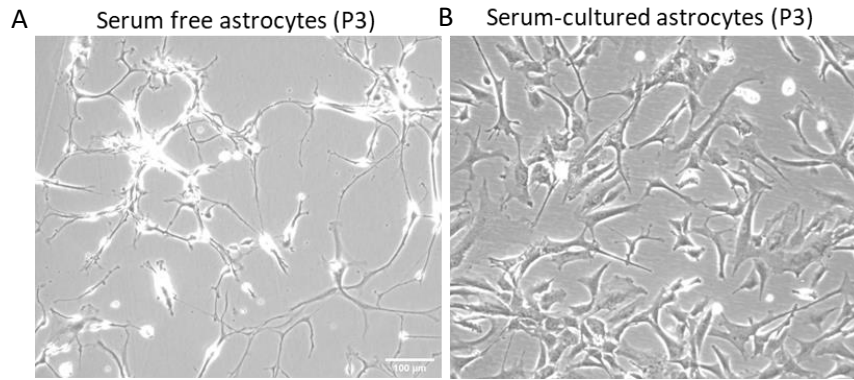


Figure 3-2 – Qualitative analysis of human primary astrocytes cultured with and without serum show distinct morphological differences typically associated with reactive and non-reactive phenotypes, respectively. (A) Serum-free astrocytes have smaller, less hypertrophic cell bodies with more distinct processes compared to (B) serum-cultured astrocytes. Astrocyte morphology was compared at passage 3 (P3) to avoid any changes due to cellular-ageing in proliferative serum-cultured astrocytes. This was the only passage available for serum-free cultures due to a lack of proliferation, and therefore these cells were seeded at passage 3. Serum-free astrocytes are maintained in DMEM G5 medium whilst serum cultures are maintained in the supplier’s recommended astrocyte medium (astrocyte medium supplemented with 2% FBS, 1% AGS and 1% Pen/Strep). Image taken at 10x magnification with scale bar representing 100 μm .

3.3.2 Quantification of astrocyte reactive morphology

Whilst subjective visual assessments indicated clear morphological differences between serum-free and serum-cultured astrocytes, a quantitative approach was required to independently compare morphologies. Previous analyses of rodent astrocyte morphology have used the ‘simple neurite tracer’ plug-in (SNT) in ImageJ software (Tavares et al., 2017; Prah et al., 2019). This was initially attempted on the brightfield images taken to assess human astrocyte morphology in this study. However, this was not successful due to a lack of contrast between the background and the cells. The use of this software was only suitable for fluorescent images where the cells are stained sufficiently so that the processes and cytoplasm of the cell are visible, as well as the nucleus.

To test the SNT plug-in, ICC images of serum-free and serum-cultured astrocytes stained for GFAP and Phalloidin (F-actin label) were analysed using the SNT plug-in (see Figure 3-3A for an example of serum-cultured astrocytes). The plug-in allows semi-automatic tracing of the cells which partially traces cells but does not accurately trace the complete cell outline (Figure 3-3B). As a test of the accuracy of this tracing, the tracings were then used to recreate the original cell morphology using the fill function at a value of 0.03 (Figure 3-3C). The reconstruction showed a similar morphology to the original cell suggesting these tracings might be suitable to measure astrocyte morphology. The region of interest (the cell outline) was then used to measure the cell area and perimeter of the astrocytes which was then compared to manual tracing of the cell. Whilst perimeter was similar in both analyses (SNT = 1233 vs Manual = 1209), area was not correctly calculated by the software (SNT = 216 vs Manual = 3200). Therefore, the plug-in was not deemed suitable for the analysis of astrocyte morphology in this study, even with GFAP staining.

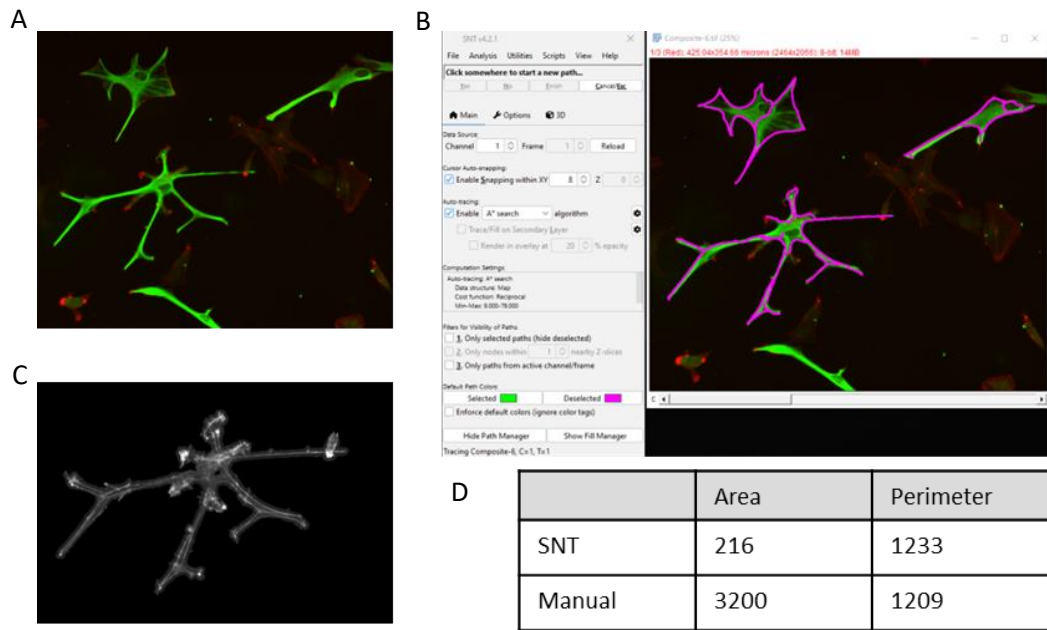


Figure 3-3 – Human primary astrocyte morphology analysis using the ‘Simple neurite tracer’ plug-in. (A) Representative ICC image of serum-cultured, human primary astrocytes used for analysis which have been stained using anti-GFAP (green) and Phalloidin (red). (B) Screenshot of the SNT plug-in after semi-automatic tracing of the astrocytes (shown in purple). (C) Reconstruction of an astrocyte using the semi-automatic tracing to show the similarity between the tracing and the original cell. (D) Measurements taken in FIJI of the astrocyte selected in C after SNT semi-automatic tracing and after manual tracing of the cells. Whilst perimeter measurements are similar, cell area was not correctly calculated by the SNT plug-in. SNT plug-in was run using FIJI software. Cells were maintained in the supplier’s recommended astrocyte medium (astrocyte medium supplemented with 2% FBS and 1% AGS).

Instead, the area and perimeter of the cells were measured using the freehand selection tool in ImageJ using brightfield images. The ratio between cell area and perimeter was calculated to account for the diversity in astrocyte morphology that is seen in culture and reduce the effect that long processes would have on the area of the cell (i.e. hypertrophy measurements focus on change in soma size). Therefore, this ratio better recapitulates any increase in volume of the cell body due to reactivity.

A significant increase in the area/perimeter ratio was found in serum-cultured astrocytes indicating cell hypertrophy in serum conditions compared to serum-free astrocytes ($P = 0.0007$; $N = 3$; Figure 3-4C). This result supports the preliminary qualitative analysis of cell morphology above (section 3.3.1). In addition to cell hypertrophy, the area of the nuclei in the cells was also analysed using DAPI staining as this commonly increases during cellular maturation or senescence (Zhao and Darzynkiewicz, 2013). A significant increase in nuclear size was observed after culture in serum compared to serum-free cultures ($P = 0.011$; $N = 3$; Figure 3-4, D-F).

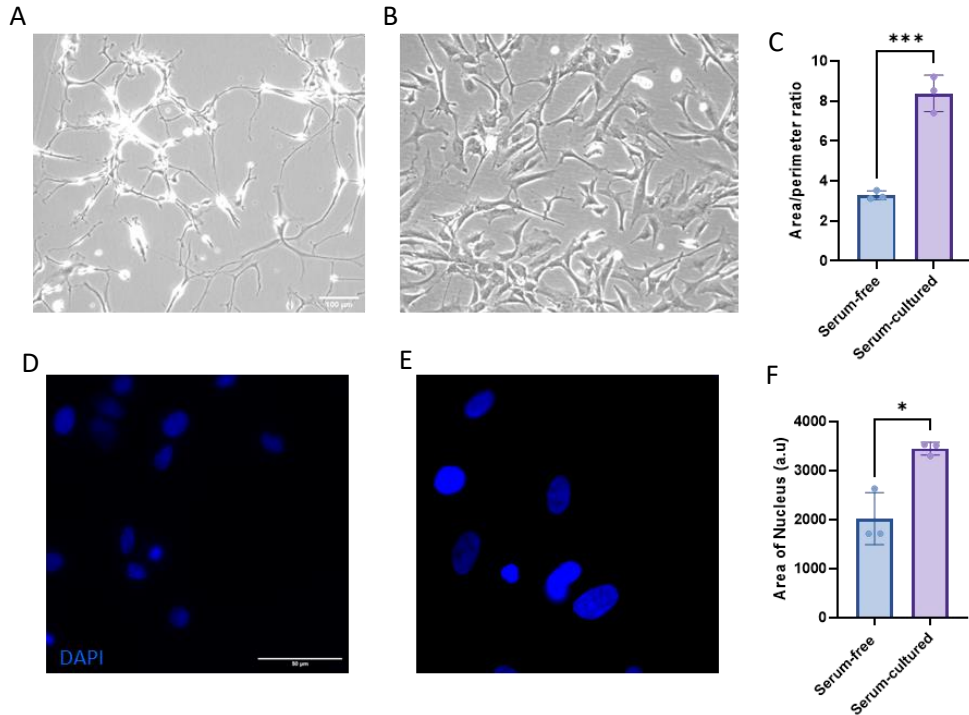


Figure 3-4 - Quantitative analysis of human primary astrocytes cultured with or without serum shows significant morphological differences. (A-B) Representative brightfield images of (A) serum-free and (B) serum-cultured astrocytes (in 2% FBS) previously depicted in Figure 3.2. (C) The area/perimeter ratio of astrocytes was used to measure cellular hypertrophy which indicated a significant increase in the size of the astrocytes ($P = 0.0007$; Serum-free = 3.29 ± 0.22 vs Serum-cultured = 8.38 ± 0.91). (D-F) Nuclear size increases in (E) serum-cultured astrocytes compared to (D) serum-free astrocytes ($P = 0.011$; Serum-free = 3448 ± 130 vs Serum-cultured = 2021 ± 531). Astrocytes were imaged whilst in culture at passage 3 for serum-free (seeded directly at passage 3) and passage 3-4 for serum-cultured astrocytes at either 10x magnification (A-B) or 40x magnification (D-E). Scale bar represents (A) 100 μm or (D) 50 μm . Statistical significance was calculated using an unpaired t-test. Error bars represent mean and standard deviation. a.u = arbitrary units. Area/perimeter ratios were calculated using a minimum of 20 cells measured per replicate with nuclei measurements using at least 70 cells per replicate, $N = 3$.

3.3.3 Serum exposure causes an irreversible morphological change in cultured human primary astrocytes

With clear morphological differences established between the serum-free and serum-cultured human astrocytes (Figure 3-4), the models allowed us to investigate the reversibility of reactivity caused by serum exposure. Healthy reactive responses should be transient and allow astrocytes to resume homeostatic functions once the detected threat/damage has been dealt with. To determine whether serum exposure was associated with a permanent morphological change, serum-cultured astrocytes were placed into serum-free media for up to 5 days. Brightfield imaging was completed at day 1 and day 4/5 to compare cellular morphology (Figure 3-5). An increase in area/perimeter ratio was found in day 4/5 measurements compared to day 1 measurements ($P = 0.011$; Day 1 = 6.17 ± 1.24 vs Day 4/5 = 7.47 ± 1.19 ; $N = 3$). This is likely due to the cells having more time to spread onto the cell culture flask after initial plating and therefore increase in size. The similarity in area/perimeter ratio to previous serum-cultured astrocytes suggests an irreversible morphological change in astrocytes after serum exposure (Day 4/5 mean = 7.48 ± 1.20 vs previous serum-culture = 8.38 ± 0.91 ; section 3.3.2). Notably, we had previously

demonstrated that astrocyte reactivity could be prevented by freezing cells at low passage number (P2) and thawing in serum-free media (see Figure 3-1). In the rest of the thesis, we therefore decided to only culture serum-free astrocytes directly from cryopreserved vials. This experimental procedure allowed the maintenance of the quiescent serum-free phenotype in human astrocytes.

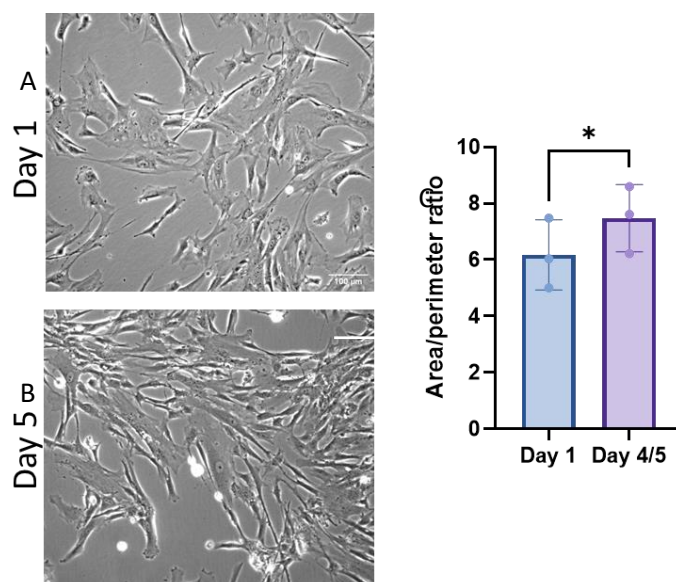


Figure 3-5 – Morphological changes in serum-cultured human primary astrocytes are irreversible. (A and B) Serum-cultured astrocytes were subsequently cultured in serum-free media for up to 5 days with no visible change in morphology suggesting an irreversible change in the astrocyte phenotype after the addition of 2% FBS. (C) Morphological analysis found an increased area/perimeter ratio in day 4/5 measurements compared to day 1 measurements which was similar to previous serum-culture analysis ($P = 0.011$; Day 1 mean = 6.17 ± 1.25 vs Day 4/5 mean = 7.48 ± 1.20 , previous serum-culture mean = 8.38 ± 0.91 ; $N=3$). Due to experimental constraints, imaging was completed on either day 4 or day 5 for quantification (pooled as day 4/5). Representative brightfield image depicted in (B) represents cell morphology at day 5. Scale bar represents $100 \mu\text{m}$ with brightfield images taken at 10x magnification. Error bars represent mean and standard deviation with statistical analysis performed using a paired *t*-test (repeated measures).

3.3.4 Comparison of *in vitro* and *ex vivo* human and rat primary astrocyte morphologies

To further explore the relevance of cultured *in vitro* astrocyte morphologies to astrocyte cells in tissue, serum-free and serum-cultured human primary astrocytes were stained for GFAP and compared to cortical human brain tissue sections also stained for GFAP, a well-characterised astrocyte marker (Figure 3-6A-C). GFAP expression in the cultured astrocytes showed similar morphology to those observed previously during brightfield imaging (see Figure 3-2), with small cell bodies and long processes observed in the serum-free astrocytes, and hypertrophic cell bodies in the serum-cultured astrocytes (more detailed GFAP analysis in section 3.4.2). Astrocytes stained using anti-GFAP antibody within human tissue typically showed a similar morphology to *in vitro* serum-free astrocytes with long, thin processes and smaller cell bodies (Figure 3-6C, white arrows).

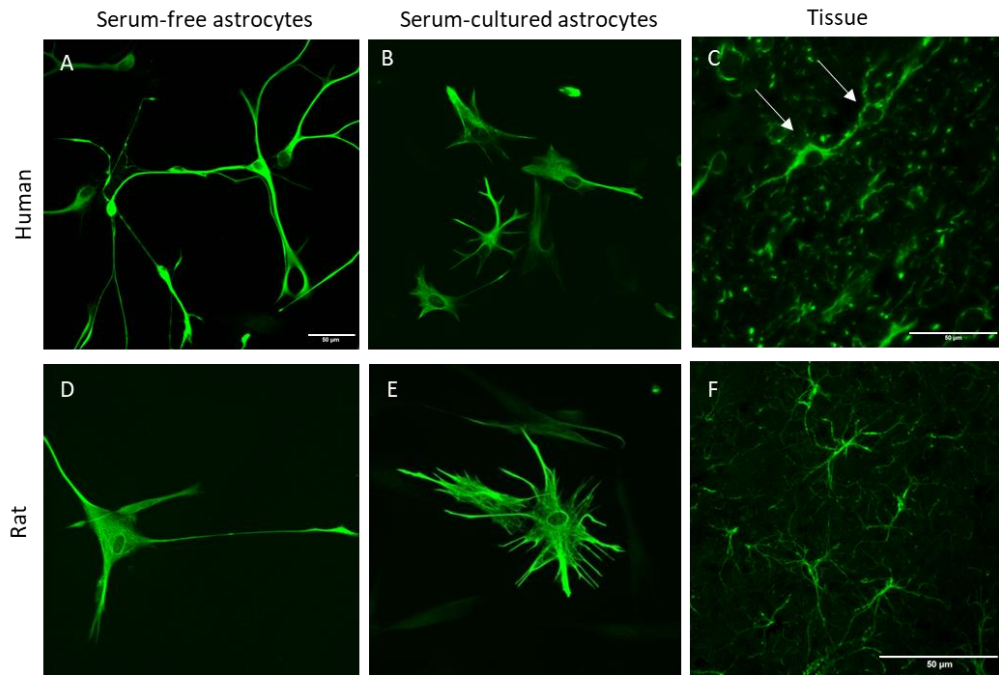


Figure 3-6 – Comparison of both human and rat GFAP expression between serum-free and serum-cultured primary astrocytes and ex vivo tissue. Serum-free astrocytes showed quiescent-like features in both (A) human and (D) rat in vitro cultures. Serum caused changes in both (B) human and (E) rat astrocytes with changes in morphology more evident in human astrocytes. Differences in size and morphology are observed between (C) human and (F) rat astrocytes in tissue. Human tissue images were taken at 40x magnification, rat tissue images taken at 63x magnification, and all in vitro images were taken using 20x magnification. Scale bar on tissue images represent 50 μm (C and F) and scale bar on ICC images represent 100 μm (A-B, D-E). White arrows highlight astrocytes identified within human brain tissue.

To compare the morphologies of rodent and human astrocytes, cultured rat primary astrocytes and adult female rat brain tissue (6-12 week old BD-IX rats) were also stained for GFAP (Figure 3-6, D-F). Briefly, rat primary astrocytes were cultured for one week using the same medium as the human primary astrocytes (in either serum-free or 2% FBS-containing astrocyte medium for a minimum of 3 days) before staining for GFAP, alongside healthy rat brain tissue. The morphology of primary rat astrocytes cultured in serum-free conditions was less comparable to astrocytes observed in rat tissue (Figure 3-6D and E). Rat astrocytes cultured without serum showed some reactive morphology, likely due to poor viability after the re-thawing process resulting in a low-density culture (Figure 3-6D). Rat primary astrocytes had a better recovery in the FBS-containing medium and showed some signs of proliferation however, there was still poor viability. Of the surviving rat primary astrocytes, cell morphology was similar to that of the serum-cultured human astrocytes. Due to the lack of viability in the primary rat cultures, it was difficult to quantify morphology in the same way as the human primary astrocytes.

3.4 Stability of serum-cultured human primary astrocytes over time

3.4.1 Astrocyte morphology changes with increasing passage number in serum-cultures

Unlike immortalised cell lines, primary cells are known to have a finite culture period and therefore it is important to define the useable age limit of the serum-cultured human primary astrocytes before the cells begin to change phenotype. To investigate the effect of passage number on the growth of serum-cultured astrocytes, astrocytes were imaged using brightfield microscopy after each passage until passage 12 (not shown) where there was visible reduced cell viability (Figure 3-7). In early passage numbers, cell bodies were small and mostly uniform in size with a fibroblastic morphology (Figure 3-7, A and B). With increasing passages, cell bodies became increasingly larger with a more varied morphology (Figure 3-7, C-E). Visual inspection of cell proliferation rate indicated this declined after passage 7, with cells reaching 70% confluency after ~7 days instead of 4 days from passage 7. This led to more available space in the cell culture flask and this may have contributed to the increased size of the cells. In comparison, serum-free astrocytes were not found to proliferate and so did not require passaging, even after 4 weeks of culture (equivalent time point for serum-culture would be passage 9 based upon 2 passages per week). Unlike serum-cultured astrocytes, no clear change in morphology was evident in the serum-free cells over that time frame (Figure 3-7F).

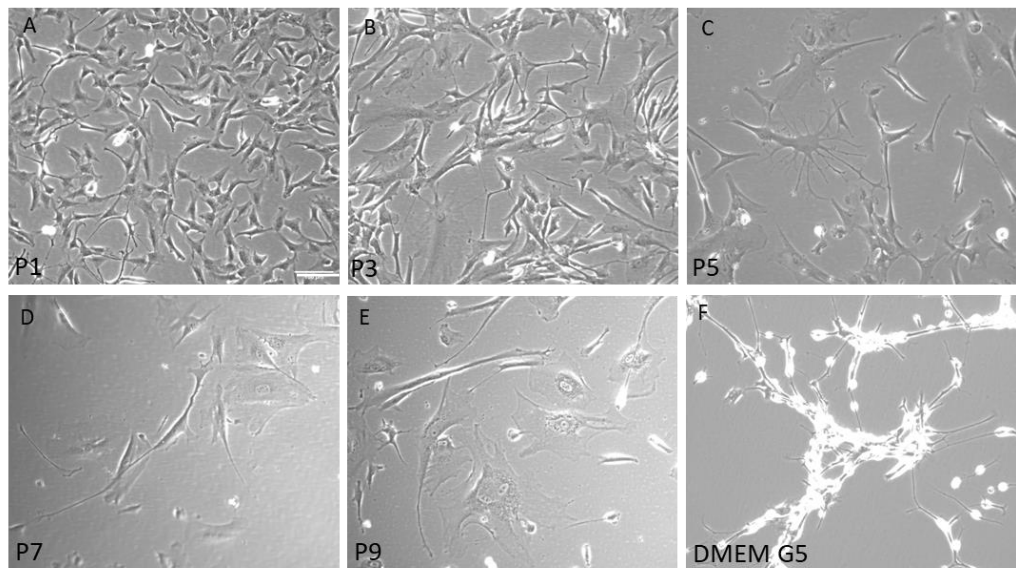


Figure 3-7 – The morphology of serum-cultured human primary astrocytes changes between P1 and P9 in comparison to serum-free astrocytes which remain the same after 4 weeks in culture. (A-E) Morphological differences were observed in serum-cultured astrocytes (in 2% FBS and 1% AGS) as they become larger and have a more varied morphology in later passages. (F) In comparison to serum-free astrocytes, no morphological difference was found after 4 weeks in culture (equivalent to passage 9; image repeated from Figure 3-1) Images were taken at 10x magnification and scale bar represents 100 μ m.

For quantitative analysis of astrocyte morphology, data for similar passage numbers were grouped to increase sample size (from N=2 to N=4). Quantitative analysis revealed an increase in the area/perimeter ratio with increasing passage, confirming cellular hypertrophy increases with passage (e.g. P1/2/3 vs P10/11, $P = 0.0022$; $N = 3-4$; Figure 3-8A). Nuclear area also showed an increasing trend with passage number

but due to a limited sample size, statistical analysis was not completed (Figure 3-8B). For experimental reasons, nuclear area could not be completed for P10/11.

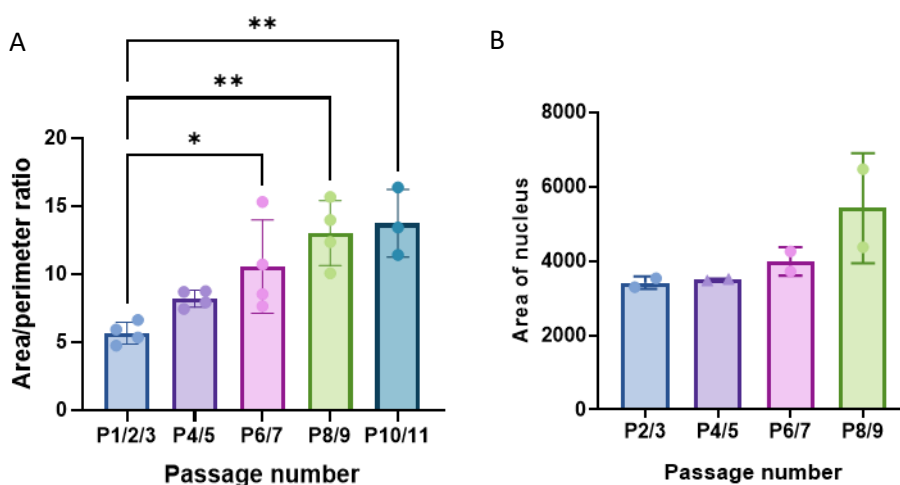


Figure 3-8 - Serum-cultured human primary astrocytes have increased hypertrophy with increasing passage number. (A) A significant increase in hypertrophy was observed as passage number increased (P1/2/3 vs P10/11, $P = 0.0022$; $N=3-4$). (B) An increasing trend was observed in nuclear area as passage number increased, however was found not to be significant (P2/3 vs P8/9, $P = 0.18$; $N=2$). Statistical analysis was completed using One-way ANOVAs followed by Tukey's multiple comparison's test. Error bars show mean and standard deviation.

3.4.2 GFAP expression reduces in serum-cultured human primary astrocytes with increasing passage number

GFAP expression is the most widely used marker of astrocytes and has been consistently shown to increase in reactive astrocytes (Escartin et al., 2021; Jurga et al., 2021). GFAP is an intermediate filament protein that is found throughout the cytoplasm of astrocytes and therefore, is integral to the morphology of the astrocytes. With morphological changes observed with increasing passage number in serum-cultured astrocytes (section 3.4.1), we anticipated that GFAP expression may also change in the serum-cultured astrocytes. Therefore, GFAP expression was examined using ICC in serum-cultured astrocytes and compared across passage numbers (Figure 3-9).

The morphological changes observed over different passages in the serum-cultured astrocytes using GFAP staining matched those observed previously through brightfield imaging (see Figure 3-7), with hypertrophic bodies and shorter processes (Figure 3.9A). This was more evident in later passages with GFAP staining revealing astrocytes typically have only one or two main processes creating a bipolar-shaped morphology. GFAP expression also decreased with passage number with a significant reduction in expression in later passages (5.6-fold reduction between P2/3 vs P10/11/12, $P = 0.037$; $N = 2-3$; Figure 3-9B). Visual analysis noted that until passage 6, there was very little GFAP staining in the nucleus and high expression in the cytoplasm of the cells. However, in later passages, nuclear staining of GFAP was more evident than cytoplasmic staining despite no increase in GFAP expression in the nucleus (Figure 3-9A; nuclear GFAP intensity remained between 20,000 and 30,000 a.u regardless of passage number, data not shown). Therefore, an increase in the

nuclear/cytoplasmic ratio of GFAP was observed with passage number (P2/3 vs P10/11/12, $P = 0.006$; $N = 2-3$; Figure 3-9C).

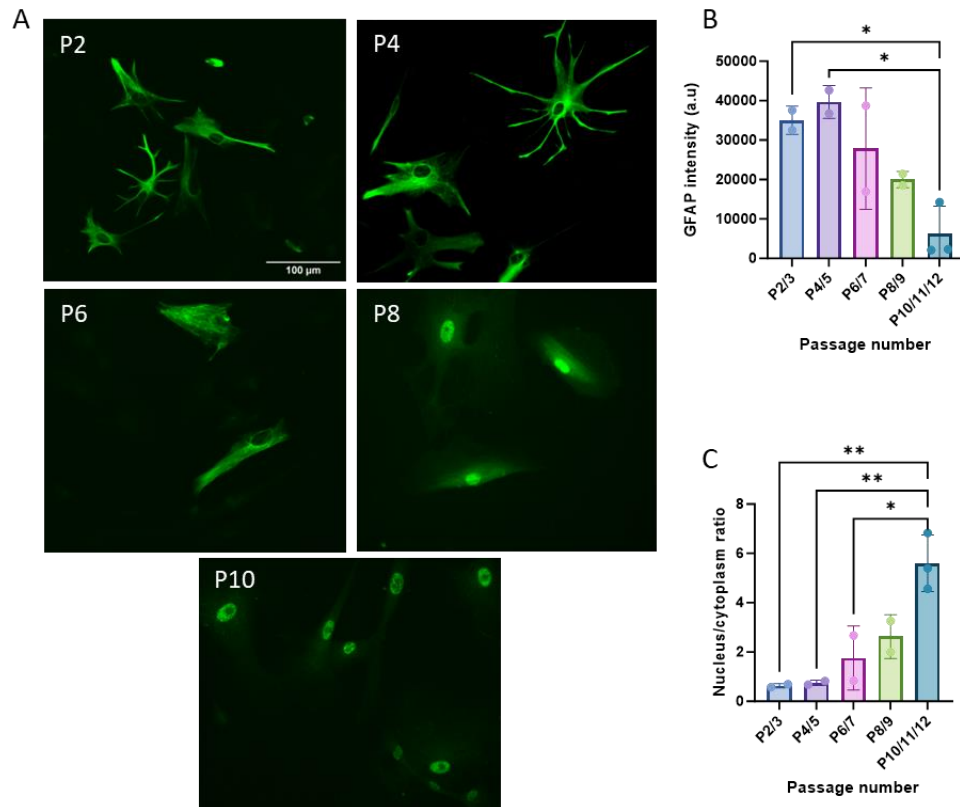


Figure 3-9 - GFAP expression reduces in serum-cultured human primary astrocytes with increasing passage number. (A) GFAP staining of human primary astrocytes cultured in 2% FBS from P2 to P10 displays a changing phenotype with fewer processes and a bipolar morphology observed in later passages. (B) A significant decrease in GFAP expression in the cytoplasm was observed at later passages compared to early passages (P2/3 vs P10/11/12 $P = 0.037$). Large variability was observed at passage 6 and 7 due to the presence of both early (more processes and smaller cell bodies) and late (fewer processes and bipolar morphology) phenotypes. (A and C) Despite nuclear staining appearing brighter in later passages (P8+), there was no change in nuclear expression of GFAP (data not shown) resulting in a significant difference in the nucleus/cytoplasm ratio of GFAP expression in later passages (P2/3 vs P10/11/12 $P = 0.0062$). Significant differences were calculated using a one-way ANOVA followed by Tukey's multiple comparison's test ($N=2-3$). Images were taken at 20x magnification. Scale bar represents 100 μ m. Error bars represent mean and standard deviation.

Interestingly, astrocytes displayed a mix of both early (more processes and smaller cell bodies alongside high cytoplasmic GFAP expression) and late (fewer processes and bipolar morphology, reduced cytoplasmic GFAP staining) passage phenotypes at passage 7 suggesting key physiological changes are occurring within the cells around this passage number (Figure 3.9A). Given these changes matched the time point of changes observed in nuclear size and cell area (see previous Figure 3-8), it was decided that serum-cultured astrocytes in future experiments would be used until passage 7 to better match the physiological status of serum-free cultures and avoid phenotypic changes. This agreed with previous work where SC1800 human primary astrocytes were also used until passage 7 (Baxter et al., 2021).

3.5 Expression of astrocyte markers in serum-free and serum-cultured human primary astrocytes

3.5.1 GFAP expression is lower in serum-cultured human primary astrocytes compared to serum-free astrocytes

As noted previously, GFAP is the most widely used astrocyte marker and is considered the 'gold standard' for astrocyte staining (Jurga et al., 2021). In addition, increased GFAP expression is often associated with astrocyte reactivity in response to brain disease or injury (Hol and Pekny, 2015). Therefore, GFAP expression was investigated using a variety of techniques in serum-free and serum-cultured astrocytes. GFAP staining was evident in serum-free and serum-cultured astrocytes using ICC, particularly at low passage number in the serum-cultured astrocytes, with staining observed throughout the cytoplasm and absent in the nucleus (Figure 3-10A and B).

GFAP gene expression was compared between serum-free and serum-cultured astrocytes using RT-qPCR (Figure 3-10C). Ct values were normalised using the mean of three housekeeping genes (GAPDH, B2M and β -actin; Supplementary figure 2). Fold change was calculated against the serum-free condition to investigate GFAP expression change caused by serum. GFAP gene expression was found to significantly decrease in serum-cultured astrocytes compared to serum-free astrocytes (SF mean = 1.16 ± 0.70 vs SC = 0.08 ± 0.08 , $P = 0.0093$, $N = 5$; Figure 3-10C). This is contradictory to previous published work with GFAP commonly shown to increase with reactivity (Prah et al., 2019).

With many post-translational regulatory processes occurring within cells, RNA expression may not always correlate with protein expression. Therefore, western blotting was also completed to compare GFAP protein expression in the serum-free and serum-cultured astrocytes (Figure 3-10D and E). GAPDH expression was used as a housekeeping protein to normalise the data. Overall GFAP expression was significantly higher in serum-free astrocytes compared to serum-cultured astrocytes despite serum-free astrocytes displaying quiescent morphology (SF mean = 129.1 ± 7.0 vs SC = 69.7 ± 18.6 , $P = 0.007$; Figure 3-10D). This was consistent with the GFAP gene expression found in the astrocytes indicating GFAP expression decreases when astrocytes are cultured in serum. This may indicate that GFAP is not a reliable marker of reactivity after long-term (chronic) exposure to FBS in these human astrocyte cultures.

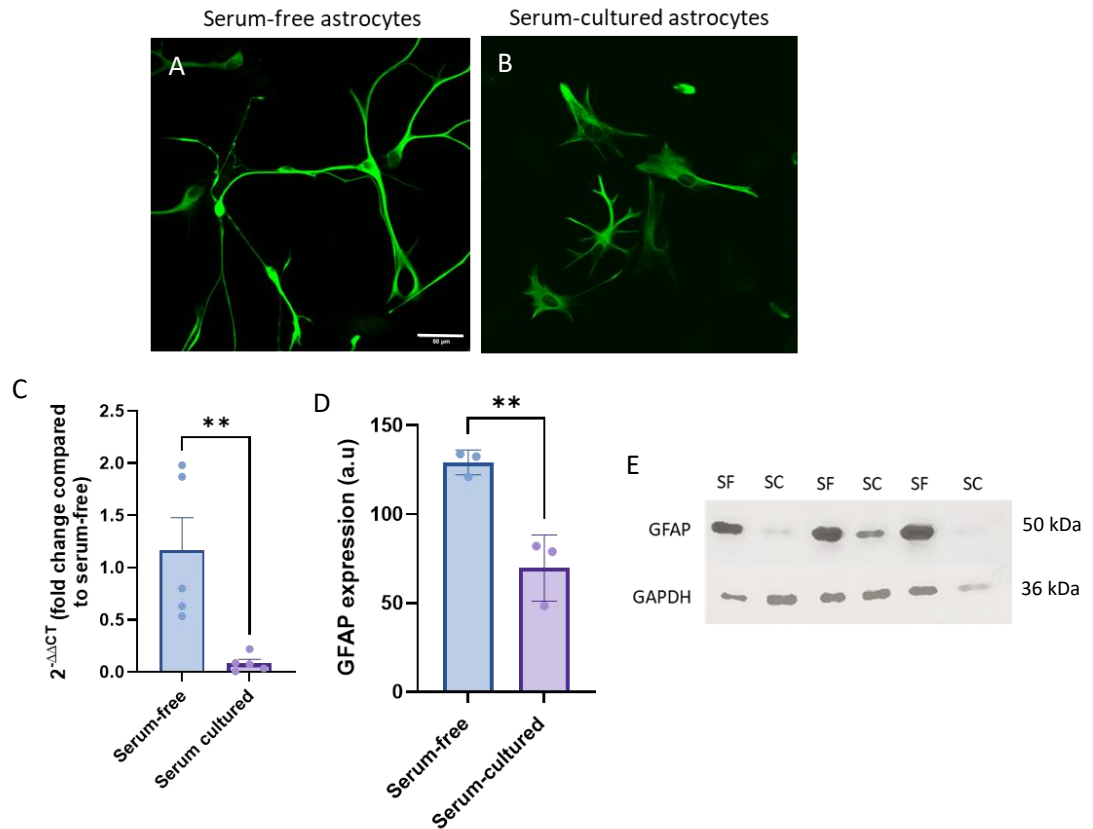


Figure 3-10 - GFAP expression is lower in serum-cultured human primary astrocytes compared to serum-free astrocytes. (A and B) Representative ICC images of serum-free and serum-cultured astrocytes taken from Figure 3.4 (images shown at passage 2). (C) RT-qPCR analysis found a significant decrease in GFAP expression in serum-cultured astrocytes compared to serum-free astrocytes (SF mean = 1.16 ± 0.70 vs SC = 0.08 ± 0.08 , $P = 0.0093$; $N = 5$). (D and E) Western blotting found 2-fold higher GFAP expression in serum-free astrocytes compared to serum-cultured astrocytes after normalisation to GAPDH expression (SF = 129.1 ± 7.0 vs SC = 69.7 ± 18.6 , $P = 0.007$; $N = 3$). Statistical analysis was completed using unpaired t-tests, data represents mean and standard deviation (only upper bar present on RT-qPCR due to lower range falling below 0). Images were taken of human primary astrocytes at passage 2 at 20x magnification with scale bars representing 50 μm .

While GFAP is well established as an astrocyte marker, there are astrocyte populations in the healthy brain that do not express GFAP at detectable levels (Walz and Lang, 1998; Cahoy et al., 2008). Further, inspection of the GFAP-stained ICC images indicated variable expression of GFAP across populations of serum-free and serum cultured astrocytes (Figure 3-11). From a simple subjective classification of GFAP-positive cells (clear GFAP staining) compared to total numbers of cells (co-staining with F-actin label phalloidin), a significant, 6-fold decrease in the percentage of GFAP⁺ cells was identified in serum-cultured astrocytes compared to serum-free astrocytes (SF mean = $49.5\% \pm 11.3$ vs SC = $8.3\% \pm 2.1$, $P = 0.0004$; $N = 4$; Figure 3-11E). In fact, the percentage of GFAP⁺ cells was surprisingly low in the serum-cultured cells with an average of only 8% of cells showing GFAP expression compared to ~50% in the serum-free astrocytes. This would suggest the increase in GFAP expression in serum-free human primary astrocytes could be due to an increase in the number of GFAP-positive astrocytes within the cultures.

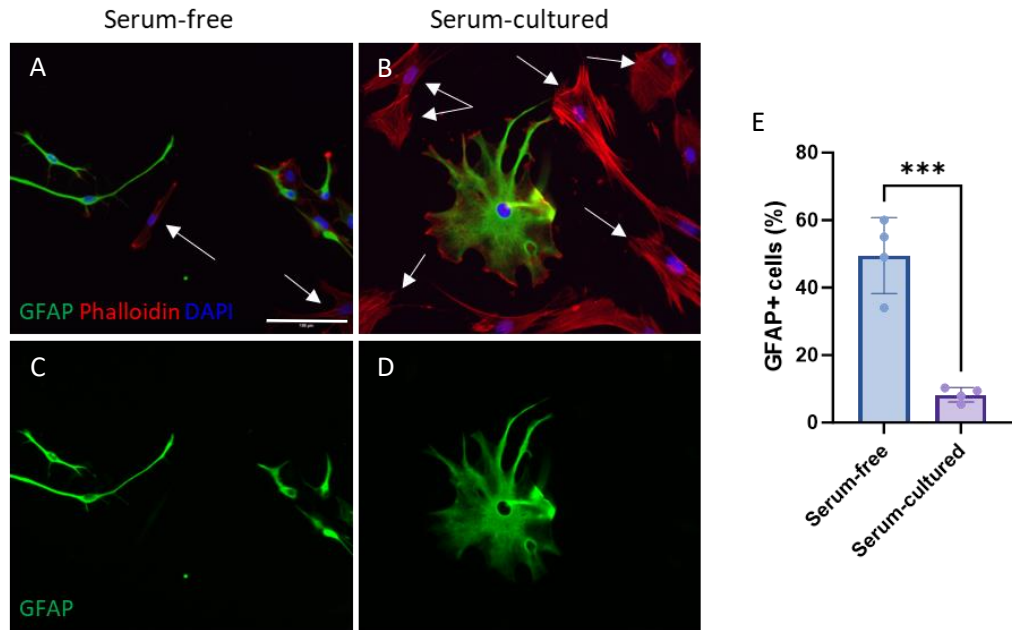


Figure 3-11 – The percentage of GFAP-positive cells is higher in serum-free human primary astrocytes compared to serum-cultures. (A-D) Representative ICC images of serum-free and serum-cultured human astrocytes stained with anti-GFAP, phalloidin and DAPI. White arrows highlight GFAP-negative cells (A and B). The percentage of GFAP-negative cells were counted using Phalloidin to distinguish cells. (E) An unpaired t-test showed a significant decrease in the percentage of GFAP-positive cells when astrocytes were cultured in serum compared to serum-free astrocytes (SF mean = 49.5% ± 11.3 vs SC = 8.3% ± 2.1, $P = 0.0004$; $N=4$). Images were taken at 20x magnification with the scale bar representing 100 μm . Error bars represent mean and standard deviation.

3.5.2 S100 β expression in serum-free and serum-cultured human primary astrocytes

S100 β is a brain-specific calcium binding protein, often elevated in neurodegeneration and brain injury, that is also commonly used as a marker of astrocytes (Rothermundt et al., 2003). Much like GFAP, S100 β expression is often associated with reactive astrocytes, but is typically expressed in different populations of astrocytes (e.g. some GFAP-negative astrocytes express S100 β ; Steiner et al., 2007). To compare S100 β protein expression in our human primary astrocyte cultures to GFAP expression, serum-free and serum-cultured astrocytes were co-stained with anti-S100 β and anti-GFAP antibodies (Figure 3-12, A-F). S100 β protein expression displayed different localisation within the cell compared to GFAP, with highest expression found in the nucleus. The majority of cells exhibited both GFAP and S100 β expression in both serum-free and serum-cultured astrocytes, but low levels of S100 β expression were also observed in GFAP-negative cells (Figure 3-12E and F, white arrows).

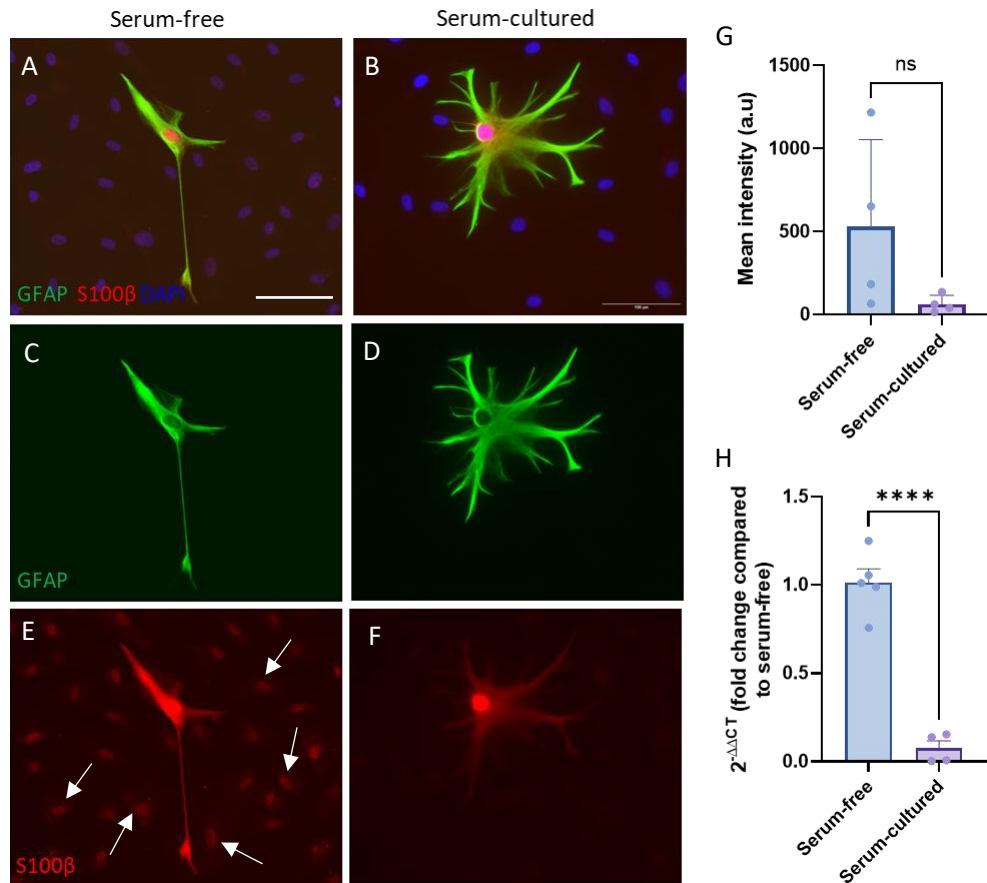


Figure 3-12 - S100β and GFAP co-expression in serum-free and serum-cultured human primary astrocytes. (A-F) Representative images of serum-free and serum-cultured human primary astrocytes shows GFAP and S100β expression overlaps. Whilst GFAP was limited to cytoplasmic staining in early passages (before P7), S100β was expressed throughout the cell, with much higher expression in the nucleus than in the cytoplasm. Some serum-free astrocytes also display low levels of S100β expression despite no GFAP expression (white arrows; E). (G) S100β protein expression measured using ICC staining showed a decreasing trend in serum-cultured astrocytes compared to the serum-free condition, however it was not statistically significant (SF mean = 529.6 ± 523.4 vs SC = 63.0 ± 52.1 , $P = 0.126$; $N = 4$). (H) RT-qPCR analysis found a significant decrease in S100β gene expression in serum-cultured cells compared to serum-free astrocytes (SF mean = 1.01 ± 0.18 vs SC = 0.08 ± 0.08 , $P < 0.0001$; $N = 5$). Statistical analysis was completed using unpaired t-tests with error bars representing mean and standard deviation. Images were taken at 20x magnification with scale bar representing 100 μm.

Unlike GFAP protein analysis, immunoblotting was not possible using the S100β antibody due to the antibody being pre-diluted by the supplier to be optimal for immunofluorescence. Therefore, to investigate changes in S100β protein expression between serum-free and serum-cultured human primary astrocytes, S100β staining intensity was measured through ICC (Figure 3-12G). Efforts were made to reduce bias by selecting areas for S100β analysis whilst viewing anti-EAAT2 co-staining in a different channel (i.e. when S100β staining was not visible). S100β protein expression showed a decreasing trend in serum-cultured astrocytes compared to serum-free astrocytes, however it was found to not be statistically significant (SF mean = 529.6 ± 523.4 vs SC = 63.0 ± 52.1 , $P = 0.126$; $N = 4$). This is likely due to the variability observed between replicates in the serum-free condition. To investigate S100β gene expression, RT-qPCR analysis was completed on the serum-free and serum-cultured astrocytes (Figure 3-12H). A significant decrease in S100β RNA expression was identified in serum-cultured astrocytes compared to serum-free

cultures supporting the decreasing trend observed in S100 β protein expression (SF mean = 1.01 ± 0.18 vs SC = 0.08 ± 0.08 , $P < 0.0001$; $N = 5$).

3.5.3 EAAT2 expression in serum-free and serum-cultured human primary astrocytes

A marker of astrocyte function is the glutamate transporter EAAT2 (GLT-1 in rodents) which is responsible for 90% of synaptic glutamate clearance (Lehre and Danbolt, 1998). Loss of EAAT2 is often observed in reactivity and neurodegenerative disease leading to reduced glutamate uptake and excitotoxicity (Pajarillo et al., 2019). To investigate whether our serum-cultured astrocytes may have reduced glutamate uptake compared to the serum-free astrocytes, EAAT2 expression was analysed using ICC, RT-qPCR and immunoblotting. ICC analysis identified EAAT2 expression throughout the cell in both serum-free and serum-cultured astrocytes, with low expression in the nuclei (Figure 3-13, A and B). Interestingly, RT-qPCR analysis found a significant decrease in EAAT2 gene expression in serum-cultured astrocytes compared to serum-free astrocytes (SF mean = 1.10 ± 0.61 vs SC = 0.008 ± 0.009 , $P = 0.033$; $N = 5$ Figure 3-13C). However, whilst a difference was observed when comparing gene expression, there was no difference in the protein expression of EAAT2 between serum-free and serum-cultured astrocytes after immunoblotting (SF mean = 73.8 ± 5.1 vs SC = 79.2 ± 12.1 , $P = 0.52$; Figure 3-13, D and E).

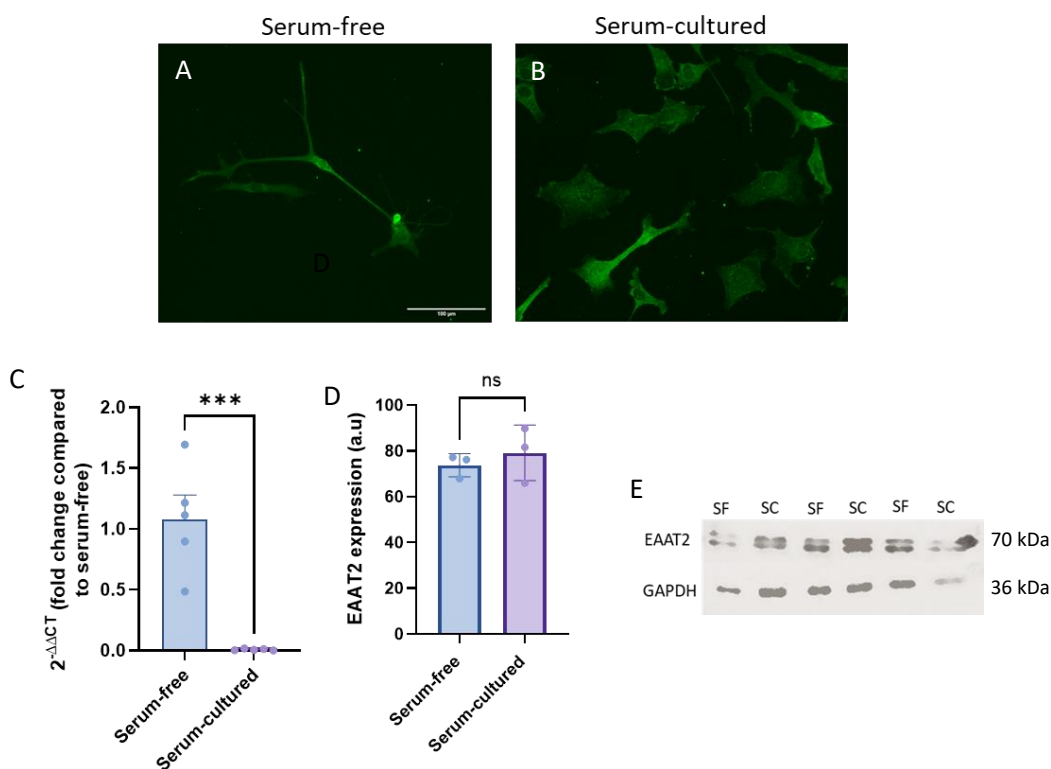


Figure 3-13 - EAAT2 expression in serum-free and serum-cultured human primary astrocytes. EAAT2 was detected in both serum-free and serum-cultured astrocytes using (A-B) ICC, (C) RT-qPCR and (D and E) immunoblotting. (C) A significant decrease in EAAT2 gene expression was found in serum-cultured cells compared to serum-free astrocytes (SF mean = 1.08 ± 0.4 vs SC = 0.008 ± 0.007 , $P = 0.0006$; $N = 5$). (D and E) No difference was observed during western blotting between the conditions after normalisation to GAPDH (SF mean = 73.8 ± 5.1 vs SC = 79.2 ± 12.1 , $P = 0.52$). Statistical analysis was completed using unpaired t-tests with error bars representing the mean and standard deviation.

3.6 Other markers of astrocyte reactivity

The expression of GFAP, S100 β and EAAT2 were investigated in the human primary astrocytes in detail because they are commonly used to characterise astrocyte phenotypes. However, as previously discussed (see section 1.3), there are no optimal astrocyte markers for reactive or quiescent states so there is a need to explore multiple markers when understanding astrocyte phenotypes (Escartin et al., 2021; Jurga et al., 2021). RT-qPCR analysis was completed on more novel astrocyte markers in the serum-free and serum-cultured human primary astrocytes. *NDRG2* expression, a marker for mature non-reactive astrocytes, *ITGA6* (CD49f), a proposed marker of astrocytes regardless of phenotype, and two interleukins *IL10* and *IL1 β* , both of which are released during inflammation, were chosen to investigate astrocyte reactivity (Flügge et al., 2014; Barbar et al., 2020). Three housekeeping genes were used for normalisation after finding no difference in their expression between conditions, GAPDH, B2M and β -actin (Supplementary figure 2).

No significant expression differences were found in any of the genes of interest, however a decreasing trend was observed in *NDRG2* expression in serum-cultured compared to serum-free astrocytes ($P = 0.0905$; $N = 5$; Figure 3-14). An increasing trend was observed in the expression of *IL-10* and *IL1- β* in the serum-cultured astrocytes compared to the serum-free astrocytes, however this was not statistically significant (*IL-10*, $P = 0.19$; *IL1- β* , $P = 0.25$; $N = 5$). This would suggest that the astrocytes in our model have a mixed inflammatory response (both anti-inflammatory and inflammatory cytokines) in response to serum.

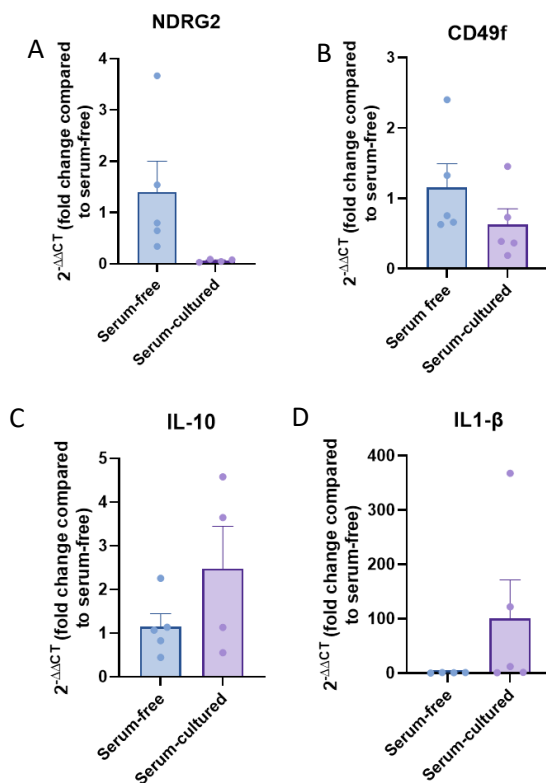


Figure 3-14 – Gene expression comparisons between serum-free and serum-cultured human primary astrocytes. No significant differences were identified after RT-qPCR analysis of (A) *NDRG2*, (B) *CD49f*, (C) *IL-10* and (D) *IL1- β* after normalisation to three housekeeping genes, GAPDH, B2M and β -actin. Error bars represent mean and upper standard deviation with statistical testing completed using unpaired t-tests ($N=5$). Fold changes were calculated based upon the mean Ct values for serum-free astrocytes.

3.7 Reactivity of serum-free human primary astrocytes in response to different stimuli

3.7.1 Changes in morphology of serum-free human primary astrocytes after acute (24 h) cytokine or FBS treatment

A key aspect of quiescent astrocytes is their ability to react to harmful stimuli, resulting in a phenotypic change in the cells (termed reactivity). With the serum-free human primary astrocytes potentially showing a quiescent phenotype, it was hypothesised that the astrocytes would change phenotype to better resemble the serum-cultured, 'reactive' human primary astrocytes when treated with a combination of cytokines (IL1 α , TNF α and C1q) previously shown to induce inflammatory reactivity in other studies (Liddelow et al., 2017; Barbar et al., 2020). Serum-free human primary astrocytes were cultured for a minimum of 14 days before the cells were treated for 24 h with either the cytokine cocktail (IL1 α at 3 ng/ml, TNF α at 30 ng/ml and C1q at 400 ng/ml) or 2% FBS, to determine if short-term exposure of serum could induce the same inflammatory reactivity as long-term chronic culture (serum-cultured astrocytes, see sections 3.3 and 3.5).

Reactive morphology was observed in the majority of astrocytes within the 2% FBS treated condition using both brightfield microscopy (live cell imaging) and fluorescent microscopy after ICC staining with anti-GFAP antibody (Figure 3-15, A-F). Astrocytes that were treated with 2% FBS had a significantly higher area/perimeter ratio than untreated cells, indicative of hypertrophic cell bodies, which better resembled serum-cultured astrocyte morphology (Untreated mean = 3.62 ± 1.15 vs FBS = 5.24 ± 0.61 , $P = 0.017$; $N = 6$; Figure 3-15G). Astrocytes treated with the cytokine cocktail had a more subtle morphological change than the 2% FBS treated condition with only an increasing trend observed in area/perimeter ratio (Untreated mean = 3.62 ± 1.16 vs Cytokine = 4.70 ± 2.08 , $P = 0.28$; $N = 6$).

With a decrease in GFAP expression previously observed in serum-cultured human primary astrocytes (see section 3.5.1), GFAP expression was analysed in the serum-free astrocytes treated with either the cytokine cocktail or 2% FBS for 24 h to determine whether their GFAP expression was more comparable to serum-free or serum-cultured human primary astrocytes. No difference was found in GFAP expression in either of the treated conditions compared to the untreated control, suggesting they are more similar to serum-free astrocytes after a 24 h treatment (Figure 3-15H-I). Measurements were normalised to the untreated control for each replicate in an effort to reduce the variation between replicates.

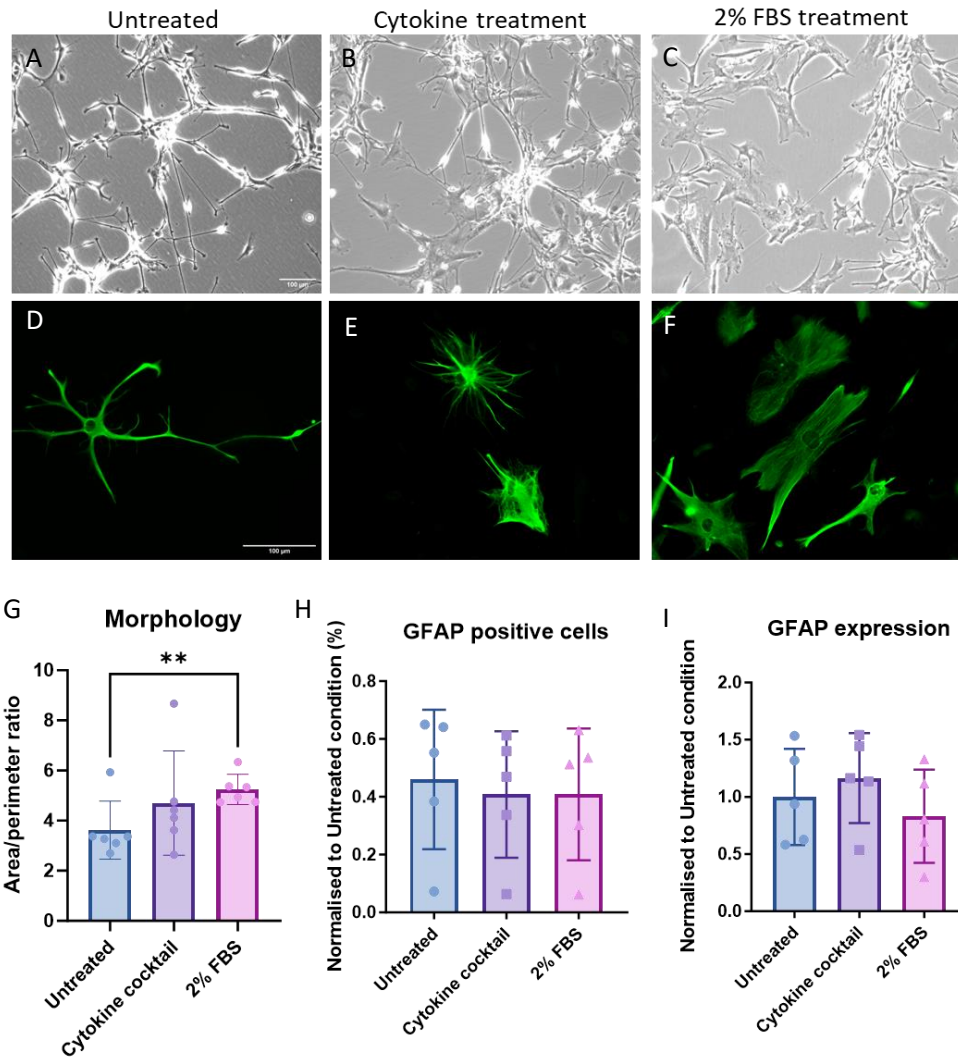


Figure 3-15 – Serum-free human primary astrocytes display changes in morphology but not GFAP expression after treatment with either a cytokine cocktail or 2% FBS for 24 h. (A-C) Representative brightfield images of serum-free human primary astrocytes after 24 h treatment with either a cytokine cocktail previously shown to elicit an inflammatory phenotype (IL1 α , TNF α and C1q), or 2% FBS. (D-F) Representative images of serum-free astrocytes stained with anti-GFAP antibody to measure GFAP expression after 24 h cytokine or 2% FBS treatment. (G) A significant increase in the area/perimeter ratio was observed in serum-free astrocytes treated with 2% FBS (Untreated mean = 3.62 \pm 1.16 vs FBS = 5.24 \pm 0.61, P = 0.004, N = 6). No significant increase was observed when astrocytes were treated with cytokines, however an increasing trend is observed (Untreated mean = 3.62 \pm 1.16 vs Cytokine = 4.70 \pm 2.08, P = 0.167, N = 6). No difference in GFAP expression was observed when (H) defining the percentage of GFAP positive cells, nor (I) the intensity of GFAP expression in the cells (N = 5). Due to high variability between biological replicates, GFAP expression was normalised to the untreated control in each replicate (H-I). Scale bars represent 100 μ m, with brightfield images taken at 10x magnification (A-C) and fluorescent images taken at 20x magnification (D-F). Data represents mean and standard deviation with one way ANOVA tests used to calculate statistical significance (G-I).

To determine whether the 24 h cytokine or 2% FBS treated serum-free astrocytes had a reactive transcriptome, gene expression of astrocyte markers (GFAP, S100 β , EAAT2, CD49f and NDRG2) and inflammatory markers (IL1- β , IL10 and TNF α) were investigated using RT-qPCR. As above, serum-free astrocytes were treated for 24 h with either the cytokine cocktail or 2% FBS before RNA was isolated from the cells

and processed for RT-qPCR. Three housekeeping genes were selected (GAPDH, actin and B2M) for normalisation.

To determine whether the housekeeping genes were suitable for normalisation, the Ct values were compared across conditions to identify any changes in the genes induced by the cytokine or FBS treatments (Figure 3-16). Both GAPDH and Actin expression remained consistent across the conditions with a difference of <1.5 cycles. On the other hand, B2M expression was found to vary by >3 cycles between the untreated condition and the cytokine condition (difference = 3.57) and was found to be significantly different ($P = 0.006$; $N = 8$). Therefore, only GAPDH and actin expression were used to normalise the genes of interest. The difference between the untreated and 2% FBS treated condition was found to be <1 cycle suggesting B2M can be used in future RT-qPCR when cytokine treatment is not used.

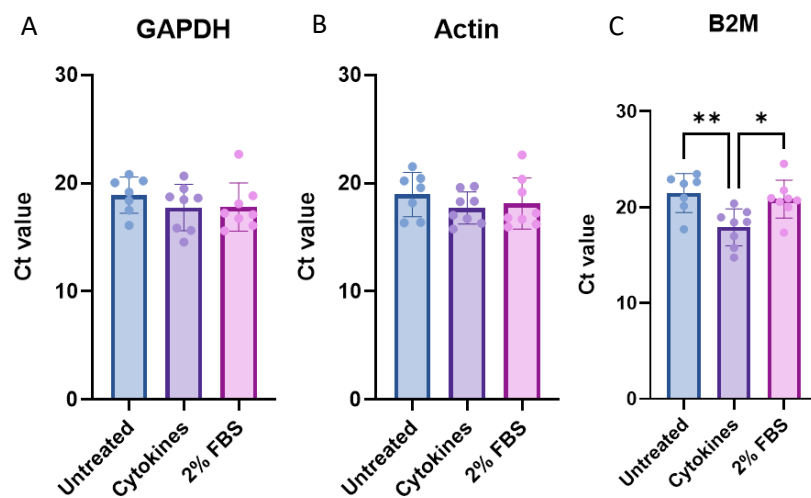


Figure 3-16 - Raw Ct values of GAPDH, Actin and B2M to determine suitability as housekeeping genes for RT-qPCR of human primary astrocytes treated for 24 h with cytokines or 2% FBS. Ct values of (A) GAPDH, (B) Actin and (C) B2M were compared across untreated, cytokine and 2% FBS treated conditions to determine whether their expression remain consistent. GAPDH and Actin both have < 2 cycle variation across all three conditions (GAPDH = 1.24, Actin = 1.23), but B2M had a difference of > 2 cycles when comparing untreated and cytokine-treated astrocytes suggesting it is not suitable as a housekeeping gene (B2M = 3.57, $P = 0.006$). Statistical analysis was completed using a One-way ANOVA followed by a Tukey's multiple comparison's test. Error bars represent mean and standard deviation with annotations displaying the mean value ($N = 8$).

After normalisation to the mean of the two suitable housekeeping genes, GAPDH and Actin, a fold change was calculated using the mean of the untreated condition for each gene of interest (Figure 3-17). No significant differences were identified in any of the astrocyte markers suggesting 24 h is not sufficient for transcriptional changes to have occurred, to compliment those observed in serum-cultured human primary astrocytes (see section 3.5). On the other hand, pro-inflammatory markers IL1- β and TNF α expression were found to significantly increase after cytokine treatment compared to the untreated control, supporting previous studies that show the cytokine cocktail induces an inflammatory response in the astrocytes (IL1- β $P = 0.008$; TNF α $P = 0.0095$; Liddelov et al., 2017; Barbar et al., 2020; Guttenplan et al., 2020). No difference between the untreated and FBS-treated astrocytes were found in these markers. No change in expression was observed in the anti-inflammatory marker IL10.

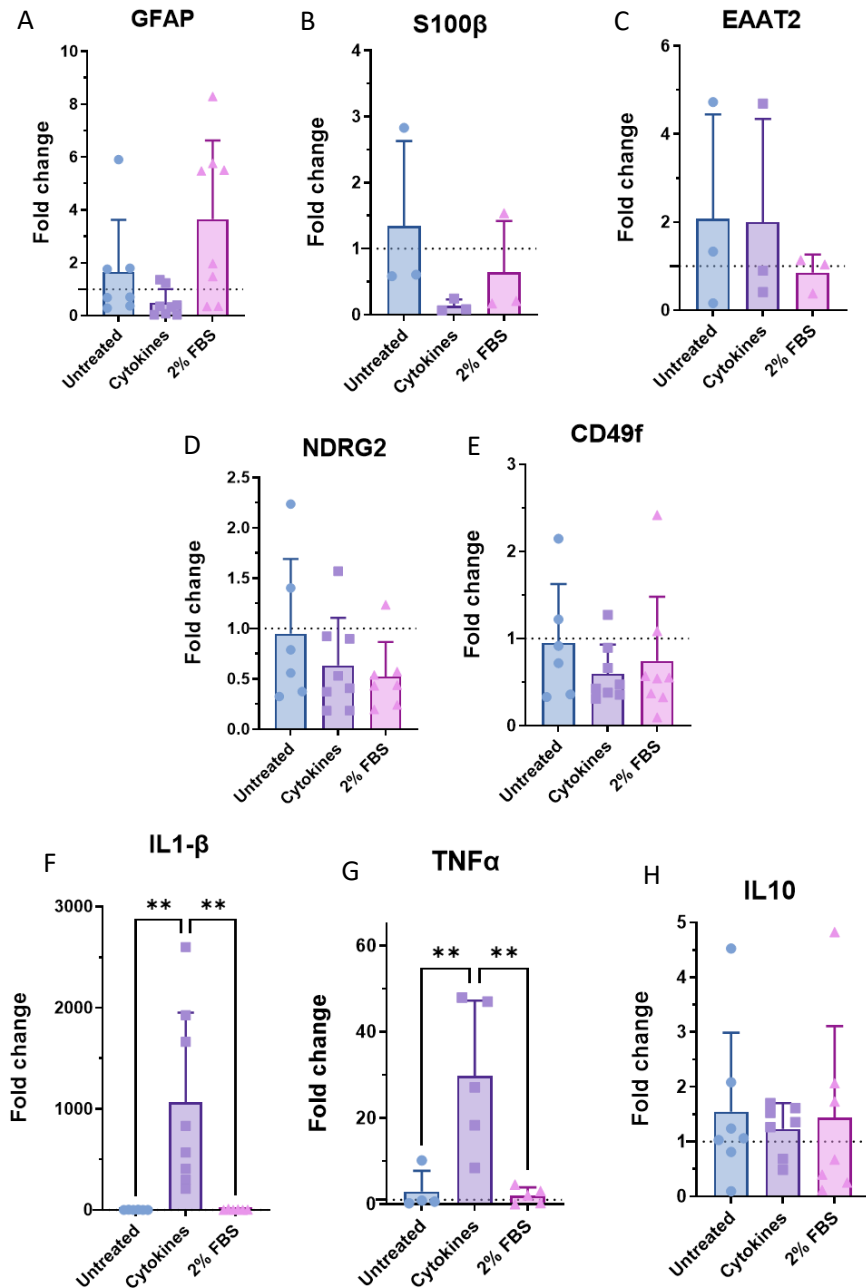


Figure 3-17 - RT-qPCR analysis of astrocyte markers and inflammatory cytokines in serum-free astrocytes treated with either 2% FBS or cytokines for 24 h. Genes of interest were normalised to housekeeping genes GAPDH and Actin, and then a fold change calculated using the mean of the untreated (serum-free) condition. (A-E) No significant differences were found in any of the astrocyte markers after statistical analysis. Pro-inflammatory markers (F) IL1-β and (G) TNFα were found to significantly increase in the cytokine treated condition but not the FBS treated condition (IL1-β untreated vs cytokine, $P = 0.0081$; TNFα untreated vs cytokine, $P = 0.0095$). (H) No difference was found in the anti-inflammatory marker IL10. Statistical analysis was carried out using a One-way ANOVA followed by Tukey's multiple comparisons test (For A, D-H, $N = 8$; For B and C, $N = 3$). Outliers were removed using ROUT's method ($Q = 1\%$). Data represents mean and upper standard deviation with annotations depicting the mean value.

3.7.2 Serum concentration affects reactive human primary astrocyte morphology

The results so far suggest that 2% FBS induces changes in the phenotype of human primary astrocytes that recapitulate pro-inflammatory reactivity. With 10% FBS also commonly used for astrocyte *in vitro* cultures, we examined whether these phenotypic changes were dose dependent. Serum-free human primary astrocytes were treated with either 2% or 10% FBS for 24 h with morphological changes assessed using brightfield imaging and ICC.

Distinct morphological changes were evident in the brightfield images taken 24 h after FBS treatments (Figure 3-18). Reactive phenotypes were seen in both of the FBS treated conditions, with astrocytes having hypertrophic bodies (measured by the area/perimeter ratio). A significant difference in the area/perimeter ratio can be seen in astrocytes treated with 2% FBS (Untreated mean = 3.15 ± 0.44 vs 2% = 5.07 ± 0.23 , $P = 0.0004$) and 10% FBS (Untreated mean = 3.15 ± 0.44 vs 10% = 5.89 ± 0.30 , $P < 0.0001$) compared to the untreated control. A significant increase in hypertrophy can be seen in the 10% FBS treatment compared to the 2% treatment ($P = 0.025$) suggesting FBS-induced reactivity is dose-dependent.

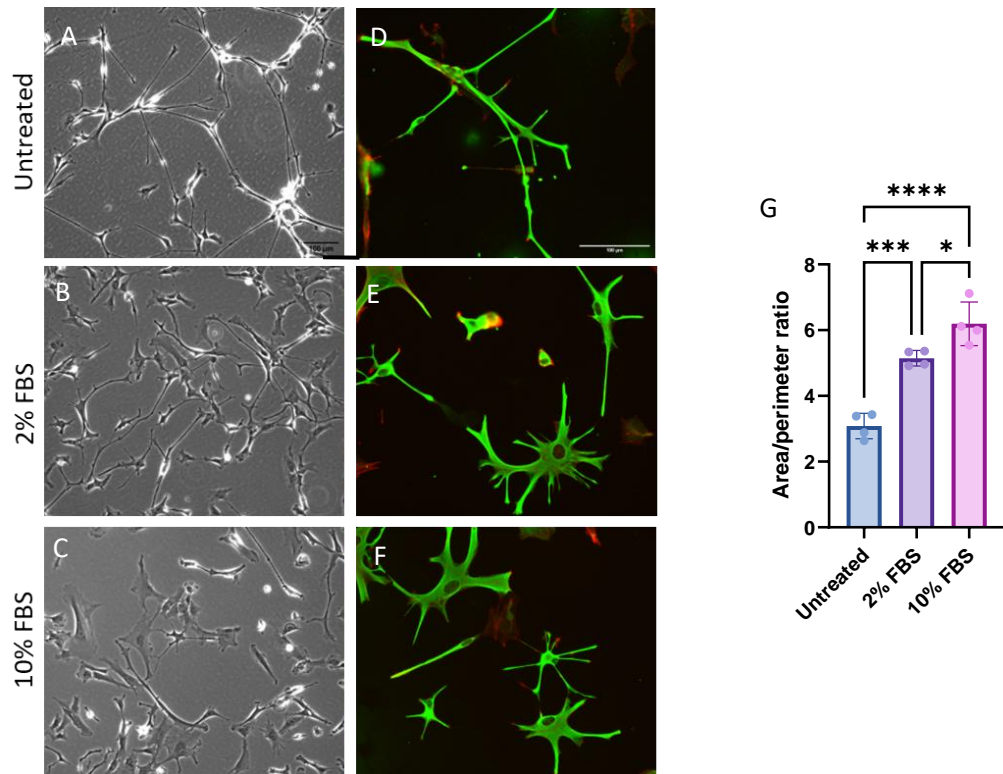


Figure 3-18 – 24 h treatment with higher concentrations of FBS (10%) cause a greater morphological change in serum-free human primary astrocytes than 2% FBS. (A-C) Representative brightfield images of serum-free human primary astrocytes after treatment for 24 h with either 2% FBS or 10% FBS. (D-F) Serum-free astrocytes stained with anti-GFAP antibody and phalloidin after 24 h treatment with either 2% or 10% FBS. (G) Morphology analysis using brightfield images shows a significant increase in the area/perimeter ratio after 24 h treatment with 2% FBS (Untreated mean = 3.15 ± 0.44 vs 2% = 5.07 ± 0.23 , $P = 0.0004$) and 10% FBS (Untreated mean = 3.15 ± 0.44 vs 10% = 5.89 ± 0.30 , $P < 0.0001$). A significant difference between 2% and 10% FBS treatments indicates a dose-response to FBS ($P = 0.025$). Significance was calculated using a one-way ANOVA followed by Tukey's multiple comparison's test. Error bars represent mean and standard deviation ($N = 4$). Scale bars represent $100 \mu\text{m}$ with brightfield images taken at 10x magnification and fluorescent images taken at 20x magnification.

3.7.3 Serum concentration does not affect the expression of astrocyte markers

With morphological changes observed in serum-free human primary astrocytes after treatment with 2% and 10% FBS for 24 hr, it was hypothesised that 10% FBS treatment may elicit a transcriptional change in the astrocytes to replicate the changes observed when astrocytes are cultured in serum (see section 3.5). Astrocyte markers GFAP and S100 β were selected due to the previous changes observed in serum-cultured astrocytes compared to serum-free astrocytes. A more novel astrocyte marker, CD49f, was also measured to investigate its suitability as a marker of astrocytes. Expression of inflammatory cytokines IL1 β and TNF α were also investigated alongside caspase-1 expression which matures pro-inflammatory IL1 β (Molla et al., 2020).

The Ct values of GAPDH, B2M and 18s were initially compared to determine their suitability as housekeeping genes for the current experiment (Figure 3-19). Both GAPDH and B2M were identified as reliable housekeeping genes with the difference between the untreated and FBS-treated conditions being < 2 Ct values (GAPDH = 1.86, B2M = 0.35). On the other hand, 18s was found to have high variation between replicates and the difference between the conditions was > 2 Ct values (2.48). Therefore, 18s was deemed not to be a reliable housekeeping gene and was excluded from analysis. Instead, the mean of GAPDH and B2M was used to normalise genes of interest.

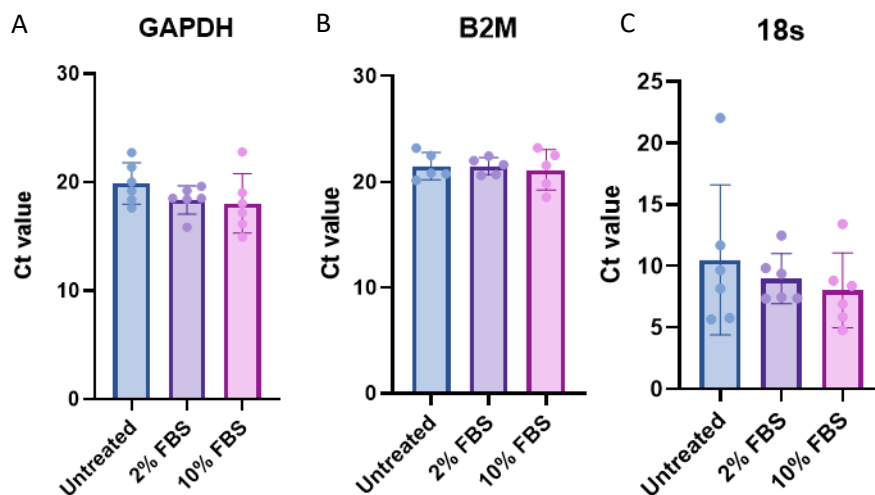


Figure 3-19 – Raw Ct values of GAPDH, B2M and 18s to determine suitability as housekeeping genes for RT-qPCR of human primary astrocytes treated for 24 h with 2% or 10% FBS. Ct values of (A) GAPDH and (B) B2M did not vary between conditions (difference is < 2 Ct values) and therefore could be used for normalisation of the genes of interest. (C) 18s varied between conditions with a difference of 2.48 between the untreated (serum-free) and 10% FBS condition. There was also higher variation between the replicates compared to the other housekeeping genes. Error bars show mean and standard deviation with annotations displaying the mean Ct value (N = 5).

With two reliable housekeeping genes identified, RT-qPCR was completed for the remaining genes of interest with fold change calculated using the mean of the untreated condition (i.e. serum-free astrocytes; Figure 3-20). No significant differences were identified in any of the genes of interest, likely due to the variability between replicates. The variability can be clearly seen within the untreated condition

for each gene, which would be expected to closely centre around 1 (baseline fold change for untreated conditions, dotted line).

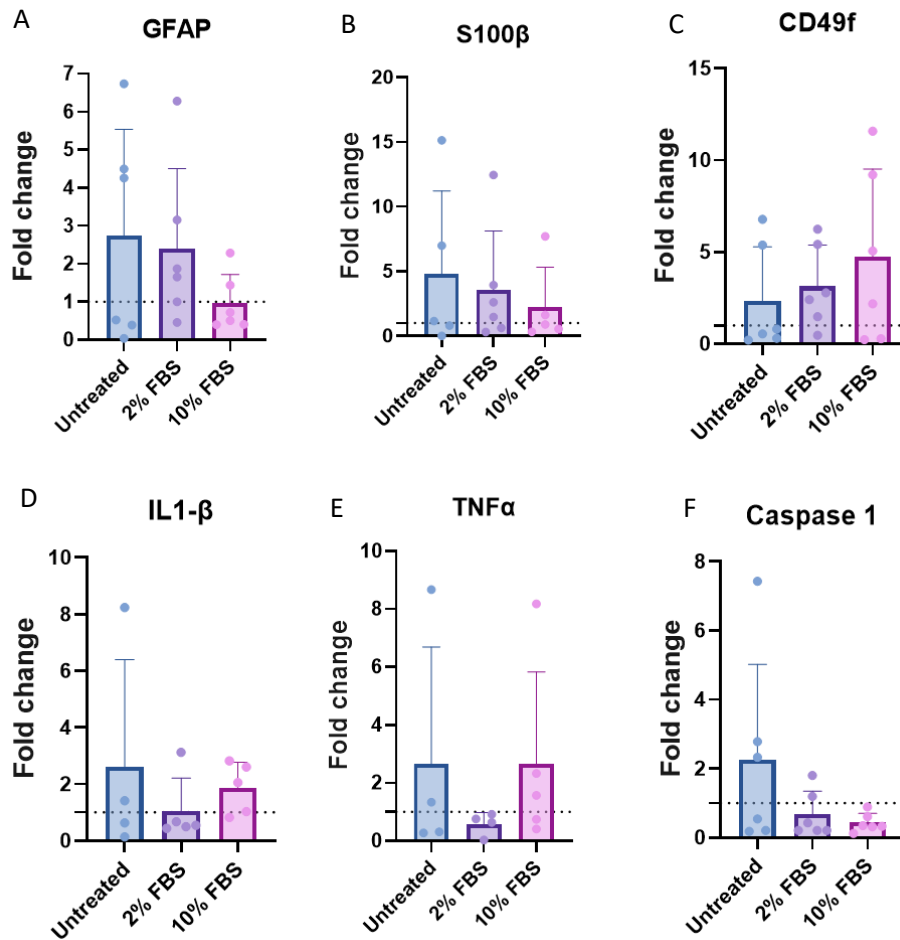


Figure 3-20 – No transcriptional differences in astrocyte markers and pro-inflammatory cytokines in serum-free human primary astrocytes after treatment with either 2% or 10% FBS for 24 h. (A) GFAP expression shows a decreasing trend after treatment with 10% FBS but due to high variation between biological repeats, this difference was not significant ($P = 0.336$). (B) S100 β expression shows a decreasing trend but was not significant (2% $P = 0.718$; 10% $P = 0.748$). No significant differences were found in (C) CD49f, (D) IL1- β , (E) TNF α or (F) Caspase-1. Normalisation was completed using the mean of the untreated condition for each gene of interest. Statistical analysis was completed using a mixed effects analysis followed by Tukey's multiple comparison's test ($N=6$). Annotation displays mean value and error bars represent mean and upper standard deviation.

3.7.4 Cytokines produced by astrocytes change in the presence of serum

The analysis so far suggests exogenous serum causes a reactive phenotype in human primary astrocytes with serum-free cultures maintaining a quiescent phenotype.

With a change in phenotype observed, changes in the secretome of the serum-free and serum-cultured astrocytes were predicted, given the astrocyte secretome has a critical role in the communication between cells in the CNS. A cytokine array containing antibodies for a range of growth factors, pro-inflammatory and anti-inflammatory cytokines was completed using conditioned media from both serum-free and serum-cultured human primary astrocytes. Serum-cultured astrocytes were incubated in FBS-free astrocyte medium for 72 h to remove any potential

contamination from the FBS itself. Figure 3-5 had previously showed incubation with serum-free media did not alter the phenotype of the serum-cultured astrocytes over this time frame.

Serum-free astrocyte conditioned medium had more cytokines present (23/105) than the serum-cultured astrocyte conditioned medium (7/105; Figure 3-21). Four cytokines were found in both conditions with SERPIN-E1 having a similar expression in both. IGFBP2 and Osteopontin had higher expression levels in the serum-free astrocyte conditioned media, whilst MCP-1 had a higher level of expression in the serum-cultured conditioned media. MCP-1 is an inflammatory cytokine which enhances the expression of other inflammatory factors and attracts inflammatory cells (Singh et al., 2021). Chitinase-3 like-1 is also highly expressed in the serum-cultured astrocytes with no expression observed in the serum-free astrocytes. This cytokine is primarily expressed by astrocytes and is increased in the neurotoxic reactive phenotype seen in inflammation and disease (Connolly et al., 2023; Song et al., 2024).

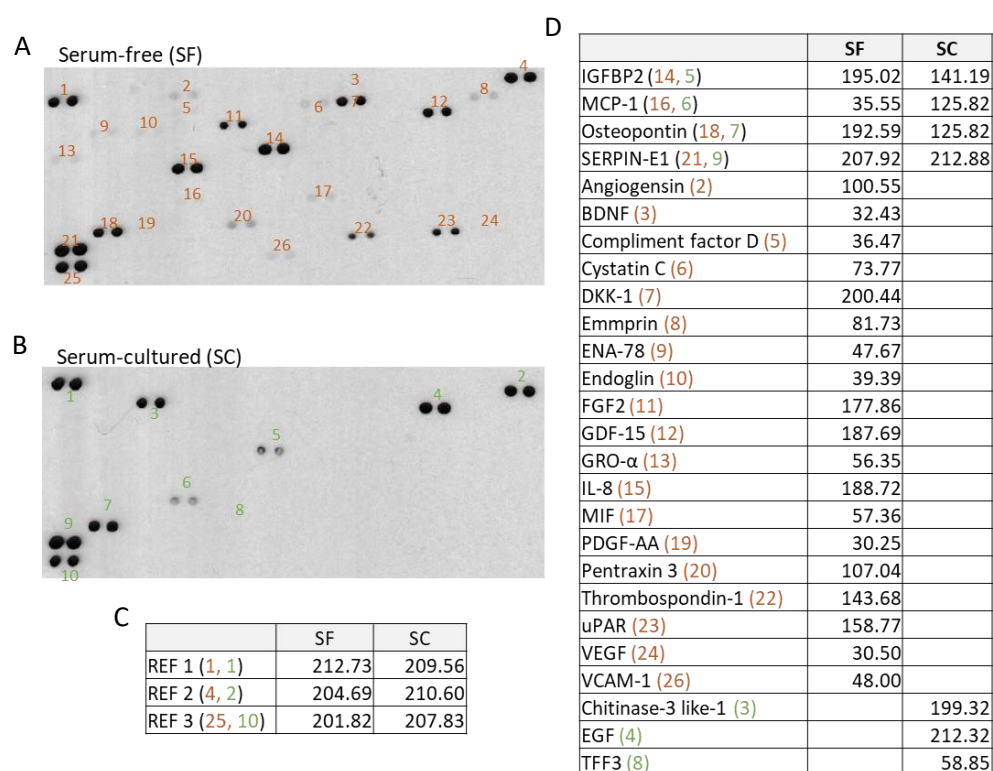


Figure 3-21 - Serum-free astrocytes have a more diverse secretome than serum-cultured astrocytes. (A) Serum-free astrocytes have more cytokines present in their conditioned media with 23/105 secretory proteins detected compared to (B) serum-cultured astrocytes which only detected 7/105. (C) Reference spots were used as a control. (D) Values represent mean intensity across duplicates for each cytokine (N = 1). Four proteins were detected in both conditions (IGFBP2, MCP-1, Osteopontin and SERPIN-E1) with SERPIN-E1 having similar expression across both conditions. IGFBP2 and Osteopontin had higher expression in the serum-free astrocyte conditioned medium, but MCP-1 was more highly expressed in the serum-cultured conditioned medium. Immunoblotting was captured with a 10 min exposure using enhanced ECL.

3.8 Discussion

3.8.1 Summary

In this chapter, serum-free culture of human primary astrocytes was characterised and found to recapitulate quiescent *in vivo* phenotypic traits when assessing morphology and their molecular and genetic phenotype. Using this model, the effect of serum on human primary astrocytes was also investigated with a distinct, reactive phenotype observed after culture in serum, with reduced expression of key astrocyte genes. During optimisation of the serum-cultured model, the effect of passage number on the morphology and transcriptome was also investigated with a distinct change in phenotype observed after passage 7. Therefore, all future work completed using the serum-cultured human primary astrocytes should be completed before passage 7 (ideally between passages 3-6) as a better comparator to the serum-free astrocyte cultures.

With the serum-free human primary astrocytes displaying quiescent features, their ability to react to stimuli, including FBS, was investigated. Astrocytes showed reactive phenotypes upon cytokine and FBS treatments and were also shown to have a dose-dependent response to FBS. Interestingly, the acute response of serum (serum-free astrocytes treated with FBS for 24 hr) differed to the chronic response (serum-cultured astrocytes) suggesting different mechanisms are occurring and potentially recapitulate a healthy reactive response (acute) compared to a pathological response (chronic). In the serum-cultured astrocytes, an increase in nuclear size and a reduction of astrocyte protein and gene expression (i.e. GFAP and S100 β) suggests a potentially mature or senescent phenotype.

Finally, the effect of serum on the secretome of the astrocytes was explored using a cytokine array. Much like the muted expression of astrocyte genes in serum-cultured astrocytes, fewer cytokines were detected in serum-cultured astrocyte conditioned medium. Whilst more cytokines would be expected to be released from reactive astrocytes due to their role in inflammation, many of the cytokines detected in serum-free astrocytes were found to be important growth factors and cytokines involved in homeostatic processes. Of those highly expressed in the serum-cultured astrocytes, MCP1 and chitinase-3 like-1 are potent inflammatory cytokines suggesting serum does cause a reactive, inflammatory phenotype.

3.8.2 Optimisation of a suitable serum-free medium for quiescent human primary astrocyte culture

In this work, serum-free medium has been confirmed to be able to maintain the human primary astrocytes in a quiescent, resting state in line with previous studies of serum-free rodent primary astrocyte cultures (Foo et al., 2011; Zhang et al., 2016; Prah et al., 2019). Our findings indicate that serum-free human primary astrocytes closely resemble the morphology of *in vivo* human astrocytes with long thin processes and a small cell body. This morphology was observed in all of the serum-free media compositions tested with the best condition found to be DMEM medium with G5 supplement. A limitation of this work is the lack of quantitative comparisons completed at this early optimisation stage. Whilst it is unlikely that morphological analysis would have shown a difference between serum-free media conditions which

was not observed through visual inspection, viability assays such as resazurin or MTT could have been completed to produce a quantitative comparison of astrocyte viability. Alongside the quiescent morphology and good viability observed in the DMEM G5 medium, G5 supplement was also chosen due to its astrocyte-focused composition. G5 supplement composition is clearly documented unlike supplements such as AGS or B27 supplement, making the supplement ideal for future analysis involving conditioned media and the ADEVs. Addition of other molecules could have been trialled, however the aim for this work was to optimise a simple, reproducible human astrocyte culture which was successful without the addition of further molecules.

3.8.3 Morphological analysis identifies distinct phenotypes in serum-free and serum-cultured human primary astrocytes

In contrast to serum-free human primary astrocyte cultures, serum-cultured astrocytes display a fibroblastic morphology with observable hypertrophy that has also been shown in other studies such as Prah et al (2019) using rodent cells, as well as enlarged nuclei. Morphological analysis was completed to quantify the hypertrophy, however with such a large difference in overall morphology observed between serum-free and serum-cultured astrocytes, the correct analysis needed to be identified to show the true difference in hypertrophy between the conditions. In Prah et al (2019), where a similar comparison was completed, cell area and the number of processes were analysed using a SNT plug-in. Whilst attempts were made to replicate this in the current work, morphology analysis was completed using brightfield images to avoid issues with ICC staining such as ensuring the entirety of the cell is stained, or artifacts caused by the ICC process (the fine processes observed in serum-free astrocytes were often damaged/folded during ICC). For example, GFAP stains the cell body and larger processes but often does not stain fine processes, and as shown in this work, GFAP is not highly expressed in all astrocytes. However, using brightfield images, the plug-in did not always detect the entirety of the cell or their processes due to a lack of contrast with the background.

There is also an issue with defining astrocyte processes. In particular, the serum-cultured astrocytes often had a bipolar morphology but it is not always clear where a process begins in order to start the measurements. In Prah et al (2019), the measurement started from the nuclei, however with serum-cultured astrocytes having a hypertrophic cell body, the actual processes of the astrocytes would in fact be much shorter than described using this method. For this reason, alongside the issues with measuring brightfield images using plug-ins, number or length of processes were not measured in the current study. Future work could attempt to measure differences in processes using live cell staining (such as membrane dyes), which would avoid any damage caused by the ICC process and allow automation of the measurement by plug-ins such as SNT.

Instead, cell area and perimeter were measured by manually tracing the astrocytes in FIJI software. Given the diversity in astrocyte morphology and the length of some astrocyte processes, particularly in the serum-free astrocyte cultures, the area/perimeter ratio was thought to be the most suitable measurement. This would

account for an increase in area caused by long processes, and therefore the measurement would better reflect cellular hypertrophy, rather than overall cell size. This measurement also confirmed the observations seen during visual inspection and therefore was used for the remainder of the work completed.

3.8.4 Serum causes changes in proliferation and nuclear size of human primary astrocytes

Serum-free human primary astrocytes displayed no proliferation throughout their culture with passaging not required. This supports observations made *in vivo* with mature astrocytes found not to proliferate unless in a reactive state (Colodner et al., 2005; Sofroniew and Vinters, 2010). Other studies have found that HB-EGF promotes astrocyte proliferation, but this was not found in this study when included in the NB and DMEM B27 cultures during serum-free optimisation (Foo et al., 2011; Puschmann et al., 2014; Prah et al., 2019). This may be due to the low concentration used in these media, and HB-EGF was not tested in the DMEM G5 media. Further work could investigate whether HB-EGF would encourage proliferation, however with mature astrocytes having limited proliferation abilities, the serum-free model used in this study is more representative of *in vivo* astrocytes.

On the other hand, serum-cultured astrocytes readily proliferated, particularly at low passages reminiscent of reactive astrocytes. The proliferation rate slowed with increasing passage number alongside other differences such as increasing nuclear size and reduced GFAP expression. Nuclear size is often used as a measure of senescence or maturation so alongside the reduced proliferation, we may suggest that either the increasing passage number or prolonged exposure to FBS causes a senescent phenotype in the later passages (Mitsui and Schneider, 1976; Heckenbach et al., 2022; Huang et al., 2022). Cellular senescence in the serum-cultured astrocytes was not explored further in this work, however investigation into senescent markers could be completed in the future. Instead, serum-cultured astrocytes were limited to passage 7 to avoid the senescent phenotype which complements other studies that have used the same human primary astrocytes (Baxter et al., 2021).

3.8.5 Cytokine treatment did not elicit a clear reactive response in serum-free human primary astrocytes

A cytokine cocktail of TNF α , IL1 α and C1q is commonly used to induce an inflammatory reactive phenotype in astrocytes (Liddelow et al., 2017; Guttenplan et al., 2020; Ziff et al., 2022). In this work, a morphology change was not observed when serum-free human primary astrocytes were treated with the cytokines for 24 hours, in contrast to treatment with 2% FBS. On the other hand, significant increases in the gene expression of IL1 β and TNF α were observed after cytokine treatment suggesting cytokines may cause a reactive phenotype in the astrocytes. The inclusion of the cytokine treatment in this work was to compare the serum phenotype to a well-documented 'A1' phenotype (Zamanian et al., 2012; Liddelow et al., 2017). A higher concentration of cytokines may elicit a stronger response leading to morphological changes as well as greater transcriptional changes, but this was beyond the scope of this work. Future work could the effect of hypoxia treatment on

human primary astrocytes which has previously been established as inducing an 'A2' protective phenotype (Zamanian et al., 2012).

3.8.6 Serum-free human primary astrocytes have a dose-dependent response to FBS

Whilst 2% FBS was used throughout this work for serum-cultured astrocyte culture due to this concentration being recommended by the supplier of the astrocytes, 24 h treatment with 10% FBS was shown to induce a more reactive phenotype than 2% treatment, indicating a dose-dependent increase. This has implications for studies that use high concentrations of FBS for astrocyte culture such as 10% or 15% FBS concentrations (for example, 10% FBS was used within Prah et al (2019)). Lower concentrations of FBS were not tested in the current work but it would be interesting to determine at what concentration reactivity is observed.

Interestingly, serum-free astrocytes treated with 2% FBS had a different transcriptional response than serum-cultured astrocytes despite the concentration of FBS remaining the same. This would suggest there is an acute and chronic response to serum which may reflect a healthy reactive response (treated) and a pathological response (cultured). Whilst not completed in the work, omics analysis of both FBS-treated and serum-cultured human primary astrocytes in comparison to the serum-free astrocytes would highlight how different these phenotypes are, but also allow a better comparison to disease-associated astrocytes.

3.8.7 Transcriptional differences between serum-free and serum-cultured human primary astrocytes

Surprisingly, when human primary astrocytes were cultured in 2% FBS (serum-cultured), GFAP expression was significantly lower than serum-free astrocytes when comparing both protein and RNA expression, in contrast with previous work comparing serum-free and serum-cultured rodent primary astrocytes (Roybon et al., 2013; Prah et al., 2019). GFAP is considered the gold-standard astrocyte marker and is well documented to increase in reactive astrocytes (Jurga et al., 2021; Kim et al., 2023). However, GFAP is not exclusive to astrocyte reactivity with higher concentrations identified in particular regions of the brain as well as during development (Roybon et al., 2013; Escartin et al., 2019, 2021). In fact, repetitive trauma was shown to decrease GFAP expression in mouse brains (Escartin et al., 2019).

GFAP expression is also not found in all astrocytes, with distinct populations expressing other markers such as S100 β (Walz and Lang, 1998; Jurga et al., 2021). Here we show that only 50% of serum-free and 10% of serum-cultured human primary astrocytes express high levels of GFAP. This difference in GFAP-positive populations may begin to explain the increased expression of GFAP in serum-free astrocytes as it may suggest higher GFAP expression is due to more GFAP-positive cells instead of individual astrocytes expressing more GFAP. This also shows the necessity of using multiple markers to assess astrocyte phenotypes instead of focusing solely on GFAP expression (Escartin et al., 2021; Jurga et al., 2021).

Notably, the expression of other well-known astrocytic genes (such as S100 β and EAAT2) were at least five-fold higher in serum-free human primary astrocytes compared to serum-cultured astrocytes. This may suggest that serum-cultured astrocytes preferentially focus on the production of proteins involved in cellular proliferation instead of more specific astrocyte markers. In contrast, when serum-free human primary astrocytes were treated with 2% FBS for 24 hours, GFAP was shown to increase, supporting evidence that GFAP expression increases in reactivity. This highlights the importance of understanding acute and chronic reactivity in astrocytes.

3.8.8 Overall limitations of the work

One of the greatest challenges with *in vitro* astrocyte culture is their immaturity with most models using embryonic and immature astrocytes. The human primary astrocytes used in this work are of foetal origin and therefore will likely behave differently to mature astrocytes. Neurodegenerative disease occurs in the ageing brain with age being the highest risk factor for spontaneous neurodegenerative disease. Therefore, using immature models does not accurately represent these aged astrocytes. Studies are working to induce a more mature phenotype but there is currently no widely used method to age these cells (Roybon et al., 2013; Savchenko et al., 2019; Hergenreder et al., 2024). To overcome this issue, any findings should be confirmed in *in vivo* models or in aged human tissue postmortem.

Another issue that was identified throughout this work was the reproducibility between replicates, particularly in RT-qPCR data. Large variation was observed in many of the studies, likely masking differences identified between conditions. To overcome this, the sample sizes of the studies were increased to reduce type 1 and type 2 errors. Another way to overcome this was to undertake similar experiments using different techniques to ensure consistency. For example, ICC staining allows semi-quantitative measurement of protein expression but can be subject to bias and issues with technical variation. Therefore, western blotting was also completed where possible to confirm any differences in protein expression. Both RNA and protein expression were measured which also validated any findings, however it is important to note that many post-translational modifications and pathways occur, meaning RNA expression does not always match protein expression (Morris and Mattick, 2014; Wang et al., 2014). This was observed in this study when measuring EAAT2 expression, indicating the importance of a multi approach analysis.

The cytokine array completed at the end of this chapter suffers from low sample size with only one replicate completed due to cost issues. Instead, this experiment was completed as a preliminary, exploratory analysis of astrocyte secretion with future work aiming to further investigate astrocyte secretions (ADEVs were the focus of the current thesis but many other proteins/RNA are secreted alongside).

3.8.9 Conclusions

Serum causes a reactive phenotype in human primary astrocytes which supports previous findings found in rat primary astrocytes (Prah et al., 2019). This chapter

details a serum-free human astrocyte culture which can survive for up to 4 weeks, and that displays many features of quiescent astrocytes with the ability to react to inflammatory stimuli. Whilst serum-free astrocytes are more difficult to work with due to a lack of proliferation, future work needs to move towards serum-free cultures when studying quiescent astrocyte function due to the permanent reactive changes induced by serum. Instead, this work has demonstrated a use for serum cultures when studying reactive or 'diseased' astrocytes.

The next chapter of this work continues to profile the serum-free and serum-cultured astrocytes but instead focuses on larger scale, unbiased omics analysis using RNA-sequencing and mass spectrometry. This will allow the identification of differentially expressed genes/proteins as well as differences in cellular pathways.

Chapter 4: Effects of serum exposure on the transcriptome and proteome of human primary astrocytes

4.1 Introduction

4.1.1 The importance of multi-omics analysis

The aim of the previous thesis chapter was to characterise the phenotypes of commercially available human primary astrocytes when cultured in both serum-free and serum-containing media, to establish a model of serum-induced reactivity. However, the molecular characterisation was completed using a candidate approach where genes and proteins of interest were selected based upon previous literature, such as GFAP and EAAT2. This approach is very useful when investigating specific pathways or targets within cells, but this only visualises changes in a few select genes/proteins and therefore does not provide detailed information on the overall molecular phenotype of astrocytes. Immunoblotting and ICC also rely on the availability of suitable antibodies, and only permit relative quantification of protein expression, so it is difficult to reliably compare expression between different proteins. Whilst several markers were explored in the previous chapter, it is unrealistic to investigate a large number of targets using these methods and therefore different methods must be applied to analyse the totality of genes and proteins within the human primary astrocytes.

In order to investigate changes in whole cellular pathways as well as quantify differences in gene and protein expression amongst many targets, omics-based analysis is required. As shown in the previous chapter, it is important to compare both gene and protein expression as not all changes in gene expression will correlate with protein expression due to post-transcriptional regulatory mechanisms such as nonsense-mediated decay (Greenbaum et al., 2003). For global gene expression analysis, RNA-sequencing was performed to identify changes in the transcriptome of serum-cultured astrocytes compared to the serum-free astrocytes. In parallel, protein mass spectrometry was then used to characterise protein expression in both serum-free and serum-cultured astrocytes.

4.1.2 RNA-sequencing

RNA-sequencing uses high-throughput, next-generation sequencing methods to provide quantitative snapshot of the cell transcriptome (Wang et al., 2009; Kukurba and Montgomery, 2015). Providing quantification of the mRNAs identified within the astrocyte 'RNAome', assumptions can be made as to which pathways are enriched within the cells and thus enables the characterisation of the molecular phenotype in human primary astrocytes. As well as providing details of mRNA transcripts, RNA-sequencing can also be applied to investigate small RNA such as miRNAs, tRNAs and ribosomal profiling (Holley and Topkara, 2011; Abbott et al., 2014). In this work, only mRNA was investigated with the analysis focused on protein-coding genes by using

polyA selection to enrich for mRNA. PolyA selection enriches mRNAs as well as non-coding RNAs that have polyA tails whilst reducing ribosomal RNAs (80% of total RNA) and pre-mRNAs in the sample (Chen et al., 2020).

4.1.3 Mass spectrometry

Liquid chromatography with tandem mass spectrometry (LC-MS/MS) allows the unbiased identification of large numbers of proteins within a sample, here providing a detailed picture of the astrocyte proteome, without the need to rely on antibody quality or target selection. Unlike RNA sequencing, quantification is traditionally more challenging with mass spectrometry due to a variety of factors. In order to detect proteins using mass spectrometry, proteins are fragmented into smaller, more manageable peptides before sequence detection which are then used to identify the original protein. This fragmentation process will not be the same for each protein with some proteins producing far more peptide fragments than others, which could easily be interpreted as more abundant than proteins with fewer fragments. On the other hand, some forms of mass spectrometry analysis, such as sequential window acquisition of theoretical mass (SWATH), have been developed in recent years to make relative quantification between samples possible.

In this work, two forms of protein mass spectrometry (conventional LC-MS/MS and SWATH-MS) will be completed to identify differences in the proteomes of serum-free and serum-cultured human primary astrocytes. Both forms of mass spectrometry use label-free, data-independent acquisition methods to produce a catalogue of proteins detected in the samples. Other data-dependent forms of mass spectrometry can be completed but require a list of targets to identify and quantify.

Conventional LC-MS/MS uses fragmentation (tryptic digestion and then physical fragmentation of peptides in a collisions cell) to identify peptide sequences of proteins within a sample, which can then be mapped to specific parent proteins. However, between runs, the analysis may dedicate different time windows to peptide sequencing, resulting in data that is at best only semi-quantitative. In contrast, SWATH-MS uses analysis windows of a fixed size to identify all peptides within frame and will spend the same time identifying each peptide within the window. This improves the accuracy and reproducibility of the analysis compared to conventional LC-MS/MS. This method also allows relative quantification between samples as all peptides are documented equally during analysis. However, due to the method of fragmentation, it is difficult to compare expression of different proteins, as some proteins will more easily fragment than others, leading to increased detection.

4.1.4 Aims of the chapter

This chapter aims to further characterise the phenotype of serum-free and serum-cultured human primary astrocytes using an unbiased multi-omics approach. Transcriptomic data will be collected using RNA-sequencing, and proteomic data collected using two types of mass spectrometry analysis (conventional LC-MS/MS and SWATH-MS). Comparisons will be made to previously published 'omics' datasets

of quiescent and reactive astrocytes to determine the validity of these findings. Only once the astrocyte models are fully characterised can their ADEVs be investigated and compared to these whole cell references (see chapter 5).

4.2 RNA-sequencing analysis of serum-free and serum-cultured human primary astrocytes

With transcriptional changes in candidate genes observed between serum-free and serum-cultured human primary astrocytes using RT-qPCR in the previous chapter, it was predicted that broader transcriptional changes would be observed, potentially distinguishing the astrocytes into quiescent and reactive phenotypes. Therefore, RNA was isolated from four biological replicates of both serum-free and serum-cultured human primary astrocytes before RNA sequencing was completed by Novogene (UK) to identify changes in the protein-coding transcriptome (mRNA). Briefly, data was mapped to the reference genome (*Homo sapiens*) and gene expression quantified to obtain FPKM values for each gene identified (see section 2.3.4 for more detail of RNA sequencing analysis).

4.2.1 Overall distribution of the samples

A principal component analysis (PCA) was first completed on the zFPKM values from the RNA sequencing data obtained from four biological replicates of serum-free and serum-cultured human primary astrocytes to determine the similarity between samples. A clear distinction was identified between the serum-free and serum-cultured astrocytes with 85.1% of the variation described by the first principal component (PC1; Figure 4-1). The four biological replicates from each condition were tightly clustered showing little variation between the samples. A small variation from the main clusters was seen in sample 8 and sample 1 for the serum-free and serum-cultured astrocytes respectively, however this difference is exaggerated by the PCA, with only 6.1% of the variation described by this principal component (PC2). Therefore, we can conclude that major differences in the transcriptome are observed when human primary astrocytes are cultured in serum compared to serum-free culture.

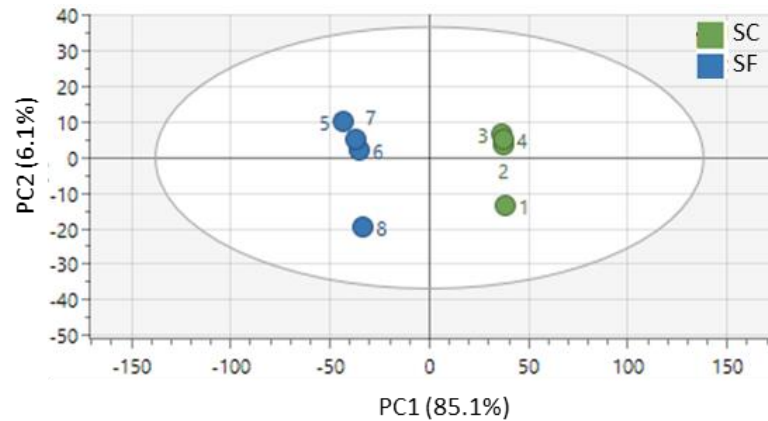


Figure 4-1 - Principal component analysis shows clear separation in mRNA expression between serum-free and serum-cultured astrocyte replicates. PCA shows a distinct difference between the transcriptomes of serum-free (blue) and serum-cultured astrocytes (green) with 85.1% of variation described by this principal component (PC1). Only 6.1% of the variation was described by the second principal component which accounts for variations between the biological replicates. Biological replicates were tightly clustered within each condition (N=4).

To identify which genes were most responsible for this difference between serum-free and serum-cultured astrocytes, a partial least squares discriminant analysis (PLS-DA) was completed. Of the top 20 genes identified during this analysis, *SRGN*, *KRT19*, *GPRC5A*, *IGFBP1*, *MMP*, *TRPC6* and *DSP* were highly expressed in serum-cultured astrocytes and *CHL1*, *DPYSL5*, *GRIK3*, *A2M*, *PMP2*, *LMO*, *C1orf61*, *MLC1*, *S100B*, *SORCS1*, *PTPRZ1*, *SPARCL1* and *ATP1B2* were more highly expressed in serum-free astrocytes (Figure 4-2). Interestingly, the observation for *S100B* supports RT-qPCR data obtained in chapter 3 where a significant difference in *S100B* gene expression was found between serum-free and serum-cultured astrocytes (see Figure 3-12G).

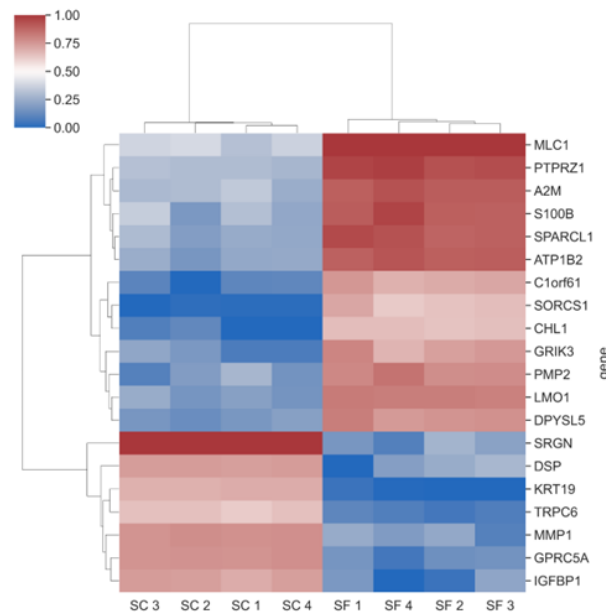


Figure 4-2 – Partial least squares discriminant analysis identified the 20 most influential genes on the separation of serum-free and serum-cultured astrocyte transcriptomes. Of the 20 genes identified, 13 genes were found to be highly expressed in the serum-free astrocytes and 7 identified as highly expressed in serum-cultured astrocytes. Red indicates high expression and blue, low expression in each of the biological repeats (SC = serum-cultured, SF = serum-free; N=4). Both samples and genes were clustered based on similarity using hierarchical clustering.

Due to the polyA enrichment completed during the RNA sequencing, the majority of RNA detected was identified as corresponding to protein-coding genes. These protein-coding genes were then filtered to identify RNA that was present in multiple biological replicates to increase confidence in the mRNA that was detected for each condition (Figure 4-3). The majority of RNA detected was identified in all 4 replicates (> 80%) suggesting high similarity between the replicates. Only protein-coding RNAs identified in at least 2 replicates (i.e. 50% of replicates) were included in downstream analysis.

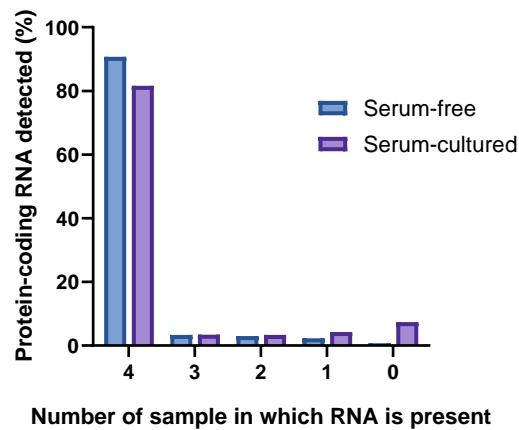


Figure 4-3 - The majority of protein-coding mRNAs were identified in all 4 replicates of serum-free and serum-cultured human primary astrocytes. Protein-coding mRNA was filtered based upon the number of biological replicates that each mRNA was identified in. The majority of mRNA was identified in all 4 replicates with less than 20% of the data found in 3 replicates or less. More unique mRNAs were identified in the serum-free condition, with 7.35% of total mRNA detected not being identified in any of the serum-cultured samples. Percentages were calculated using the total number of RNA detected across both serum-free and serum-cultured conditions.

After removal of mRNA which were not detected in 2 or more of the biological replicates, 11,273 protein-coding genes were identified in the serum-free astrocytes and 10,107 protein-coding genes identified in the serum-cultured astrocytes (Figure 4-4). Of these genes, 9630 were identified in both conditions (82% of total genes) suggesting similar mRNAs are expressed in the astrocytes, with differences between conditions likely due to differential expression of these genes. Of those exclusively identified in each condition, 1643 unique mRNA were exclusively identified in the serum-free astrocytes and 477 identified in the serum-cultured astrocytes.

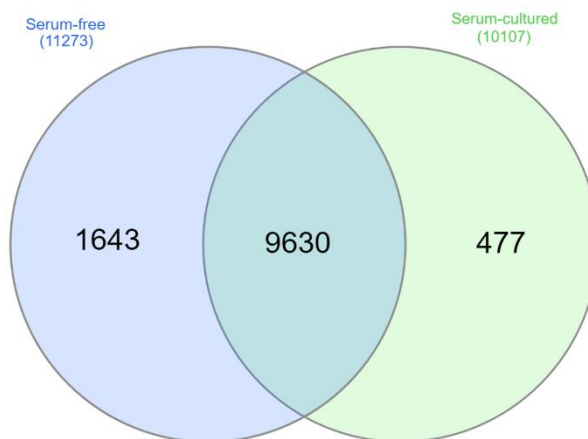


Figure 4-4 - The majority of protein-coding mRNAs were identified in both serum-free and serum-cultured astrocytes. A total of 11,750 protein-coding mRNAs were identified in the RNA-sequencing of the astrocytes with the majority identified in both conditions (9630, 82%). 1643 mRNAs were identified exclusively in the serum-free astrocytes and 477 genes exclusively in the serum-cultured astrocytes.

4.2.2 Differentially expressed genes in serum-free and serum-cultured human primary astrocytes

Whilst the analysis of exclusively detected mRNAs can identify key genes involved in each astrocyte phenotype, this mostly describes genes that are expressed at low levels (low readcounts). It is more likely that transcriptional changes between phenotypes will occur through the upregulation or downregulation of genes, rather than cells expressing 'new' mRNA. To investigate differential expression across both astrocyte conditions, statistical analysis was completed on the protein-coding RNAs identified within the samples. Genes with ≥ 2 -fold increase in either condition were identified as differentially expressed. Due to the high number of differentially expressed genes across the conditions, a false discovery rate (FDR; q value) was calculated to reduce the number of false positives.

Using a cut-off of $< 1\%$ FDR, 6134 genes were identified as differentially expressed, with 3602 found to be more expressed in the serum-free astrocytes and 2532 found to more expressed in the serum-cultured astrocytes (Figure 4-5, A and B). This means more genes were downregulated in serum-cultured astrocytes. Interestingly, *AQP4*, a homeostatic gene in astrocytes, was found to be very highly expressed in serum-free astrocytes compared to serum-cultured, with the gene found to be the 5th most differentially expressed gene in serum-free astrocytes (Figure 4-5C).

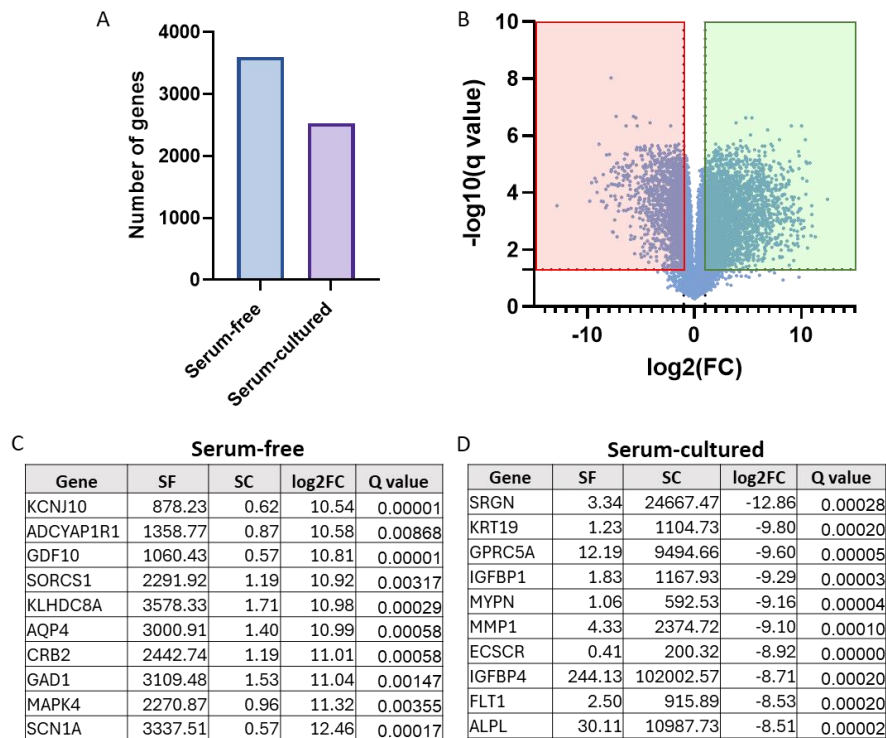


Figure 4-5 - Differential expression of protein-coding genes in serum-free and serum-cultured astrocytes. (A) Number of genes significantly upregulated in serum-free and serum-cultured astrocytes with a fold change ≥ 2 . (B) Volcano plot of all protein-coding genes identified in at least 2/4 biological repeats of both conditions. Genes found within the red region are significantly upregulated in serum-free astrocytes and genes found within the green region are significantly upregulated in serum-cultured astrocytes. (C) The 10 most differentially expressed genes that are upregulated in serum-free astrocytes. (D) The 10 most differentially expressed genes that are upregulated in serum-cultured astrocytes. Values within the SF (serum-free) and SC (serum-cultured) columns represent average zFKPM values from the four biological replicates. Significance was calculated using multiple t tests and corrected for by a two-step approach (Q value; Benjamini et al., 2006).

Other common astrocyte markers (listed in Table 1-1) were highlighted in the RNA sequencing data, in order to probe changes between human primary astrocyte phenotypes. This also allowed validation of the findings by RT-qPCR completed during Chapter 3 (see sections 3.5 and 3.6). The majority of astrocyte markers were found to be upregulated in serum-free astrocytes compared to serum-cultured astrocytes with only *CD44* and *VIM* remaining consistent between conditions, further supporting evidence of a global reduction in astrocyte markers in the serum-cultured astrocytes after 2 weeks in serum culture (Table 4-1). Only *CXN-43* (a gap junction protein) was found to increase in serum-cultured astrocytes potentially suggesting increased adherence between cells. These findings were also compared to RT-qPCR data published by Prah *et al.* (2019) comparing serum-free and serum-cultured (10% FBS) rodent primary astrocytes. Most astrocyte markers followed the same trend as those measured in the Prah study with the exception of *GFAP* and *AQP4* (shown by red arrows in Table 4-1, direction of arrows indicates the direction of expression described if cultured in serum). The RNA-sequencing also matched our previous RT-qPCR data described in chapter 3 (sections 3.5 and 3.6), however with a greater difference observed between conditions during the RNA sequencing. This may be due to the lower variability between biological replicates in the RNA sequencing compared to the RT-qPCR.

Inflammatory markers were also analysed based upon the RT-qPCR data of the Prah study as well as our own. IL1- β and IL-6 were found to be significantly upregulated in serum-cultured astrocytes suggesting they have a more inflammatory-reactive like phenotype, confirming RT-qPCR evidence (Table 4-1). TNF α and LCN2 were not identified in the RNA-sequencing analysis and IL10 was only found in serum-free astrocytes at a low expression.

Table 4-1 - Expression of astrocyte and inflammatory markers in serum-free and serum-cultured astrocytes in comparison to RT-qPCR data from Prah et al. (2019) and RT-qPCR analysis completed in Chapter 3. Of the astrocyte markers described in Table 1-1, the majority were upregulated in serum-free astrocytes with only CD44 and VIM remaining consistent between conditions. Of those measured in Prah et al (2019), most follow the same trend (green arrows) with the exception of GFAP and AQP4 (Red arrows). Inflammatory markers IL1- β and IL-6 were found to be upregulated in the serum-cultured astrocytes suggesting an inflammatory phenotype, which matched findings within the Prah study. RT-qPCR results completed in chapter 3 were confirmed by the RNA-sequencing analysis with significance found to be higher in RNA-sequencing than in RT-qPCR. Direction of arrows indicates the direction of expression change identified after culture in serum within the Prah study and our previous RT-qPCR data.

Gene	Serum-free	Serum-cultured	Log2(FC)	Q value	Prah et al, 2019	RT-qPCR
GFAP	48829.738	392.238	6.9606	0.000026	↑ Significant, P < 0.01	↓ Significant, P = 0.0093
S100B	3512.853	5.691	9.3547	0.000142	↓ Not significant	↓ Significant, P < 0.0001
ALDH1L1	124.949	9.459	3.7543	0.000804	No change	Not measured
EAAT1	22821.510	502.619	5.5060	0.000042	↓ Not significant	Not measured
EAAT2	2115.837	39.988	5.7412	0.00019	↓ Significant, P < 0.01	↓ Significant, P = 0.006
GS	10374.045	3983.426	1.3810	0.000145	↓ Significant, P < 0.05	Not measured
CD44	14450.047	17316.748	-0.2611	0.093089	Not measured	Not measured
NDRG2	405.330	17.597	4.5217	0.007735	Not measured	↓ Not significant
CD49f	4172.112	786.268	2.4077	0.000094	Not measured	↓ Not significant
AQP4	3000.906	1.399	10.9932	0.00058	↑ Not significant	Not measured
CXN-43	12116.513	34473.837	-1.5085	0.000084	↑ Significant, P < 0.05	Not measured
VIM	56785.661	67571.300	-0.2509	0.241716	↑ Significant, P < 0.05	Not measured
IL1-B	0.634	12.398	-4.3055	0.002145	↑ Not significant	↑ Not significant
IL6	7.008	29.249	-2.0618	0.012537	↑ Significant, P < 0.05	Not measured

4.2.3 Pathway analysis of differentially expressed genes in serum-free and serum-cultured human primary astrocytes

With differentially expressed genes identified, pathway analysis was completed to identify the biological pathways of human primary astrocytes that were impacted following chronic serum exposure. Pathway analysis was completed using the Kyoto Encyclopaedia of Genes and Genomes (KEGG) database. A total of 23 pathways were significantly upregulated in serum-free astrocytes compared to serum-cultured astrocytes including key homeostatic functions such as calcium signalling, axon guidance and, synaptic pathways (i.e. GABAergic, glutamatergic and cholinergic) suggesting key functions associated with quiescent astrocytes are reduced in after culture in serum (Figure 4-6A). There was also an increase in specific metabolic pathways such as alanine, aspartate and glutamate metabolism in serum-free quiescent astrocytes. Alanine is involved in ammonia detoxification produced during the glutamate/glutamine recycling process and therefore is vital for homeostatic functions in astrocytes (Dadsetan et al., 2013; Voss et al., 2021).

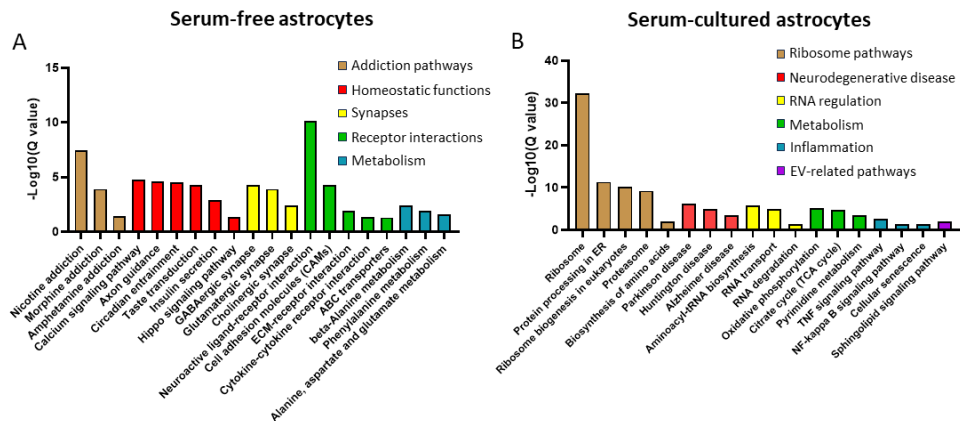


Figure 4-6 – KEGG pathway analysis of serum-free and serum-cultured human primary astrocytes suggests pathway differences in quiescent and reactive phenotypes, respectively. (A) Serum-free astrocytes were found to have 23 significantly upregulated pathways, with many pathways involved in homeostatic functions or synapse-related functions, suggestive of a quiescent phenotype. (B) Serum-cultured astrocytes were found to have 46 significantly upregulated pathways including a range of neurodegenerative diseases, protein-processing pathways and inflammatory pathways, suggestive of a reactive phenotype. Pathways relevant to astrocyte biology were categorised (see key) to allow easier visualisation of upregulated pathways.

In contrast, 46 pathways were significantly upregulated in serum-cultured astrocytes (Figure 4-6B). Protein production and processing pathways were upregulated such as ribosome pathways, protein processing in the endoplasmic reticulum, and the proteasome pathway. There was also an increase in a range of metabolic pathways such as oxidative phosphorylation, the TCA cycle, purine, pyrimidine and carbon metabolism. A range of disease pathways were also up-regulated such as HIV infection, Alzheimer’s disease, Parkinson’s disease and Huntington’s disease. Reactive astrocyte phenotypes are observed within these diseases suggesting the current astrocytes may replicate this reactive phenotype after serum culture. As well as disease pathways, TNF and NF-κB signalling were increased suggesting the serum elicits an inflammatory phenotype. Cellular senescence was significantly upregulated supporting nuclear size increases compared to serum-free astrocytes observed during passaging (see Figure 3-4).

4.2.4 Comparison of serum-free and serum-cultured astrocyte phenotypes to published ‘A1’ and ‘A2’ astrocyte phenotypes

A simplified explanation of astrocyte reactivity was proposed by Liddelw *et al.* (2017) to describe the range of opposing functions observed in astrocytes (see section 1.1.2.1 for more details). ‘A1’ astrocytes are described as having an inflammatory phenotype and ‘A2’ astrocytes are described with anti-inflammatory functions. To identify whether the serum-cultured astrocytes better resemble the ‘A1’ or ‘A2’ phenotype, a set of 38 reactive markers commonly used to describe astrocyte reactivity were assessed (Figure 4-7). Pan-reactive genes are genes that are identified in reactive astrocytes regardless of phenotype and include common astrocyte markers such as *GFAP* and *Vimentin* (*Vim*). The majority of these markers showed similar expression between the serum-free and serum-cultured astrocytes with the exception of *GFAP* and *CP* which were highly upregulated in serum-free astrocytes (Figure 4-7A). *STEAP4*, *CXCL10* and *SERPINA3* were also more highly expressed in the serum-free astrocytes however these genes were not highly

expressed in either astrocyte cultures. Five other markers, including *S1PR3* and *HSPB1* were more highly expressed in the serum-cultured astrocytes suggesting a more reactive phenotype compared to the serum-free astrocytes.

Of the 13 'A1' inflammatory genes, 6 were found to have higher expression in the serum-cultured astrocytes compared to the serum-free astrocytes (Figure 4-7B). In contrast, only 3 genes had higher expression in the serum-free astrocytes, further confirming the more reactive phenotype of the serum-cultured astrocytes. The greatest difference between serum-free and serum-cultured astrocytes was observed in the A2 reactive markers with many of the 'A2' markers found to be more highly expressed in serum-cultured astrocytes (Figure 4-7C). In contrast to previous work using cytokine treatments or hypoxia models, the serum-cultured astrocytes had high expression of both A1 and A2 astrocyte markers suggesting a more complex reactive phenotype than other astrocyte models using cytokines to initiate inflammation, or hypoxia to stimulate an A2 response (Zamanian et al., 2012; Liddelow et al., 2017a; Sancho et al., 2022; Ziff et al., 2022). This is more similar to a disease phenotype where both inflammatory and anti-inflammatory responses are observed simultaneously (Ziff et al., 2022). In summary, serum-cultured astrocytes display a combination of characteristic A1 and A2 reactive transcriptomes in comparison to serum-free astrocytes suggesting FBS elicits a complex reactive phenotype, which is similar to the complex reactive response observed in disease.

A		SF	SC	Log ₂ (FC)
Pan-reactive	LCN2	X	X	
	STEAP4	13.18	X	-3.72
	S1PR3	1355.34	4352.42	-1.68
	TIMP1	9962.51	10873.31	0.13
	HSPB1	5755.76	13805.56	1.26
	CXCL10	4.95	0.57	-3.11
	CD44	14450.05	17316.75	0.26
	OSMR	3721.80	6259.97	0.75
	CP	283.44	0.91	-8.28
	SERPINA3	9.17	2.20	-2.06
	ASPG	X	X	
	VIM	56785.66	67571.30	0.25
	GFAP	48829.74	392.24	-6.96

B		SF	SC	Log ₂ (FC)
A1 - Inflammatory	C3	4.53	3.55	-0.35
	HLA-A	8957.34	6285.69	-0.51
	HLA-B	5610.79	11989.06	1.10
	HLA-C	8182.99	9667.36	0.24
	SERPING1	760.85	277.45	-1.46
	GGTA1	X	X	
	GBP2	291.56	37.91	-2.94
	FBLN5	1406.50	1223.65	-0.20
	UGT1A1	X	X	
	FKBP5	544.72	8974.89	4.04
	PSMB6	2292.12	4365.25	0.93
	SRGN	3.34	24667.47	12.85
	AMIGO2	1601.29	3452.81	1.11

C		SF	SC	Log ₂ (FC)
A2 - Anti-inflammatory	S100A10	2217.14	8663.76	1.97
	EMP1	6033.34	12082.83	1.00
	CLCF1	140.54	597.81	2.09
	TGM1	83.82	25.52	-1.72
	PTX3	453.90	9029.55	4.31
	SPHK1	322.33	3410.40	3.40
	CD109	1143.35	3481.88	1.61
	PTGS2	165.40	200.65	0.28
	SLC10A6	1.68	X	-0.75
	TM4SF1	625.58	6839.18	3.45
	B3GNT5	678.33	1283.62	0.92
	CD14	9.46	26.91	1.51

Figure 4-7 - Serum-cultured astrocyte transcriptome resembles both 'A1' and 'A2' reactive astrocyte phenotypes defined by Liddelow et al (2017). (A) Many of the pan-reactive genes have similar expression across both astrocyte cultures (e.g. *TIMP1* and *VIM*) or were lowly expressed in the astrocyte cultures (e.g. *STEAP4* and *SERPINA3*). The majority of (B) A1 and (C) A2 reactive astrocyte markers were upregulated in serum-cultured astrocytes suggesting the serum-cultured astrocytes have a reactive phenotype compared to the serum-free astrocytes. Green indicates an upregulation in serum-cultured astrocytes. Red indicates an upregulation in serum-free astrocytes. Numbers for serum-free (SF) and serum-cultured (SC) astrocytes indicate average zFKPM values. These were then log₂ transformed to calculate log₂ fold changes in comparison to the serum-free astrocytes.

4.3 Proteomic analysis by LC-MS/MS analysis

It is clear from the RNA sequencing analysis that the serum-free and serum-cultured astrocyte transcriptomes vary considerably, which is solely due to differences imparted by culture medium composition (given the cells originate from the same vial). Whilst changes in RNA expression do not always result in a corresponding proteomic change, differences in the proteomes of the serum-free and serum-cultured astrocytes would be expected given the magnitude of difference observed in the transcriptomes. Therefore, LC-MS/MS was completed on 20 µg of protein from whole-cell lysates of serum-free and serum-cultured human primary astrocytes.

4.3.1 Protein identification in serum-free and serum-cultured human primary astrocyte whole-cell lysates

LC-MS/MS was completed by the Cambridge Centre for Proteomics (Cambridge, UK) to produce a list of proteins detected within each astrocyte sample. For identification, proteins were required to have a minimum of two peptides with a peptide threshold of over 95% as well as a protein threshold of >99% for identification. Manual filtering of the data for common contaminants (i.e. keratin, albumin) was completed, as well as for bovine proteins that were identified due to the presence of serum in the serum-cultured astrocyte medium.

Proteins were then filtered to identify those present in multiple biological replicates in order to increase confidence in the proteins that were detected for each condition (Figure 4-8). More 'missing' values were identified in the proteomic LC-MS/MS replicates compared to the RNA-sequencing replicates with only ~60% of serum-free and ~20% of serum-cultured astrocyte proteins identified in all three replicates, reflecting the stochastic nature of proteomic analysis. The serum-free astrocyte replicates had less variation between samples than the serum-cultured astrocytes, with serum-cultured astrocytes having far fewer proteins identified in two or more replicates. This is most likely due to technical variation between samples with serum-cultured astrocyte samples analysed in different mass spectrometry runs (i.e. on different occasions), unlike the serum-free astrocytes which were analysed in the same mass spectrometry run. Due to the nature of detection of mass spectrometry (proteins are fragmented before identification), proteins are more likely to be mis-identified than in other methods such as RNA-sequencing. Therefore, it is important to include proteins found in multiple samples to increase the confidence that a protein has been genuinely identified. Therefore, only proteins identified in two or three replicates were included in downstream analysis.

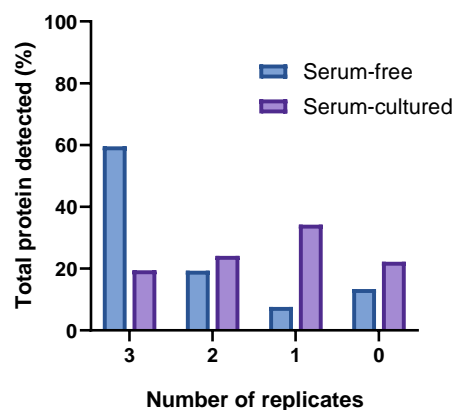


Figure 4-8 - More proteins were identified in all three replicates from the proteomic analysis of serum-free astrocytes compared to the serum-cultured astrocytes. High variation between the biological replicates is evident with a large proportion of the total proteins identified, not found in all 3 replicates (>40% found in 2 or less replicates of serum-free astrocytes; > 80% found in 2 or less replicates of serum-cultured astrocytes). The serum-free astrocyte replicates have less variation than the serum-cultured astrocytes with 3-fold more proteins identified in all 3 replicates compared to the serum-cultured astrocytes. 0 replicates represent proteins that were only identified in the opposite condition (i.e. a protein identified in serum-free replicates, but not serum-cultured replicates would be identified as 0 in the serum-cultured condition). Percentages were calculated using the total number of proteins detected across both serum-free and serum-cultured conditions.

After removal of proteins detected in only one replicate for each condition, there was a significant difference in the number of unique proteins identified in serum-free and serum-cultured astrocytes with serum-free astrocytes found to have almost 2-fold more proteins (Figure 4-9A; $P = 0.049$; $N = 3$). This difference is likely a result of the variation seen between samples with more proteins excluded in the serum-cultured astrocytes due to their presence in only one replicate. A total of 1161 proteins were identified across both astrocyte cell lysates with 581 proteins common to both conditions (50%), with 543 proteins unique to serum-free astrocytes and 37 unique to serum-cultured astrocytes (Figure 4-9B). These proteins presumably represent a subsample of the most highly expressed astrocyte proteins, which likely contains tens of thousands of proteins in its entirety.

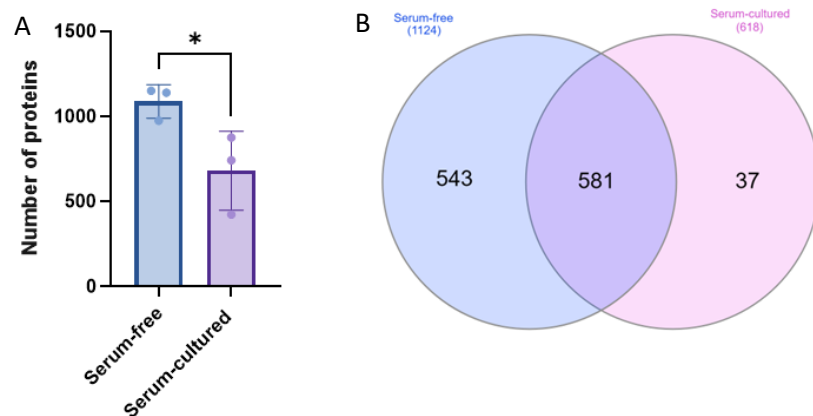


Figure 4-9 - Proteins identified in serum-free and serum-cultured astrocytes by LC-MS/MS. (A) Significantly more individual proteins were identified in each biological replicate of serum-free astrocytes compared to serum-cultured astrocytes ($P=0.049$). Statistical analysis was completed using an unpaired t -test with error bars representing mean and standard deviation ($N=3$). (B) A total of 1161 proteins were identified after manual filtering with 581 proteins found in both conditions (50%).

4.3.2 Pathway analysis of human primary astrocyte proteomes

With a list of proteins identified for each condition (serum-free and serum-cultured astrocytes), KEGG pathway analysis was completed for both conditions. For the serum-free astrocytes, 134 enriched pathways were identified compared to 80 enriched pathways in the serum-cultured astrocytes. Of these enriched pathways, 76 were found in both conditions indicating a similar proteome between the cells, in contrast to the findings from RNA-sequencing. Notably, the 11 most enriched pathways at the proteome level were the same in both conditions (Supplementary figure 3).

4.3.3 Limitations of LC-MS/MS analysis

One issue with analysis of proteomic data of this type was the lack of quantitative values for each of the proteins identified (LC-MS/MS favours protein identification over quantification). By only investigating the simple presence or absence of a protein, changes in protein expression will be overlooked. Likewise, proteome coverage can be relatively low using LC-MS/MS with only a small percentage of the overall predicted proteome detected (~20,000 proteins predicted in cells). In this case, only ~1000 proteins were confidently detected and therefore changes in less

abundant proteins would likely be missed. High variation was seen between replicates when comparing the number of detected proteins, particularly in the serum-cultured samples which may have been due to the samples being analysed at different times resulting in technical variations affecting the results. Whilst the LC-MS/MS data provides an initial glimpse into the proteomes of the astrocytes, a more detailed, quantitative analysis was required to better compare the proteomes of the astrocytes cultured with and without serum.

4.4 Sequential Window Acquisition of all Theoretical Mass Spectra (SWATH-MS)

SWATH-MS is a more powerful, data independent acquisition method of mass spectrometry which generates relative, quantitative values for detected proteins with deeper proteome coverage. To improve upon the LC-MS/MS analysis, 5 µg of protein from whole-cell lysates of serum-free and serum-cultured human primary astrocytes were analysed using SWATH-MS at Nottingham Trent University (NTU, Van Geest Cancer Research Centre), with all biological repeats analysed at the same time to reduce technical variation.

4.4.1 SWATH analysis pipeline

Whilst more detailed descriptions of the methodology are available in the methods (see sections 2.4.4.2 and 2.4.4.3), Figure 4-10 shows an outline of the processing that was completed to analyse the SWATH-MS data. In brief, peptide hits were mapped to known proteins using the SwissProt database for identification. Whilst cell lysate samples were initially normalised by loading the same amount of protein (5 µg) for analysis, a further normalisation step was completed by normalising the overall traces between samples. This produces a list of proteins and their relative abundance in each sample. Peptide sequences can match multiple proteins (often closely related proteins) so some protein hits may be identified as two or more potential proteins, for example 'PMM1:PMM2'. As these hits could not be confidently attributed to a specific protein, they were removed from the analysis.

After PCA and missing data analysis, proteins that were only present in one biological replicate were removed as well as common contaminants including keratin and albumin, in the same way as the conventional LC-MS/MS analysis. Once a list of proteins for each condition were identified, KEGG pathway analysis was completed. The list was also compared to online databases of particular protein groups such as metabolic proteins and RNA-binding proteins to determine whether there is an enrichment in certain groups of proteins. Unlike the LC-MS/MS analysis, quantitative analysis between samples was possible. Limma analysis was completed on proteins that were identified in two or three replicates for both conditions, identifying differentially expressed proteins between the serum-free and serum-cultured astrocytes. KEGG pathway analysis was then completed on these differentially expressed proteins to determine any changes in whole molecular pathways.

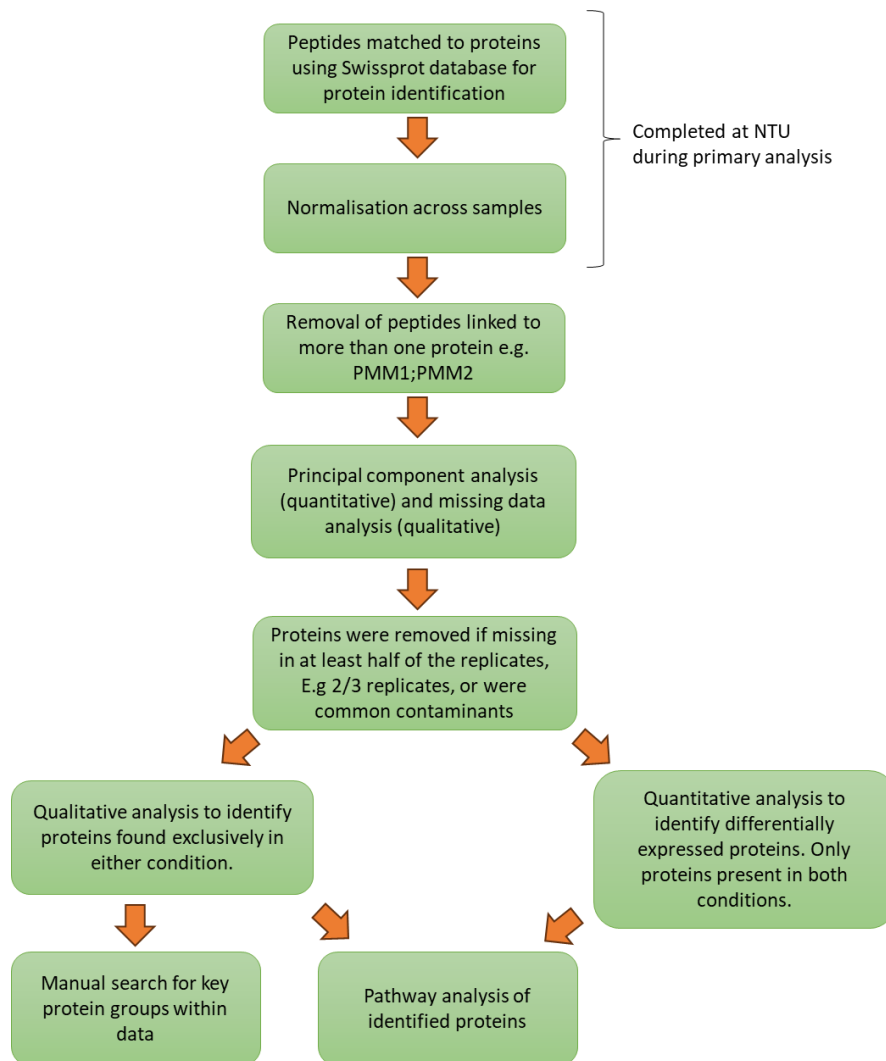


Figure 4-10 - Analysis pipeline completed to analyse the SWATH-MS data from human primary astrocytes.

4.4.2 Measuring similarity between the proteomic samples

A PCA was completed on the relative abundance of each protein detected in the three replicates of serum-free astrocytes and serum-cultured astrocytes to determine the similarity between samples (completed prior to removal of contaminants and missing replicates but after removal of peptides linked to more than one protein; Figure 4-10). A small distinction was identified between serum-free and serum-cultured astrocytes with 37.1% of the data described by the first principal component (PC1; Figure 4-11). The second principal component shows a difference in one of the FBS replicates with PC2 accounting for 27.6% of the separation. The replicates are not as tightly clustered as the RNA-SEQ analysis with replicates showing a substantial amount of variation between samples. This suggests more replicates would be required for a more confident characterisation of the proteomes between samples. Due to a lack of clear separation between the conditions, a PLS-DA would not be predictive for each condition and was therefore not completed.

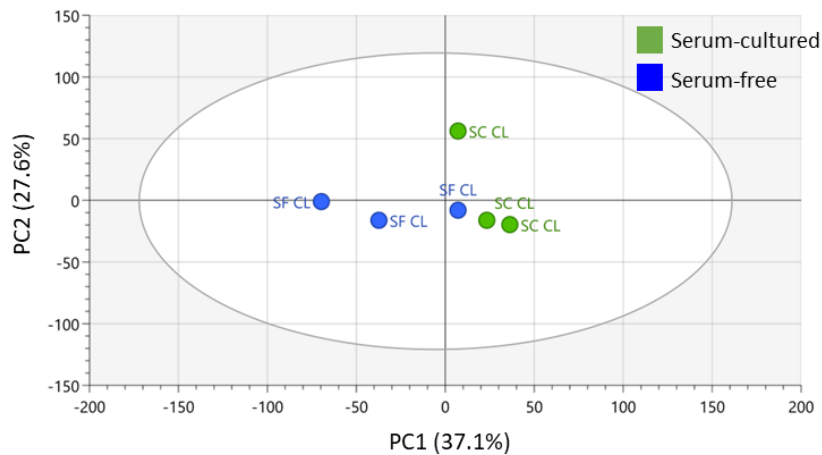


Figure 4-11 - Principal component analysis of proteins identified in serum-free and serum-cultured astrocytes. PCA shows some separation between the proteomes of serum-free (blue) and serum-cultured astrocytes (green), however the difference is not as distinct as the PCA of the transcriptomes. PC1 accounts for 37.1% of the difference between groups and PC2 accounts for 27.6% (total data described = 64.7%). Proteins and their relative abundance were used to identify overall similarities and differences between replicates as well as between serum-cultured and serum-free human primary astrocytes.

The number of missing values were also investigated to determine the similarity between replicates as well as to determine the number of proteins to be included for further analysis. The serum-cultured replicates were similar with the majority of proteins identified in all three biological replicates (~84%), and very few proteins found in only replicate (1%; Figure 4-12). In contrast, there was high variation in the serum-free astrocyte replicates with the majority of proteins identified in only 1, or 2 replicates. As with the previous LC-MS/MS analysis, further analysis was completed on the proteins that were identified in two or more biological replicates for serum-free and serum-cultured astrocytes.

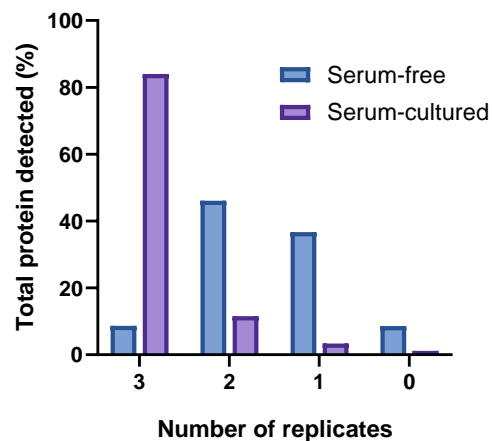


Figure 4-12 - More proteins were identified in all three biological replicates in the proteomic analysis of serum-cultured astrocytes compared to the serum-free astrocytes. High variation between the biological replicates is evident in the serum-free astrocytes with a large proportion of the total proteins identified, not identified in all three replicates (>80% found in two or less replicates of serum-free astrocytes). In contrast, the serum-cultured astrocyte replicates were very similar with the majority of proteins identified in all three biological replicates (84%). 0 replicates represent proteins that were only identified in the opposing condition (i.e. a protein identified in serum-free replicates, but not serum-cultured replicates would be identified as 0 in the serum-cultured condition). Percentages were calculated using the total number of proteins detected across both serum-free and serum-cultured conditions.

When comparing the number of proteins identified in the serum-free and serum-cultured human primary astrocytes, far more proteins were identified in the serum-cultured astrocytes with little variation in the number of proteins between biological replicates (Figure 4-13A). In contrast, a large difference was observed in the number of proteins identified in each of the biological repeats for the serum-free condition, ranging from 462 proteins to 4077 proteins. This difference is likely due to an issue with sample preparation and suggests further work should include more than three biological replicates with an effort to have similar numbers of proteins identifications.

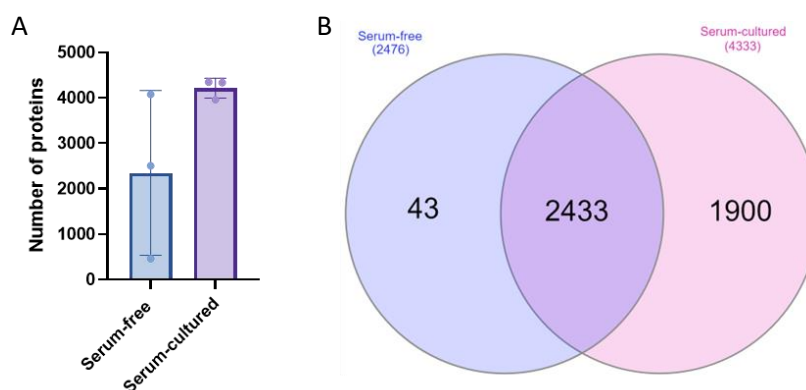


Figure 4-13 – Many unique proteins were identified in serum-free and serum-cultured astrocytes through SWATH analysis. (A) Number of unique proteins identified in each of the biological repeats. Error bars represent mean \pm standard deviation ($N=3$). (B) The majority of proteins (55.6%) were identified in both serum-free and serum-cultured astrocytes with few unique proteins identified in serum-free astrocytes. For inclusion, protein identification must be in at least 2 replicates of the same condition.

To generate a list of proteins for each condition for qualitative analysis, proteins that were only present in one biological repeat were removed, leaving a total of 4376 proteins that were identified in ≥ 2 biological repeats (Figure 4-13B). The majority of proteins were identified in serum-cultured astrocytes with only 43 proteins found to be unique to serum-free astrocytes. In contrast, 55.8% of all proteins were identified in both conditions with 1900 proteins found to be unique to serum-cultured astrocytes. This is most likely due to the large difference in protein identification numbers between serum-free and serum-cultured astrocytes.

4.4.3 Qualitative analysis of serum-free and serum-cultured astrocyte proteomes

Whilst SWATH analysis allows for quantitative analysis, it is still important to compare the presence and absence of proteins between samples with subsequent quantitative analysis only taking into account proteins identified in both conditions. KEGG pathway analysis was completed on the proteins that were identified exclusively in either the serum-free or serum-cultured astrocytes to identify pathways that may be remodelled upon serum exposure. No KEGG pathways were significantly enriched in the serum-free astrocytes, and this is likely due to the small number of proteins that were analysed (only 43 uniquely identified proteins). In contrast, 34 KEGG pathways were significantly enriched in the serum-cultured

astrocyte uniquely identified proteins, including 13 of those identified through LC-MS/MS such as 'Ribosome' and 'Amyotrophic lateral sclerosis' (Figure 4-14).

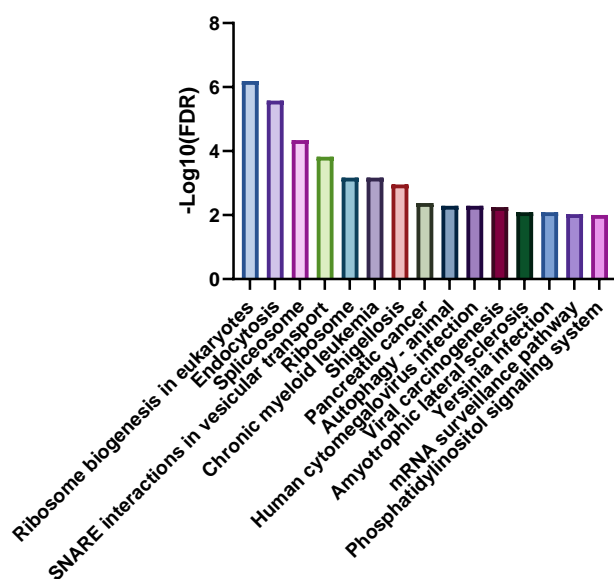


Figure 4-14 – The top 15 enriched KEGG pathways identified in uniquely identified proteins in serum-cultured astrocytes after SWATH analysis. A total of 34 enriched pathways were identified with 13 pathways also identified in the LC-MS/MS analysis of the complete serum-cultured proteome.

4.4.4 Differentially expressed proteins

Thus far, qualitative analysis of the astrocyte proteome has not been able to analyse expression differences in proteins identified in both serum-free and serum-cultured astrocytes. Unlike the previous LC-MS/MS analysis, relative abundance (across samples) of each identified protein was measured by SWATH-MS spectral counting, allowing a quantitative comparison. To identify differentially expressed proteins, spectral counts (post-normalisation) of each identified protein were input into StatsPro software to calculate a fold change between conditions and an adjusted significance (P_{adj}). Two methods of adjusting the stringency of the analysis are by altering the allowance for missing values (NA value) or by altering the coefficient of variation (CV) threshold. The NA value is the number of missing values allowed across replicates for protein inclusion. For example, to include proteins found in $\geq 2/3$ replicates per condition (accounting for the stochastic nature of proteomics), less than 33.3% of the replicates can be missing values (therefore NA value = 0.34, rounded to 0.4 for analysis). By reducing the NA value, less proteins will be included and therefore the analysis will be more stringent. The CV value will exclude proteins that have a variance of more than the set criteria. A CV value of 0.5 will only include proteins that have a variance below 50% across all replicates.

To identify the most appropriate criteria to analyse whole-cell lysate samples, a range of NA and CV values were empirically tested (Table 4-2). Two NA values were trialled, with 0.4 including proteins found in ≥ 2 replicates and 0.2 including proteins found in all 3 biological replicates. Three different CV values were trialled representing 30%, 50% and 100% variance criteria with a value of 1 including all proteins despite the variance observed between replicates. The P-adjusted value was calculated during a Limma analysis using the Benjamini-Hochberg procedure which accounts for the number of proteins analysed to reduce false positives. By increasing

the number of proteins analysed, the threshold for the adjusted P-value increases and therefore likely results in false-negatives.

Table 4-2 - Differentially expressed proteins in serum-free and serum-cultured astrocytes identified using Limma analysis with different NA and CV criteria. To determine the most appropriate criteria for the proteomic analysis, different NA (missing values) and CV (variance) values were trialled on the samples. The NA value is based upon the number of replicates where the protein was present (0.4 = 2/3 samples, 0.2 = 3/3 samples). The CV value is the threshold for the coefficient of variation. Any proteins above this level of variation between replicates were removed from the analysis (e.g. 0.3 = only proteins with <30% variance). P-values were calculated using a Limma test with P-values adjusted using the Benjamini-Hochberg procedure. Green highlight indicates the criteria selected for further analysis.

NA (Missing values)	CV (Variance)	Total Proteins	P<0.05	Padj<0.05
0.4	0.3	1082	178	26
0.4	0.5	1760	272	0
0.4	1	2387	268	0
0.2	0.3	50	18	18
0.2	0.5	126	27	15
0.2	1	300	31	0

It was determined that a NA value of 0.4 (i.e. ≥ 2 replicates required) and a variance of 0.3 (variance of $\leq 30\%$ across biological replicates) was most suitable for whole-cell lysate comparisons (Table 4-2, green highlight). This allowed a large proportion of the proteins detected to be included in the analysis but was strict enough to yield differentially expressed proteins. In total, 26 proteins had a P-adjusted value below 0.05, and of these proteins, all 26 were also found to have a fold change above ± 1.5 (common criteria for proteomic analysis; Figure 4-15; proteins listed in more detail in section 4.5).

To determine whether these proteins were related, KEGG pathway analysis was completed on the 20 proteins upregulated in serum-free astrocytes (highlighted in red in Figure 4-15), revealing an enrichment in glutathione metabolism (RRM2B, GCLM and GSTM2; FDR = 0.008). Glutathione metabolism is a homeostatic function of astrocytes to prevent toxicity in both neighbouring astrocytes and neurones from reactive oxygen species (ROS) and oxidative stress, as well as supplying neurones with cysteine which is required for neuronal glutathione metabolism (Dringen et al., 2015). Therefore, this pathway would be expected in homeostatic, quiescent astrocytes. No enrichment was found between the 6 proteins upregulated in the serum-cultured astrocytes (highlighted in green in Figure 4-15; proteins listed in more detail in section 4.5) but this is likely due to the low number of proteins analysed.

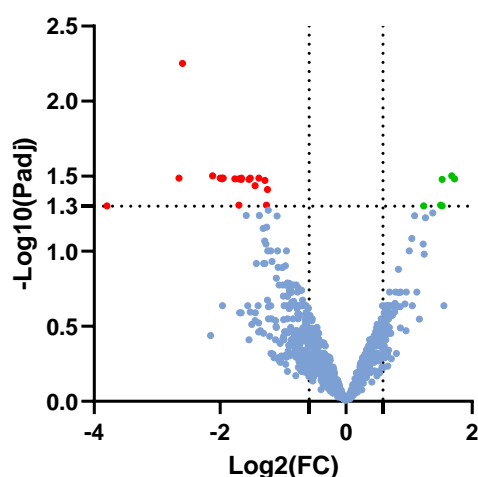


Figure 4-15 – 26 differentially expressed proteins were identified between serum-free and serum-cultured astrocytes. 26 differentially expressed proteins were identified using a Limma analysis with 20 upregulated in serum-free astrocytes, and 6 upregulated in serum-cultured astrocytes. Proteins highlighted in red are upregulated in serum-free astrocytes and those highlighted in green are upregulated in serum-cultured astrocytes. Criteria for significance was a P-adjusted value of 0.05 (-Log10 = 1.30) and a fold change of more than ±1.5 (Log2 = 0.58).

4.4.5 Comparison of conventional LC-MS/MS and SWATH-MS to describe the astrocyte proteome

The main difference between both mass spectrometry analyses is the quantitative potential of the SWATH analysis. Whilst qualitative analysis produces an overview of the proteins in the sample, it is difficult to identify enrichment between samples without measuring protein abundance. The differentially expressed genes identified within section 4.4.4 would simply appear as present in both samples in qualitative analysis, but SWATH analysis also identifies expression differences within the samples.

More proteins were identified during the SWATH analysis across both conditions with SWATH analysis identifying >2-fold more protein in the serum-free astrocytes and 7-fold more in the serum-cultured astrocytes than conventional LC-MS/MS (Table 4-3). This is likely due to improved sample preparation and all samples being analysed at the same time with SWATH analysis (completed later in the project), in contrast to the LC-MS/MS. There was high similarity between the mass spec techniques with >85% of the proteins identified by conventional LC-MS/MS also identified within the SWATH analysis. With more proteins consistently identified in the samples, SWATH analysis provides deeper proteome coverage whilst using less sample than conventional LC-MS/MS.

Table 4-3 – High similarity in the proteins identified by LC-MS/MS and SWATH analysis after manual filtering. More proteins were identified by SWATH analysis than by LC-MS/MS, particularly in the serum-cultured condition. The proteins identified were very similar with >85% of LC-MS/MS proteins also identified in the SWATH analysis. Number of proteins were calculated after manual filtering for proteins identified in two or more biological replicates as well as filtering for common contaminants.

	LC-MS/MS	SWATH	Similarity
Serum-free	1124	2476	85.5%
Serum-cultured	618	4333	94.0%

4.5 Comparison of RNA sequencing and Mass spectrometry techniques to describe astrocyte phenotype

Both RNA sequencing and mass spectrometry are very powerful techniques for producing a non-targeted characterisation of RNA and protein expression, respectively. It is difficult to directly compare the expression of the two 'omics techniques given that not all protein-coding RNA will be directly translated into protein, with post-transcriptional regulation tightly controlling gene expression. However, general trends in expression should be similar between RNA and protein.

RNA sequencing provided a very detailed characterisation of the mRNA expression in the astrocytes with over 15,000 protein-coding RNAs detected in at least 2 of the biological replicates for both serum-free and serum-cultured human primary astrocytes (Table 4-4). On the other hand, far fewer targets were identified in SWATH-MS with only 2476 proteins detected in serum-free astrocytes and 4333 proteins detected in the serum-cultured astrocytes. Despite far fewer unique identifiers, there was high similarity between the proteins identified and the corresponding mRNA (>95% of SWATH proteins also identified as mRNA).

Table 4-4 – High similarity between protein-coding RNA and corresponding protein identified during RNA sequencing and SWATH mass spectrometry, respectively. Far more unique mRNA was detected during RNA sequencing with more than 15,000 protein coding genes identified in each of the conditions. The majority of proteins identified in SWATH-MS were also detected as mRNA in RNA sequencing (>95% of proteins).

	RNA-SEQ	SWATH	% SWATH proteins identified as mRNA in RNA sequencing
Serum-free	17,052	2476	96.5%
Serum-cultured	15,531	4333	97.5%

With the majority of the proteins identified in both RNA sequencing (as mRNA) and SWATH-MS, the 26 differentially expressed proteins identified during SWATH-MS analysis were compared against the RNA sequencing analysis to compare overall expression trends between serum-free and serum-cultured astrocytes. Of the 26 proteins, 23 were identified in the RNA sequencing analysis with 15 also found to be differentially expressed in the RNA sequencing ($\text{Log}_2(\text{FC}) > 1$ and Q value below 0.05; Table 4-5). Only 3 proteins were amongst the top 20 differentially expressed mRNA (*SPTBN1*, *DSP* and *JUP*) with most of the other differentially expressed proteins found to be much lower ranking in the differentially expressed mRNA. The direction of change was also compared to determine whether the differences between serum-free and serum-cultured astrocytes were consistent. Of the 23 proteins identified as mRNA in the RNA sequencing analysis, 18 followed the same trend (i.e both upregulated or both downregulated; highlighted in green) with 9 of these also differentially expressed in both analyses. Of the 6 proteins that did not follow the same trend (highlighted in orange), *DSP* had the greatest difference with a 7.8-fold increase identified in serum-cultured astrocytes identified in the RNA sequencing analysis, in contrast to a 1.8-fold decrease found in SWATH analysis.

Table 4-5 - Comparison of differentially expressed proteins identified in SWATH analysis, with the corresponding mRNA identified in RNA sequencing analysis. The majority of the 26 differentially expressed proteins identified during SWATH analysis were also identified as mRNA during RNA sequencing analysis (23/26). However, only 3 of these were identified within the top 20 most differentially expressed genes with the majority being much lower ranked in the RNA sequencing analysis. Of the 23 proteins also identified in the RNA sequencing, 18 were found to follow a similar trend between serum-free and serum-cultured astrocytes (highlighted in green; those that did not are highlighted in orange). Numbers written in italics identifies non-significant results in the RNA sequencing analysis ($\text{Log}_2(\text{FC}) < 1$ or $Q \text{ value} > 0.05$ were not significant). Both P_{adj} and $Q \text{ value}$ represent adjusted P values, however, were calculated using different techniques. Positive $\text{log}_2(\text{FC})$ values represent an upregulation in serum-cultured astrocytes, and a negative $\text{log}_2(\text{FC})$ represents a downregulation in serum-cultured astrocytes.

	SWATH analysis		RNA-SEQ analysis	
	Log ₂ (FC)	Rank (P_{adj})	Log ₂ (FC)	Rank ($Q \text{ value}$)
EPHX1	-2.57	1	-2.54	4320
EPS8	1.68	2	2.80	463
JUP	-2.12	3	1.21	19
CMBL	-1.95	4	-1.05	2607
DCN	-2.65	5	3.83	240
DDAH2	-1.52	6	-1.07	2650
GSTM2	-1.38	7	-1.53	3324
MACROH2A2	-1.97	8	x	x
NAGLU	-2.00	9	-0.17	12864
RRM2B	-1.66	10	-0.85	5247
ALCAM	1.72	11	2.39	600
ASAH1	-1.70	12	-0.74	2668
CYRIA	-1.97	13	x	x
DSP	-1.77	14	7.79	18
PHPT1	-1.54	15	-0.12	13879
PLIN2	-1.66	16	0.99	5113
SERBP1	1.53	17	0.92	960
LMCD1	-1.29	18	-1.43	3200
PTGFRN	-1.45	19	-0.85	1954
GCLM	-1.25	20	-0.07	14844
ARL6IP1	-1.27	21	-1.20	2850
CPQ	-1.70	22	0.34	8871
TMEM214	1.50	23	1.39	1460
CCN1	1.52	24	x	x
GPNMB	-3.80	25	-1.79	3637
SPTBN1	1.23	26	-1.62	11

4.6 Discussion

4.6.1 Summary

This chapter aimed to produce an unbiased multi-omics analysis for both serum-free and serum-cultured human primary astrocytes to complement the targeted characterisation of astrocyte phenotype completed in chapter 3. RNA sequencing produced a thorough characterisation of the protein-coding genes within the astrocytes, and whilst there was a large number of overlapping genes, the transcriptomes of the astrocytes were shown to be distinctly different after culture with and without serum. A total of 6134 genes were shown to be differentially expressed between the astrocytes, with expression of known astrocyte markers matching previous RT-qPCR characterisation by Prah et al. (2019; with the exception of *GFAP* and *AQP4* expression) as well as the RT-qPCR analysis completed in Chapter 3. Pathway analysis of the astrocytes at the mRNA level suggests the serum-free astrocytes have a more quiescent phenotype with homeostatic pathways upregulated such as axon guidance, and synapse-associated pathways such as the glutamatergic and GABAergic synapses. Serum-cultured astrocytes had an

upregulation in ribosomal pathways as well as inflammatory pathways such as the TNF and the NF- κ B signalling pathways.

Two types of mass spectrometry were completed to understand the proteome of the serum-free and serum-cultured human primary astrocytes which were traditional LC-MS/MS and SWATH analysis. Traditional LC-MS/MS only allowed qualitative data analysis with only a small number of proteins identified (~600 – 1200 proteins). SWATH analysis produced a more comprehensive proteome (~2500 – 4400 proteins) and also measured relative abundance so quantitative comparisons could be made between samples. Therefore, for future work, SWATH analysis should be prioritised for proteomic research where possible.

Despite a more detailed proteome analysis, relatively few differences were identified between the serum-free and serum-cultured astrocytes when comparing the proteome, with only 23 differentially expressed proteins identified. In comparison to the RNA sequencing analysis, SWATH-MS analysis was far less detailed, but this partially reflects differences between RNA and protein expression in cells as well as difference sensitivities between the techniques. Overall, the majority of protein identified using SWATH analysis was also found within the RNA sequencing as mRNA (>95%) suggesting the techniques are complimentary when investigating astrocyte phenotype. The combination of these comparisons highlights the value of a multi-omics approach compared to use of a single technique to fully appreciate the differences between conditions. Whilst RNA sequencing shows a very detailed transcriptome, not all of these mRNA will be translated into protein and therefore may not accurately reflect the proteome of the cells.

4.6.2 Consistency between biological replicates

The RNA-sequencing analysis provided an in-depth characterisation of the astrocyte protein-coding transcriptome. The data was very consistent amongst samples with tight clustering observed in the PCA analysis in both the serum-free and serum-cultured replicates, with a clear distinction between the conditions. Two samples (one serum-free and one serum-cultured) appear to be more variable than the other samples in the PCA, however this is due to the nature of PCAs with differences often exaggerated by the principal components. 85% of the data was described by the first component which clearly distinguishes the conditions (see Figure 4-1). Therefore, the second principal component has sought to identify any further differences which only accounts for 6.1% of the data. However, by plotting onto a 2D graph, the principal components appear to have the same weight and therefore the two samples appear to be different from the other replicates.

The tight clustering of the RNA-sequencing replicates is in contrast to the SWATH analysis where there was high variation between replicates, with the serum-free replicates ranging from 462 - 4077 proteins identified per sample. There was a much smaller difference between the serum-cultured replicates, which led to ~2-fold more proteins found in two or three replicates for the serum-cultured condition (SF = 2476 vs SC = 4333). A similar variation was observed within the LC-MS/MS analysis with only 618 proteins identified in two or three replicates of the serum-cultured condition compared to 1124 proteins in the serum-free condition.

Initially, this was thought to be due to technical variation in the LC-MS/MS analysis because the serum-cultured samples were not analysed at the same time. However, efforts were made to avoid this technical variation in the SWATH analysis with all samples analysed at the same time. Instead, this variation likely results from the mass spectrometry preparation and methodology itself. To overcome this issue, more replicates should be completed for future mass spectrometry so outliers can be identified, and more proteins will be included in the final analysis (i.e. present in more than one replicate). For RNA sequencing, four replicates appear to be an appropriate number of samples to distinguish conditions and confidently identifies a large population of mRNA within the samples.

4.6.3 RNA sequencing analysis

In the RNA sequencing analysis, there was a high number of differentially expressed protein-coding genes despite using the adjusted P-value (Q value) to reduce the number of false positives (6134 differentially expressed genes). This high number may indicate that the thresholds for significance were too lenient, leading to true differences being masked between the astrocytes by false positives. In the current work, genes were identified as significantly different if they had a Q value <0.05 and a fold change above 2. This threshold was recommended by Novogene for their RNA sequencing analysis but with such a small variance between samples, a stricter threshold may be more suitable for this data. In contrast, different threshold criteria were trialled when analysing the SWATH data which showed the importance of fitting the threshold to the data.

The differences observed between conditions are supported by previous research with the same differences observed through RT-qPCR (Chapter 3) and similar differences found in Prah et al. (2019). The exceptions were *GFAP* and *AQP4* where the opposite trend was observed in their analysis. As discussed in Chapter 3, *GFAP* expression was unexpectedly higher in serum-free astrocytes compared to serum-cultured astrocytes. However, almost all general astrocyte markers investigated were found to have higher expression in the serum-free astrocytes, which supports the theory that serum-cultured astrocytes may be focused on producing proteins required for proliferation and reactivity instead. In contrast, when investigating genes associated with different types of reactivity (inflammatory and anti-inflammatory), serum-cultured astrocytes were found to have higher expression of both A1 and A2 reactive markers suggesting a complex reactive response similar to that observed in disease (Ziff et al., 2022). This shows that FBS culture elicits a reactive phenotype that can be used to model the complex, reactive response often seen in disease.

Whilst the RNA-sequencing has produced a thorough analysis of protein-coding genes expressed in the astrocytes, other forms of RNA have important roles within the cells which were not analysed. For example, miRNAs tightly control protein expression by binding to mRNA, leading to a reduction in protein expression. MiRNAs have been shown to be dysregulated in neurodegenerative disease and therefore, an RNA sequencing which focused on small RNAs, such as miRNAs, would be useful in

further characterising the astrocytes (Goodall et al., 2013; Lafourcade et al., 2016; Bai et al., 2021; Marton et al., 2023).

4.6.4 Conventional LC-MS/MS vs SWATH analysis when comparing the proteome of serum-free and serum-cultured astrocytes

Two types of LC-MS/MS were completed during this work on the serum-free and serum-cultured human primary astrocytes. The conventional LC-MS/MS only allowed qualitative analysis of the astrocyte proteomes, unlike SWATH-MS analysis which determined relative abundance between the samples, allowing quantitative comparisons between conditions. Qualitative analysis is important when comparing the conditions as this likely shows the greatest difference between cells, where expression is very different between conditions (i.e. presence vs absence). Quantitative analysis identifies changes in protein expression, but proteins must be expressed in both conditions and variance must be below the threshold selected. It is also difficult to compare the abundance of different proteins with mass spectrometry analysis so quantitative comparisons are only possible between samples, rather than between proteins. This is because the protein values are normalised, so they are relative between samples for each protein rather than their relation to other proteins. Also to be identified, the proteins are fragmented to produce different peptide fragments that can be detected. Fragments that are unique to a particular protein can then be used to identify the presence of that protein. However, based upon the protein sequence, proteins will fragment differently with some proteins fragmenting more than others. Because of this fragmentation approach, it is difficult to establish that a particular protein is more abundant than another.

It is therefore important to compare both presence and absence (qualitative), as well as differentially expressed proteins (quantitative). Interestingly, despite different samples being analysed using the two techniques, a similar proteome was identified in both analyses showing a consistency between the mass spectrometry analyses. Due to the consistency between techniques, the increased number of proteins identified and the quantitative nature of SWATH analysis, SWATH analysis will be used for future proteomic analysis instead of conventional LC-MS/MS.

4.6.5 Importance of a multi-omics analysis

RNA sequencing analysis may appear to provide a more thorough understanding of the astrocyte phenotypes, with >3.5-fold more protein-coding genes identified compared to proteins identified in SWATH analysis, and many more differentially expressed genes identified between conditions. However, it is important to consider both the transcriptome and the proteome when completing a thorough characterisation, as many regulatory processes occur between the transcription of the mRNA and the translation into protein, such as miRNA binding leading to mRNA degradation.

Alternatively, other less-used types of 'omics analysis exist that could be used to characterise the astrocytes such as metabolomics (analysis of metabolites) or lipidomics (analysis of lipids). In the RNA sequencing pathway analysis, metabolic

pathways were differentially expressed between the astrocytes suggesting differences would be identified between the conditions in metabolomic analysis. Lipidomics would also be particularly interesting when comparing the astrocytes and their EVs, with EVs being lipid membrane-bound particles. Characterising astrocyte-derived EVs (ADEVs) will be the main focus of chapter 5 of this thesis with a particular focus on using SWATH-MS to identify protein cargo within the ADEVs.

4.6.6 Other limitations of the work within this chapter

As described previously, an increase in the sample size would benefit the current analysis, leading to more confident conclusions from the data. However, it would also be beneficial to include other conditions that were trialled in the previous chapter. For example, analysis of the cytokine-treated astrocytes would allow a direct comparison between previous RNA sequencing work completed by other groups on primary astrocytes (Liddelow et al., 2017; Barbar et al., 2020; Hasel et al., 2021; Ziff et al., 2022). This would also allow a better comparison of the FBS and cytokine treatments to determine how similar the reactive phenotypes are between the two types of treatments. Acute and chronic treatments could also be compared if FBS-treated astrocytes were also analysed because in the previous chapter, differences were observed between serum-cultured and FBS-treated astrocytes. Whilst these conditions would yield interesting comparisons in astrocyte reactive phenotypes, the current work was limited in funding and therefore was only able to focus on a comparison between serum-free and serum-cultured astrocytes with a limited sample size.

4.6.7 Conclusions

In this chapter, an unbiased characterisation of the astrocyte transcriptome and proteome was completed to investigate the effect of serum on human primary astrocytes. In combination with the more targeted characterisation completed in chapter 3, we have demonstrated that human primary astrocytes have a quiescent phenotype in serum-free culture, which changes to a reactive-like phenotype upon exposure to serum. With quiescent and reactive astrocyte cultures established, their EVs can be explored to investigate differences between reactive and quiescent ADEVs. These ADEVs will also be compared to brain-derived EVs (BDEVs) from both healthy and diseased brain tissue to determine their relevance to endogenous human EVs as well as disease EVs, and whether ADEVs can be used as a unique measure of brain health.

Chapter 5: Investigating the characteristics and functions of human astrocyte-derived extracellular vesicles

5.1 Introduction

5.1.1 The importance of understanding extracellular vesicles

The previous results chapters have shown the effect of serum on human primary astrocyte phenotypes, with FBS exposure rapidly causing changes that resembles reactive remodelling. The cytokine assay in Chapter 3 has also revealed that serum exposure can cause changes in the secretome of the astrocytes, with astrocytes cultured in serum releasing inflammatory cytokines (MCP-1 and Chitinase-3 like-1) and far fewer supportive growth factors (such as IGFBP2, FGF2 and GDF-15). The rest of this thesis will investigate in greater detail how reactivity changes the secretome of human primary astrocytes and in particular, their extracellular vesicles (EVs).

EVs have been shown to elicit positive changes in neighbouring cells in many studies and therefore are being trialled as therapeutics (Duong et al., 2023). Both mesenchymal and neural stem-cell derived EVs have demonstrated beneficial effects when applied to the CNS, including enhanced tissue repair and prevention of neuronal death (Mahdavi-pour et al., 2020; Apodaca et al., 2021; Garcia-Contreras and Thakor, 2021). However, therapeutic effects have not only been observed using stem-cell derived EVs, but also with ADEVs (Ranjit et al., 2018; Leggio et al., 2022). ADEVs are of particular interest due to the astrocyte's key roles in neuronal support and protection. ADEVs contain supportive molecules such as growth factors (FGFs or PDGFs) or neurotrophic factors (BDNF or CNTF) that will protect and promote neuronal survival (Linnerbauer and Rothhammer, 2020). Further research needs to be conducted on the potential therapeutic aspect of ADEVs on neighbouring cells to decide how best to utilise them as a therapeutic tool.

As well as a potential therapeutic use, ADEVs may represent a unique window into understanding astrocyte phenotypes, and by identifying changes in reactive ADEV, they may present as unique markers of brain health which can be monitored within the blood circulation. Astrocyte reactivity is a good measure of brain health with reactivity observed in almost all neurodegeneration but is very difficult to quantify accurately with current technology *in vivo* (Pekny and Pekna, 2014; Escartin et al., 2019; Brandebura et al., 2023). By measuring changes in reactive ADEVs within the blood or CSF, brain health could be monitored non-invasively, allowing earlier diagnosis of neurological disease and therefore administer preventative treatment earlier. For example, circulating 'free' GFAP has been identified as upregulated in the plasma of dementia patients up to 10 years before diagnosis (Guo et al., 2024).

We hypothesise that ADEV contents will reflect the phenotype of astrocytes at the time of release and therefore, there will be changes in the content of EVs released

between the reactive serum-cultured astrocytes, and the quiescent serum-free astrocytes. To investigate this, a thorough characterisation of ADEVs from both quiescent and reactive astrocytes needs to be performed. Any changes can then be confirmed in brain-derived EVs (BDEVs) from human neurodegenerative tissue (ALS and Alzheimer's disease) to determine whether findings from the human primary astrocytes can be translated.

5.1.2 Current knowledge of ADEVs

EV research is still a relatively new field of research so current knowledge on ADEVs is incomplete. However, within the past few years, there has been a flurry of interest focusing on the role of ADEVs in a range of diseases, as well as investigating the functional effects of ADEVs on other cell types (Goetzl et al., 2016; Patel and Weaver, 2021; Sun et al., 2022; Varcianna et al., 2019; Winston et al., 2019). Many of these studies have caveats associated with other *in vitro* cell culture that have been highlighted previously in this thesis, with many studies utilising rodent cells and FBS for *in vitro* culture (Chaudhuri et al., 2020; Sun et al., 2022; You et al., 2020). To date, little is known about the cargo of human quiescent ADEVs which is needed as a baseline for studying changes induced upon reactive remodelling.

There have been recent advances in understanding ADEVs in neurodegenerative diseases, with a focus on how ADEVs might facilitate the spread of these diseases in the brain. As described in section 1.3.3, many studies have shown that EVs facilitate the transport of pathological proteins to healthy cells (Grad et al., 2014; Westergard et al., 2016; Wang et al., 2017; Sardar Sinha et al., 2018; Guo et al., 2020; Pérez-González et al., 2020; Vandendriessche et al., 2020). It is still unclear why cells package pathological proteins into EVs and whether this is a net detrimental or protective mechanism. By preventing the release of EVs containing these pathological proteins, there may be greater neuronal loss due to the build-up of these toxic proteins within the cells. On the other hand, preventing EV release may also halt disease transmission between cells, slowing disease progression.

As well as disease transmission, EVs could also be involved in the neurotoxic secretion by reactive astrocytes in ALS (Liddelow et al., 2017; Guttenplan et al., 2020; Kushwaha et al., 2021). Recent research has identified key components of this toxicity as the excessive release of inorganic polyphosphate (PolyP) and long-chain saturated lipids (Guttenplan et al., 2021; Arredondo et al., 2022). PolyP was found to be associated with vesicles that were secreted into the extracellular space (Angelova et al., 2018; Arredondo et al., 2022). With EVs formed using a lipid bilayer, these long-chain saturated lipids may also be present in the EV membranes and the lipid rafts found within EV membranes, suggesting EVs themselves (as opposed to just their cargo) may form a key component of this toxicity. ADEVs have also been linked to astrocyte toxicity through the transport of alternative miRNAs that are subsequently delivered to neurones (Varcianna et al., 2019). By investigating ADEVs from reactive astrocytes, other factors associated with this toxicity may be identified which would lead to the discovery of novel targets for therapeutic development. If EVs are involved in this toxicity, therapeutics could target EV released from reactive astrocytes to reduce toxicity and improve neuronal survival in disease.

5.1.3 A multi-targeted approach is required for the study of EVs

One of the major challenges with EV research is their nanoparticle nature, which requires any measurements or analyses to be very sensitive. They are also released from cells alongside many other particles resulting in preparations with potential contaminants such as lipoproteins, free proteins or free RNA. To ensure any observed features or effects are due to EVs rather than these other co-isolates, extensive controls and characterisation are required. To maintain and improve the quality of EV research, MISEV guidelines were produced through the consensus of many researchers within the EV field (Lötvall et al., 2014; Théry et al., 2018; Welsh et al., 2024). These guidelines are updated regularly to encompass new knowledge and technologies that have been applied to EVs with the latest guidelines published earlier this year (Welsh et al., 2024).

Current MISEV guidelines discuss eight main topics which are nomenclature, sample collection and pre-processing, EV separation and concentration, EV characterisation, technique-specific reporting considerations, EV release and uptake, functional studies and *in vivo* EV analysis (Welsh et al., 2024). Many of these guidelines focus on the inclusion of relevant controls and what should be reported when publishing EV research. For example, one key issue with EV research for models based on mammalian cell culture is the contamination of FBS-derived EVs, with FBS commonly used in many cell culture methods. To mitigate this, researchers can either complete serum-starvation (used in this work) or use EV-depleted FBS created through ultracentrifugation of the FBS before addition to media. Guidelines suggest running an unconditioned media control during experiments as well as detailing the exact culture conditions in the methodology. Guidelines also discuss the potential issues with both methods such as changing cellular behaviour with serum starvation or EV-depleted FBS. This allows more open discussions in the field ultimately improving the transparency and therefore quality of EV publications.

A further important consideration for the techniques used for EV isolation and characterisation is the downstream analysis that will be completed. For example, for proteomic analysis that will be completed in this work, minimal contamination is important and therefore serum-removal is needed (i.e. astrocytes are initially cultured in serum, then placed into serum-free medium for collection), rather than culture conditions with EV-depleted FBS. Size exclusion chromatography (SEC) was also selected as the isolation technique instead of ultracentrifugation to reduce free-protein contamination and preserve the integrity of the EVs for later functional studies (Benedikter et al., 2017; Lobb and Möller, 2017; Mol et al., 2017; Takov et al., 2019; Kaddour et al., 2021).

5.1.4 Aims of this chapter

This chapter aims to characterise ADEVs from both reactive and quiescent human primary astrocyte cultures analysed in the previous chapters. The ADEVs will then be compared to BDEVs isolated from healthy or disease brain tissues to determine their relevance to endogenous human EVs and whether reactive ADEV cargo overlaps with BDEV cargo observed in disease. A range of techniques will be used to characterise

the EVs including TEM, NTA and protein mass spectrometry with efforts made to conform to the latest MISEV guidelines. To investigate functionality in the EVs, reactive ADEVs (serum-cultured) will be applied to quiescent astrocyte cultures (serum-free) to determine if ADEVs can elicit changes to quiescent astrocyte phenotypes.

5.2 Isolation and visual confirmation of EVs from cultured astrocytes and human tissues

5.2.1 Optimisation of ADEV isolation from serum-free and serum-cultured astrocytes

Serum-free culture of human primary astrocytes allows the continuous collection of conditioned medium without the need to remove contaminant FBS-derived EVs from the medium. However, due to the lack of proliferation, cell number is limited meaning multiple collections were required to harvest sufficient EVs for downstream analysis. Previous work with non-proliferative cells within our group had found that 4x 6-well plates (~48 ml media, 1.75×10^5 cells/cm² seeding density) of primary mouse neurones were required to collect sufficient EVs per individual preparation to observe functional effects on recipient cells and for sufficient characterisation of the EVs (Mesquita-Ribeiro et al., 2021). With the rate of EV release predicted to be similar between neurones and non-proliferative astrocytes compared to other cell types, the same approach was used as a basis for EV isolation in the serum-free human astrocyte culture. The serum-free astrocytes had been shown to survive for up to 4 weeks in chapter 3, so media was collected from 1x 6-well plate of astrocytes over the course of 2 weeks (4x collections resulting in ~48 ml conditioned media, seeding density was lower at $\sim 1.6 \times 10^4$ cells/cm² due to their larger size).

Serum cultured astrocytes required a different method of collection due to the presence of FBS-derived EVs that would co-isolate with the ADEVs. Other researchers have used EV-depleted FBS to culture cells in the presence of serum, whilst reducing contamination. However, this approach does not completely remove FBS-derived EVs, and the removal of EVs from FBS still alters the growth of cells compared to non-EV-depleted serum (Aswad et al., 2016; Lehrich et al., 2018; Urzì et al., 2022). Therefore, serum removal was completed on serum-cultured astrocytes for 72 hours to collect ADEVs whilst avoiding contamination of FBS-derived EVs. As shown in section 3.3.3, the reactive phenotype observed in serum-cultured cells remains during serum-removal, with little cell death and therefore was suitable for ADEV isolation (Figure 3-5, repeated below as Figure 5-1). Given that serum induces proliferation and therefore more cells were available per experiment, 4x T75 flasks were used (~48ml conditioned media, seeding density of $\sim 4 \times 10^4$ cells/cm² resulting in $\sim 1.3 \times 10^5$ cells/cm² at collection). Cells did not attach if initially seeded in FBS-free astrocyte media, thus cells were seeded in normal astrocyte media for 24 hours before serum-removal for 72 hours (cultured in astrocyte medium without FBS).

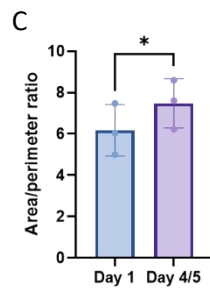
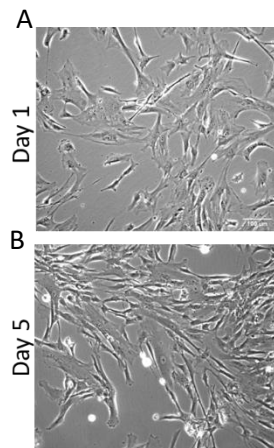


Figure 5-1 - Serum-removal does not change reactive astrocyte morphology, with astrocytes surviving for up to 5 days without serum (repeat of Figure 3-5). Representative brightfield image of serum-cultured astrocytes after 1 day (A) and 5 days (B) of serum removal showed no change in reactive morphology. (C) Area/perimeter was similar to previous serum-cultured levels, with an increase in ratio after 4-5 days. Images were taken at 10x magnification with scale bar representing 100 μ m. Statistical significance was calculated using an unpaired t-test with error bars showing mean and standard deviation.

After collection of ~48 ml conditioned media from either serum-free or serum-cultured astrocytes, ADEVs were isolated using ultrafiltration followed by SEC. Ultrafiltration was required prior to SEC to concentrate the large volume of conditioned medium (48 ml in this work) to a suitable volume required for the qEV columns (500 μ l of concentrated conditioned medium). SEC was preferential over ultracentrifugation to isolate the EVs due to the gentle nature of the isolation and the increased purity of the EV fractions compared to ultracentrifugation. The qEV 70nm columns (Izon, France) used to isolate the EVs are designed to produce ~2.9 ml of void fraction (PBS buffer that was already in the column as the sample was added to the column), followed by three fractions of EV enriched fractions, and then a series of smaller 'free' protein fractions. To maximise yield, all three EV fractions were utilised for downstream applications.

5.2.2 Isolation of tissue-derived BDEVs

BDEVs were isolated from frontal lobe brain tissue donated from people who were diagnosed with AD or ALS alongside age and sex-matched controls for both diseases (Supplementary table 3-6). Two sets of control tissue were required due to the difference in age between the AD and ALS patients (Average ages of patients: ALS = 59, ALS-Ctrl = 60, Alz = 79, Alz Ctrl = 88). BDEVs were isolated using a previously published technique followed by SEC (Huang et al., 2020). For ease of comparison with ADEVs, BDEVs isolated from AD tissue will be abbreviated to Alz BDEVs, and BDEVs isolated from ALS tissue will be abbreviated to ALS BDEVs.

5.2.3 TEM analysis of ADEV and BDEV fractions confirms the presence of extracellular vesicles

To confirm the presence of ADEVs within isolated samples, we first sought to visualise ADEVs. Due to the nanoparticle size of EVs, electron microscopy is currently the only microscopic method that is sensitive enough to visualise EVs. Transmission electron microscopy (TEM) was completed using a concentrated combination of the three EV-enriched fractions. EVs were fixed with 3% glutaraldehyde and negatively stained with 2% uranyl acetate to allow visualisation (Figure 5-2). Classical cup-shaped vesicles (middle is concaved) were observed in both preparations indicating a

successful EV isolation. No observable differences were subjectively identified between serum-free and serum cultured ADEVs; however, it is difficult to determine true EV morphology and size due to the artificial changes caused by the preparation of the samples such as the cup-shaped morphology. EVs are typically vesicular but they collapse under the vacuum required for TEM, creating the cup-shaped morphology (Rikkert et al., 2019; Emelyanov et al., 2020).

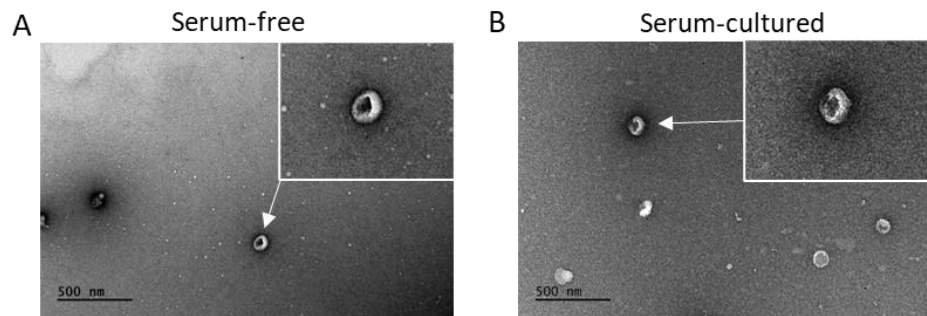


Figure 5-2 - ADEVs were visible in EV fractions after isolation from both serum-free and serum-cultured human primary astrocyte conditioned media. Representative image of (A) serum-free ADEVs and (B) serum-cultured ADEVs. Classical cup-shaped morphology (centre of the EV is concaved) can be observed due to the vacuum conditions of the TEM. A zoomed image is shown in the top right of each image for clearer morphological observation. Images were taken at 9300x magnification with scale bars representing 500 nm (N = 3).

TEM showed that the ADEVs were not highly concentrated within the 500 μ l fractions, with only a few ADEVs visible within a single image confirming the need to concentrate the EVs before use in other techniques such as western blotting or mass spectrometry. In contrast, frontal lobe BDEVs were far more abundant from the tissue samples (which were not subsequently concentrated due to their predicted abundance), with the typical cup-shaped morphology also observed (Figure 5-3). No visual difference was noted between control and disease BDEVs but comparisons are difficult due to the artificial morphology.

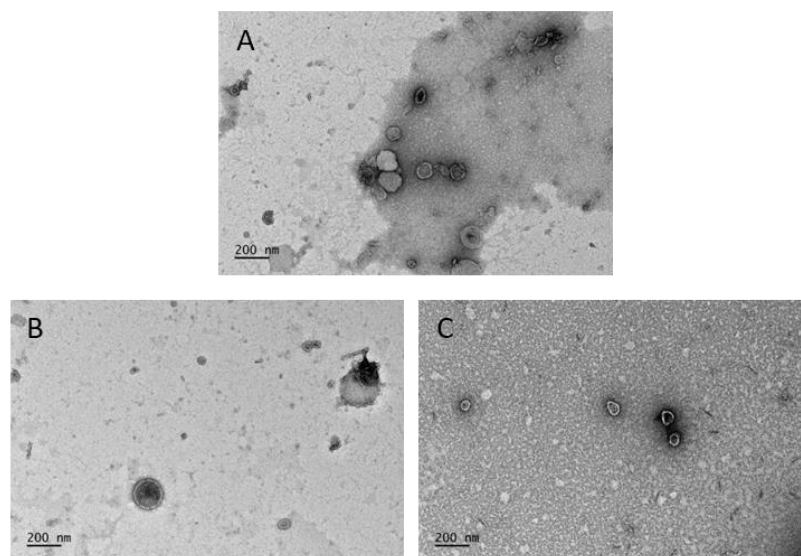


Figure 5-3 - Brain-derived EVs were successfully isolated from frontal lobe tissue of control, AD and ALS patients. (A-C) Representative image of (A) control BDEVs, (B) Alz BDEVs and (C) ALS BDEVs. Classical cup-shaped morphology can be observed due to the vacuum conditions of the TEM. No differences were noted between conditions. Images were taken at 11,000x magnification with scale bars representing 200 nm (N = 1).

5.3 Analysis of EV size and concentration

To measure the size and overall concentration of ADEVs with EV-enriched fractions, two techniques were available allowing a quantitative analysis that can directly compare serum-free and serum-cultured ADEVs. Therefore, nanoparticle tracking analysis (NTA; completed using the Zetaview®) and super resolution microscopy (direct stochastic optical reconstruction microscopy, dSTORM) were trialled, with the results compared to determine which technique should be continued for EV quantification.

5.3.1 Direct stochastic optical reconstruction microscopy (dSTORM) analysis of ADEVs

dSTORM analysis uses a mathematical approach to calculate the size and concentration of particles within a sample. For EV analysis, a lipophilic, fluorescent dye is used to stain the EV membrane which is then activated by the stochastic flickering motion of suitable lasers (i.e. observed as 'blinking' particles). This allows precise localisation of the individual fluorophores as not all particles will be active at the same time. By using fluorescence, only particles with a lipid membrane will be analysed, excluding any contaminants such as free protein.

Only EV fraction 2 (1/3rd of total EV fractions) was measured for each ADEV sample, with EV fraction 2 expected to have the highest concentration of EVs based upon the manufacturer's publications on the IZON columns used to isolate the EVs. The median diameter of the particles as well as the particle concentration were calculated to characterise the EVs. The size distribution was then calculated by summing data for the particles counted across the four images taken for each condition.

The diameter of the particles was not significantly different between conditions, however the serum-free ADEVs had a larger trend in diameter than serum-cultured ADEVs (SF mean = 81.3 ± 6.9 nm vs SC mean = 71.2 ± 2.4 nm, $P = 0.11$; Figure 5-4A). There was a significant difference in the number of particles within each sample type with serum-free ADEVs having 6-times more particles than serum-cultured samples ($P = 0.005$; Figure 5-4B). The difference in the number of particles is likely due to differences in the collection methods for each condition rather than differences in release rate of EVs with large differences in cell number (1x 6-well vs 4x T75 flasks) and collection time (72 h vs 2 weeks) between the serum-free and serum-cultured conditions. A better method for normalisation is required between the collection methods to determine if there is a true difference in size and particle number between the conditions.

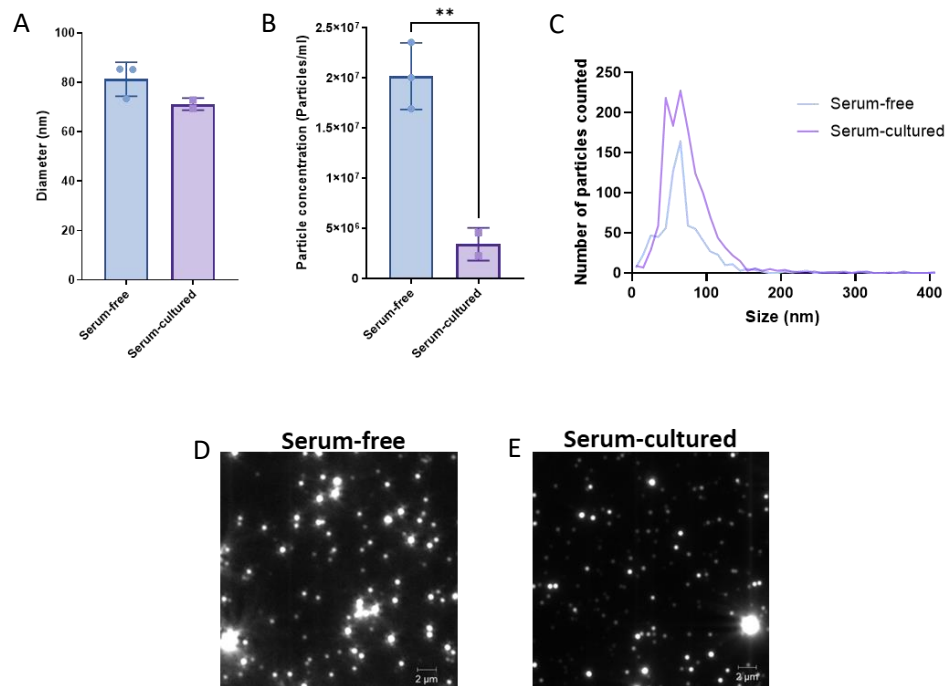


Figure 5-4 - DSTORM analysis identified a difference in particle concentration between serum-free and serum-cultured ADEVs, but not average size. (A) No significant difference in size was detected between serum-free and serum-cultured ADEVs (SF mean = 81.3 ± 6.9 nm vs SC mean = 71.2 ± 2.4 nm; $P = 0.11$). (B) There was a significant difference in the concentration of ADEVs with a 6-fold increase in particle number detected in serum-free ADEVs compared to serum-cultured ADEVs (SF mean = 2.0×10^7 vs SC mean = 3.4×10^6 particles/ml; $P=0.005$). (C) Size distribution shows a peak at ~ 65 nm for both conditions but also a second peak in the serum-cultured ADEVs at ~ 45 nm. More particles were counted in the serum-cultured condition despite fewer ADEVs in the sample overall, but this is due to serum-free samples requiring a 1:10 dilution. (D-E) 16 averaging snapshots taken prior to dSTORM imaging shows the fluorescence labelling of the particles in (D) serum-free and (E) serum-cultured ADEVs. Statistical analysis was completed using an unpaired t-test with a Welch's correction ($N = 2-3$). Error bars represent mean and standard deviation.

The number of particles counted across four different fields of view for each biological replicate was used to plot the size distribution of particles. A peak at ~ 65 nm was observed for both samples, but in the serum-free samples, a much narrower peak was observed compared to the serum-cultured samples, possibly due to a shift to a smaller size range in the serum-cultured ADEVs (Figure 5-4C).

5.3.2 Zetaview analysis of ADEVs

NTA uses light scattering and Brownian motion to measure size distribution of particles in solution. Using the Zetaview[®], the median size, concentration and size distribution is calculated without the need to alter the EV fractions (e.g. no lipophilic dyes are needed). Samples are simply diluted in PBS to achieve a concentration of particles within the optimal measurable range of the machine. A medium only control was included to determine any contribution of particles by the non-conditioned media. This involved a combination of non-conditioned G5 media and astrocyte medium which was processed alongside the astrocyte conditioned media. Due to the ease of sample preparation and measurement, all three EV fractions were analysed per biological replicate.

The median size of the three EV fractions was calculated for both serum-free and serum-cultured ADEVs and compared using a two-way ANOVA. No difference was found between the fractions within each condition ($P = 0.29$; Figure 5-5A). However, the two-way ANOVA revealed a significant decrease in the overall median size of serum-cultured ADEVs compared to serum-free ADEVs, despite no significance detected in the individual fractions when analysed using a Šídák's multiple comparisons test ($P = 0.036$). When the median size of the fractions were combined (i.e. one value for all three fractions), serum-free particles were significantly larger than serum-cultured particles confirming the results of the two-way ANOVA (SF mean = 151.4 ± 19.0 nm vs SC mean = 130.6 ± 4.4 nm, $P = 0.006$; $N = 7-9$; data not shown). In summary, when using NTA to measure particle size, there is a significant decrease in diameter of serum-cultured ADEVs compared to serum-free ADEVs.

When measuring particle concentration, no significant difference was observed between serum-free and serum-cultured ADEVs despite the differences in methodology for collecting both ADEVs (i.e. different number of cells and time period for collection; Figure 5-5B). There was a small difference in the number of particles calculated between fractions, but this was not statistically significant using a two-way ANOVA ($P = 0.16$). The non-conditioned media control had a similar particle size to the EV fractions however it had >1000-fold fewer particles showing that the majority of the particles were released from the astrocytes and thus there were not significant contaminants present in the media. This media control underwent the same processing (ultrafiltration and SEC) as the conditioned media. Pure PBS was found to have a concentration of 1.4×10^6 particles/ml suggesting both PBS and the non-conditioned media control had very little influence on the particle number and size in the EV fractions (media only = 1.3×10^8 particles/ml).

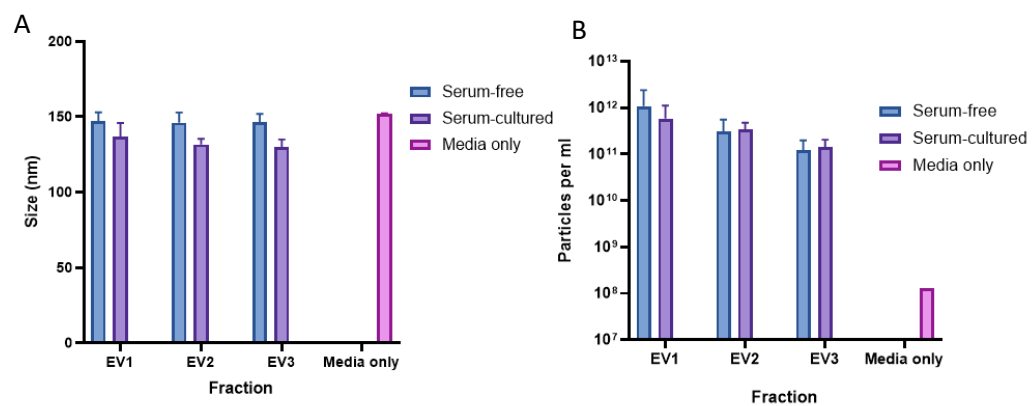


Figure 5-5 - NTA analysis of ADEV fractions from serum-free and serum-cultured human primary astrocytes. (A) Median size of particles is consistent between EV fractions and is similar to particles found within the media only control. However, a significant size difference was observed between serum-free and serum-cultured conditions with serum-free particles having an average size of 146.4 nm across the three fractions, compared to 132.6 nm in serum-cultured fractions ($P = 0.036$). (B) Particle concentration found within the three EV fractions of serum-free and serum-cultured samples shows a decreasing trend amongst the EV fractions, but this was not statistically significant. No difference in concentration was observed between the serum-free and serum-cultured conditions, however there was >1000-fold fewer particles in the media only control than either ADEV condition. Statistical significance was measured using a Two-way ANOVA followed by Šídák's multiple comparisons test. Error bars show mean and standard deviation ($N = 3$).

With a difference in median size observed between serum-free and serum-cultured ADEVs, size distribution plots were created to compare the distribution of particle sizes found within the samples. There was an overall shift in particle size with a uniform decrease observed in the serum cultured ADEVs (Figure 5-6A). Much like the median size of the particles, there was no difference in size distribution between fractions within each condition (Figure 5-6B and C). There were differences in the number of particles counted for each fraction, but this is due to the methodology used to count the particles as the sample dilutions were not accounted for when calculating the size distribution. EV3 fraction was often diluted 50-fold compared to EV1 and EV2 fractions which required a dilution of 100-fold to reach an optimal measurement range. In some cases, EV1 fraction was diluted 200-fold and therefore less particles were present during counting compared to EV2 and EV3, resulting in less traces being included for size distribution analysis. Overall, size distribution shows a global shift in the size of serum-cultured ADEVs compared to serum-free ADEVs.

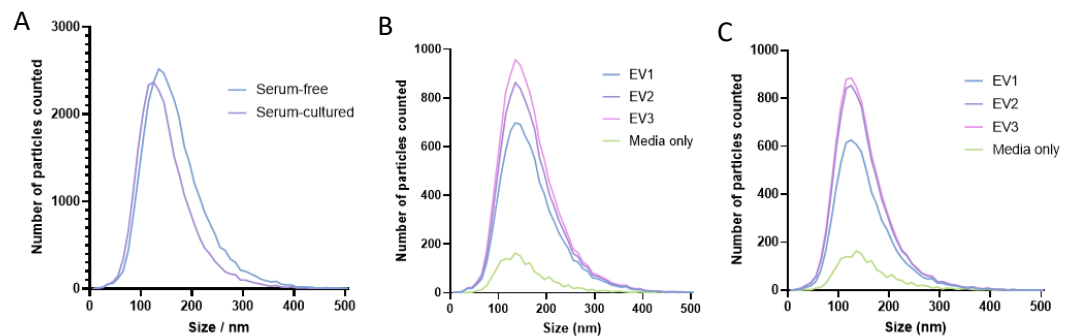


Figure 5-6 - Size distribution of particles identified a shift in serum-cultured ADEV fractions compared to serum-free ADEV fractions. (A) Serum-cultured ADEV fractions have more, small particles detected (<100 nm) with an overall shift to the left compared to serum-free ADEVs. (B and C) EV fractions have the same size distribution of particles with peaks between (B) 120-170 nm for serum-free and (C) 100-150 nm for serum-cultured ADEVs.

5.3.3 Comparison of dSTORM and Zetaview techniques for analysing ADEV size and concentration

5.3.3.1 Size of ADEVs

Both NTA and dSTORM allow quantitative characterisation of particle size and concentration in the samples but produce different results (Table 5-1, comparison using EV fraction 2). NTA indicated a larger median size than dSTORM for both conditions, with a significant decrease in size in serum-cultured ADEVs using NTA but not dSTORM analysis, despite the same trend observed. This size difference between NTA and dSTORM is likely due to the different methods that are used to calculate the size of the particles.

Table 5-1 - Comparison of size and concentration of EV fraction 2 using NTA and dSTORM analysis. NTA and dSTORM analysis show different results for both size and concentration of ADEVs produced from serum-cultured and serum-free astrocytes. Fraction EV2 was used for comparison due to this being the only fraction analysed during dSTORM analysis. Data shows mean and standard deviation, with values corrected for any dilution required for measurement.

	Serum-free ADEVs		Serum cultured ADEVs	
	NTA	dSTORM	NTA	dSTORM
Median size (nm)	146.1 ± 0.5	81.3 ± 6.9	131.6 ± 3.5	71.2 ± 2.4
Concentration (P/ml)	3.12 x10 ¹¹ ± 2.42 x10 ¹¹	2.0 x10 ⁷ ± 3.3 x10 ⁶	3.47 x10 ¹¹ ± 1.33 x10 ¹¹	3.4 x10 ⁶ ± 1.6 x10 ⁶

The Zetaview® uses polystyrene beads to calibrate the machine at the start of every session, often leading to small variations between imaging sessions. The EVs also remain in solution during imaging so it is difficult to focus precisely on all the particles in the field of view. Together, this is likely to overestimate the size of the particles in solution. On the other hand, dSTORM uses mathematics based upon the clustering of the fluorescence to calculate the size of the particles. The particles also settle onto the glass slide used to image the sample resulting in mostly stationary particles being analysed. Alongside the automatic focusing used throughout the experiment, focusing is much easier using dSTORM and therefore would produce more accurate size calculations. However, given that dSTORM uses fluorescence staining of lipid membranes and a mathematical approach to calculate the size of the particles, this method is likely under-representing the size of the particles. The true size of the ADEVs is likely between these two values.

5.3.3.2 Concentration of particles

The concentration of the particles varies considerably between the two techniques with NTA detecting >1000-fold more particles than the dSTORM analysis (Table 5-1; comparison of EV fraction 2). A significant decrease in particle concentration was observed in the serum-cultured ADEVs using dSTORM, but no difference was observed through NTA analysis. dSTORM utilises a lipophilic dye to stain the EVs and therefore will only detect lipid-based particles, such as EVs or liposomes, that have incorporated the dye. However, this relies on all EVs taking up the dye equally, with particles with less than five measurements excluded from analysis. The lasers also photobleach the sample resulting in far fewer hits as the experiment continues. Simply by searching for an area and taking the widefield image, some hits are already lost and therefore would not be included in the analysis. Therefore, dSTORM is likely to under-estimate the number of EVs in the sample. In contrast, the NTA is more likely to over-estimate particle number as it will also measure other non-EV particles that co-isolate with EVs, as seen in the non-conditioned medium and PBS-only controls.

5.3.3.3 Sample preparation and ease of use

Zetaview® sample preparation is easier with samples simply requiring a PBS dilution before injection into the machine, compared to dSTORM which requires sample incubation with a lipophilic dye followed by slide preparation. Excess dye also needs

to be removed so the dye needs to be added before SEC. The Zetaview® is also much easier to use with automated post-capture processing, unlike dSTORM which requires extensive post-capture processing. Therefore, there is less manual alteration to the raw data using NTA reducing any processing errors. The advantage of dSTORM over NTA is the use of fluorescence to identify sub-populations of EVs that can be tagged using fluorescent antibodies. For example, if GFAP was found to be a good ADEV marker, GFAP⁺ ADEVs could be identified in CSF or blood samples. This could be used alongside another fluorescent antibodies for co-localisation studies. Whilst the Zetaview® is capable of measuring fluorescence and could be used to identify sub-populations, dSTORM allows better resolution and better separation of EV clusters resulting in more accurate co-localisation of markers. Within this current work, fluorescent markers were not used so the benefit of dSTORM is outweighed by the speed and ease of use for quantifying ADEVs provided by the Zetaview® (see Table 5-2 for summary).

Table 5-2 – Technical comparison summary between dSTORM and NTA techniques for the quantification of EV concentration and size.

dSTORM	NTA (Zetaview®)
Automatic focusing, with EVs settling on the glass microscope slide (i.e. mostly stationary so easier to maintain focus)	Difficult to focus on EVs with particles remaining in solution
Requires fluorescent labelling of EVs so will only measure a subset of particles (more specific, but will likely miss EV particles with limited staining)	Detects all particles using Brownian motion (PBS-only control still has a high particle count of $\times 10^6$ particles/ml)
Requires extensive preparation of samples, with incorporation of dye/antibody into EV isolation as well as microscope slide set up (use of spacers required for microscope slide)	No modification to EV fractions, with samples simply requiring a dilution in PBS prior to analysis
Manual image capture with evidence of photobleaching whilst moving around the sample (therefore leading to underestimation of particle concentration)	Automatic image capture of 11 positions, which are then averaged post-capture
Long image capture time (~10 min), with each image made from the compression of 5000 frames (image capture is completed using a video)	Short capture time (~2 min) with only 11 positions combined for a final result
Extensive, manual post-capture processing which requires optimisation of inclusion threshold criteria	Automatic post-capture processing

5.3.3.4 Conclusions

Overall, the Zetaview® was cheaper, easy to use and provided data that was easier to interpret in comparison to dSTORM (Table 5-2). Fluorescent conjugated antibodies were not used in the current project with the work focusing on unbiased cargo

characterisation rather than specific markers. ADEVs were isolated from a monoculture of astrocytes and therefore these ADEVs do not need to be separated from EVs released by other cell types which would be important when using more complex samples such as blood or CSF. Whilst the Zetaview® may result in over-estimations of size and concentration, the work in this thesis is focused on comparing conditions and therefore, absolute measurements are less important than the consistency between the measurements of the samples. Therefore, NTA using the Zetaview® will be used for the remainder of the work presented in this thesis. To ensure consistency between samples, samples will be analysed during the same imaging session where possible to remove technical variability.

5.3.4 ADEVs were isolating in earlier fractions than expected using generation 2 IZON columns

Due to improvements in the manufacturing process, generation 2 IZON columns were used to isolate EVs in subsequent work, instead of the original columns used for ADEV characterisation. For generation 2 columns, the manufacturer suggests that EVs will elute in the first three 400 µl fractions (EV1 - EV3, total 1200 µl instead of the original 500 µl fractions, total 1500 µl) after the 2.9 ml PBS void. The manufacturer also indicates that the middle EV fraction (EV2) should have the highest concentration of EVs. This was not observed in our subsequent NTA using the generation 2 columns with EV1 fraction having the highest concentration of particles, suggesting the EVs are eluting earlier than expected (observed in Figure 5-5B). Therefore, the final 400 µl fraction of the PBS void was also collected and measured using the Zetaview® (SEC fractions = 2.5 ml PBS void followed by collection of a final void fraction of 400 µl, 3x EV fractions and 2x Protein fractions, each of 400µl). Particle concentration found that EV-sized particles were eluting earlier than expected with many particles present in the last void fraction of the ADEVs (V1; Figure 5-7A). There was no change in median size across any of the fractions collected (Figure 5-7B). This suggested that the final void fraction (V1) should be used in subsequent experiments alongside the other three EV fractions.

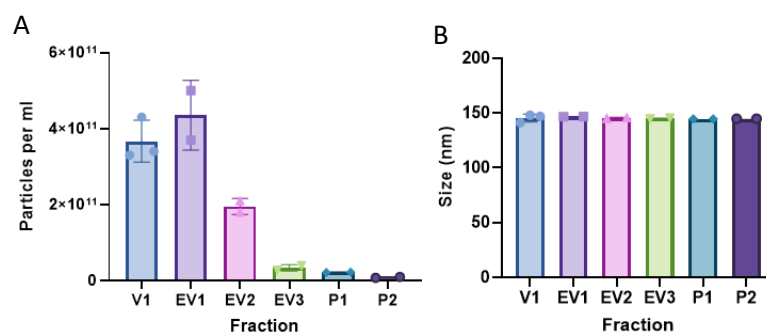


Figure 5-7 – Using generation 2 IZON columns, EVs were eluting earlier than expected from the columns with many particles identified within the final void fraction. (A) A large proportion of serum-cultured ADEV particles were detected within the final 400 µl of the void (V1 fraction) suggesting EVs were eluting earlier than expected. (B) No difference in size was detected between any of the fractions. Error bars represent mean and standard deviation of technical repeats for each fraction tested (N = 1). V1 represents the final void fraction, EV1-3 represents the predicted EV fractions by the manufacturer of the qEV columns and, P1 and P2 represent the predicted protein fractions.

5.3.5 The effect of freezing on ADEV size and concentration

Whilst optimal to utilise EVs for downstream analysis immediately after isolation, this is not always possible and the EVs require storage at -80°C . There have been conflicting results regarding the effect of freezing on EV integrity, so this was investigated within the ADEVs (Gelibter et al., 2022; Görgens et al., 2022; Wright et al., 2022). Particle size and concentration were measured immediately after EV isolation (fresh) and again, after a week of storage at -80°C (frozen). No difference in particle concentration was found when freezing the purified ADEVs for 1 week, however there was a decrease in the size of particles (Figure 5-8). A reduction in particle size could be explained by the presence of larger EVs dividing into multiple smaller EVs during the freezing process. However, if this was true, an increase in the particle concentration would be expected. Instead, this reduction in size is likely due to technical variation observed when using the Zetaview[®] for analysis. Due to small differences in calibration with polystyrene beads and focusing before each image, differences in median size can be observed between different sessions. For example, the average size may vary between 150-160 nm during analysis, whereas in another session, the average size may vary between 120-130 nm. This highlights the importance of comparing samples within the same analytical session to reduce the effect of technical variability. This is not possible when measuring the effect of freezing due to the nature of the experiment.

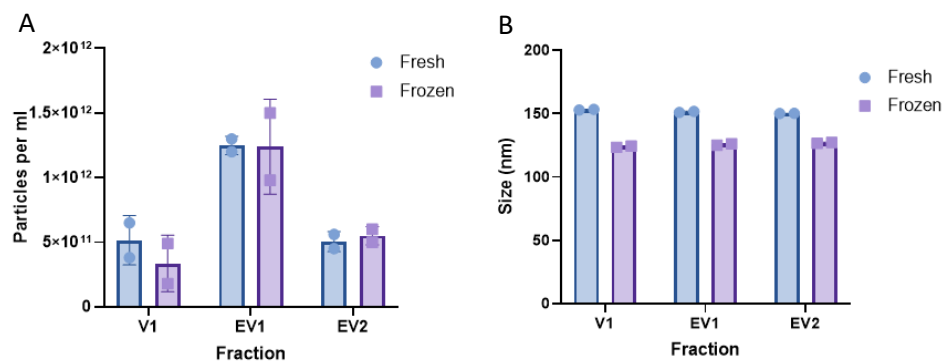


Figure 5-8 – Freezing human primary ADEVs at -80°C does not affect particle concentration. (A) No change in particle concentration was found after one week of storage at -80°C . (B) Median particle size was found to decrease but this is likely due to technical variation of the Zetaview[®]. Error bars represent mean and standard deviation of technical repeats of serum-cultured ADEVs ($N = 1$).

As well as it being advantageous to stockpile conditioned media, allowing experiments to be conducted on all biological replicates at the same time (thereby reducing technical variation), storing conditioned media is necessary for serum-free conditioned media collections with media collected over two weeks from four separate collections. Therefore, the effect of freezing the conditioned media from human primary astrocytes prior to EV isolation was also investigated to determine how this effected the ADEV yield. Conditioned media was collected from serum-cultured astrocytes after 72 hours (using the serum-removal method) and either frozen at -80°C for 1 week before isolation or isolated immediately. NTA analysis was then completed to compare size and concentration. Of the EVs isolated from fresh conditioned medium, EVs were either stored for 1 week at 4°C or were frozen at -80°C for 1 week before re-analysis to confirm the results seen in Figure 5-8.

When investigating the effect of freezing conditioned medium on particle concentration, very little difference was observed between fresh and frozen conditioned medium (Figure 5-9A). In fact, there was a small increase in particle concentration after freezing the conditioned medium suggesting there may be some budding of larger particles into smaller particles. However, there was a decrease in particle concentration after freeze-thawing EVs isolated from fresh conditioned medium suggesting freezing conditioned medium is preferable to freezing isolated EVs from fresh conditioned medium. Storage of conditioned media for 1 week at 4 °C had no effect on particle concentration. No difference in medium size was found between any of the conditions contrasting the previous findings, confirming the difference observed in Figure 5-8 was due to variations in the NTA analysis (Figure 5-9B). Statistical analysis was not completed due to the limited biological repeats for the experiment (N = 1). In summary, the size and concentration of ADEVs appear to be unaffected by storing conditioned media for 1 week at either -80 °C or at 4 °C. In fact, it appears to be preferable than storing isolated EVs at -80 °C for 1 week.

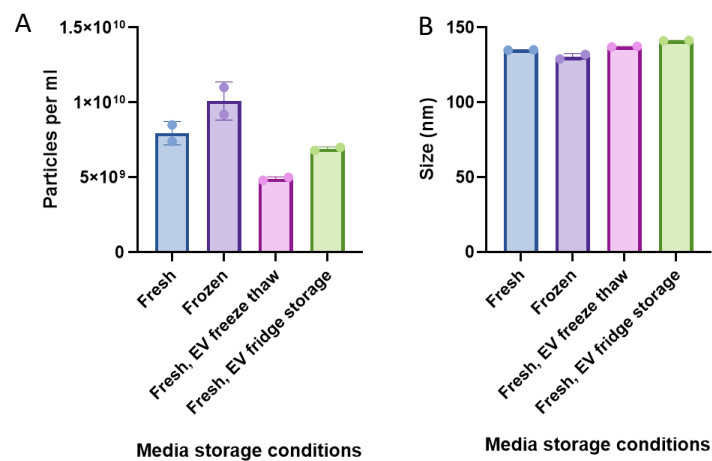


Figure 5-9 – Storage of astrocyte conditioned media at either 4 °C or -80 °C does not affect ADEV concentration and is preferable to freeze-thawing isolated EVs. (A) Freezing astrocyte conditioned media had limited effect on the particle concentration after EV isolation, compared to fresh conditioned medium. In fact, a reduction in particle concentration was observed in EVs after isolation from fresh medium when frozen for 1 week and thawed (pink) compared to isolated EVs which were stored at 4 °C (green). (B) No difference in the size of particles was detected between fresh and frozen astrocyte conditioned medium. Error bars represent mean and standard deviation of the two technical repeats completed using serum-cultured ADEVs (N = 1).

Future analysis will aim to measure particle size and concentration within the same session when comparing conditions to reduce the variation seen in the NTA. Efforts will also be made to use fresh ADEVs for functional analysis to avoid any differences due to storage, however when required, conditioned media should be frozen prior to EV isolation. Freezing is less problematic when using ADEVs for proteomic analysis as EV integrity is not required. Proteins are stable when frozen and therefore freezing is likely to benefit the samples by reducing the activity of proteases which would degrade any proteins.

5.3.6 Zetaview analysis of control and disease BDEVs

As an endogenous comparison to ADEVs, BDEVs isolated from control and disease (ALS and Alzheimer's disease) human frontal lobe tissue were also analysed using the Zetaview®. NTA showed no difference in the size of particles isolated from the diseased tissue compared to the matched controls (Figure 5-10A and B). Alz BDEVs were larger than the ALS BDEVs, however this is likely due to technical differences between measurements (analysis completed during separate sessions) because the size of BDEVs from the Alz-controls were also larger than those of the ALS-controls (143.4 ± 0.4 nm vs 125.6 ± 0.1 nm). To ensure true comparison of control vs disease particle size, the disease BDEVs were analysed at the same time as their matched controls. Size distribution plots from all BDEV samples show a similar pattern to previous ADEV analysis suggesting successful isolation of EVs (Figure 5-10C and D).

Similar concentrations of particles were observed across the ALS and ALS-control conditions (ALS = $1.55 \times 10^{13} \pm 1.06 \times 10^{13}$ vs ALS control = $1.65 \times 10^{13} \pm 1.13 \times 10^{13}$ particles/ml per 100 mg; Figure 5-10E). For Alz BDEVs, similar concentrations were also observed in the disease and matched control (Alz = $2.31 \times 10^{13} \pm 1.54 \times 10^{13}$ vs Alz control = $1.87 \times 10^{13} \pm 1.58 \times 10^{13}$ particles/ml per 100mg; Figure 5-10F).

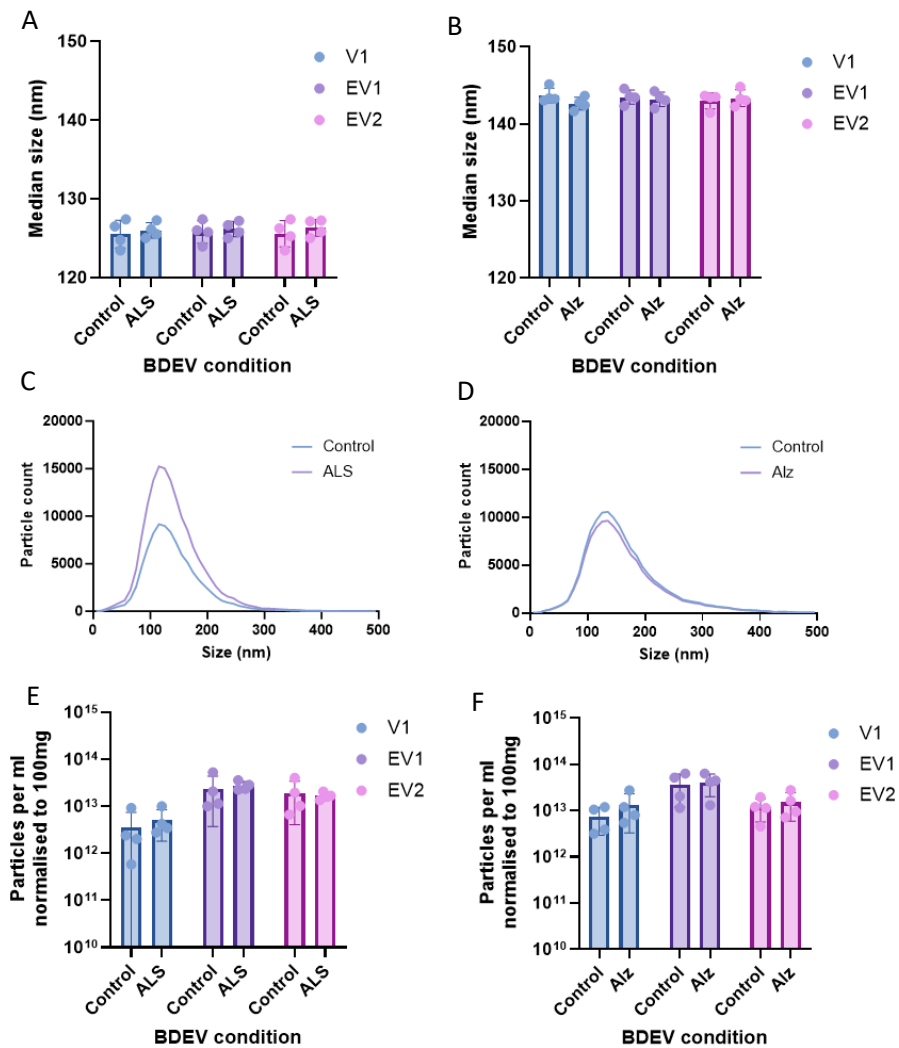


Figure 5-10 - NTA analysis of BDEVs isolated from human control, Alzheimer's disease and ALS tissues shows no difference in the size or concentration of BDEVs between conditions. (A-B) No difference in median size of (A) ALS and (B) Alz BDEVs compared to their matched controls. (C-D) A similar size distribution was observed between disease and their matched control BDEVs. (E-F) No difference in the concentration of particles between disease and control BDEVs. Statistical analysis was completed using a two-way ANOVA followed by Šidák's multiple comparisons test. Error bars represent mean and standard deviation (N = 4).

5.3.7 Comparison of particle size and concentration between ADEVs and BDEVs

Whilst it is difficult to directly compare the concentration of ADEVs and BDEVs due to the different origins of EVs (cell culture vs tissue) and collection methods, some comparisons can be made between the size of the EVs. Similar size distributions were observed between all EV samples, with median size ranging from 125 – 146 nm which is expected using SEC isolation (Table 5-3). Whilst a difference in size was observed between quiescent (serum-free) and reactive (serum-cultured) ADEVs, no

difference was observed between control and disease BDEVs. ~50-fold fewer particles were found within cell culture EV fractions compared to BDEV fractions, which is most likely due to the number of cells in culture being far fewer than the number of cells within the tissue (Table 5-3; von Bartheld et al., 2016).

Table 5-3 - Comparison of the size and concentration of ADEVs and BDEVs using NTA (Zetaview®). Median size and mean particle concentration were calculated using NTA for both ADEVs and BDEV fractions. For BDEVs, particle concentration was calculated per 100 mg of tissue to normalise between samples (ADEVs N= 3, BDEVs N = 4).

	Median size (nm)	Particle concentration (Particles/ml)
Serum-free ADEVs	146.4	5.05 x 10 ¹¹
Serum-cultured ADEVs	132.6	3.58 x 10 ¹¹
ALS BDEVs	126.2	1.55 x 10 ¹³
ALS control BDEVs	125.6	1.65 x 10 ¹³
Alz BDEVs	143.1	2.31 x 10 ¹³
Alz control BDEVs	143.4	1.87 x 10 ¹³

5.4 Detection of EV-associated markers in ADEV and BDEVs

At present, there are no established universal markers of EVs and in particular, no markers to confidently distinguish between different sub-types of EVs such as microvesicles and exosomes. Instead, MISEV guidelines recommend immunodetection of multiple endosomal (exosome origin) and membrane markers that are thought to be enriched within EVs, as well as the absence of proteins that would not be expected within EVs such as Golgi-apparatus or mitochondrial markers. There are also issues with comparing protein expression due to many EV samples having undetectable levels of protein using regular protein assays (such as Bradford or BCA assays) and no well-established housekeeping proteins identified for normalisation.

5.4.1 Western blotting of EV markers within ADEVs

To initially identify EV-related proteins within the ADEVs four EV-associated markers (CD63, CD81, FLOT1 and ALIX) were measured using immunoblotting on serum-free and serum-cultured ADEVs. CD63 and CD81 are endosomal proteins associated with exosomes, whereas FLOT1 and ALIX are associated with the cell membrane and cytosol. Calnexin expression was investigated as a negative EV marker to identify the level of cell debris contamination in the samples. Calnexin is an endoplasmic reticulum protein and therefore would not be expected within small EVs.

Despite extensive optimisation, not all markers were detected within the ADEVs which is likely due to the sensitivity of the technique. Concentrating the EV fractions using further ultrafiltration did improved signal when staining for calnexin, ALIX and FLOT-1 but no signal was detected in CD81 or CD63 despite detection within the cell lysate (Figure 5-11). Flow-through from the protein concentrators were also analysed to confirm the EVs remained within the concentrator at a smaller volume. Calnexin displayed a strong signal suggesting EV fractions may contain some cell debris. It is difficult to compare expression between proteins (due to variations between

antibodies) and between conditions through immunoblotting and a lack of housekeeping proteins within the EVs.

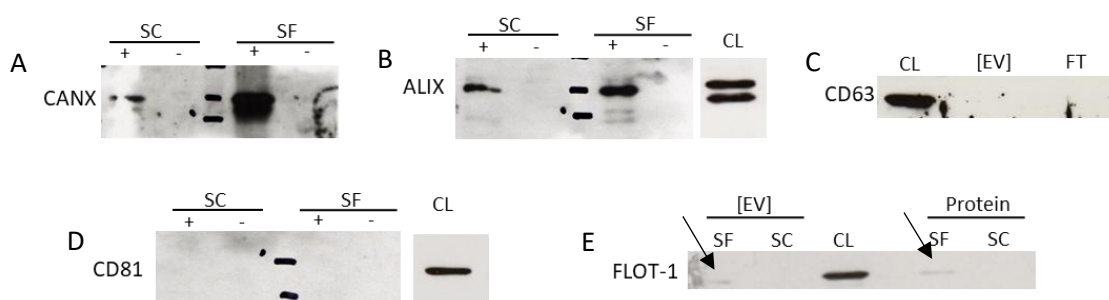


Figure 5-11 - Immunoblotting identifies some EV-associated markers in serum-free and serum-cultured ADEVs. (A-B) Protein bands were detected using (A) anti-calnexin (CANX) and (B) anti-ALIX antibodies in both the serum-free and serum-cultured ADEVs after concentration (+ represents EV sample). No protein was detected in the flow-through from the EV concentrators (represented by -) confirming EVs were concentrated by further ultrafiltration. (C) CD63 and (D) CD81 were not detected in concentrated ADEV fractions but were present in cell lysate samples. (E) FLOT-1 was faintly detected in both the concentrated EV fraction and the protein fraction of serum-free ADEVs (black arrows) but was not detected in the serum-cultured ADEVs. Cell lysate (CL) controls were also included to ensure a lack of signal was due to the samples and not due to the technique, with the exception of CANX because the signal intensity was too high to be distinguishable. EV fractions were combined using further ultrafiltration to increase EV concentration and therefore the concentration of protein within the sample.

5.4.2 Identification of EV protein markers in ADEVs

Due to the many issues identified with immunoblotting of EV samples, SWATH mass spectrometry was completed to identify EV-associated proteins within the samples. SWATH-MS is far more sensitive than immunoblotting with less reliance on antibody quality, as well as providing an unbiased relative quantification. For SWATH-MS analysis, purified ADEV fractions V1, EV1, EV2 and EV3 were combined and concentrated using further ultracentrifugation to approximately 50 μ l. Samples were then processed as described in section 2.4.4.2 alongside parent astrocyte whole cell lysates (described in section 4.4). SWATH-MS analysis was completed in the same way as the astrocyte cell lysates and will be described in more detail later in this chapter (see Figure 4-10 for analysis pipeline; section 5.5 for full analysis of ADEV proteome by SWATH-MS). In total, 526 proteins were identified in more than two replicates of serum-free ADEVs and 300 proteins identified in the serum-cultured ADEVs.

As alluded to previously, MISEV guidelines introduces 5 categories of proteins to investigate within EVs – 1: Transmembrane proteins associated with membrane/endosomes, 2: Cytosolic proteins, 3: Non-EV co-isolates, 4: Transmembrane, lipid-bound soluble proteins associated with intracellular compartments other than membranes and endosomes, 5: Secreted proteins recovered with EVs. The suggestion is to investigate at least one protein from each of the categories, with the immunoblotting above (section 5.4.1) already measuring category 1 (CD63 and CD81), category 2 (ALIX and FLOT1) and category 4 (Calnexin). Due to the large number of proteins detected within SWATH analysis, multiple proteins from each category are possible to detect so a thorough analysis can take place (Figure 5-12).

Of the category 1 proteins identified, many were enriched within the ADEVs with the exception of LAMP1. CD63 and CD81 were identified by SWATH-MS in the ADEVs despite their absence in previous immunoblotting highlighting the improved sensitivity of mass spectrometry (Figure 5-12A). Category 2 proteins were also identified within the ADEVs, supporting evidence of EV-enrichment in the fractions. However, in contrast to category 1 proteins, these proteins were also highly expressed in the cell lysates (Figure 5-12B). The difference in expression between category 1 and 2 proteins is likely due to the ratio of cell membrane and cytoplasm within EVs and cell lysates. EVs have a high membrane to cytoplasm ratio due to their small size, in comparison to cell lysates which will have a greater cytoplasm area. Therefore, more cytosolic proteins will be expected in cell lysates than EVs in respect to cell membrane proteins.

More category 3 lipoprotein markers were identified within serum-free ADEVs compared to serum-cultured ADEVs (Figure 5-12C). APOB and APOE were not detected within serum-cultured ADEVs despite high relative abundance in the serum-free ADEVs. High levels of albumin were detected in all samples which is a likely a contaminant of the cell culture medium. Very low expression of category 4 proteins within the ADEVs suggests that the fractions are free of cell debris contaminants and therefore the proteins detected are likely secreted by the cells or found within EVs (Figure 5-12D). Calnexin was not identified within the ADEVs despite identification by immunoblotting. Secreted proteins (category 5) were found in high abundance within ADEV samples with higher expression found in ADEVs than cell lysate samples suggesting co-isolation with EVs (Figure 5-12E).

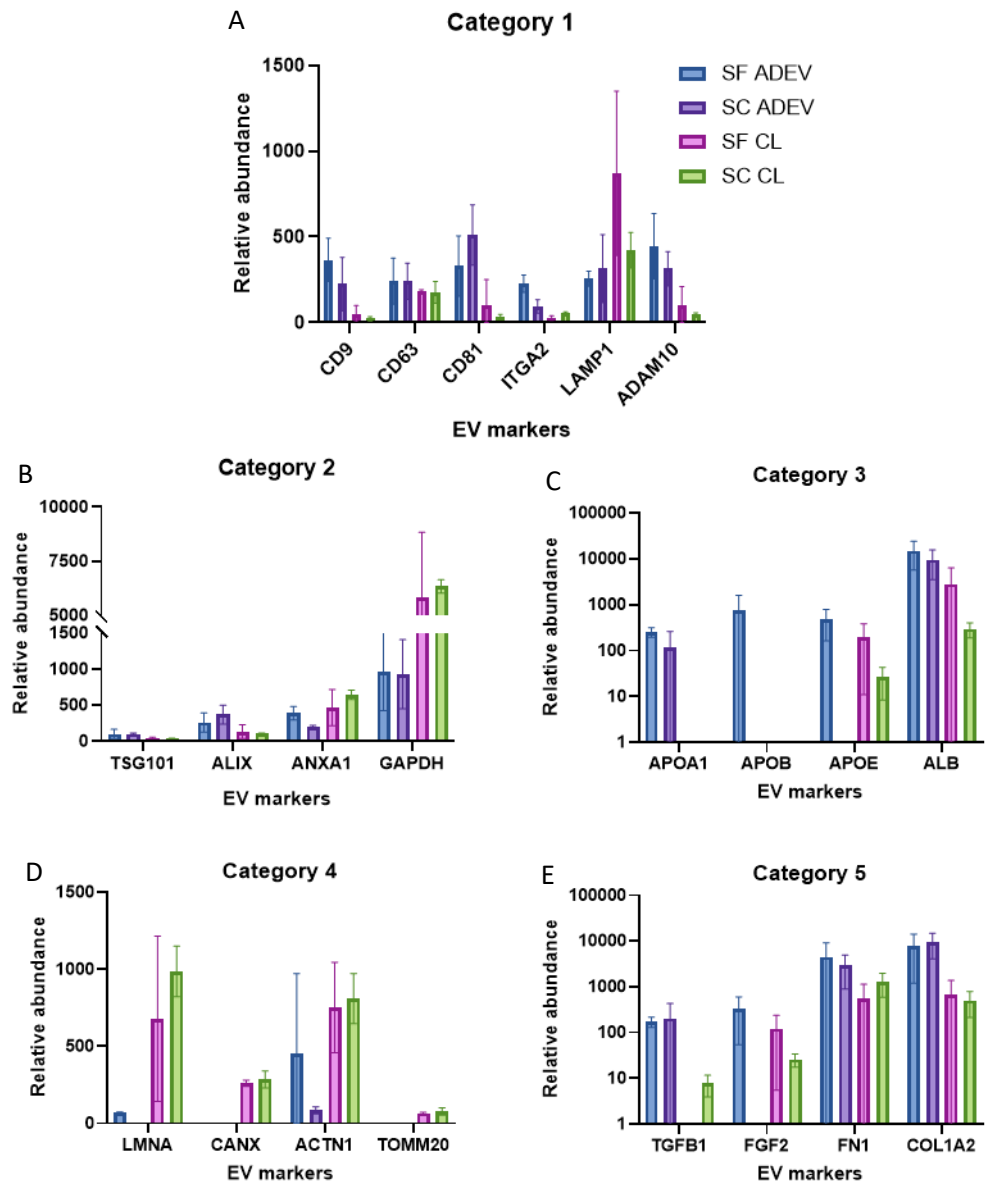


Figure 5-12 – Relative abundance of EV-associated proteins (category 1 and 2) and cell-associated proteins (category 3-5) identified within human ADEV and their parent astrocyte lysate samples using SWATH-MS. (A) Five of the six EV-associated membrane proteins identified had a higher abundance than the parent cell lysate samples suggesting EV enrichment. (B) Cytosolic proteins were identified within EVs as well as their parent cell lysates. (C) Lipoprotein markers were identified in the serum-free ADEVs but often not in the serum-cultured ADEVs, with only APOA1 and ALB expressed in serum-cultured ADEVs. (D) Organelle associated markers were rarely expressed in the ADEVs despite expression within the parent cell lysates. (E) Secreted proteins were common co-isolates with ADEVs which were often enriched in ADEV samples compared to cell lysate samples. Error bars represent mean and standard deviation (N = 3). Protein abundance was relative across samples due to the nature of SWATH analysis (arbitrary units).

5.4.3 EV markers within BDEVs

With SWATH analysis providing a more extensive characterisation of protein expression compared to immunoblotting, BDEVs were also analysed by SWATH-MS. BDEVs were processed using the same methodology as the ADEVs, with between 1377 and 1617 proteins identified in at least four of the eight biological replicates analysed for each BDEV condition (full analysis described in section 5.6). The five MISEV categories were also investigated with similar proteins identified to those observed in the ADEVs (see previous Figure 5-12). A similar expression between control and disease BDEVs was identified across category 1 and 2 proteins (Figure 5-13A and B). TSG101 was not identified in the BDEVs so FLOT1 was used instead for characterisation. ITGA2 was also not identified within at least 4 replicates for each of the conditions but ITGA1 was identified.

Category 3 lipoproteins and category 4 cell-markers were identified within the BDEVs suggesting some contamination with liposomes and cell debris (Figure 5-13C and D). This is probably due to the destructive nature of the technique used to isolate the EVs (mechanical chopping and collagenase), which would likely lead to some cell debris. The brain is also highly myelinated and therefore has a much higher lipid content. Whilst SEC should remove the majority of the cell debris (both larger and smaller than EV size range), debris of a similar size to the EVs would naturally co-isolate in the samples. TOMM20 was not identified within the BDEVs but another mitochondrial protein, IMMT was identified. Very few secreted proteins were identified in the samples suggesting these proteins were separated from EVs during isolation in contrast to the ADEV proteins. Some of the secreted proteins identified within the ADEVs, such as FGF2, may be found within the original cell culture medium and therefore would not necessarily be abundant within human tissue.

Together with the TEM and NTA, the mass spectrometry analysis suggests that EVs can be isolated from both human primary astrocyte cell culture medium (ADEVs) and human tissue (BDEVs). Similar sizes of particles were identified within both sets of samples as well as similar morphology and EV-associated proteins indicating that the ADEVs are comparable to those observed endogenously. With high confidence that the EV fractions are indeed enriched with EVs, further analysis of the SWATH-MS data was completed on the ADEV and BDEV cargoes.

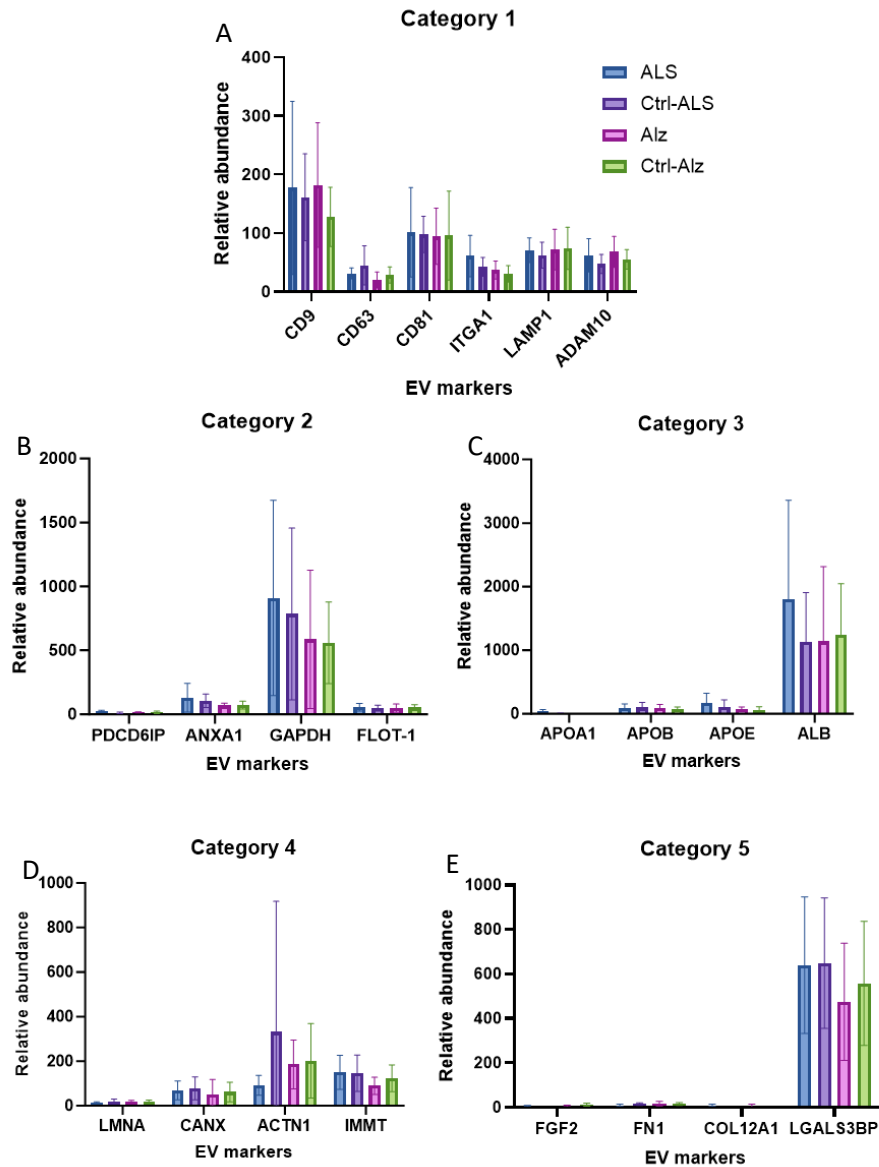


Figure 5-13- Relative abundance of EV-associated proteins (category 1 and 2) and cell-associated proteins (category 3-5) identified within healthy and disease BDEVs using SWATH-MS. (A) Category 1 and (B) category 2 proteins had a similar relative abundance across the 10 markers identified within BDEVs (C) Lipoprotein markers were identified in the BDEVs but in low abundance with the exception of albumin. (D) Some organelle associated markers were identified suggesting some cellular contamination. (E) Secreted proteins were not highly expressed in BDEVs with the exception of LGALS3BP. Error bars represent mean and standard deviation (N = 8). Protein abundance was relative across samples due to the nature of SWATH analysis.

5.5 SWATH analysis of ADEVs to understand the ADEV proteome

For SWATH-MS analysis, concentrated serum-free and serum-cultured ADEVs (all EV fractions as well as 400 μ l void fraction combined) were analysed by SWATH-MS at the same time as the parent astrocyte cell lysates, previously described in section 4.4 (N = 3). As with parent cell lysates, peptides which mapped to more than one protein

were removed, and the samples normalised using the total spectra. Unlike the cell lysates, the ADEVs were not normalised to protein concentration due to the undetectable protein levels on a standard BCA assay. However, as determined in section 5.3.2, no significant difference in particle concentration was found between the serum-free and serum-cultured ADEVs suggesting protein concentration would be comparable. Finally, common contaminants albumin and keratin were removed from the analysis (albumin was only included when investigating EV markers, above).

5.5.1 Comparing similarity between the proteomes of serum-free and serum-cultured ADEV biological replicates

A PCA was completed on the relative abundance of proteins obtained from three replicates of serum-free and serum-cultured ADEVs to determine the similarity between samples (completed prior to removal of contaminants and missing replicates but after removal of peptides linked to more than one protein, see Figure 4-10 for analysis pipeline). A small distinction was identified between serum-free and serum-cultured ADEVs with 73% of the data described by the first principal component (PC1) and the second principal component (PC2) accounting for 25% of the separation. The replicates were not clustered showing a substantial amount of variation between samples. This suggests more replicates would be required for a more confident characterisation of the proteomes between samples, much like the cell lysate comparison. With no clear difference between the conditions, a PLS-DA was not completed (normally identifies proteins which are most responsible for any difference).

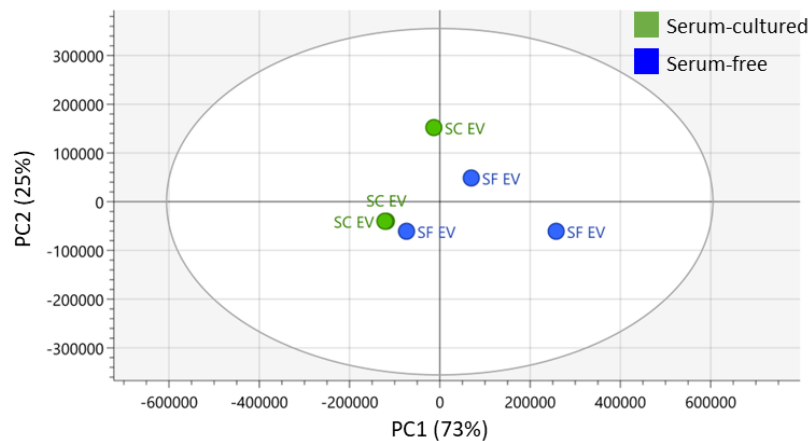


Figure 5-14 - PCA of ADEV proteins indicates no distinct difference between serum-free and serum-cultured ADEV proteomes by SWATH-MS. PCA shows some separation between the proteomes of serum-free (blue) and serum-cultured (green) ADEVs, however the samples are not tightly clustered showing high variability between replicates. PC1 accounts for 73% of the difference between groups and PC2 accounts for 25% (total data described = 98%).

The number of missing values were investigated to determine the similarity between replicates as well as to identify the proportion of proteins to be included for further analysis (Figure 5-15). As with the previous SWATH cell lysate analysis (see section 4.4), further analysis was completed on the proteins that were identified in at least

two biological replicates for serum-free and serum-cultured ADEVs which included 35-40% of identified proteins.

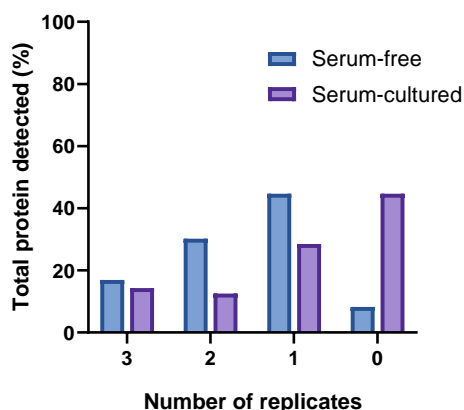


Figure 5-15 – High variation between biological replicates by SWATH-MS, with the majority of proteins only identified in either 1 or 2 biological replicates for both serum-free and serum-cultured ADEVs. High variation between the biological replicates is evident in the serum-free and serum-cultured ADEVs with a large proportion of the total proteins identified, not found in all 3 replicates (>80% found in 2 or less replicates). 0 replicates represent proteins that were only identified in the opposing condition (i.e. a protein identified in serum-free replicates, but not serum-cultured replicates would be identified as 0 in the serum-cultured condition). Percentages were calculated using the total number of proteins detected across both serum-free and serum-cultured conditions.

When comparing proteins identified within each replicate, the serum-free and serum-cultured ADEVs had a fairly consistent number of proteins within each condition, and no difference between serum-free and serum-cultured ADEVs (SF mean = 580 ± 267 vs SC mean = 359 ± 119 proteins, P = 0.99, Figure 5-16A). As expected, the number of proteins identified were much lower in ADEVs than parent cell lysates with a significant difference identified between the serum-cultured condition (P = 0.004).

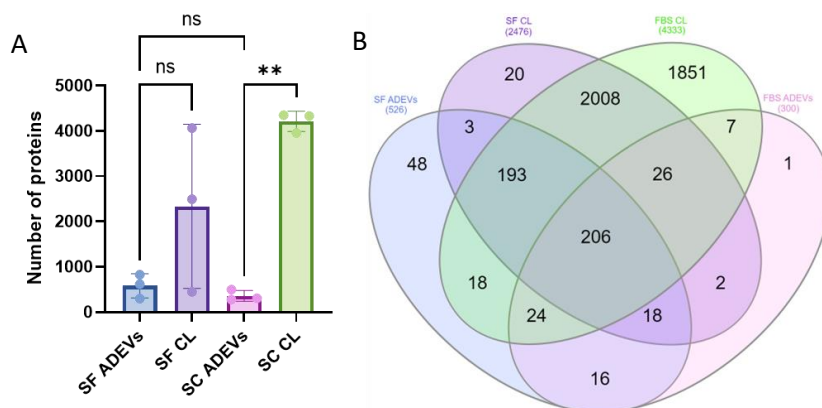


Figure 5-16 – Fewer proteins were identified by SWATH-MS in serum-free and serum-cultured ADEVs compared to their parent cell lysates. (A) Number of unique proteins identified in each of the biological repeats. (B) The majority of proteins (55.6%) were identified in multiple conditions with few unique proteins identified exclusively in ADEVs. Error bars represent mean ± standard deviation (N=3).

Similar to the SWATH-MS analysis completed on the cell lysates in section 4.4, proteins were excluded that were only present in one replicate of each sample to improve confidence that the protein was identified correctly. After applying this

criteria, 526 proteins were identified within the serum-free ADEVs compared to only 300 within the serum-cultured ADEVs, with 264 proteins found in common between the ADEVs (Figure 5-16B). There were few proteins that were exclusive to the serum-free or serum-cultured conditions (ADEV and CL) suggesting the proteome of astrocytes and their ADEVs does not change after culture in serum. Interestingly, 16 proteins were identified within both ADEV conditions but not in the astrocyte cell lysates, suggesting these proteins may be enriched within ADEVs (Table 5-4). STRING analysis was completed on these proteins to determine their connectivity and subcellular location. Of the 16 proteins, 9 were highly connected (bold and italicised in Table 5-4) with 13 found to be associated with the “extracellular region” using GO compartment analysis. Of the 13 extracellular proteins, 6 were also associated with “extracellular vesicles” supporting the hypothesis that these proteins are enriched in ADEVs (GC, PLG, APOA1, ITIH4, IGSF8 and SDC1).

Table 5-4 – 16 proteins were identified within serum-free and serum-cultured ADEVs but not their parent cell lysates. Of the 16 proteins identified, 9 were highly connected within the STRING analysis (Italicised and in Bold, STRING connectivity not shown).

A1BG	GC	IGSF8	PLG
APOA1	HAPLN1	ITIH1	SDC1
CFI	HAPLN3	ITIH3	SERINC5
EVA1A	IGHG4	ITIH4	SSC5D

5.5.2 Qualitative analysis of the ADEV proteome

5.5.2.1 Pathway analysis

Whilst half of all ADEV proteins were identified in both serum-free and serum-cultured ADEV conditions (264 proteins), 262 proteins were unique to serum-free ADEVs and 36 were exclusive to the serum-cultured ADEVs (Figure 5-16B). KEGG pathway analysis was completed on these proteins to identify pathways that may be over-represented within the ADEVs. No pathways were upregulated in the proteins exclusive to the serum-cultured ADEVs, likely due to the limited number of proteins. On the other hand, 33 pathways were significantly upregulated in the unique serum-free ADEV proteins (Figure 5-17). These pathways were very similar to those observed within both cell lysates in section 4.4.3 such as “Ribosome” and “Carbon metabolism”, suggesting these pathways are only upregulated in serum-free ADEVs due to the increased number of proteins identified compared to the serum-cultured ADEVs, and not because of the ADEV phenotype.

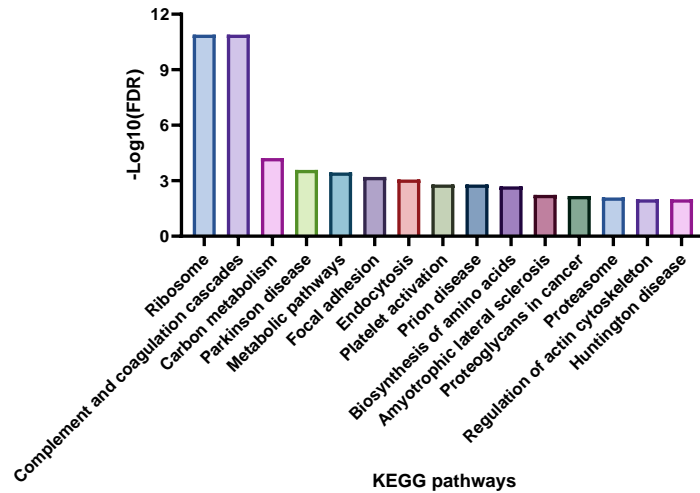


Figure 5-17 - The 15 most significantly upregulated KEGG pathways in ADEV proteins identified exclusively in ADEVs purified from serum-free cultures. A total of 33 KEGG pathways were identified as significant amongst the 262 proteins found exclusively in serum-free ADEVs.

Pathway analysis was also completed on all proteins identified within the serum-free and serum-cultured ADEVs (in at least two replicates) to identify which pathways were over-represented in EVs. In the serum-free ADEVs, 68 pathways were upregulated compared to 50 pathways in the serum-cultured ADEVs. Many of these pathways were identified in both ADEVs (43 pathways), consistent with the high number of proteins found in both ADEV conditions (Figure 5-18).

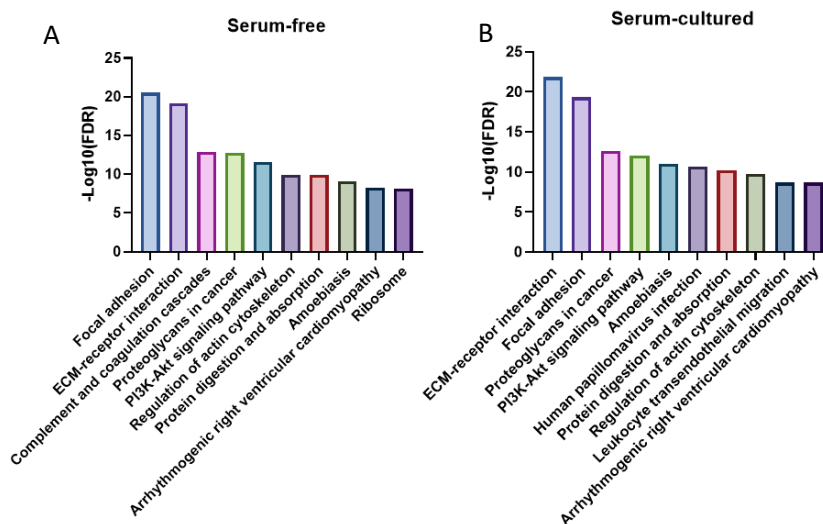


Figure 5-18 - Top 10 KEGG pathways upregulated in serum-free and serum-cultured human primary ADEV proteins. (A) Serum-free ADEVs had a total of 68 upregulated KEGG pathways. (B) Serum-cultured ADEVs had 50 upregulated pathways. Similar pathways were identified in both serum-free and serum-cultured ADEV proteomes suggesting little difference in the ADEV proteomes between the conditions.

5.5.2.2 Vesiclepedia database shows ADEV proteome is similar to previously published EV datasets

The Vesiclepedia database was created to provide a comprehensive list of RNA, protein, lipid and metabolite cargoes within EVs from both published and

unpublished studies (Pathan et al., 2019). However, when searching specifically for CNS datasets such as neurones and astrocytes, very few datasets are included. In fact, there is only one study included in the database for ADEVs, with only one protein identified (Nkpd1 in rat ADEVs). Therefore, ADEV proteins identified within our dataset, which are also not present in the Vesiclepedia database, could be CNS specific proteins found in EVs. The majority of ADEV proteins were present within the Vesiclepedia database (from analyses of other published EV datasets) indicating the EV preparations in this study are of a good quality and are similar to those published in other studies (526 proteins out of 562 ADEV proteins; Figure 5-19). Seven proteins were identified in both serum-free and serum-cultured ADEV conditions but had not been previously recorded in Vesiclepedia (Figure 5-19). However, of these seven proteins, only QRICH2 is highly expressed in astrocytes (as described in the human protein atlas) suggesting many of these proteins may simply be contaminants. For example, XP32 is involved in keratinization and therefore is a likely contaminant from skin cells. Other potential contaminants may have arisen from the preparation steps (environmental contamination, such as keratin) or carry over from previous samples which were analysed using the mass spectrometer.

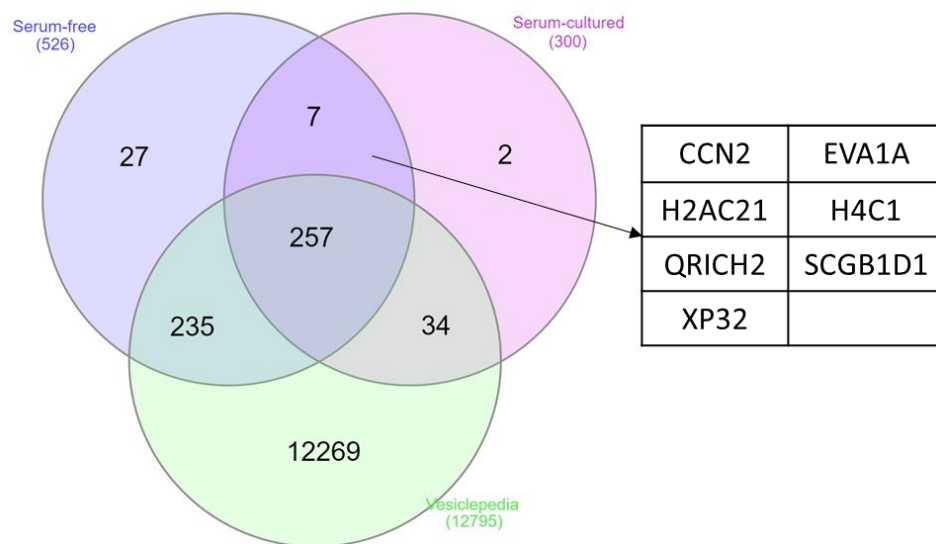


Figure 5-19 – The majority of serum-free and serum-cultured ADEV proteins were also present within the Vesiclepedia database. The majority of proteins found within the ADEVs were previously found within the Vesiclepedia database made up of previously published EV datasets. Seven proteins were identified within both ADEVs that were not in the database. Of the 27 proteins found in the serum-free ADEVs, many were immunoglobulins and therefore likely represent contamination.

5.5.2.3 Comparison of ADEV proteomes to parent whole cell lysates

There are still many outstanding questions surrounding the loading of protein cargo into EVs, and whether this process is selective. If proteins were non-selectively loaded for removal from the cell (secretory autophagy), the proteome of the EVs would be directly comparable to the parent cell lysates. The ADEV proteomes were compared to the parent cell lysates to determine whether there was any protein enrichment within the ADEVs (Figure 5-20). 65 proteins were exclusive to the ADEV samples, with 16 of these proteins found in both serum-free and serum-cultured

ADEV proteomes suggesting EVs are not direct reflections of the parent cells and therefore selective loading likely occurs as part of EV loading.

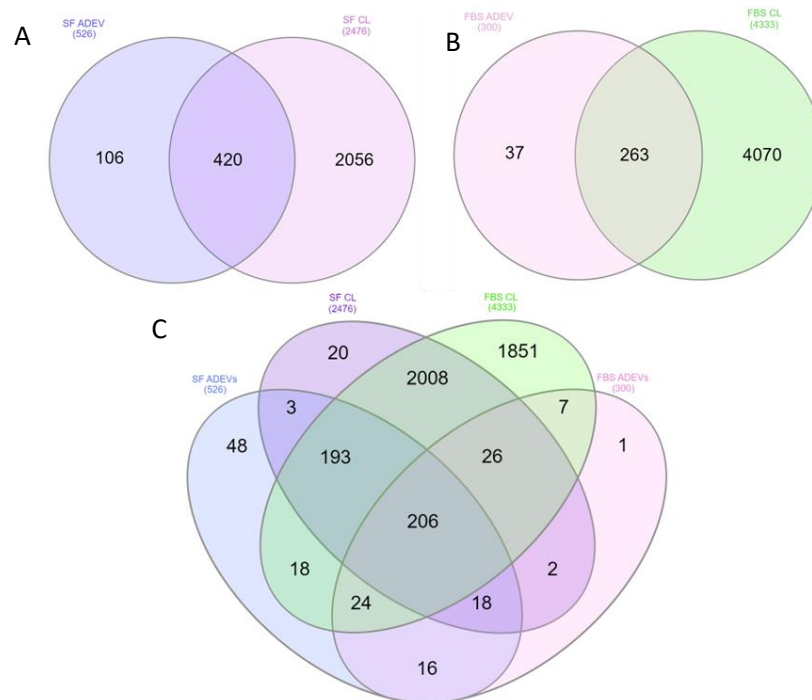


Figure 5-20 - Qualitative differences in human primary ADEV and their parent cell lysate proteomes by SWATH-MS. (A) Serum-free ADEVs have 106 proteins that were not identified in two or more replicates of the parent serum-free astrocytes compared to (B) serum-cultured ADEVs which had 37 proteins exclusive to the EVs. (C) Comparison between samples taken from Figure 5-16 to show distribution of proteins across the samples. Of the exclusively ADEV proteins (i.e. not found in the cell lysates), 16 were found in both serum-free and serum-cultured conditions.

It is difficult to quantitatively compare the ADEVs and cell lysates due to the differences in complexity and protein concentration between an EV and cell. Protein concentrations within the EVs were too low to detect on a standard BCA assay and therefore was not quantified before SWATH analysis. Whilst normalisation to spectra was completed to allow quantitative comparisons between samples, this is only accurate when below 2-3-fold differences in protein concentration. Protein concentration differences between cell and EV samples are likely 10-fold different and therefore would not be accurately normalised.

5.5.2.4 Enrichment of disease-associated proteins categories within ADEVs

To identify whether certain protein “groups” (such as metabolic proteins or ALS-associated proteins) were enriched within the ADEVs compared to the parent cells, ADEV proteins were compared to online databases of key proteins that have been associated with CNS diseases (and therefore reactivity) or are expected to be involved in cargo loading (such as RNA-binding proteins or autophagy proteins; Leidal and Debnath, 2021). Autophagy proteins were investigated due to the shared pathways between autophagy and EV secretion (see section 1.2.3 for more detail about secretory autophagy) as well as RNA binding proteins due to their suspected role in RNA loading within EVs. Where protein databases were not available, gene databases were utilised due to a similar nomenclature between gene and proteins.

Parent cell lysates were also compared to the online datasets to determine enrichment within ADEVs.

In order to compare the ADEV groups to their parent cell lysates for enrichment analysis, the number of proteins identified within the samples must be considered. For example, the serum-free astrocytes have ~4-fold more proteins identified in the cell lysates compared to the ADEVs, and therefore, their ADEVs would be predicted to have 4-fold fewer proteins identified in the protein groups. If the ADEVs have more proteins than expected, this suggests a possible enrichment of this protein group. For the serum-cultured ADEVs, there is a 15-fold reduction in ADEV protein number compared to the parent cell lysates and a 1.5-fold decrease compared to the serum-free ADEVs.

Mutant proteins associated with neurodegenerative diseases have already been identified within EVs suggesting EVs are involved in the transmission of disease (Saman et al., 2012; Silverman et al., 2016; Sardar Sinha et al., 2018). Therefore, ALS and Alzheimer's disease protein databases were utilised to identify whether any of these disease-associated proteins would be enriched within our ADEVs (Abel et al., 2012; Hu et al., 2017). A multiple sclerosis protein dataset was also compared against the ADEV samples as an inflammatory neurodegenerative disease without a clear proteinopathy (Joy Shepard et al., 2019). Finally, metabolic processes were investigated to determine whether any evidence of possible functionality could be found within the ADEVs.

More ALS proteins were identified within the ADEVs than expected compared to their parent cells suggesting ALS-associated proteins are enriched in the ADEVs (Table 5-5; expected proteins calculated based upon the number of parent cell proteins identified and normalised for the difference in the number of proteins identified). This increase in disease-associated proteins was also found in Alzheimer's disease proteins supporting previous research showing the presence of disease-associated proteins within EVs (Iguchi et al., 2016; Sardar Sinha et al., 2018; Silverman et al., 2019). Very few multiple sclerosis-associated proteins were identified in any of the astrocyte samples suggesting the reactive phenotype observed in the serum-cultured astrocytes may not be the same as the inflammatory, reactive phenotype seen in MS. This supports our previous findings with different gene expression observed between FBS-treated and cytokine-treated serum-free astrocytes (see section 3.7).

Table 5-5 - Protein sub-types identified in the ADEVs and their parent cells using online databases. ADEV proteins were compared to their parent cell lysates to identify potentially enriched protein groups. The values described in the cell columns represent the number of proteins identified in the cell lysates as well as the number of proteins also identified within their ADEVs (in brackets). By accounting for protein number between the cell lysates and ADEVs, ADEV proteins were highlighted as ‘increased expression’ (green) or ‘decreased expression’ (orange) according to the expected number of proteins present if the ADEVs were simply smaller copies of the parent cells. No highlight represents values that are very similar to the expected number of proteins.

Protein type	Database	SF ADEVs	SC ADEVs	Shared (EV)	SF cells	SC cells	Shared (CL)
ALS proteins	ALSoD (Abel et al., 2012; 154 proteins)	15	6	6	40 (13)	58 (6)	39
Alzheimer’s disease	Hu et al., 2017 (430 genes)	29	20	19	89 (26)	121 (19)	88
Multiple sclerosis	Joy Shepard et al., 2019; (95 genes)	5	2	2	9 (5)	19 (2)	9
Autophagy proteins	Human autophagy database (222 proteins)	18	14	12	59 (17)	98 (14)	59
RNA binding proteins	RNA-binding protein Database (Cook et al., 2011; 407 proteins)	8	3	3	112 (8)	182 (3)	111
Metabolic enzymes	Mammalian metabolic enzyme database (Corcoran et al., 2017; 1647 proteins)	60	23	20	408 (59)	584 (22)	406

The expected number of autophagy proteins was found in the serum-free ADEVs, but an increase was found within the serum-cultured ADEVs (Table 5-5). Alongside the reduction in median size measured using the Zetaview® (see Figure 5-5), this may suggest more exosomes are released due to increased secretory autophagy, and therefore a greater proportion of autophagy-related proteins were detected compared to the serum-free ADEVs (Leidal and Debnath, 2021). Less RBPs were detected than expected for both ADEV conditions. The small number of RBPs may reflect a mechanism where the RNA is loaded into the EVs and released by the RBPs so the RBPs would not be actively loaded into the EVs. Another explanation may be that a few, specific RBPs may be involved in the active loading of RNA into EVs.

Fewer metabolic enzymes were found in the ADEVs than expected if the EV cargo simply reflected parent cell lysates (Table 5-5). This is likely due to fewer metabolic processes occurring within the ADEVs than the parent cells, with any metabolic functionality likely to be limited to a few specific processes. The metabolic need of an EV is likely very limited compared to a normal functioning cell. On the other hand, many of the glycolytic enzymes were observed within the ADEVs suggesting a possible process for generating ATP within EVs, allowing them to function as independent metabolic units (see below, Table 5-6).

Ten essential glycolysis enzymes alongside lactate dehydrogenase (LDH; required for converting between pyruvate and lactate) were searched for within the ADEV and parent cell lysate samples (Table 5-6). Due to the specific nature of the search, proteins were identified as present if found in any of the three biological replicates for each condition, but those only present in one replicate were highlighted in blue (i.e. would have been removed from general analysis). All 10 glycolysis enzymes were identified within at least one replicate of the serum-free ADEVs suggesting the

possibility of glycolysis occurring within EVs. Only 6 of the glycolysis enzymes were identified in the serum-cultured ADEVs suggesting these EVs may be less metabolically active and may be released for a different purpose, such as secretory autophagy to expel proteins. Alternatively, the difference between the glycolytic enzyme number in the two ADEV conditions may simply be due to less proteins being identified within the serum-cultured ADEVs. As a comparison, all glycolytic enzymes were identified within at least two replicates of the parent cell lysates. Both sub-types of LDH were identified within all of the samples (required for the conversion between pyruvate and lactate) suggesting this process may be active within ADEVs.

Table 5-6 - Glycolytic enzymes were identified within ADEVs and their parent cell lysates. All glycolytic proteins were identified within the serum-free ADEVs suggesting the possibility of active glycolysis within the EVs. Less glycolytic proteins were detected within the serum-cultured ADEVs than serum-free ADEVs but this may be due to fewer proteins identified overall. Proteins were classed as present if identified within any of the replicates, however if only present in one of the replicates, they were highlighted in blue. LDH was also investigated due to the enzyme's key role in astrocyte-neurone metabolism.

Glycolytic enzymes	SF EVs	SC EVs	SF CL	SC CL
HK1/2/3	HK1	No	HK1	HK1/2
GPI	Yes	No	Yes	Yes
PFKM/PFKL/PFKP	Yes (L+P)	No	Yes (all 3)	Yes (all 3)
ALDOA/ALDOB/ALDOC	Yes (A)	Yes (A)	Yes (A+C)	Yes (A+C)
TPI1	Yes	Yes	Yes	Yes
GAPDH	Yes	Yes	Yes	Yes
PGK1	Yes	Yes	Yes	Yes
PGM1/2/3	Yes (1)	No	Yes (all 3)	Yes (all 3)
ENO1/ENO2/ENO3	Yes (1)	Yes (1)	Yes (1+2)	Yes (1+2)
PKM	Yes	Yes	Yes	Yes
LDHA/LDHB	Yes (A+B)	Yes (A+B)	Yes (A+B)	Yes (A+B)

5.5.3 Differentially expressed proteins between serum-free and serum-cultured human primary ADEVs

SWATH-MS allows quantitative analysis to be completed to investigate protein expression differences between the samples. Significance was set at an adjusted P-value of <0.05 and a fold change of > ±1.5 as with the previous analysis completed on the cell lysates (see previous section 4.4.4). With far fewer proteins identified overall in the ADEVs compared to the parent cells, different thresholds for inclusion were required, with ADEV protein comparisons benefitting from a less stringent analysis than parent cell comparisons (NA = 0.4, CV = 0.3). Whilst proteins were still required to be present in at least two biological replicates (NA = 0.4), three different variances were trialled (0.3, 0.5 and 1; CV value) to identify the best condition for each of the comparisons (Table 5-7).

Table 5-7 – Lowering the threshold for variance increased the number of differentially expressed proteins between serum-free and serum-cultured ADEVs identified by SWATH-MS. To determine the most appropriate criteria for protein expression analysis, different variance thresholds (CV values) were trialled on the samples prior to statistical testing. Three different coefficient of variation values (CV value) were trialled with any proteins above this level of variation were removed from the analysis (E.g. 0.3 = only proteins with <30% variance between replicates). As with previous cell lysate analysis (section 4.4.4.) proteins were required to be present in at least two biological replicates (NA = 0.4). P-values were calculated using a Limma test with the P-values adjusted using the Benjamini-Hochberg procedure. A CV value of 0.5 (<50% variance) analysed the highest number of proteins (65 proteins) with 17 of these found to be differentially expressed using $P_{adj} < 0.05$.

NA (Missing values)	CV (Variance)	Total Proteins	P<0.05	Padj<0.05
0.4	0.3	19	7	6
0.4	0.5	65	28	17
0.4	1	210	18	0

With a variety of EV sub-types expected within the EV samples (e.g. exosomes, microvesicles), a higher variance was expected between ADEV biological replicates than between cell lysates. The highest number of significant, differentially expressed ADEV proteins were found with a CV of 0.5 (<50% variance between replicates) so these values were chosen for further analysis of the ADEVs (65 proteins reached threshold criteria of 264 proteins identified in both serum-free and serum-cultured ADEVs; Table 5-7).

Of these 65 proteins, 28 were found to be differentially expressed after Limma analysis, with 17 proteins still differentially expressed after the p-value was adjusted (Figure 5-21A). Of the 17 differentially expressed proteins, 9 were found to be upregulated in the serum-cultured ADEVs and 8 upregulated in serum-free ADEVs (Figure 5-21B, left and right, respectively). STRING analysis was completed on the differentially expressed proteins to identify any connections between these proteins. No KEGG pathways were identified within the two groups of differentially expressed proteins (upregulated in serum-free and serum-cultured ADEVs) indicating that there is not a particular pathway that is upregulated in either of the conditions.

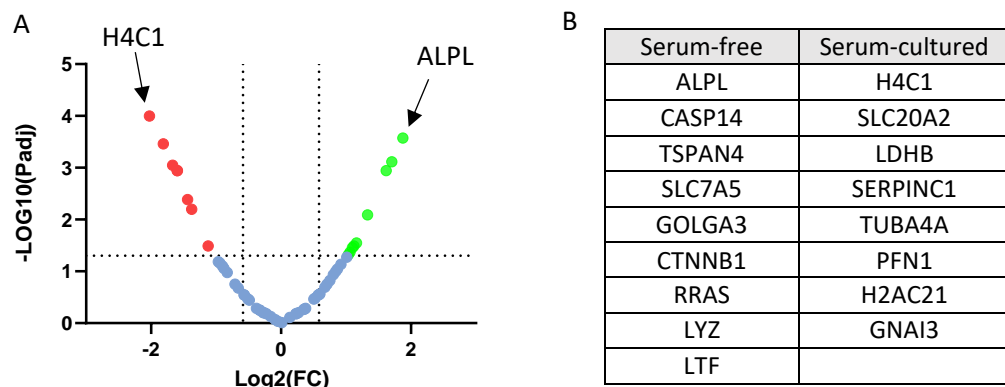


Figure 5-21 - Differentially expressed proteins identified in serum-free and serum-cultured ADEVs by SWATH-MS. (A) Of the 65 proteins analysed, 17 were found to be differentially expressed after P-value adjustment. 9 were found to be upregulated in serum-cultured ADEVs (Green) and 8 were upregulated in serum-free ADEVs (Red; listed in B). Dotted lines represent the thresholds for significance ($P_{adj} < 0.05$, Fold change <1.5). Blue dots represent proteins that were included in the analysis but were not found to be significant. (B) H4C1 and ALPL were most upregulated in the serum-free and serum-cultured ADEVs, respectively.

5.6 SWATH-MS analysis of BDEVs

The human primary astrocyte cultures used in this work are limited by the monoculture style which lacks the influence of neighbouring cell types such as neurones and microglia. Microglia are known to have a major role in inducing astrocyte reactivity through the secretion of cytokines and therefore, the *in vitro* FBS-induced reactivity used in this work may not truly reflect endogenous astrocyte biology (Pascual et al., 2012; Liddelow et al., 2017; Shinozaki et al., 2017; Joshi et al., 2019; Xia et al., 2022). The astrocytes are also foetal cells which likely limits the model when used to study neurodegenerative disease, with ageing being the greatest risk factor for many of these diseases (Hou et al., 2019; Azam et al., 2021). Therefore, to compare the relevance of the ADEV analysis to endogenous human EVs, BDEVs isolated from both healthy (comparison for 'quiescent' serum-free ADEVs) and disease (comparison for 'reactive' serum-cultured ADEVs) frontal-lobe brain tissue were analysed using SWATH analysis. Due to the variation seen between three biological replicates within the ADEV analysis, eight biological replicates for each BDEV condition were analysed to allow for sample variability and to improve the quality of the analysis. The same analysis pipeline used to analyse the astrocyte cell lysates and ADEVs was used to analyse the BDEVs (see section 4.4.1).

5.6.1 Principal component analysis of control and disease BDEVs analysed using SWATH-MS

A PCA was completed on the relative abundance of protein obtained from each of the BDEV samples (8 biological replicates per condition) to determine the similarity between samples (Figure 5-22). No distinction was identified between the conditions despite 81.8% of the data being described by two principal components (PC1 = 63.3%, PC2 = 18.5%). The replicates for each condition are not clustered indicating the variation between replicates is similar to the variation between conditions. A PLS-DA analysis was not completed due to more than 2 conditions being analysed as well as no differences being observed between conditions.

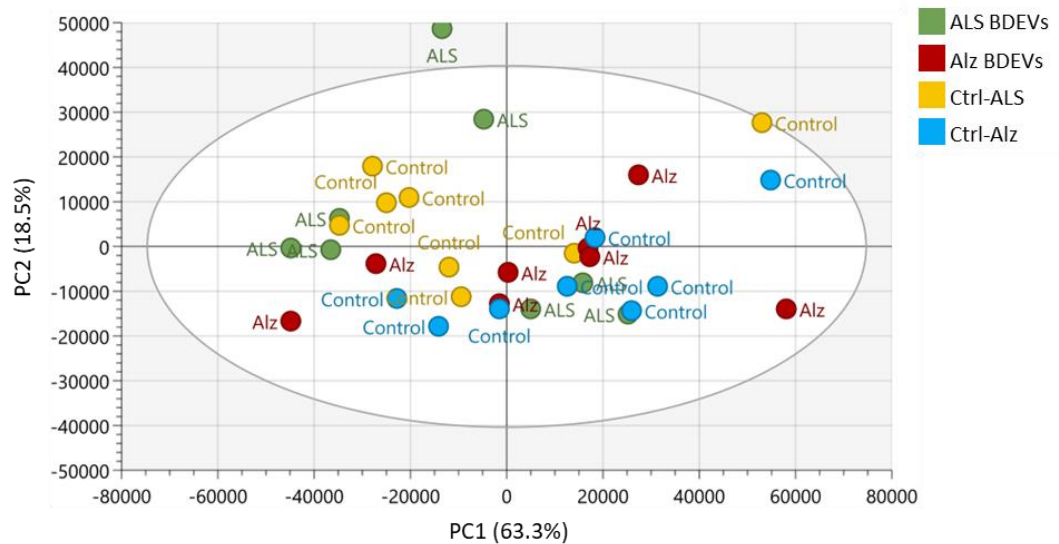


Figure 5-22 - Principal component analysis of BDEVs shows no clear differences in the proteomes between control and disease conditions as well as between ALS and Alzheimer's BDEVs by SWATH-MS. No clustering of replicates for each condition suggests no clear differences were identified between BDEV conditions despite 81.8% of the data being described by two principal components (PC1 = 63.3%, PC2 = 18.5%; N = 8).

5.6.2 Qualitative analysis of BDEV proteomes from control and disease frontal lobe tissue by SWATH-MS

With more replicates used in the SWATH-MS analysis, a different threshold was needed for the number of replicates a protein must be present in to be identified within a condition. The number of proteins that were present in more than 2, 4, 6 and in all 8 replicates of each BDEV condition were compared to determine which criteria to select for further analysis (Figure 5-23). Across all conditions, the number of proteins identified were similar with standard deviation increasing with the stringency of the criteria. Due to the diverse nature of EV populations and the range of parent cells that would release EVs in the tissue samples, more relaxed criteria were selected. This criterion included between 1389 and 1631 proteins identified for each BDEV conditions with a standard deviation between conditions below 10% of the mean (Figure 5-23A). This also included a high proportion of the total proteins identified (between 67-78% per condition). Therefore, all further analysis was completed on proteins found in four or more replicates for each BDEV condition.

A

	≥2 replicates	≥4 replicates	≥6 replicates	≥8 replicates
ALS	1847	1483	1004	444
Ctrl-ALS	1806	1389	966	465
AD	1889	1542	1174	726
Ctrl-AD	1934	1631	1258	728
Average	1869 ± 48	1511 ± 88	1101 ± 120	591 ± 136

B

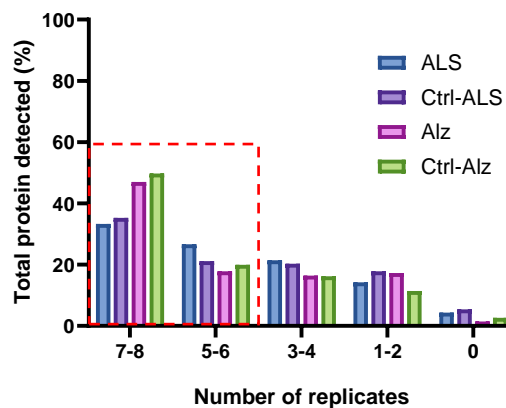


Figure 5-23 – The number of proteins identified by SWATH-MS in multiple biological replicates across different BDEV conditions. (A) The average number of proteins between the conditions was calculated alongside the standard deviation to demonstrate the variation observed across the disease conditions. A high number of proteins were identified in ≥4 replicates with a low standard deviation between conditions. (B) The highest proportion of proteins were identified in 7-8 replicates demonstrating low variation between biological replicates, with more than 50% of proteins identified in ≥5 replicates (indicated by red box). 0 replicates represent proteins that were not identified in the specific BDEV condition but were identified in other BDEV conditions.

BDEV proteins identified in four or more replicates for each condition were compared to identify proteins unique to each condition (Figure 5-24). The majority of the EV proteins were found across multiple conditions with only 5-10% of proteins identified exclusively in one condition. When comparing disease conditions to their matched controls, 183 proteins were unique to ALS and 73 proteins unique to Alz BDEVs (Figure 5-24A and B, respectively). KEGG pathway analysis was completed on the unique disease proteins that were identified in ALS BDEVs (but not in the matched controls) to determine which pathways were over-represented in the ALS BDEVs (i.e. more proteins in a particular pathway within the selected group of proteins than would be expected from a random selection of proteins). This identified two significantly enriched pathways within the ALS BDEVs - 'Huntington's disease' (P= 0.005) and 'Metabolic pathways' (P=0.003). Metabolic dysfunction has been described in ALS with impaired mitochondrial and glycolytic processes, as well as other metabolic pathways such as lipid and RNA metabolism (Droppelmann et al., 2014; Vandoorne et al., 2018; Lee et al., 2021). The enrichment of Huntington's disease-associated proteins in the ALS BDEVs implies similar pathways are involved across different neurodegenerative diseases. KEGG pathway analysis was also completed on the Alz BDEV proteins that were not identified in the control-Alz BDEVs but this only identified 'spliceosome' as significantly enriched compared to controls (P= 0.045).

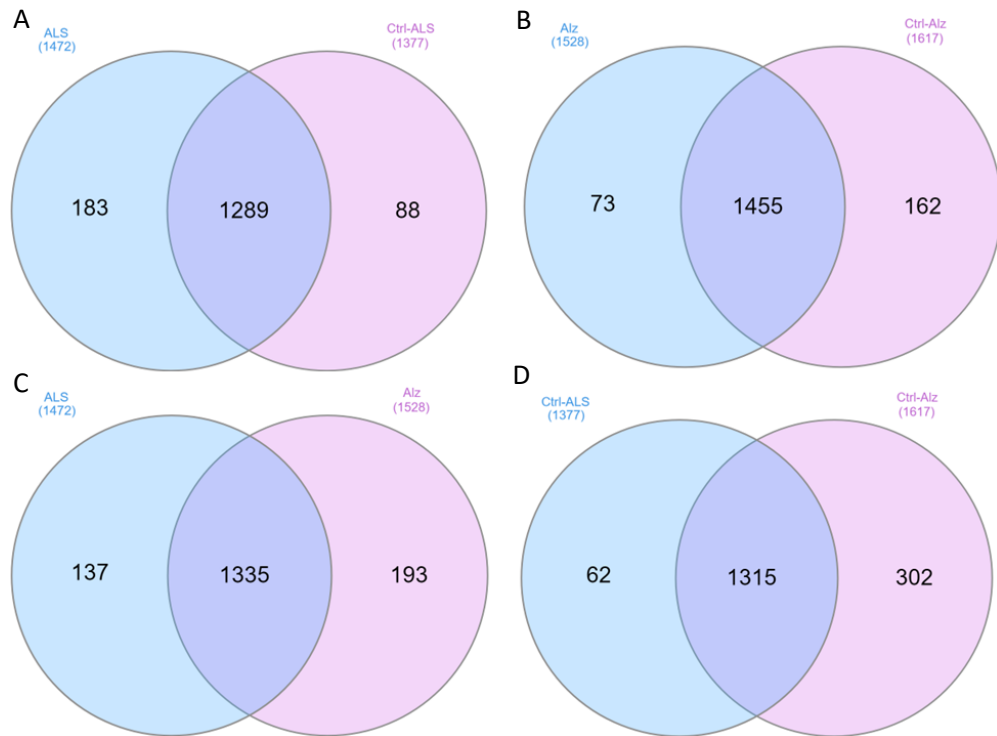


Figure 5-24 - Comparison of BDEV proteins identified by SWATH-MS in four or more replicates for each condition. Proteins identified in (A) ALS and (B) Alz BDEVs were compared to their matched controls to identify the number of disease-specific proteins. (C) Disease BDEV proteins were also compared to identify potentially unique proteins attributed to a particular disease. (D) The control conditions were compared to identify variation between the datasets with few differences expected between these groups (i.e. no change due to disease).

Proteins identified in BDEVs isolated from both ALS and Alzheimer's disease frontal lobe tissue were also compared to identify any EV protein differences between the neurodegenerative diseases. 137 proteins were found to be unique to the ALS BDEVs compared to 193 unique within the Alz BDEVs (Figure 5-24C). There was still a large amount of similarity between the samples with 1335 proteins found in both disease groups. Finally, to compare the variation between the different control groups, proteins identified in each of the control BDEVs were compared (Figure 5-24D). As the control BDEVs are isolated from healthy tissue, the groups were expected to be similar. Any differences would be due to technical differences or age-associated differences that would also likely affect the comparison between diseases (Average ages of patients: ALS = 59, ALS-Ctrl = 60, Alz = 79, Alz Ctrl = 88). The majority of proteins were identified in both control groups (95.5% control-ALS vs 81.3% control-Alz BDEV proteins) suggesting any differences identified between conditions are due to changes in disease. The control-Alz group had the most proteins identified across all the conditions so more unique proteins were expected in this condition and explains why ~20% of proteins were not found in the control-ALS condition.

5.6.2.1 Comparison of BDEV proteins to previously published EV datasets using the Vesiclepedia database

To identify the number of proteins identified within our BDEVs that had been previously reported in EVs, the BDEVs were compared to the Vesiclepedia database (Figure 5-25). More than 90% of BDEV proteins were identified within the Vesiclepedia database suggesting high consistency with other published studies. Of the proteins that were not identified in the Vesiclepedia database, many were found in both the disease conditions and the matched controls. These proteins were further analysed through STRING analysis to determine whether any of these proteins are CNS proteins that may have been missed from the Vesiclepedia database, or whether these proteins represent potential contaminants in the samples.

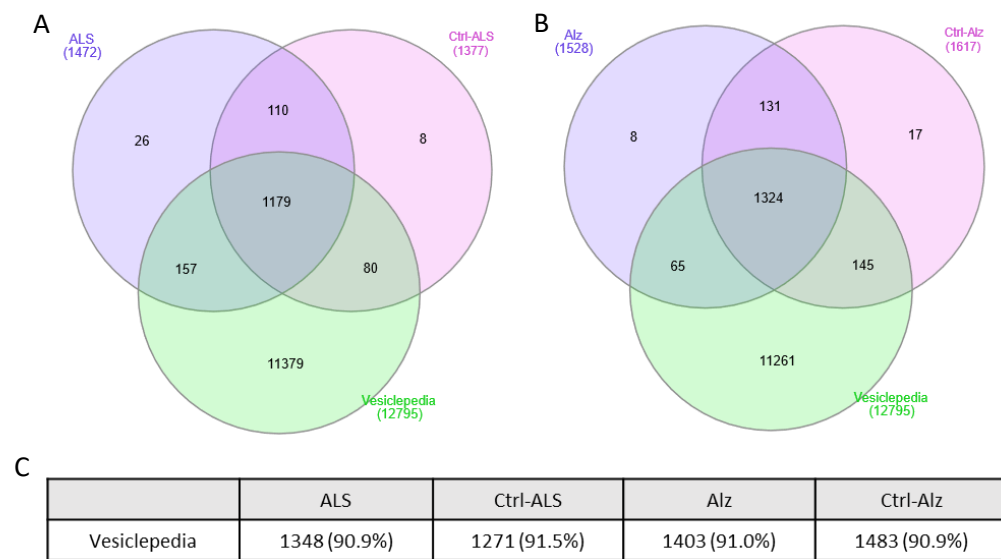


Figure 5-25 – The majority of BDEV proteins were identified within the Vesiclepedia database. (A-B) Of the proteins that were not identified within the Vesiclepedia database, the majority were found in both disease and control BDEVs. (C) More than 90% of the proteins in all conditions were found within the Vesiclepedia database. Numbers within the table represent the number of BDEV proteins found in the Vesiclepedia database as well as the percentage of the overall proteins within the condition.

KEGG pathway analysis of the 110 ALS and control proteins not found within Vesiclepedia identified 8 pathways as significantly upregulated, 4 of which were neurodegenerative disease pathways (Parkinson’s disease, Huntington disease, prion disease and ALS; $P < 0.05$; Figure 5-26A). Using GO analysis, 84 of these proteins were associated with the CNS suggesting that a large proportion of these proteins may be found within EVs but are missing from the Vesiclepedia database. Much like astrocytes, very few proteins have been identified in neuronal cells within the database highlighting that CNS derived-EVs are not well-represented within Vesiclepedia.

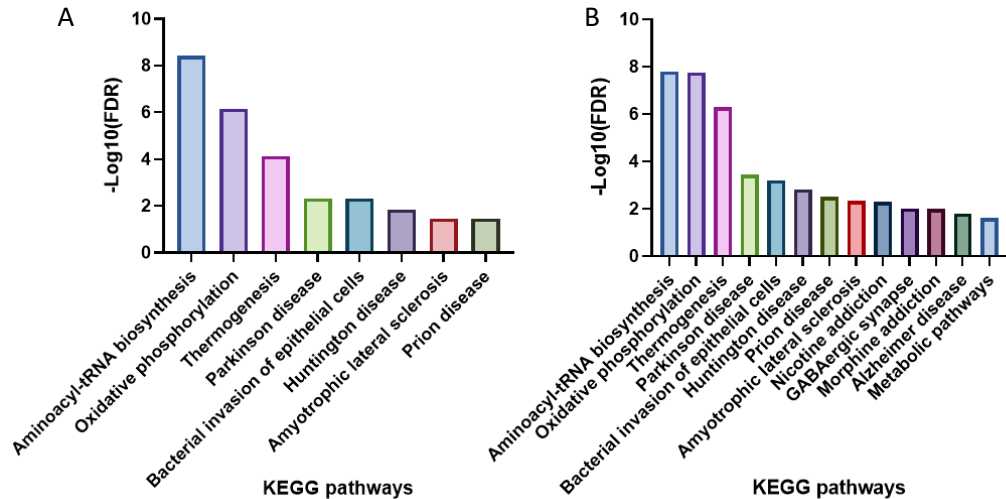


Figure 5-26 - Proteins identified in BDEVs by SWATH-MS that were not found within the Vesiclepedia database are enriched in neurodegenerative disease pathways. (A) KEGG pathway analysis identified 8 enriched pathways in proteins found in both ALS and ALS-Control BDEVs that were not documented in the Vesiclepedia database. Four of these pathways were neurodegenerative disease pathways (Parkinson's disease, Huntington's disease, ALS and Prion disease). (B) 13 enriched pathways were identified in proteins found within Alz and Alz-control BDEVs that were not found within the Vesiclepedia database. Five of these pathways were neurodegenerative disease pathways (Parkinson's disease, Huntington's disease, Prion disease, ALS and Alzheimer disease).

Other proteins include ATPase subunits (such as ATP5F1C and ATP5PD) that form the ATPase found within the mitochondria. Oxidative phosphorylation was upregulated with other mitochondrial proteins such as MT-CO2 and TOMM20, identified ($P = 7.06 \times 10^{-7}$). The presence of these proteins highlights the possibility of mitovesicles (a subtype of EV containing mitochondrial proteins) or mitochondria being found within the BDEVs (D'Acunzo et al., 2021, 2022; Liang et al., 2023). Mitochondrial ATPase subunits were also identified within the ADEVs.

The non-Vesiclepedia proteins identified in both the Alz BDEVs and the matched control BDEVs also underwent KEGG pathway analysis. This identified 13 enriched pathways with 5 of the pathways associated with neurodegenerative diseases, including Alzheimer's disease and ALS (Figure 5-26B). Like the ALS/control proteins, GO analysis identified 93 of the proteins as associated with the CNS. When comparing the non-Vesiclepedia proteins, 96 were found to be in all 4 BDEV conditions.

5.6.2.2 Glycolytic enzymes and transporters identified within BDEVs

With glycolytic enzymes found to be abundant in ADEVs (see section 5.5.2.3, Table 5-6), the 10 enzymes required for glycolysis were also investigated in the BDEVs. All glycolytic enzymes were identified within all BDEV conditions alongside both subunits of lactate dehydrogenase (Table 5-8). No difference was observed between the four BDEV conditions when comparing different isoforms of the proteins such as ALDOA or ALDOC. Whilst this result does not indicate whether all the enzymes are present within an individual EV, it does suggest that EVs have the potential to be metabolic units which can generate their own ATP as a source of energy. Other molecules are required for glycolysis to occur such as carbon substrates (i.e. glucose)

and co-factors (i.e. NADH) but these were not possible to detect using the current methodology.

Table 5-8 - All enzymes required for glycolysis were identified by SWATH-MS within the BDEVs with no differences observed between BDEV conditions.

Glycolytic enzymes	ALS	Ctrl-ALS	AD	Ctrl-AD
HK1/2/3	HK1	HK1	HK1	HK1
GPI	Yes	Yes	Yes	Yes
PFKM/PFKL/PFKP	Yes (all 3)	Yes (all 3)	Yes (all 3)	Yes (all 3)
ALDOA/ALDOB/ALDOC	Yes (A+C)	Yes (A+C)	Yes (A+C)	Yes (A+C)
TPI1	Yes	Yes	Yes	Yes
GAPDH	Yes	Yes	Yes	Yes
PGK1	Yes	Yes	Yes	Yes
PGM1/2/3	Yes (1)	Yes (1)	Yes (1)	Yes (1)
ENO1/ENO2/ENO3	Yes (all 3)	Yes (all 3)	Yes (all 3)	Yes (all 3)
PKM	Yes	Yes	Yes	Yes
LDHA/LDHB	Yes (A+B)	Yes (A+B)	Yes (A+B)	Yes (A+B)

Active transporters such as ABCB1 and ABCG2, as well as subunits of the Na⁺/K⁺ ATPase were identified within the BDEVs which all require ATP to function. ABCB6 and subunits of the Na⁺/K⁺ ATPase were also detected within the ADEVs suggesting these are commonly found within EVs. With the presence of glycolytic enzymes within the EVs, there is the possibility that EVs may generate ATP in order for these transporters to be functional. Solute carrier transporters (SLCs) such as SLC1A2 (EAAT2) and SLC1A3 (EAAT1) were also present on the BDEVs suggesting that if an electrochemical gradient were created through ATPases such as the Na⁺/K⁺ ATPase, these transporters could also be functional in EVs.

5.6.3 Differentially expressed proteins between healthy and disease BDEVs identified by SWATH-MS

5.6.3.1 Identifying suitable thresholds for quantitative analysis

As with the previous SWATH analysis of ADEVs, suitable thresholds for quantitative analysis were empirically determined by adjusting the missing value threshold (NA value) and the variance threshold (CV value). Previous thresholds for ADEVs were set at 0.4 NA and 0.5 CV which also appeared to also be suitable for the BDEVs, and therefore these thresholds were used for quantitative analysis (Supplementary Table 2). This still required the proteins to be identified in the majority of replicates ($\geq 5/8$; NA = 0.4) whilst also allowing some variability between samples (<50% variance). A higher variability is expected within the BDEVs compared to cell culture-derived EVs due to the variability of disease progression within each disease condition, the biological variability that occurs between humans and the technical variations in tissue preservation.

5.6.3.2 *Differentially expressed proteins between control and disease BDEVs identified by SWATH-MS*

After selecting the criteria for inclusion, proteins identified in ALS and Alz BDEVs were compared against proteins found within their matched control BDEVs to identify significant differentially expressed proteins (Supplementary Table 2). Only 1 protein was identified as differentially expressed in each comparison after P-value adjustment. In the ALS BDEVs, HPCAL4 (Hippocalcin-like protein 4) was found to be significantly downregulated compared to the control BDEVs. HPCAL4 is a calcium binding protein which is highly expressed in excitatory interneurons (Alvaro et al., 2020). Whilst not a well-studied protein, HPCAL4 is thought to be involved in the inactivation of Cav2.1 channels. MPO (Myeloperoxidase) was found to be the most up-regulated protein in ALS BDEVs compared to the matched control BDEVs, but this difference was not significant ($P_{adj} = 0.10$). MPO is an inflammatory, lysosomal enzyme which promotes the production of reactive oxygen/nitrogen species (ROS/RNS) as well as catalysing the production of hypochlorous acids (HOCl) which are used to defend against invading pathogens (Kargapolova et al., 2021). In fact, MPO has been shown previously to be upregulated in ALS brains with aggregated SOD1 mutants thought to activate the MPO/HOCl pathway resulting in motor neurone death (Peng et al., 2022; Xiong et al., 2022). In the Alz BDEVs, only GNB2 (Guanine nucleotide-binding protein subunit $\beta 2$) was significantly downregulated with no proteins upregulated in the Alz BDEVs. GNB2 is a G-protein subunit which has previously been associated with schizophrenic pathways and in particular, the dopaminergic synapse pathway (Liu et al., 2022). The protein is involved in modulating neuronal signalling within the glutamatergic and dopaminergic pathways.

A final comparison was completed to identify differentially expressed proteins between the ALS and Alz BDEVs to determine if BDEVs can potentially be used to differentiate between diseases (Figure 5-27). 12 proteins were found to be differentially expressed between the diseases with 11/12 proteins up-regulated in the Alz BDEVs compared to only one (JCHAIN; Immunoglobulin J chain) up-regulated in the ALS BDEVs. STRING analysis did not identify any pathways or connections between the proteins. Two of the most upregulated proteins in the Alz BDEVs, PPT1 and MAOB, have been shown to be upregulated in Alzheimer's disease mice models with MAOB utilised as a potential therapeutic target for Alzheimer's disease treatment (Schedin-Weiss et al., 2017; Aladeokin et al., 2019; Park et al., 2019). In fact, MAOB is involved in GABA production in reactive astrocytes with aberrant expression leading to memory impairment. This has led to MAOB expression being utilised as a PET biomarker for reactive astrocytes in Alzheimer's disease and other related dementias (Jaisa-aad et al., 2024). The other 9 proteins upregulated in Alz BDEVs had limited associated with Alzheimer's disease, often only identified in large gene expression studies with little research conducted into their association with the disease. The results identified when comparing disease BDEVs must be considered with caution due to the diseased samples not being age-matched, unlike comparisons between control and disease BDEVs (ALS average age = 59 ± 11 vs AD age = 79 ± 14). The differences highlighted should be confirmed with age-matched tissue where possible and should be reproducible in future experiments.

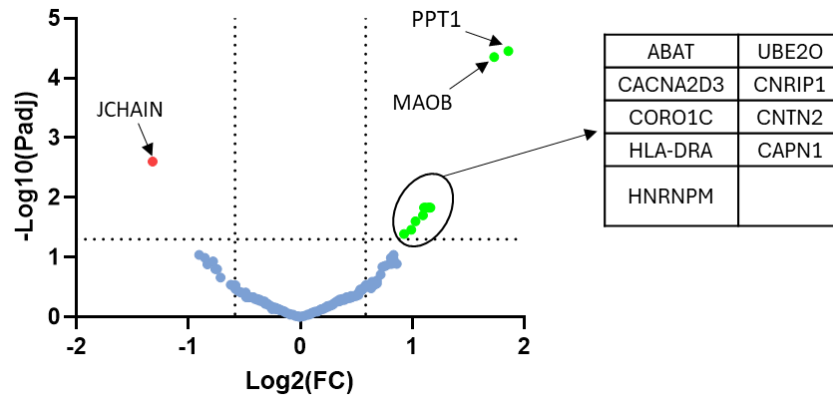


Figure 5-27 - 12 differentially expressed proteins were identified when comparing ALS BDEVs and Alz BDEVs by SWATH-MS. Thresholds for significance was set at $P_{adj} < 0.05$ and fold change > 1.5 . P -adjusted values were transformed using $-\log_{10}$. Dotted lines represent thresholds for significance. JCHAIN was found to be the only protein significantly upregulated in ALS BDEVs (red). On the other hand, 11 proteins were identified as significantly upregulated in the Alz BDEVs, with PPT1 the most upregulated of any of the proteins. Statistical analysis was completed using a limma test followed by P -value adjustment using the Benjamini-Hochberg procedure. Proteins included in the analysis were in $\geq 5/8$ biological repeats and had a variance of below 50% ($N = 8$).

5.6.4 Cell-specific markers within BDEVs that could be used to isolate cell-specific BDEVs

5.6.4.1 Astrocyte markers in BDEVs

A major issue with EV research is the lack of cell-specific markers that have been identified in EVs which can distinguish their cellular origin. Almost all cells release EVs, with all CNS cells shown to release EVs that can pass through BBB into the blood (Shi et al., 2019). Reactive astrocytes are often observed in the early stages of neurodegenerative disease and therefore, changes in ADEVs due to reactivity present useful measurements of disease progression. By isolating ADEVs from other EVs, these changes will be easier to detect. As described in section 1.3, there is a general lack of astrocyte-specific markers which makes distinguishing ADEVs from other EVs very difficult. Therefore, a panel of cellular markers are likely required to confidently identify the origin of select EVs. To identify which neural markers are present in EVs, cell-specific markers found commonly within the literature for astrocytes (Table 1-1), neurones, oligodendrocytes and microglia were investigated within the BDEV proteins. Those with high expression within the BDEVs represent markers that could be used to distinguish between neural EVs.

12/13 markers associated with astrocytes (discussed in Table 1-1) were identified across all 4 BDEV conditions with detection in at least 4 replicates for each condition (Figure 5-28). GFAP was highly expressed, with the highest expression found within the Alz BDEVs. High GFAP expression is associated with neurodegenerative disease and has been shown to be increased in the blood of Alzheimer's disease patients (Kim et al., 2023b). High GFAP expression is also expected in ALS however this would likely be detected within the spinal cord or the CSF where neurodegeneration is evident rather than in the frontal lobe of patients (Benninger et al., 2016; Verde et al., 2023). GFAP would likely be higher in ALS patients that also have cognitive decline and therefore would have reactivity in the frontal lobe of the brain. In this study, none of the ALS patients demonstrated cognitive deficits at the time of death

(Supplementary table 3). GFAP expression in EVs is also high in the control conditions suggesting this would be a useful marker of ADEVs, but not necessarily a useful marker for neurodegeneration. GFAP increases with age and because age is the main contributing factor for neurodegeneration, increases in GFAP due to age could be easily mistaken for neuropathology (Nichols et al., 1993). On the other hand, research has shown it can be a good marker for predicting some diseases, particularly Alzheimer’s disease patients with high A β load which would now benefit from early intervention with new treatments such as Lecanemab and Donanemab (Chatterjee et al., 2021). These drugs target A β to reduce disease progression, so patients benefit most from early intervention (Sims et al., 2023; van Dyck et al., 2023).

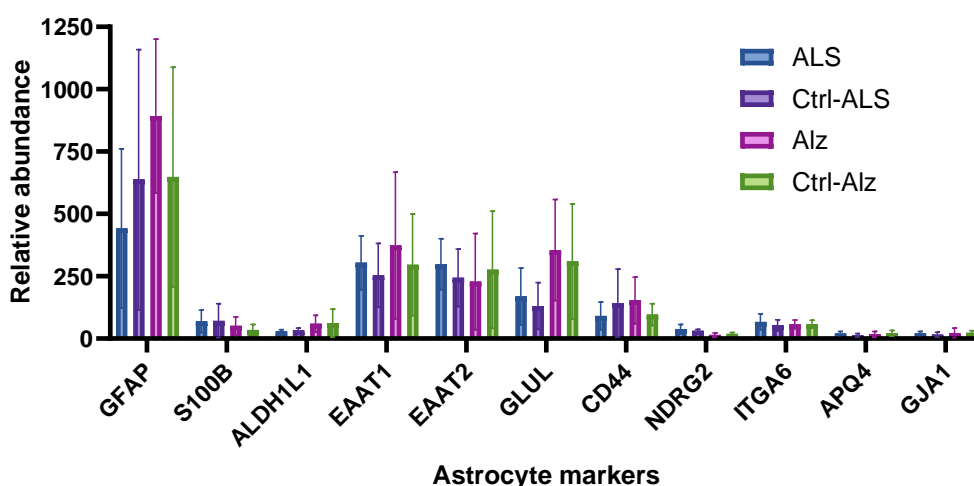


Figure 5-28 – Many astrocyte markers were identified within control and disease BDEVs by SWATH-MS. 12 of the 13 astrocyte markers investigated were identified within the BDEVs. Due to the nature of SWATH analysis, abundance is relative between the samples and therefore it is difficult to compare expression between different proteins. Error bars represent mean and standard deviation between replicates (N = 8).

Alongside GFAP, other astrocyte markers that were expressed within the BDEVs were the glutamate transporters, EAAT1 and EAAT2, as well as glutamine synthetase (GLUL, also known as GS; Figure 5-28). Similar expression was observed across the conditions for both glutamate transporters, but GLUL expression was higher in both the Alz and Ctrl-Alz BDEVs. With high presence in both the Ctrl-Alz and Alz tissues, this does not appear disease associated and may instead reflect a change caused by ageing, observed previously in senescent rodent astrocytes (Matias et al., 2023). Other astrocyte makers were expressed in lower abundance such as S100 β , ALDH1L1, CD44 and ITGA6 (CD49f) with very little expression of NDRG2, AQP4 and GJA1 observed in the BDEVs. These proteins would not be good markers of ADEVs as they would not likely be found in many EVs within the population.

5.6.4.2 Neuronal markers in BDEVs

As well as astrocyte markers, 17 common neuronal markers were investigated within the BDEVs to identify potential neuronal-derived EV (NDEV) markers. 13 of these proteins were identified within at least 4 replicates of both disease and control

BDEVs (Figure 5-29). SYP and THY1 were particularly abundant within the BDEVs and were found within the 25 most abundant proteins detected by SWATH-MS across the BDEVs (SYP in the top 25 in 3/4 conditions, THY1 in all 4 conditions). This may suggest these proteins would be very useful to separate NDEVs from ADEVs and other EVs in complex samples. An issue with THY1 is that it is also highly expressed in other cell types such as endocrine cells so could only be used within a panel of other neuronal markers. Much like astrocytes, many neuronal markers are also identified within other cell types so a panel of markers would be more beneficial to confirm the origin of cells.

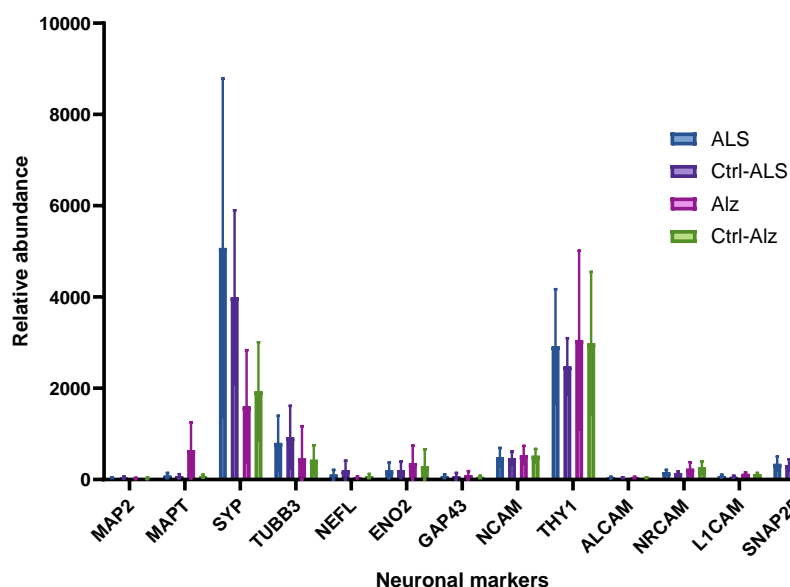


Figure 5-29 - Neuronal markers were also identified within BDEVs. 13 of the 17 neuronal markers investigated were identified within the BDEVs. SYP and THY1 were particularly abundant in BDEVs suggesting high expression in EVs but like the astrocyte marker analysis, abundance is relative between the samples and therefore it is difficult to accurately compare expression between proteins. Error bars represent mean and standard deviation between replicates (N = 8).

TUBB3 was also highly expressed in the BDEVs so would also be a good marker of NDEVs (Figure 5-29). TUBB3 (also known as TUJ1) is a commonly used neuronal marker but has been identified in other cell types such as melanocytes (Locher et al., 2014). MAPT (tau protein) was found to be more highly expressed in the Alz BDEVs compared to any other condition, but this is not surprising with tau shown to be a major contributor of Alzheimer’s disease pathology (Ballatore et al., 2007). Tau has been identified within Alz BDEVs and these EVs are thought to be involved in the spread of tau pathology (Saman et al., 2012; Guix et al., 2018; Ruan et al., 2021; Fowler et al., 2023). Abundance of MAPT in the control or ALS conditions was >7-fold lower so MAPT could be a valuable marker of Alzheimer’s disease pathology within NDEVs.

Other markers of neurones that were detected in lower abundance were NEFL, ENO2, NCAM, NRCAM and SNAP25. Very little expression of MAP2, GAP43, ALCAM and L1CAM were observed. L1CAM is commonly used as a marker of NDEVs and has been used in immunocapture to separate NDEVs. However, it remains controversial as to whether this protein is indeed present within EVs, or simply co-isolates as free

protein (Norman et al., 2021; Gomes and Witwer, 2022). The BDEV dataset analysed in this work would suggest other markers may be better when isolating NDEV with many of the markers analysed shown to be highly abundant. NeuN, DCX and C-FOS were not found within the BDEVs and DLG4 was not found in at least 4 replicates of any conditions.

5.6.4.3 Other glial cell markers in BDEVs

Alongside astrocytes, two other major glia cell types are present within the brain which will also release EVs to the extracellular environment – microglia and oligodendrocytes. 10 microglial markers were investigated in the BDEVs however only 2 markers were identified in ≥ 4 replicates for all conditions (Figure 5-30A). The abundance of these two markers, CD11b and CD45, was also low compared to other proteins suggesting either the microglial markers investigated are not present in microglia-derived EVs (MDEVs), or MDEVs were in low abundance in the BDEV populations. TMEM119, CD64 and CD163 were present in some BDEV replicates but were in fewer than 4 replicates for each condition, and again, were found in low abundance. IBA1, CX3CR1, F4/80, CD68 and CD40 were not found in any of the BDEV replicates.

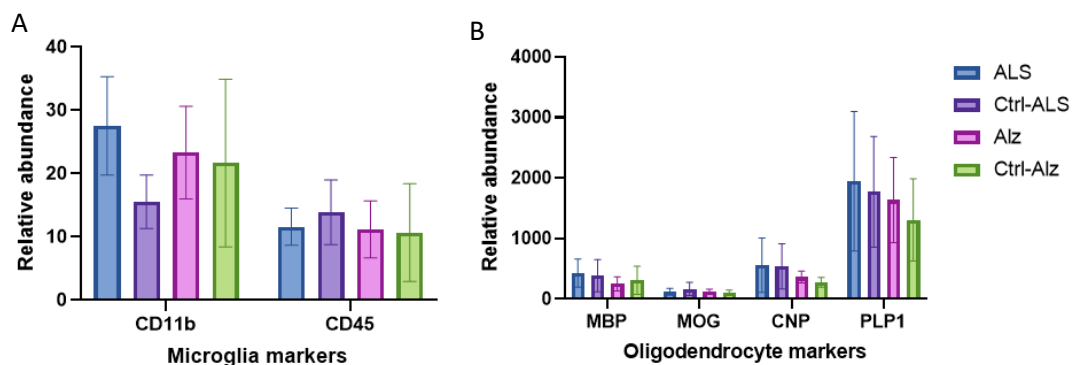


Figure 5-30 - Microglial and oligodendrocyte markers identified within BDEVs. (A) Only 2 microglial markers (CD11b and CD45) were identified within BDEVs and were not abundant. (B) 4 oligodendrocyte markers were identified within the BDEVs. Error bars represent mean and standard deviation between replicates (N = 8).

10 oligodendrocyte markers were investigated within the BDEVs however only 4 markers were identified in the BDEVs (Figure 5-30B). PLP1 was a very abundant oligodendrocyte marker followed by CNP and MBP which are all associated with ensuring the integrity of the myelin sheath. MOG was also identified but at a less abundant level than the other oligodendrocyte proteins. Unlike the other cell-specific markers described in this section, myelin-associated proteins are specific to oligodendrocytes due to the unique nature of these myelin-producing cells. Some of these proteins are also identified in Schwann cells within the peripheral nervous system, however, to a lesser extent. OLIG1/2/3, OSP, SOX10 and TMEM10 were not found within the BDEVs.

5.7 Comparison of ADEVs and BDEV proteomes by SWATH-MS

Overall, the BDEV analysis has generated a database of endogenous human EV proteins that can be used to compare to the ADEV proteins as well as future analysis on other EV types such as NDEVs or MDEVs. Therefore, a final analysis was completed to compare the ADEV and the BDEV proteomes identified by SWATH-MS. 60-70% of both the serum-free and serum-cultured ADEV proteins were identified within the BDEVs with similar proteins observed across all BDEV conditions (Table 5-9). Differences were to be expected between the ADEVs and the BDEVs due to the human primary astrocytes utilising foetal cells which are not representative of the aged cells from the post-mortem tissue. The ADEVs will therefore have developmental proteins that are not highly expressed within mature cells. In contrast, the BDEVs were isolated from subjects with an average age of 59 (ALS tissue) and 83 (Alz tissue) and therefore the parent cells will likely be made up of a mixture of mature and senescent CNS cells. Technical variation will also likely affect the results with the ADEVs and BDEVs being analysed at different times. High variation was observed between different technical runs during the qualitative mass spectrometry in section 4.3 demonstrating the effect this will have on the results. Therefore, with >60% proteins found in both samples, there was high similarity between the EVs groups.

Table 5-9 - Comparison of ADEV proteins and BDEV proteins identified by SWATH-MS indicates high similarity between the EV proteomes. Proteins found in at least 2 replicates of ADEVs as well as proteins found in ≥ 4 replicates of BDEVs for each condition. 60-70% of ADEV proteins were also identified within the BDEVs. Total protein numbers compared are presented in brackets alongside each condition.

	ALS (1472)	Ctrl-ALS (1377)	Alz (1528)	Ctrl-Alz (1617)
Serum-free ADEVs (526)	347 (66.0%)	327 (62.2%)	342 (65.0%)	352 (66.9%)
Serum-cultured ADEVs (300)	184 (61.3%)	178 (59.3%)	184 (61.3%)	187 (62.3%)

5.8 Investigating ADEV functionality beyond cargo transport

The work completed so far has shown that a wide variety of proteins are present within EVs with high similarity between *in vitro* ADEVs and endogenous BDEVs. What is still unclear is how these proteins effect recipient cells, and whether EVs simply act as cargo carriers, or if they have independent functionality. The final section of this thesis presents preliminary work completed to begin answering these questions.

5.8.1 The induction of astrocyte reactivity in serum-free astrocytes by serum-cultured ADEVs

Inflammatory reactive astrocytes and microglia release inflammatory cytokines into the environment which signals to other neighbouring cells that a harmful stimulus or tissue damage has been detected. These signals will then cause quiescent astrocytes

to respond by changing into a reactive phenotype. It is unclear whether EVs released by reactive astrocytes will also play a role in eliciting this reactivity in other astrocytes. Therefore, ADEVs purified from serum-cultured astrocytes (reactive phenotype) were added to the medium of serum-free 'quiescent' astrocytes in order to investigate whether reactive ADEVs could elicit a reactive response. Morphology analysis was completed using brightfield imaging before the cells were harvested for qPCR analysis.

5.8.1.1 Morphology analysis

To optimise the application of EV treatment, images were taken over 72 h after treatment to identify any morphological changes within the cells. Two different concentrations of ADEVs were also trialled to determine the optimal concentration for future work. By considering the concentration of EVs taken from each well of a 6-well plate of serum-free astrocytes, it was calculated that $\sim 7.5 \times 10^9$ particles/well would result in a representative concentration (the number of EVs released from a single well in one collection). Therefore, $\sim 3.8 \times 10^9$ and $\sim 3.8 \times 10^{10}$ particles from serum-cultured ADEVs were added to the human primary serum-free astrocytes.

Fresh ADEVs (purified as in section 2.5) were used for treatment to avoid any potential degradation or bursting caused by freezing the ADEVs. ADEV concentration was measured prior to treatment to determine the number of EVs with an average concentration of 3.6×10^{11} particles/ml. Brightfield images of the EV-treated astrocytes were taken at 90 min as well as 3, 6, 24, 48 and 72 h to determine any changes in morphology that may be indicative of reactive remodelling.

No obvious change in morphology of the EV-treated quiescent astrocytes was observed through visual inspection and therefore, quantification of morphology was not completed (Figure 5-31). Due to high confluency of the serum-free astrocytes at seeding, some of the serum-free astrocytes appeared reactive prior to EV treatment so morphological changes may have been missed in the current experiment. Instead, transcriptional changes were measured due to the high sensitivity of RT-qPCR, which should identify any subtle changes in the quiescent astrocytes after EV treatment.

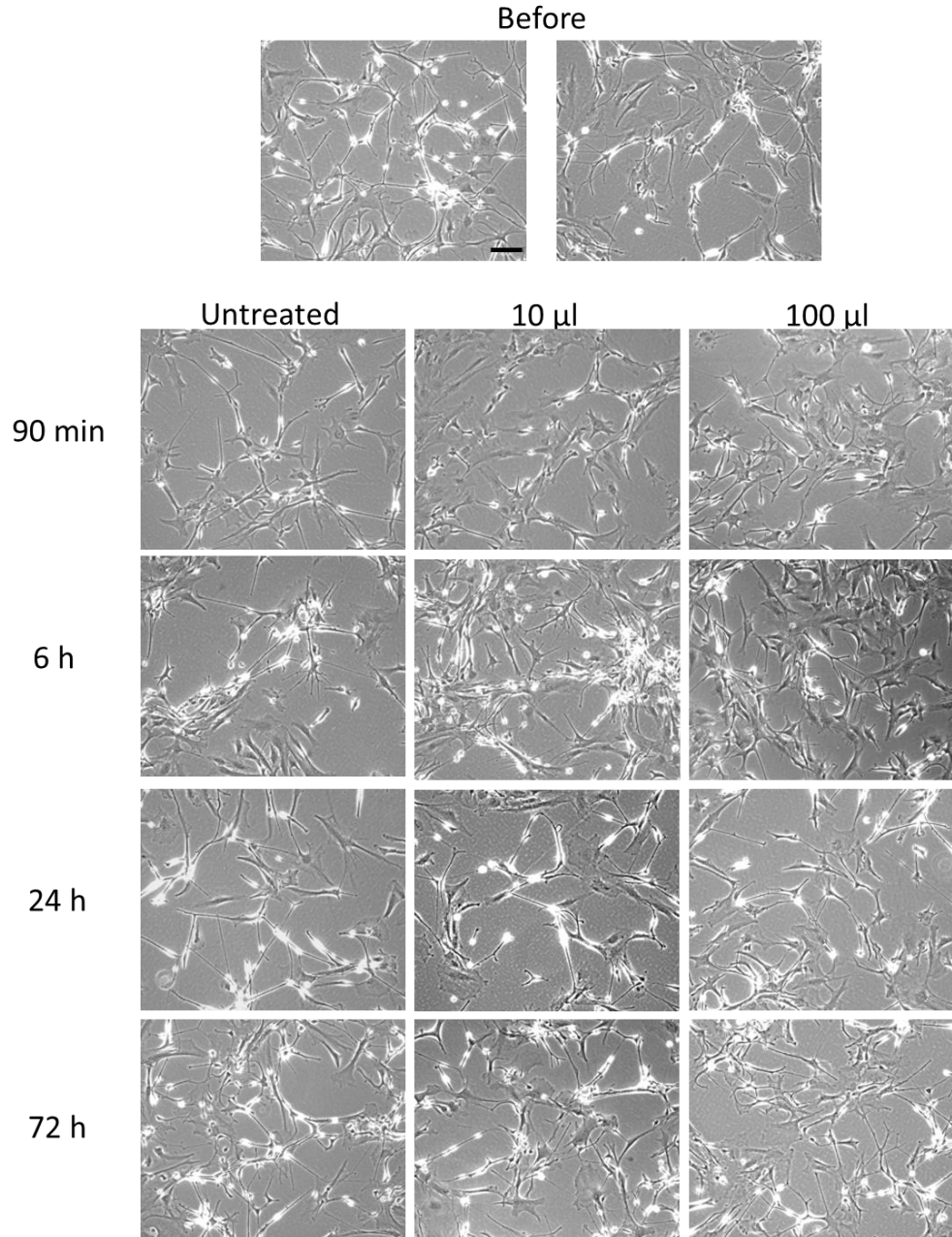


Figure 5-31 – No morphological differences were observed after 72 h of reactive ADEV treatment in human primary serum-free astrocytes. Representative brightfield images of serum-free astrocytes treated with serum-cultured ADEVs over 72 h. Serum-free astrocytes were treated with either 10 µl or 100 µl of serum-cultured ADEVs ($\sim 3.8 \times 10^{11}$ particles/ml) for 72 h. Astrocytes were imaged using brightfield microscopy at 90 min as well as 3, 6, 24, 48 and 72 h. Images were taken at 10x magnification with scale bar representing 100 µm (N = 2).

5.8.1.2 Gene expression changes of astrocyte and inflammatory markers in serum-free quiescent astrocytes after reactive ADEV treatment

RNA was harvested from serum-free astrocytes after 72 h treatment with serum-cultured ADEVs by RNA extraction for RT-qPCR analysis. Reactive astrocyte markers were selected as genes of interest (GFAP, S100β, EAAT2, and CD49f) as well as the inflammatory markers, IL-1β and IL10. TNFα was also investigated but was not

consistently detected within the samples, and therefore was not included in the final analysis. GAPDH, B2M and actin were tested for their suitability as housekeeping genes. Variation was observed across conditions (> 2 Ct values) in GAPDH so was not used for normalisation (Figure 5-32A). B2M and actin had similar Ct values across conditions, so the mean of these genes was used to normalise expression of genes of interest (Figure 5-32,B and C).

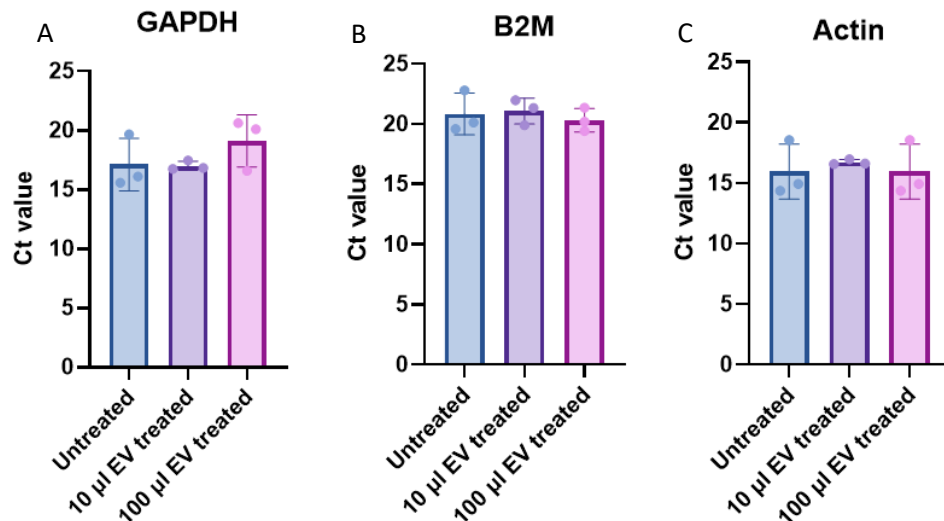


Figure 5-32 – B2M and Actin are suitable housekeeping genes when comparing gene expression changes in EV-treated serum-free astrocytes. Three housekeeping genes, GAPDH, B2M and actin, were compared to determine their suitability as housekeeping genes. (A) GAPDH had >2 Ct values difference across conditions indicating the gene is not stably expressed after EV treatment (2.1 cycles). (B) B2M and (C) actin had less variation across the conditions (0.75 and 0.78 Ct value difference, respectively) so would be suitable as housekeeping genes. Error bars represent mean and standard deviation (N = 3).

Gene expression was normalised to the mean of both B2M and actin with a fold change calculated against the average of the untreated condition for each gene of interest. GFAP expression significantly increased after serum-free astrocytes were treated with 100 µl of serum-cultured ADEVs ($\sim 3.8 \times 10^{10}$ particles/ml) but not after 10 µl treatment ($\sim 3.8 \times 10^9$ particles/ml) suggesting high doses of serum-cultured ADEVs can elicit reactivity in neighbouring astrocytes (Figure 5-33A; 100 µl fold change = 7.6 vs untreated; P = 0.046; N = 3). No other genes of interest were found to significantly change, however S100 β expression had an increasing trend with increased EV dosage (Figure 5-33B). CD49F and IL10 expression had decreasing trends with increasing EV dosage. With more biological repeats, these differences may become significant, supporting the hypothesis that EVs from reactive astrocytes are involved in eliciting a reactive phenotype in neighbouring quiescent astrocytes.

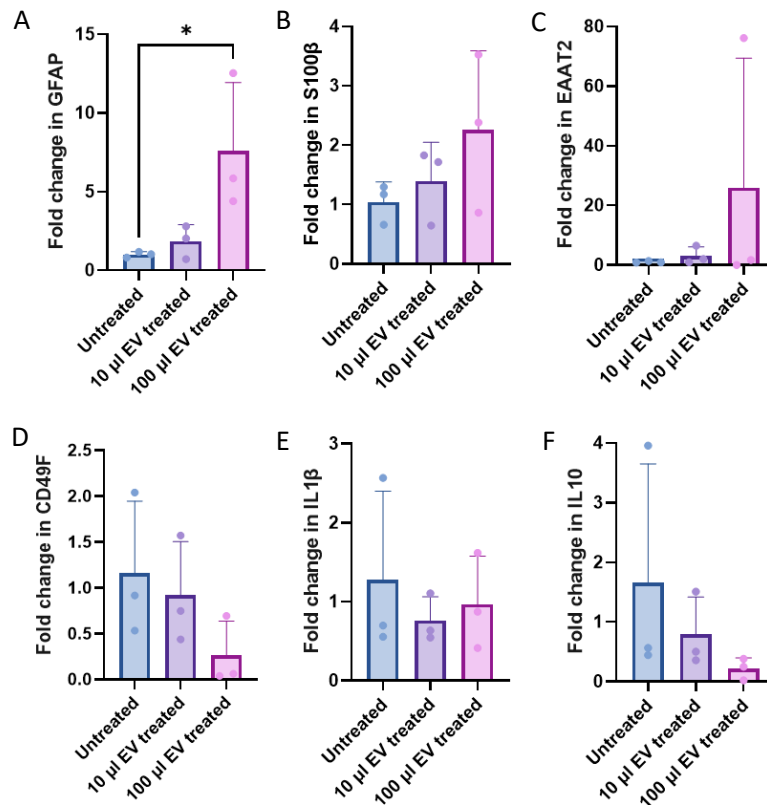


Figure 5-33 - Transcriptional changes in serum-free human primary astrocytes after treatment with purified ADEVs from serum-cultured cells. (A) GFAP expression significantly increased after serum-free astrocytes were treated with 100 µl but not 10 µl (100 µl Fold change = 7.603 vs untreated; $P = 0.046$). No differences were identified in the other astrocyte markers (B) S100β, (C) EAAT2 or (D) CD49F. However, an increasing trend was observed in S100β expression, and a decreasing trend observed in CD49F expression when astrocytes are treated with higher EV doses (100 µl). (E) No difference was observed in IL1β expression despite reactive EV treatment. (F) A decreasing trend was observed in IL10 when serum-free astrocytes were treated with reactive ADEVs but was not found to be significant. Statistical analysis was completed using One-way ANOVAs followed by Tukey's multiple comparisons tests. Error bars represent mean and upper standard deviation ($N = 3$).

5.9 Glycolysis within EVs: Are EVs metabolically active?

ABC and solute carrier (SLC proteins) transporters as well as the subunits of Na^+/K^+ ATPase were amongst the proteins identified within ADEVs and BDEVs by SWATH mass spectrometry. Whether these proteins are simply being transported to adjacent cells or if these transporters are active within the EVs is yet to be determined. For the transporters to be functional, ATP would be needed either to directly provide the energy required by the transporter (active transport) or used by other proteins such as the Na^+/K^+ ATPase to establish a concentration gradient within the ADEV that would facilitate molecular movement using the electrochemical gradient (such as glutamate transporters EAAT1 and EAAT2, secondary transporters). Glycolysis enzymes were also identified within the ADEV and BDEV mass spectrometry (see sections 5.5.2.3 and 5.6.2.2) indicating a potential pathway for EVs to generate ATP. Therefore, the presence of ATP as an indicator of independent functionality within EVs was investigated.

5.9.1.1 ATP is detected within ADEVs

To detect the presence of ATP within the purified ADEVs, a luminescent ATP detection assay (Abcam, #ab113849) was completed. Initially, the assay was used to measure ATP within the parent astrocyte whole cell lysates to determine if there were differences between serum-free and serum-cultured human primary astrocytes (Figure 5-34A). ATP luminescence was normalised to the serum-free control due to variations between technical repeats of the assays. No difference was identified between serum-free and serum-cultured astrocytes (SF = 1.00 vs SC = 1.05; $P = 0.84$; $N = 8$). ATP concentrations were then analysed within three biological replicates of serum-free and serum-cultured ADEVs. ATP was detected in the ADEVs with luminescence higher than the blank control (PBS) confirming the presence of ATP within ADEVs (Figure 5-34B). Luminescence was normalised to the median size and concentration of the ADEVs (measured by NTA) due to size differences previously observed between serum-free and serum-cultured ADEVs (see Figure 5-5). However, after normalisation, no difference was found between the conditions (SF ADEV = 811.7 ± 198.3 vs SC ADEV = 900.0 ± 70.0 a.u.; $P = 0.51$; $N = 3$).

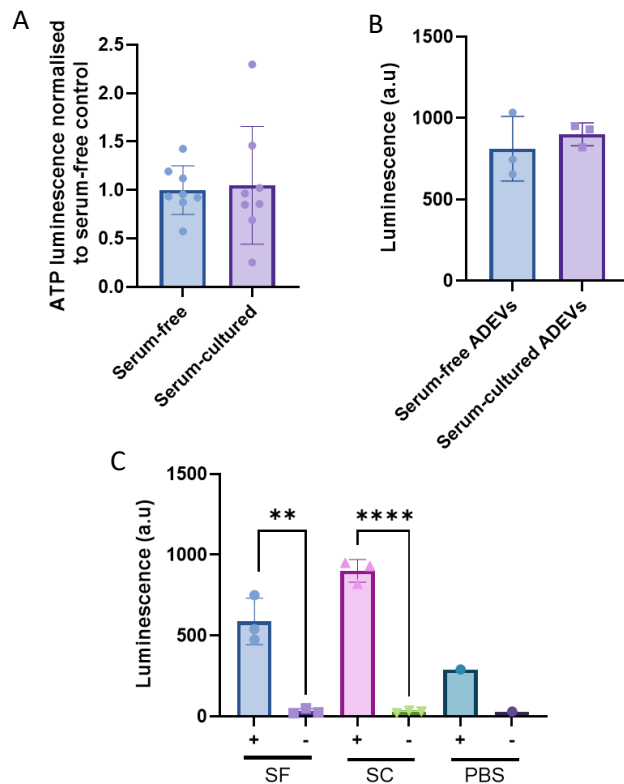


Figure 5-34 - ATP concentration is similar in serum-free and serum-cultured human primary ADEVs. (A) ATP concentrations were not different in serum-free and serum-cultured human primary astrocyte whole-cell lysates after normalisation to the serum-free control (SF = 1.00 vs SC = 1.05; $P = 0.84$; $N = 8$). Normalisation was completed on the cell lysates due to variations observed between assays. (B) There was also no difference in luminescence between serum-free and serum-cultured ADEVs after luminescence was normalised to the size and concentration of particles measured using NTA. (SF ADEV = 811.7 ± 198.3 vs SC ADEV = 900.0 ± 70.0 ; $P = 0.51$; $N = 3$). (C) ATP was present within ADEVs with very little luminescence observed when detergent was not included in the assay (+ = with detergent, - = without detergent; SF ADEV $P = 0.0026$, SC ADEV $P < 0.0001$; $N = 3$). Statistical analysis was completed using unpaired t-tests. Error bars represent mean and standard deviation.

To ensure the ATP that was detected in the ADEVs was in fact within the EVs and not a co-isolate (i.e. free ATP), the assay was completed with and without detergent (supplied with the ATP luminescent assay). When detergent was not added to the samples, luminescence was almost undetectable suggesting the ATP is inside the EVs (Figure 5-34C). PBS with and without detergent was used as a control to determine the effect of the detergent on luminescence. This showed some increase after detergent was added, but not to the same scale as the ADEVs.

5.9.1.2 *Measuring glycolysis within EVs*

With ATP detected within ADEVs, work began to investigate whether this ATP was generated within the EVs, or whether the ATP was loaded into the EVs prior to release from the cell. Glycolytic activity has previously been detected in neuronal intracellular vesicles where ATP generated by glycolysis is used to facilitate the movement of vesicles along microtubules in axons (Hinckelmann et al., 2016). In this experiment, glycolysis was detected using a similar luminescent ATP assay to the assay used in section 5.9.1.1, and therefore, a similar approach was taken to explore glycolysis within the ADEVs. To do this, a high concentration of EVs were required so subtle increases in ATP concentrations could be observed. Whilst ATP was found within ADEVs (above), luminescence was very close to the blank value and therefore it is unlikely that if glycolysis was occurring, this change would be detectable within the ADEVs. Instead, EVs derived from a neuroblastoma cell line (N2A cells) were utilised. Due to their neoplastic origin, N2A cells release far more EVs than the human primary astrocytes in a shorter collection timeframe and therefore had a much higher luminescence in the ATP assay (~10-fold higher, data not shown).

To detect glycolysis N2A EVs were treated with either glucose or 2-deoxy-D-glucose (2DG) as well as other substances required for glycolysis including NADH and ADP. 2DG was used as a negative control because 2DG cannot be broken down after the hexokinase step to provide carbon for energy production by glycolysis. ATP was added as this is needed to initiate glycolysis. If glycolysis was occurring within the EVs, ATP luminescence would be higher in the EVs treated with glucose as well as ADP and ATP, than those treated with 2DG. PBS was also used as a negative control to identify the raw luminescence of any of the individual substrates.

No difference in luminescence was identified between N2A derived-EVs and the PBS or 2DG controls suggesting production of ATP *via* glycolysis was not detected in the EVs (Figure 5-35). The addition of ATP and ADP did effect luminescence as expected, highlighting the need for the PBS control. It is difficult to determine whether the EVs are not capable of glycolysis or whether the assay was simply not sensitive enough to detect such a small change in ATP concentration. Future work should aim to confirm this result using different, more sensitive methodology.

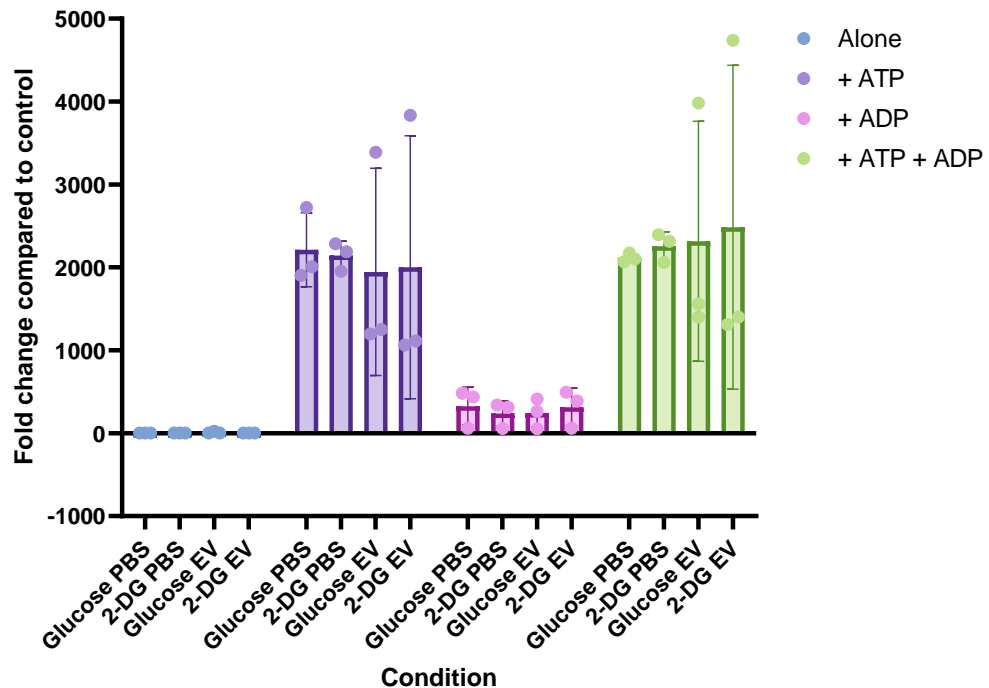


Figure 5-35 – ATP production via glycolysis was not identified within N2A EVs after treatment with glycolytic substrates. N2A-derived EVs were treated with either glucose (substrate required for glycolysis) or 2DG (cannot be broken down in glycolysis) as well as ADP and ATP which is required for glycolysis. All EVs received NADH and inorganic phosphates (present within PBS). Luminescence was normalised using the fold change compared to the EV-only control. No difference was identified between EVs and PBS or 2DG controls suggesting glycolysis could not be detected within the EVs. Error bars represent mean and standard deviation (N = 3).

5.10 Discussion

5.10.1 Summary

In this chapter, EVs were successfully isolated from both serum-free and serum-cultured human primary astrocytes as well as human brain tissue. The EVs were characterised using TEM imaging, NTA and protein mass spectrometry to confirm the presence of EVs within the EV-enriched fractions. NTA revealed a reduction in size of serum-cultured ADEVs compared to the serum-free ADEVs. No size or concentration differences were identified when comparing control and diseased BDEVs. Mass spectrometry successfully identified a range of EV-associated markers in the ADEVs and BDEVs such as the commonly used tetraspanins CD63, CD9 and CD81, as well as cytosolic proteins, TSG101 and ALIX. This highlights the advantage of protein mass spectrometry in comparison to western blotting which relies upon the quality of antibodies and requires high concentrations of EVs.

Once characterisation of the EVs were completed, the mass spectrometry datasets were further interrogated to identify any differences in protein expression between the serum-free and serum-cultured ADEVs as well as the control and diseased BDEVs. Whilst limited differences were identified between serum-free and serum-cultured ADEVs from human primary astrocytes, this work has provided a baseline dataset that can be further explored with a more directed hypothesis. Again, few differences

were identified between control and disease BDEVs suggesting frontal-lobe BDEVs do not reflect disease pathology in these cases. On the other hand, the experiment yielded a detailed dataset of frontal lobe BDEV proteomes that can be further interrogated, as well as be used as a comparison dataset for *in vitro* EV findings.

Preliminary investigations explored the functionality of ADEVs. Serum-free astrocytes were treated with serum-cultured ADEVs to determine whether reactive ADEVs could transfer reactivity. An increase in the RNA expression of astrocyte markers GFAP as well as a small, non-significant increase in S100 β and IL1- β after treatment with 100 μ l of EVs ($\times 10^{10}$ particles/ml) suggests reactivity may be transferred via ADEVs. No visible morphology change in the serum-free astrocytes was detected after treatment. However, there were issues with baseline reactivity during these preliminary experiments. More work is required to investigate the effect of ADEVs on recipient cells, but this work forms a baseline for future experiments.

With membrane transporters as well as subunits of the Na⁺/K⁺ ATPase detected during mass spectrometry, attempts to measure ATP within the ADEVs were completed using a luminescence ATP assay. ATP was detected within serum-free and serum-cultured ADEVs suggesting the possibility of these transporters being active within EVs. However, no difference was found between the conditions after normalisation using size and concentration differences. Glycolysis substrates were added to EVs to determine whether ATP was generated within the EVs themselves (i.e. can they act as independent units) or whether this ATP was packaged into the EVs prior to release from the cell. ATP production via glycolysis was not observed in the current study, but this could be due to a lack of sensitivity by the assay. Other techniques to try and measure glycolysis within EVs should be attempted before a lack of functional glycolysis within EVs is confirmed.

5.10.2 Successful EV isolation from human primary astrocytes

The isolation of EVs from both serum-free and serum-cultured astrocytes required different methodology to overcome the unique challenges in their cultures. For the serum-free astrocytes, their non-proliferative nature made it difficult to begin EV collection with a large number of astrocytes and therefore, it was difficult to collect sufficient EVs within one collection for downstream analysis. Therefore, EVs had to be collected over 2 weeks from a single 6-well plate of astrocytes, which required storing the first and second collection of conditioned media at -80°C to avoid EV degradation. The effect of freezing serum-cultured conditioned medium was explored in this work which found no difference in the size and concentration of ADEVs with freezing, but these experiments were limited by sample size, and were not completed using serum-free conditioned medium due to the difficulty in collecting ~48ml of fresh conditioned media (Figure 5-8 and Figure 5-9). Future work could further investigate the effect of freezing serum-free conditioned medium to improve the validity of functional studies completed using serum-free ADEVs.

In contrast, serum conditioned medium was not limited by the number of cells but instead required FBS removal from the media during EV collection to avoid contamination of bovine EVs that originated from the FBS. Many studies have highlighted issues with using FBS-containing medium for EV studies and show that

even EV-depleted medium still contains a large number of EVs (Aswad et al., 2016; Lehrich et al., 2018, 2021; Urzì et al., 2022). Therefore, the decision was made to use serum-deprivation to remove serum from the cultures, but this limited the time-frame conditioned media could be collected. No difference in serum-cultured astrocyte morphology was found after 5 days in FBS-free astrocyte medium (see Figure 5-1) so collections took place over 72 hours to avoid stressing the cells (one day in serum to initially seed the cells followed by 3 days in FBS-free medium before collection). However, further work should more thoroughly investigate the effect of serum-starvation (for example, using RNA sequencing or protein mass spectrometry) on the serum-cultured human primary astrocytes as well as compare to serum-cultured astrocytes cultured in EV-depleted FBS.

Due to the differences in collection method, it was difficult to compare the release rate of ADEVs from the cells. It would be interesting to test whether the difference in proliferation between the cultures would affect the EV release rate as cancer cells and stem cells release more EVs than normal tissue due to their proliferative nature (Sándor et al., 2021). Future work could increase the number of serum-free cells to match the number of serum-cultured cells at time of collection which would allow a direct comparison of EV number.

5.10.3 Importance of comprehensive EV characterisation

With EV preparations containing a wide range of EV subtypes such as exosomes and microvesicles (see section 1.2.1) as well as other contaminants such as liposomes and protein complexes, thorough characterisation needs to be completed to confirm the presence and purity of EVs. The MISEV guidelines were created to improve the quality of EV research with in-depth guidance for EV characterisation (latest version is Welsh et al, 2024)). In this work, experiments were designed to include many of the suggestions within MISEV for EV characterisation including use of a range of protein markers (in both western blotting and mass spectrometry) as well as using a range of different techniques to visualise and quantify particles within EV-enriched fractions.

Highlighted in this work is the power of mass spectrometry to characterise the protein cargo of EVs compared to standard western blotting methodology. Western blotting was challenging with the current ADEV samples and required whole EV preparations (i.e all EV-fractions concentrated and used for a single well) to detect proteins within the EVs. As well as the limited protein amount, western blotting also requires high quality antibodies that will routinely detect the protein of interest. In this work, antibodies for both CD63 and CD81 were trialled but were unsuccessfully detected in EVs using enhanced chemiluminescence, despite detection in corresponding cell lysates. In contrast, CD63 and CD81 were detected in both serum-free and serum-cultured ADEVs using SWATH mass spectrometry, alongside many other EV markers. Mass spectrometry allowed the detection of hundreds of proteins within the ADEVs allowing multiple markers from each of the categories suggested by MISEV to be explored.

5.10.4 Size differences between serum-free and serum-cultured ADEVs from human primary astrocytes

Whilst few differences were observed between serum-free and serum-cultured ADEV proteomes, a significant difference in size was observed with serum-cultured astrocytes releasing smaller ADEVs than serum-free astrocytes. This could either be due to differences in the EV population or differences in the composition of the EV membranes. There are many different subtypes of EVs documented, with the two most studied populations being exosomes (30 - 200 nm) and microvesicles (150 - 1000 nm; Couch et al., 2021). For instance, a form of small EV (median size ~80 nm) has been shown to promote cell proliferation and therefore may be released from serum-cultured astrocytes but not in serum-free astrocytes reducing the overall median size of ADEVs from reactive astrocytes (Lee et al., 2019). In contrast, changes in the composition of the EV membranes may also lead to small changes in the size of the EVs. Whilst not completed in this work, lipidomics could be completed on the ADEVs to investigate changes in the membrane composition between serum-free and serum-cultured ADEVs.

5.10.5 Comparison between ADEVs and BDEVs

BDEVs were explored in this chapter as a comparison to ADEVs to determine the translatability of the ADEV findings to endogenous human EVs, as well as to explore differences in CNS-derived EVs in both health and disease. Few differences were identified between control and disease tissue with more differences identified between ALS and Alzheimer's disease BDEVs. This suggests that other areas of the brain should be explored where more pathology is observed, instead of the frontal lobe tissue. Frontal lobe tissue was used in this work due to the availability of tissue (Alzheimer's disease frontal lobe tissue was used in a previous study within the lab group) but also because there is a common association between ALS and frontal temporal dementia (FTD; Abramzon et al., 2020). In this work, none of the subjects diagnosed with ALS were found to have cognitive symptoms which may explain why few differences were identified between ALS and control BDEVs. An interesting study comparing BDEVs from ALS tissue with no cognitive symptoms and BDEVs from ALS-FTD patients could be completed, where pathology is observed in the frontal lobe.

On the other hand, whilst not significant, GFAP expression was highest in the Alz BDEVs with a noticeable difference between Alz and the matched Alz-control BDEVs. Higher GFAP expression has previously been suggested as a potential biomarker in Alzheimer's disease with reactive astrocytes observed early in the disease (Kim et al., 2023). In particular, increased GFAP levels have been identified in the blood, which allows non-invasive measurement in patients that can be monitored repeatedly over time (Pereira et al., 2021; Oeckl et al., 2022). GFAP expression in the ALS BDEVs was similar to control BDEVs suggesting GFAP may be useful in distinguishing some neurodegenerative diseases.

Regarding the similarity of BDEVs and ADEVs, around 60-70% of ADEVs were observed within the BDEVs. Mass spectrometry is highly variable between technical repeats and the age difference between the tissue and primary cells (aged tissue vs foetal cells) meant differences were expected in the proteomes of the EVs. This

means the 60-70% similarity between ADEVs and BDEVs supports the translatability of the ADEV findings to endogenous brain tissue. Similar sizes in ADEVs and BDEVs were also observed, particularly in the Alzheimer's disease BDEVs and their matched controls, where ADEVs had an average of 139.5 nm compared to BDEVs having an average of 134.6 nm. Differences were observed in the concentration of BDEVs compared to the ADEVs but this is due to the high density of cells in tissue compared to cell culture.

There is a concern that more contaminants may be found within tissue-derived EVs such as synaptosomes and cell debris due to the harsher isolation methodology (mechanical and enzymatic dissociation is required). However, in this study as well as the previous study our methodology was based upon (Huang et al., 2020), few cellular contaminants were identified during mass spectrometry suggesting limited contamination.

5.10.6 Cell-specific proteins found on BDEVs could be used to isolate populations of EVs

The BDEVs represent a population of EVs from a range of CNS cell types and therefore provides an opportunity to identify cell-specific markers that can be used to isolate EV populations. A range of known cell markers for astrocytes, neurons, microglia and oligodendrocytes were identified within the BDEVs, however more astrocyte and neuron markers were identified suggesting EVs derived from these cell types would be easier to isolate using immunoprecipitation techniques than microglia or oligodendrocyte derived EVs (Fortunato et al., 2022; Valle-Tamayo et al., 2022). Regarding astrocyte markers, 11 markers were identified with GFAP, EAAT1/2, GLUL and CD44 all being highly expressed in the BDEVs. Previous studies have used GFAP and GLAST (rodent form of EAAT1) to isolate ADEVs from complex fluids such as blood and CSF (Willis et al., 2017; Valle-Tamayo et al., 2022b; Forró et al., 2024). However, using a range of markers would be beneficial in isolating ADEVs with it unlikely that a single marker will be abundant on the surface of all ADEVs, particularly when using GFAP which is not highly expressed in all astrocyte populations. Whilst no differences were detected between healthy and diseased BDEVs, this dataset can still be used in future work to investigate CNS EV cargo from other CNS cell types such as neuronal or microglial-derived EVs to confirm translatability.

5.10.7 Functionality of EVs

After thorough EV characterisation was completed for both the ADEVs and BDEVs, preliminary experiments were carried out to test EV functionality. Changes in the transcriptome of serum-free astrocytes were observed after treatment with a concentration of $\sim 3.8 \times 10^{10}$ particles (present in 100 μ l of combined EV fractions) suggesting this is a suitable concentration for future work. This is also similar to the concentration of particles that would be collected from each well of the serum-free astrocytes (calculated to be equivalent to 67 μ l per well). As with RT-qPCR findings in chapter 3, more replicates should be included to determine whether the trends observed in S100 β , CD49F and IL10 would become significant. Transmission of

neuroinflammation by ADEVs has been recently explored using LPS-treated organotypic spinal cord slices suggesting EVs are associated with transmitting reactivity between neighbouring microglia and astrocytes (Memo et al., 2024). Therefore, future work should focus on exploring this transmission further.

Mass spectrometry or RNA-sequencing could also be completed on EV-treated astrocytes to compare the EV-treated astrocytes to the serum-free and serum-cultured astrocyte datasets already collected in this work. Also, only serum-free and serum-cultured ADEVs were explored in this work, however other reactive phenotypes could be explored such as ADEVs from hypoxic astrocytes as well as ADEVs from astrocytes treated with inflammatory cytokines (such as the cytokine cocktail trialled in Chapter 3). Previous work has demonstrated changes in the protein and miRNA cargo of reactive ADEVs after astrocytes were treated with IL1 β and TNF α (Chaudhuri et al., 2018; You et al., 2020). In these studies, the effects of reactive ADEVs on neurons were explored rather than the effect of ADEVs on neighbouring astrocytes. However, functional changes seen within neurons after treatment with cytokines would suggest that similar functional changes would be observed in quiescent astrocytes. Future work could also investigate the effect of both reactive and quiescent human primary ADEVs on neurons and other glial cells (such as microglia or oligodendrocytes). *In situ*, ADEVs would be taken up by a range of cell types and therefore the effect of ADEVs should be explored across all CNS cell types.

At a metabolic level, measurable ATP concentrations were detected within EVs suggesting transporters found on the surface of EVs could be functional. In the case of astrocytes, it would be beneficial for ADEVs to have functional glutamate receptors to uptake excess glutamate from the extracellular space to prevent excitotoxicity. If this were possible, ADEVs could act as a possible therapeutic for a range of neurological diseases as well as trauma where excitotoxicity is documented (Armada-Moreira et al., 2020; Baracaldo-Santamaría et al., 2022). The difficulty with investigating transporter functionality in EVs is a lack of sensitivity with many of the techniques used to measure this. For example, many glutamate uptake assays exist but are designed to measure nanomolar changes. Using the ATP assay, ATP levels were detected in the picomolar range and therefore a similar level of detection will likely be needed for any uptake assays. Radioactive tracers could be attempted due to the high sensitivity of the technique but there are still issues with removing excess substrate from the EVs.

5.10.8 Limitations of EV characterisation

One of the largest limiting factors of the work completed in this chapter is the low yield of ADEVs from both serum-free and serum-cultured astrocytes. This leads to issues in downstream analysis with far fewer proteins detected via mass spectrometry compared to the BDEVs and limited resolution in assays such as the luminescent ATP assay. Detection of EV markers *via* western blotting were difficult with the limited number of ADEVs, with bands only observed when using antibodies against ALIX, calnexin and faint detection with Flotillin. N2A-derived EVs were often used to optimise techniques such as western blotting (data not shown) and the ATP

assay due to these cells releasing more EVs over a shorter period of time. However, this limits the knowledge of details exclusive to astrocyte-derived EVs.

Protein quantification was difficult within the EVs as the protein content of ADEVs was below the limit of detection of a standard BCA. Micro-BCAs are available which are far more sensitive than standard BCAs, however, this technique was not available within the current work. The absence of protein quantification likely led to the high variability seen in the biological repeats of the ADEVs. More replicates would improve the quality of the mass spectrometry analysis and would lead to more proteins being included for differential expression analysis. Only 65 proteins were included in the differential expression analysis out of the 562 proteins identified across the serum-free and serum-cultured ADEVs because of the variability observed across the replicates.

5.10.9 Conclusions

In this chapter, ADEVs were successfully isolated and characterised from serum-free and serum-cultured human primary astrocytes. The proteomes of the ADEVs were analysed creating a database for future analysis of ADEVs, despite few differences observed between serum-free and serum-cultured ADEVs at this stage. In comparison to aged, healthy and diseased BDEVs, ADEVs were similar to BDEVs with over 60% of the ADEV proteins also detected in BDEVs. Functionality of the ADEVs was explored with changes in the transcriptome of serum-free astrocytes observed after treatment with reactive ADEVs suggesting a transfer of reactivity from serum-cultured ADEVs to serum-free astrocytes. However, the functionality studies were limited by sample size and a lack of controls which should be included in future work.

Chapter 6: General discussion

6.1 Background of the work

6.1.1 Understanding astrocyte reactivity

The definition of 'reactivity' in astrocytes is fiercely debated with multiple approaches used to describe the molecular phenotypic remodelling of astrocytes (Escartin et al., 2019, 2021). Much of the research into astrocyte reactivity is in the context of disease, with neurotoxic astrocytes described in a range of neurodegenerative diseases such as Alzheimer's disease and ALS, as well as in traumatic brain injury (Liddel et al., 2017; Chun and Lee, 2018; Birger et al., 2019; Goetzl et al., 2020; Habib et al., 2020; Bellaver et al., 2023). However, reactivity is also a normal physiological response in astrocytes to protect the brain from harmful stimuli and return brain homeostasis. Therefore, the difference between 'healthy' reactivity and chronic, harmful reactivity needs to be explored. Escartin et al. (2021) have suggested the terms 'reactive' to define the astrocyte response to pathology, and 'active' to define the healthy, physiological response of astrocytes. When it is unclear whether the reactive response is modelling healthy or pathological conditions, such as in the current work, the term reactivity can be generally applied.

An issue with this terminology is that there are no unique descriptors to distinguish a healthy and a pathological astrocyte response at present. Astrocyte reactivity is described as the process where astrocytes undergo transcriptional, metabolic, biochemical and physiological remodelling, leading to a gain of new function, or loss of homeostatic functions (Escartin et al., 2021). Morphological changes, including hypertrophy, are observed in reactive astrocytes, as well as proliferation and increases in some astrocyte-associated genes such as GFAP and S100 β . However, different types of reactive response have been observed including both inflammatory and anti-inflammatory responses in the same population of astrocytes. Efforts have been made to distinguish the different types of reactivity using A1 (inflammatory) and A2 (anti-inflammatory) reactivity which are thought to be activated by different stimuli (A1 = LPS stimulation, microglia activation, A2 = ischemic stroke; Zamanian et al., 2012; Liddel et al., 2017). However, it is far more likely that astrocyte reactivity includes a spectrum of these responses. This makes defining astrocyte reactivity very challenging with a range of markers required to characterise astrocyte phenotype.

In order to experimentally study astrocyte reactivity, both quiescent and reactive astrocytes are required to identify changes specific to astrocyte reactivity. However, quiescent astrocytes are challenging to culture due to their lack of proliferation as well as requiring extensive supplementation to survive. Previous work has highlighted that FBS induces astrocyte reactivity in rodent primary astrocytes and therefore should not be used in quiescent astrocyte culture (Roybon et al., 2013; Prah et al., 2019). Despite this, many studies utilise serum-containing medium as standard to maintain astrocyte culture and encourage proliferation due to a lack of reproducible serum-free methods. In this work, the first aim was to create a serum-free, quiescent astrocyte culture method to explore the effects of serum on phenotype of human primary astrocytes. Once these models were established and

thoroughly characterised, the effect of astrocyte reactivity on their extracellular vesicles could be explored.

6.1.2 Current knowledge of human ADEVs

Current knowledge on ADEVs (prior to this study) is limited, however recent work has begun to explore the role of ADEVs in cellular communication within the CNS and beyond. ADEVs have been identified in the circulation having crossed the BBB, so ADEVs are potentially desirable targets for assessing brain health using less invasive techniques such as blood testing (Willis et al., 2017; Shi et al., 2019; Ramos-Zaldívar et al., 2022; Forró et al., 2024). To assess human brain health using ADEVs, biomarkers need to be identified that change in both reactivity and disease which can be consistently measured. Research has begun to explore the protein and miRNA cargo of ADEVs from inflammatory reactive astrocytes (often stimulated with inflammatory cytokines), but quiescent ADEV cargo are not well defined (Chaudhuri et al., 2018, 2020; You et al., 2020; Chun et al., 2021). In fact, only one protein entry for astrocytes has been included in the Vesiclepedia database (as of sept 2024) highlighting the need to characterise ADEV cargo, particularly from both reactive and quiescent human astrocytes.

It is unclear whether EVs have other roles beyond cargo delivery to recipient cells. Numerous studies have described changes in recipient cells after EV treatment highlighting their involvement in the communication between cells. For example, ADEVs contain neuroprotective and neurotrophic factors that can promote neuronal growth and survival in recipient neurones (Luarte et al., 2017; Pei et al., 2020; Chun et al., 2021; Sun et al., 2022; Xin et al., 2022). However, ADEVs have also been shown to have negative effects in disease by delivering harmful cargo to neurones, including mutant pathological proteins or inappropriate miRNAs, highlighting the complexity of astrocyte communication within the brain (Silverman et al., 2019; Varcianna et al., 2019; Zhao et al., 2021).

A study by Iraci et al. (2017) suggested EVs are independent metabolic units indicating that EVs could have functionality beyond cargo transport. In that study, human neural stem cell EVs were shown to harbour L-asparaginase activity, with Asrgl1 activity detected. Whilst this could be unique to stem cell EVs, this result implies that other metabolic functions may occur within EVs, with a role beyond cargo transport. In this work, ATP concentration within human ADEVs was investigated due to the identification of all ten glycolysis enzymes by SWATH-MS within the ADEVs and BDEVs which may indicate potential transporter activity.

6.2 Summary of findings

6.2.1 Establishing quiescent and reactive human primary astrocyte cultures

The overarching aim of this work was to thoroughly characterise both quiescent and reactive ADEVs from human primary astrocytes to determine whether they have potential as diagnostic markers of disease. In order to achieve this, quiescent and reactive astrocyte cultures using human primary astrocytes were required. In rodent

primary cultures, FBS induces a reactive phenotype, with serum-free cultures displaying quiescent features (Roybon et al., 2013; Prah et al., 2019). Therefore, in chapters 3 and 4 of this thesis, serum-free and serum-cultured human primary astrocytes were characterised using morphological analysis as well as RNA (RT-qPCR and RNA sequencing) and protein analysis (ICC, immunoblotting and protein mass spectrometry). In chapter 3, serum was found to induce a reactive phenotype which included hypertrophy (increased cell body size), proliferation and an increase in release of inflammatory cytokines such as MCP-1 and Chitinase-3-like-1 proteins (chronic serum culture). Serum-free astrocytes maintained quiescent morphology (smaller cell bodies, long thin processes) and had the ability to become reactive upon treatment with an inflammatory cytokine cocktail as well as different concentrations of FBS. Interestingly, 24 h treatment of FBS resulted in a different transcriptome response to astrocytes cultured in FBS for a minimum of 7 days (serum-cultured) suggesting two different mechanisms of reactivity when exposed acutely and chronically to FBS.

An unbiased 'multi-omic' approach was applied to the serum-free and serum-cultured human primary astrocytes in chapter 4 using RNA sequencing and protein mass spectrometry to identify key pathway differences between the astrocyte cultures, as well as to identify any genes or proteins that are differentially expressed after culture with serum for more than 7 days (chronic culture). Any significant differences may represent potential markers that could be used to assess astrocyte reactivity, particularly if this was also replicated within the ADEVs. RNA sequencing revealed that the serum-free and serum-cultured astrocytes have very distinct transcriptomes with homeostatic and neuroprotective pathways upregulated in the serum-free astrocytes such as 'axon guidance' and 'GABAergic synapse' pathways, whereas the serum-cultured astrocytes were found to have an upregulation of inflammatory pathways such as the TNF and NF- κ B signalling pathways. This supports the quiescent and reactive phenotypes attributed to the serum-free and serum-cultured astrocytes in chapter 3. In contrast, proteomic analysis did not identify major differences between the serum-free and serum-cultured astrocytes. This may be due to issues with variation between the biological replicates for each condition with future work aiming to use more than three biological replicates.

6.2.2 Isolation and characterisation of ADEVs

Once the astrocyte phenotypes were thoroughly characterised, optimisation began for the isolation of ADEVs from both serum-free (quiescent) and serum-cultured (reactive) human primary astrocytes. Due to the nano-sized nature of EVs, in-depth characterisation of the purified ADEV fractions was required to ensure the presence of EVs. Despite major differences in collection methods, a similar concentration of ADEVs were collected from ~48 ml sample of serum-free and serum-cultured conditioned medium (5.05×10^{11} particles/ml compared to 3.58×10^{11} particles/ml, respectively). Typical EV morphology was observed using TEM in both ADEV preparations, but using NTA, serum-cultured ADEVs were seen to be smaller compared to serum-free ADEVs (132.6 nm diameter compared to 146.4 nm, respectively). Common EV-associated proteins, ALIX and FLOT1 were identified in the ADEVs via immunoblotting, however other established EV markers, CD63 and CD81,

were not detected using this method. Due to the technical difficulties of detecting ADEV proteins through immunoblotting, protein mass spectrometry was used to identify key EV-associated markers as well as to catalogue the ADEV proteome. Despite a lack of detection through immunoblotting, CD63, CD81 and CD9 were all detected in the ADEVs by SWATH-MS alongside other key EV-associated proteins such as ALIX and TSG101. Similar to the parent astrocyte whole-cell lysate analysis, few differences were identified between the serum-free and serum-cultured ADEVs. Again, this may be due to the limited sample size with high variation seen between the three biological replicates for both conditions. However, when comparing the ADEV proteomes to their parent cell lysate proteomes, protein expression differences were observed supporting the theory of selective loading of proteins into EVs (Chen et al., 2021).

6.2.3 Comparing ADEVs to tissue-derived BDEVs to investigate the patient relevance of ADEV findings

Alongside ADEVs, brain-derived EVs (BDEVs) isolated from frontal lobe tissue of control and disease (Alzheimer's disease and ALS) post-mortem brains were also characterised to compare the findings from the ADEVs to endogenous human EVs, as well as to identify any differences between control and disease BDEVs. Similar size and morphology were identified by NTA between control and disease BDEVs, which was also similar to the ADEVs. Higher concentrations of particles were isolated from tissue compared to the ADEVs (100-fold more particles detected by NTA), most likely due to a far higher density of cells present within the small 100 mg section of tissue starting material compared to *in vitro* cultures. When analysed by SWATH-MS, ~2-fold more proteins were identified in the BDEVs compared to the ADEVs, most likely due to the higher concentration of particles observed in the BDEVs giving deeper proteome coverage.

Few differences were identified by protein SWATH-MS when comparing control and disease BDEVs suggesting EVs derived from frontal lobe tissue may not reflect disease pathology in Alzheimer's disease and ALS. In the current cohort of ALS samples, no cognitive symptoms were documented suggesting a possible lack of pathology in the frontal lobe. In many ALS cases, pathology is generally restricted to the spinal cord and motor cortex and therefore BDEVs may not reflect differences induced by the disease (Jankovska and Matej, 2021). In contrast, Alzheimer's pathology is thought to begin in the hippocampus and spread through the fronto-temporal cortices with disease progression so pathological changes would be expected within the frontal lobe of patients with Alzheimer's disease (Sathe et al., 2021). Future work should include immunohistochemistry analysis of the tissue prior to BDEV isolation to confirm the presence of pathology within the brain region for each patient.

With limited differences identified between control and disease BDEVs, the BDEV datasets were then compared to the human primary ADEV proteomes, with more than 60% of ADEV proteins identified in the BDEVs. This is despite low reproducibility being expected between SWATH-MS runs due to the BDEV and ADEV samples being analysed at different times. Large differences were observed between LC-MS/MS

replicates when analysed at different times (see section 4.3), highlighting the stochastic nature of mass spectrometry. As well as technical variation, biological differences between the BDEV and ADEVs were also expected to reduce the translatability of the SWATH-MS analyses because of the biological age of the parent cells, with BDEVs being released from adult cells and the ADEVs released from astrocytes with a foetal origin.

With serum-cultured astrocytes characterised as having a reactive phenotype, it was predicted that the ADEVs purified from these cultures would better resemble disease BDEVs. Reactivity is often seen in the early stages of neurodegeneration and therefore EVs derived from reactive astrocytes would be expected within the BDEV samples. However, with few differences observed by SWATH-MS between the control and disease BDEVs, as well as few differences observed between the quiescent and reactive ADEVs, it is unsurprising that a similar number of both quiescent and reactive ADEV proteins were identified across the different BDEV conditions with no clear distinction identified in the number of proteins.

6.2.4 Functionality of ADEVs

6.2.4.1 *Propagation of astrocyte reactivity to quiescent astrocytes by purified reactive ADEVs*

The final experiments in this work began to explore possible EV functionality with a focus on EV-based transmission of reactivity and ATP production. Purified reactive ADEVs were applied to serum-free astrocytes in culture to determine whether EVs could induce a reactive phenotype in recipient quiescent astrocytes. Two concentrations of reactive ADEVs were trialled with the higher concentration ($\times 10^{10}$ particles/ml, 100 μ l) inducing an increase in *GFAP* gene expression in recipient quiescent astrocytes. This increase in *GFAP* gene expression was also observed when 2% and 10% FBS was added to quiescent astrocytes in section 3.7, inducing a reactive phenotype in the astrocytes. Other genes including *S100 β* , *CD49f* and *IL10* had small changes in expression with EV treatment, however they were not found to be significant. Increasing the number of replicates would confirm whether these are true changes in gene expression and would support the hypothesis that ADEVs from reactive astrocytes can induce reactive remodelling. For these experiments, the quiescent astrocytes were incubated with reactive ADEVs for 72 hours because this time point was thought to be sufficient to induce transcriptional changes. However, a range of earlier timepoints should be trialled in future experiments to ensure any early changes are not missed. No visual change in morphology was observed after EV treatment but this may be due to baseline reactivity observed within the quiescent astrocytes and therefore should be repeated in future work.

6.2.4.2 *Presence of ATP within ADEVs*

Within the SWATH analysis of the ADEVs and the BDEVs, multiple transporters were detected such as ABC transporters and SLC transporters (such as the glutamate transporter, EAAT2). Na⁺/K⁺ ATPase subunits were also detected which are required to produce the electrochemical gradient for SLC transporters. With ATP required for ABC transporters and ATPases to function, ATP concentrations were explored within

the ADEVs. ATP was detected in the serum-free and serum-cultured ADEVs using a luminescence ATP assay suggesting the possibility of functional transporters within EVs. Glycolysis was explored by incubating the substrates required for the glycolytic process with EVs but no change in ATP concentration was detected compared to controls.

6.3 Maintaining a quiescent, serum-free human astrocyte culture

The results in this work have highlighted the need for a reproducible serum-free culture of astrocytes to study normal astrocyte physiology, with serum shown to have irreversible effects on the morphology, transcriptome and proteome of human primary astrocytes. This had been previously identified in rodent astrocytes but had not been extensively explored in human astrocytes (Prah et al., 2019). Previous studies have utilised serum-free cultures, but no consensus has been reached as to a standardised media composition for these cultures with many different variations published (Foo et al., 2011; Roybon et al., 2013; Clarke et al., 2018; Barbar et al., 2020). To determine the best medium composition to use for serum-free culture of human primary astrocytes, previously published serum-free media compositions were compared to identify necessary components. The aim was to create an accessible media composition which could be easily reproduced in other lab settings. Unlike B27 and AGS (AGS supplement is included in ScienCell medium and produced by the supplier of the human primary astrocytes), G5 supplement has a well-documented formula which is designed for astrocytes making it optimal for use within this culture. Many of the components found within this supplement were commonly used in other serum-free compositions such as FGF, EGF and insulin, reducing the need to purchase many individual peptides and growth factors.

However, despite the serum-free medium maintaining viable quiescent culture, no noticeable proliferation was observed in the cultures. It was not financially feasible to use the original vial of astrocytes (>£780 per vial) supplied by ScienCell to generate only one 6-well plate. Therefore, optimisation was completed to culture quiescent, serum-free astrocytes from astrocytes previously cultured and expanded in serum. Whilst serum caused an irreversible change to cells once established in culture, serum-free morphology was observed in early passage astrocytes (passage 2-3) that were thawed in serum-free medium after cryopreservation in liquid nitrogen. This allowed two rounds of passaging before the cells were cryopreserved, generating between 24-36 vials per original vial and allowing this serum-free model to be financially feasible in culture. It is unclear how cryopreservation 'resets' the astrocyte phenotype but this should be investigated further as it could indicate a possible protective mechanism that could be utilised in neurodegenerative disease. One hypothesis is that cold-shock proteins could have a role in resetting the astrocyte phenotype towards a more homeostatic/neuroprotective phenotype. Cold-shock proteins RBM3 and RTN3 have been shown to have neuroprotective properties and therefore should be explored in the serum-free and serum-cultured astrocytes (Bastide et al., 2017).

An issue with the human primary astrocyte cultures is the foetal nature of the astrocytes which makes it difficult to use this model to study ageing or neurodegenerative disease. Many of the proteins and growth factors detected either through protein mass spectrometry or the cytokine assay are found in development and therefore would not be directly relevant to mature, adult endogenous astrocytes. Studies have attempted to mature *in vitro* astrocytes by adding FGF to cultures, however in this work, the FGF present in the G5 supplement did not seem to mature the astrocytes (Roybon et al., 2013; Savchenko et al., 2019). A novel combination of peptides has been shown to mature some *in vitro* cells including iPSC-derived neurones, which could also be trialled in the primary astrocytes in an effort to mature the cells (Hergenreder et al., 2024).

6.4 *The effect of serum on human primary astrocytes*

It is clear from the results presented in this work as well as those published in Prah (2019), that serum causes a multitude of changes within astrocytes, including a change to a hypertrophic, more bipolar morphology as well as transcriptomic and proteomic changes suggestive of a reactive phenotype. Therefore, we advise that serum should not be used in astrocyte cultures where a quiescent phenotype is desired. This includes studies that focus on basic astrocyte function as well as studies requiring quiescent astrocytes as a control for astrocyte reactivity research. The primary reason that serum (most commonly FBS) is used in astrocyte cultures is to stimulate proliferation and support growth. In this work, serum-free astrocyte cultures were shown to survive for at least four weeks but showed no signs of proliferation during this time. Cryopreservation reset the astrocyte phenotype which may overcome the issues surrounding cell availability without serum, but this may not be suitable for all studies. Instead, the use of serum should be clearly justified in these cases where alternatives are not available (Gstraunthaler et al., 2013). Further to this, the details of the FBS used should be clearly documented due to the batch-batch variability seen in FBS composition, which will ultimately alter cell growth (Liu et al., 2023). It should be noted that only FBS was tested in the current study as this is the most common form of serum used in cell culture. The effects of horse serum or even human serum on astrocyte culture were not explored and therefore future work should confirm whether these types of serum would replicate the changes observed using FBS.

In EV studies, it is essential to remove FBS from cultures prior to collection of conditioned medium to avoid contamination of desired EV samples with endogenous bovine EVs present within FBS. A range of studies have highlighted that 'EV-depleted FBS' still contains bovine EVs and by depleting EVs by ultracentrifugation (the common method to remove EVs), the FBS also negatively effects the growth of cells in culture (Aswad et al., 2016; Lechrich et al., 2018, 2021). Instead of using EV-depleted FBS for serum cultures, in this work, serum-cultured astrocytes were grown in astrocyte medium without FBS during conditioned medium collection (over 72 h). Whilst no morphological changes in the serum-cultured astrocytes were observed during this collection time, the molecular effects of removing the serum from the serum-cultured astrocytes were not fully explored. RNA-sequencing or protein mass

spectrometry could be utilised to identify any genetic or proteomic changes during serum-removal.

One of the aims of this work was to investigate differences between quiescent and reactive ADEVs, with this being a major focus of chapter 5. Whilst limited differences were observed between the ADEVs, serum-cultured ADEVs were found to be smaller than serum-free ADEVs indicating a change in either EV population or a change in membrane composition due to serum culture. At present, it is difficult to identify different EV populations within the complex EV fractions isolated by SEC and therefore this was not completed within the current work. A small sub-type of EV (~80 nm) has been described in proliferative populations and therefore may be released in serum-cultured ADEVs and not serum-free ADEVs (Lee et al., 2019). However, markers have not yet been identified to distinguish different EV-subtypes which would be required to determine the presence of this newly identified subtype. Future work could focus on characterising the EV membrane of quiescent and reactive ADEVs using lipid-focused mass spectrometry analysis which would determine whether a change in lipid composition is responsible for this reduced size.

6.5 Multi-omics analysis of human primary astrocytes

The multi-omic approach (RNA sequencing and protein mass spectrometry) completed in this work highlights differences that occur between cellular transcriptome and proteome. Whilst many results were consistent between the techniques (i.e. differential expression between genes/proteins were in the same direction), not all changes observed in the RNA-sequencing were observed in the proteomic analysis. While this may be explained by post-transcriptional regulatory processes such as RNA interference and nonsense-mediated decay, these differences may also be due to differences in the sample processing of the techniques (Greenbaum et al., 2003). RNA sequencing allows the detection of whole-transcripts rather than relying on protein fragmentation that is required for LC-MS/MS. This removes the level of uncertainty in detection that occurs in mass spectrometry where only peptides are used for protein identification. Ultimately, this results in far more data (depth of coverage) being generated through RNA sequencing than mass spectrometry. Alongside this, the biological replicates used for RNA-sequencing were far more consistent than those used for mass spectrometry resulting in more genes being compared between samples (more genes detected in 2 or more replicates and lower variability resulting in bigger significance), than the proteins in mass spectrometry. However, it is important to note that these techniques produce different information about the physiological state of the cells and therefore should be completed in parallel.

Other omics analysis could be completed for future work such as metabolomics which would provide insight into another aspect of astrocyte physiology. In this work, only protein mass spectrometry was completed on the serum-free and serum-cultured ADEVs, with RNA sequencing only completed on the parent cells. Whilst mRNA has previously been detected within EVs, a limited EV miRNAome is expected, with research often focusing on miRNA detection within EVs (Valadi et al., 2007; Lai et al., 2022). ADEV-associated miRNAs have been shown to elicit regulatory changes

in neighbouring cells and therefore future work could explore miRNA changes in the ADEVs from quiescent and reactive astrocytes (Lafourcade et al., 2016; Luarte et al., 2017; Chaudhuri et al., 2018; Varcianna et al., 2019; Marton et al., 2023).

Lipidomic analysis of the ADEVs would also begin to explore changes in the ADEV membrane which could explain the difference in size between the serum-cultured ADEVs and serum-free ADEVs. Lipidomic analysis could also identify targets used for the selective uptake of ADEVs by specific cell types which could be manipulated for therapeutic delivery. In ADEVs, the investigation of lipids is particularly important with certain saturated fatty-acids shown to be neurotoxic in disease (Guttenplan et al., 2021). Identifying these toxic fatty acids in reactive EVs may indicate a role for EVs in astrocyte neurotoxicity. Lipidomics is not commonly completed and therefore would provide novel insight into the composition of ADEVs.

6.6 Isolation of human ADEVs and BDEVs

Different isolation methods were required to isolate ADEVs from serum-free and serum-cultured astrocytes due to restrictions with cell number (serum-free lack proliferation) and the use of FBS (serum-cultured medium). However, this did not appear to alter the outcomes of the current experiments with no difference in EV concentration found. This is an issue when comparing the EV release rates of the astrocyte cultures which would require the same starting number of cells as well as consistent collection times (rather than 72 h vs 2 weeks). This experiment could be completed in the future using microscopy or larger numbers of serum-free astrocytes to better compare to serum cultures.

In comparison, 100-fold more particles were detected in the tissue-derived BDEV samples, which is most likely due to the high density of cells within tissue sections used. Whilst a controversial topic, it is predicted that there are roughly 120 billion cells within the human brain, with an average weight thought to be ~1300 g (average weight of human brain; von Bartheld et al., 2016). Therefore, in each 100 mg of tissue that was used to isolate the BDEVs, we predict there would be roughly 900 million cells. In contrast, ADEVs were isolated from roughly 900,000 serum-free astrocytes (150,000 per well of 6 well plate) and roughly 2.5 million serum-cultured astrocytes (4x T75 flasks with an average of 600,000 cells/flask upon collection). Therefore, we would expect around 500-1000 fold more EVs from human brain tissue if the collection methods were directly comparable.

On the other hand, due to the mechanical and enzymatic digestion involved in the isolation of BDEVs, some of the particles detected are likely to be contaminants such as synaptosomes, cell debris or intracellular vesicles. However, a similar number of cell contaminants were observed in the ADEVs in comparison to the BDEVs. This supports the findings of the published BDEV analysis where the method was originally described, where few contaminants were observed (Huang et al., 2020).

Ultrafiltration will have led to many of the smaller contaminants being isolated before the SEC step with a 10k MWCO filter utilised. Smaller contaminants that remained after ultrafiltration (such as free protein) will also be removed in later protein fractions, so the SEC protocol should produce fairly pure isolations compared

to ultracentrifugation or immunoprecipitation (Benedikter et al., 2017; Lobb and Möller, 2017; Zhao et al., 2021; Benayas et al., 2023). Ultracentrifugation is the most common technique used within EV research and often leads to a higher yield than SEC but with a focus on ADEV proteomics within this work, high purity was required. Like ultracentrifugation, immunoprecipitation leads to more contaminants with the precipitation isolating any particle with a lipid membrane (i.e. cell debris, lipoproteins etc.). SEC is also a gentler method of isolation so is more suitable for functional studies where EVs and their surface proteins are required to be unaffected.

6.7 Future analysis of ADEVs to be completed

A range of analyses were carried out on the EVs in this study, including TEM, NTA and immunoblotting to profile the serum-free and serum-cultured ADEVs in line with MISEV guidance. However, other techniques could have been trialled to achieve a more complete characterisation. Flow cytometry and dSTORM microscopy analysis have been utilised to identify sub-populations of EVs using specific protein markers (for example, Mondal et al., 2019 and Ali Moussa et al., 2022). Whilst dSTORM was briefly trialled in this work, only lipophilic dyes were utilised to detect all EVs present in the sample, rather than fluorescent antibodies to tag individual populations of EVs such as GFAP-positive ADEVs. This may be useful for future work when investigating EVs from more complex samples such as plasma or CSF, with a range of astrocyte markers identified within BDEVs using SWATH-MS. Flow cytometry and dSTORM could be completed on the BDEVs to identify the proportion of ADEVs and neuronal EVs by utilising the highly expressed markers detected during SWATH-MS analysis.

Morphology could also be assessed using cryo-EM instead of more conventional TEM to better explore the morphology of the ADEVs (Zeev-Ben-Mordehai et al., 2014; Emelyanov et al., 2020). Cryo-EM preserves the spherical structure of the EVs reducing artifacts created by the vacuum of TEM. In TEM, EVs are often seen as ‘cup-shaped’ however this is not the natural morphology of the EVs and is caused by the vacuum of the TEM.

6.8 ADEV functionality beyond cargo delivery?

The presence of glutamate transporter proteins within EVs suggests the possibility of a role in glutamate recycling for the EVs, either through the transfer of transporters to areas with a high concentration of glutamate, or the possibility of EVs using the transporters to uptake glutamate from the extracellular environment. For this to occur, Na^+/K^+ ATPase pumps would be required to establish the electrochemical gradient required for the glutamate transporters to function. ATP is needed for the pumps to establish this electrochemical gradient, so glutamate uptake requires ATP. ATP was detected within the ADEVs as well as the subunits of the Na^+/K^+ ATPase. Future work could try to measure glutamate uptake directly however, this would require a high level of sensitivity which is not possible with current glutamate uptake assays. The use of radiolabelled glutamate could be explored due to the higher sensitivity, or metabolic mass spectrometry to detect small changes in glutamate

concentrations within EVs. Glycolysis was explored within the EVs using the luminescent ATP assay but either the assay was not sensitive enough to detect subtle changes in ADEV ATP concentration, or glycolysis was not occurring. Glycolysis has previously been observed in intercellular vesicles suggesting glycolysis may occur in particles of a similar size (Hinckelmann et al., 2016).

In this work, the effect of purified reactive ADEVs on other quiescent astrocytes was partially explored with changes observed after treatment with $\times 10^{10}$ particles/ml. Whilst future work should continue this investigation using protein fractions and conditioned media as a comparison, work should also begin to explore the effect of ADEVs on other cell types such as microglia or neurones. This has been explored in other studies, but this work often uses ADEVs from serum cultured astrocytes as well as rodent cultures (Luarte et al., 2017; Pei et al., 2020; Chun et al., 2021; Sun et al., 2022; Xin et al., 2022). We have shown how serum affects the ADEVs and therefore it would be interesting to explore how this changes the interaction between astrocytes and neighbouring neurones.

6.9 Overall Limitations

6.9.1 Limitations of the astrocyte models

Commercially available human primary astrocytes from ScienCell have proven to be successful in recapitulating aspects of human biology, with serum-free cells having a similar morphology to quiescent *in situ* human astrocytes, and the ADEVs having a similar proteome to tissue-derived BDEVs. However, the human primary astrocytes are of foetal origin and therefore resemble immature astrocytes with many developmental proteins observed through SWATH MS. Therefore, age-related changes cannot be explored which limits the ability of the cultures to be used for neurodegenerative disease research.

The model is also cultured in a monolayer with only astrocytes present in the culture which does not recapitulate the human brain. Co-cultures would be more representative, however ADEV research would be more difficult as the EVs would need to be separated prior to characterisation. With astrocyte and neuronal markers identified in purified BDEVs, this may be possible in future work by isolating EVs based upon the presence of either astrocyte or neuronal-specific markers by immunoprecipitation. 3D cultures could also be utilised to improve the translatability of the findings from the human primary astrocytes to the human brain (for example, Pavia et al., 2019).

Finally, FBS reactivity is not well understood and whilst useful in eliciting reactivity in the current work, other models of reactivity could be explored further. Cytokine-induced reactivity was briefly explored in chapter 3 of this work but was not found to elicit the same changes observed in other studies using the same cytokine cocktail (Liddelow et al., 2017). Hypoxia could also be explored to potentially elicit a more neuroprotective phenotype which would allow a better characterisation of how different stimuli alter the secreted ADEVs.

6.9.2 Limitations of the mass spectrometry analyses

Two types of mass spectrometry analysis were completed during this work, with SWATH-MS analysis found to be more appropriate to characterise the ADEV proteome due to the technique's quantitative nature. However, despite the quantitative nature of the technique, it is difficult to compare the expression of different proteins within a sample due to quantification relying on peptide count rather than protein count. This means that proteins that fragment into more peptides will be detected more frequently, and therefore appear to be more highly expressed. However, quantification can be done between samples for each detected protein as changes in peptide number would reflect protein number (a protein would fragment the same way each time).

A limitation of all of the mass spectrometry work completed in this thesis is that high variation was observed between samples, despite SWATH-MS analysis being completed at the same time for all biological replicates. This indicates a higher sample size is required for the ADEVs which would allow a more comprehensive analysis (four replicates was suitable for RNA-SEQ analysis and therefore would likely be suitable for mass spectrometry analysis). Inclusion criteria required proteins to be detected in at least two of the biological replicates so with four or more replicates, more proteins were likely to meet this threshold. Eight replicates of each BDEV condition were used to overcome some of the variability issues observed during previous SWATH analysis. The variation between the BDEVs likely reflects variation within human tissue (i.e. age, storage conditions) and disease progression (as well as presence of co-morbidities) and therefore cannot be avoided. Lower thresholds during the quantitative analysis (CV and NA values) were shown to increase the number of proteins included in the analysis but this ultimately raised the threshold for significance, reducing the number of differentially expressed proteins and increasing the risk of type 2 errors.

6.10 Concluding remarks

In conclusion, serum culture has been shown to alter the physiology of human primary astrocytes resulting in a reactive phenotype. Changes in size were observed between quiescent (serum-free) and reactive (serum-cultured) ADEVs, however few changes were observed in the proteomes of the ADEVs. Functionality experiments suggests that reactive ADEVs have the ability to convert quiescent astrocytes into reactive astrocytes, but more work needs to be completed to fully characterise the functional effect of ADEVs on astrocytes as well as other CNS cell types.

Chapter 7:References

- Abbott, J. A., Francklyn, C. S., and Robey-Bond, S. M. (2014). Transfer RNA and human disease. *Front Genet* 5. doi: 10.3389/fgene.2014.00158
- Abbott, N. J. (2002). Astrocyte-endothelial interactions and blood-brain barrier permeability. *J Anat* 200, 629–638. doi: 10.1046/j.1469-7580.2002.00064.x
- Abbott, N. J., Rönnbäck, L., and Hansson, E. (2006). Astrocyte–endothelial interactions at the blood–brain barrier. *Nat Rev Neurosci* 7, 41–53. doi: 10.1038/nrn1824
- Abel, O., Powell, J. F., Andersen, P. M., and Al-Chalabi, A. (2012). ALSod: A user-friendly online bioinformatics tool for amyotrophic lateral sclerosis genetics. *Hum Mutat* 33, 1345–1351. doi: 10.1002/humu.22157
- Abramzon, Y. A., Fratta, P., Traynor, B. J., and Chia, R. (2020). The Overlapping Genetics of Amyotrophic Lateral Sclerosis and Frontotemporal Dementia. *Front Neurosci* 14. doi: 10.3389/fnins.2020.00042
- Acioglu, C., Li, L., and Elkabes, S. (2021). Contribution of astrocytes to neuropathology of neurodegenerative diseases. *Brain Res* 1758. doi: 10.1016/j.brainres.2021.147291
- Agrahari, V., Agrahari, V., Burnouf, P. A., Chew, C. H., and Burnouf, T. (2019). Extracellular Microvesicles as New Industrial Therapeutic Frontiers. *Trends Biotechnol* 37, 707–729. doi: 10.1016/j.tibtech.2018.11.012
- Aguzzi, A., and Weissmann, C. (1997). Prion research: The next frontiers. *Nature* 389, 795–798. doi: 10.1038/39758
- Akiyama, H., Kaneko, T., Mizuno, N., and McGeer, P. L. (1990). Distribution of phosphate-activated glutaminase in the human cerebral cortex. *J Comp Neurol* 297, 239–252. doi: 10.1002/cne.902970207
- Aladeokin, A. C., Akiyama, T., Kimura, A., Kimura, Y., Takahashi-Jitsuki, A., Nakamura, H., et al. (2019). Network-guided analysis of hippocampal proteome identifies novel proteins that colocalize with A β in a mice model of early-stage Alzheimer’s disease. *Neurobiol Dis* 132, 104603. doi: 10.1016/J.NBD.2019.104603
- Ali Moussa, H. Y., Manaph, N., Ali, G., Maacha, S., Shin, K. C., Ltaief, S. M., et al. (2022). Single Extracellular Vesicle Analysis Using Flow Cytometry for Neurological Disorder Biomarkers. *Front Integr Neurosci* 16. doi: 10.3389/fnint.2022.879832
- Alvaro, C. G., Braz, J. M., Bernstein, M., Hamel, K. A., Craik, V., Yamanaka, H., et al. (2020). Hippocalcin-like 4, a neural calcium sensor, has a limited contribution to pain and itch processing. *PLoS One* 15. doi: 10.1371/JOURNAL.PONE.0226289
- Alzheimer’s Association (2018). 2018 Alzheimer’s disease facts and figures. *Alzheimer’s and Dementia* 14, 367–429. doi: 10.1016/j.jalz.2018.02.001

- Andersen, J. V., and Schousboe, A. (2022). Glial Glutamine Homeostasis in Health and Disease. *Neurochemical Research* 48:4 48, 1100–1128. doi: 10.1007/S11064-022-03771-1
- Andersen, J. V., and Schousboe, A. (2023). Milestone Review: Metabolic dynamics of glutamate and GABA mediated neurotransmission — The essential roles of astrocytes. *J Neurochem* 00, 1–29. doi: 10.1111/JNC.15811
- Anderson, M. A., Ao, Y., and Sofroniew, M. V. (2014). Heterogeneity of reactive astrocytes. *Neurosci Lett* 565, 23–29. doi: 10.1016/j.neulet.2013.12.030
- Angelova, P. R., Iversen, K. Z., Teschemacher, A. G., Kasparov, S., Gourine, A. V., and Abramov, A. Y. (2018). Signal transduction in astrocytes: Localization and release of inorganic polyphosphate. *Glia* 66, 2126–2136. doi: 10.1002/glia.23466
- Apodaca, L. A., Baddour, A. A. D., Garcia, C., Alikhani, L., Giedzinski, E., Ru, N., et al. (2021). Human neural stem cell-derived extracellular vesicles mitigate hallmarks of Alzheimer’s disease. *Alzheimers Res Ther* 13, 57. doi: 10.1186/s13195-021-00791-x
- Araque, A., Parpura, V., Sanzgiri, R. P., and Haydon, P. G. (1999). Tripartite synapses: Glia, the unacknowledged partner. *Trends Neurosci* 22, 208–215. doi: 10.1016/S0166-2236(98)01349-6
- Arredondo, C., Cefaliello, C., Dyrda, A., Montecino, M., Brown, R. H., van Zundert Correspondence, B., et al. (2022). Excessive release of inorganic phosphate by ALS/FTD astrocytes causes non-cell-autonomous toxicity to motoneurons. *Neuron* 0. doi: 10.1016/J.NEURON.2022.02.010
- Ashley, A. K., Hinds, A. I., Hanneman, W. H., Tjalkens, R. B., and Legare, M. E. (2016). DJ-1 mutation decreases astroglial release of inflammatory mediators. *Neurotoxicology* 52, 198–203. doi: 10.1016/j.neuro.2015.12.007
- Aswad, H., Jalabert, A., and Rome, S. (2016). Depleting extracellular vesicles from fetal bovine serum alters proliferation and differentiation of skeletal muscle cells in vitro. *BMC Biotechnol* 16. doi: 10.1186/s12896-016-0262-0
- Attwell, D., Buchan, A. M., Charkpak, S., Lauritzen, M., MacVicar, B. A., and Newman, E. A. (2010). Glial and neuronal control of brain blood flow. *Nature* 468, 232–243. doi: 10.1038/nature09613
- Azam, S., Haque, M. E., Balakrishnan, R., Kim, I. S., and Choi, D. K. (2021). The Ageing Brain: Molecular and Cellular Basis of Neurodegeneration. *Front Cell Dev Biol* 9, 683459. doi: 10.3389/FCCELL.2021.683459/BIBTEX
- Baba, M., Nakajo, S., Tu, P. H., Tomita, T., Nakaya, K., Lee, V. M. Y., et al. (1998). Aggregation of α -synuclein in Lewy bodies of sporadic Parkinson’s disease and dementia with Lewy bodies. *American Journal of Pathology* 152, 879–884.
- Baek, G., Choi, H., Kim, Y., Lee, H.-C., and Choi, C. (2019). Mesenchymal Stem Cell-Derived Extracellular Vesicles as Therapeutics and as a Drug Delivery Platform. doi: 10.1002/sctm-18-0226

- Bai, Y., Su, X., Piao, L., Jin, Z., and Jin, R. (2021). Involvement of Astrocytes and microRNA Dysregulation in Neurodegenerative Diseases: From Pathogenesis to Therapeutic Potential. *Front Mol Neurosci* 14. doi: 10.3389/fnmol.2021.556215
- Baietti, M. F., Zhang, Z., Mortier, E., Melchior, A., Degeest, G., Geeraerts, A., et al. (2012). Syndecan-syntenin-ALIX regulates the biogenesis of exosomes. *Nat Cell Biol* 14, 677–685. doi: 10.1038/ncb2502
- Baixauli, F., López-Otín, C., and Mittelbrunn, M. (2014). Exosomes and autophagy: Coordinated mechanisms for the maintenance of cellular fitness. *Front Immunol* 5, 403. doi: 10.3389/fimmu.2014.00403
- Bak, L. K., Schousboe, A., and Waagepetersen, H. S. (2006). The glutamate/GABA-glutamine cycle: Aspects of transport, neurotransmitter homeostasis and ammonia transfer. *J Neurochem* 98, 641–653. doi: 10.1111/j.1471-4159.2006.03913.x
- Ballatore, C., Lee, V. M. Y., and Trojanowski, J. Q. (2007). Tau-mediated neurodegeneration in Alzheimer’s disease and related disorders. *Nat Rev Neurosci* 8, 663–672. doi: 10.1038/nrn2194
- Baracaldo-Santamaría, D., Ariza-Salamanca, D. F., Corrales-Hernández, M. G., Pachón-Londoño, M. J., Hernandez-Duarte, I., and Calderon-Ospina, C. A. (2022). Revisiting Excitotoxicity in Traumatic Brain Injury: From Bench to Bedside. *Pharmaceutics* 14. doi: 10.3390/pharmaceutics14010152
- Barbar, L., Jain, T., Zimmer, M., Herbert, J. M., Liddelow, S. A., Fossati, V., et al. (2020). CD49f Is a Novel Marker of Functional and Reactive Human iPSC-Derived Astrocytes. *Neuron* 107, 1–18. doi: 10.1016/j.neuron.2020.05.014
- Barker, R. A., Parmar, M., Studer, L., and Takahashi, J. (2017). Human Trials of Stem Cell-Derived Dopamine Neurons for Parkinson’s Disease: Dawn of a New Era. *Cell Stem Cell* 21, 569–573. doi: 10.1016/j.stem.2017.09.014
- Basso, M., Pozzi, S., Tortarolo, M., Fiordaliso, F., Bisighini, C., Pasetto, L., et al. (2013). Mutant copper-zinc superoxide dismutase (SOD1) induces protein secretion pathway alterations and exosome release in astrocytes: Implications for disease spreading and motor neuron pathology in amyotrophic lateral sclerosis. *Journal of Biological Chemistry* 288, 15699–15711. doi: 10.1074/jbc.M112.425066
- Bastide, A., Peretti, D., Knight, J. R. P., Grosso, S., Spriggs, R. V., Pichon, X., et al. (2017). RTN3 Is a Novel Cold-Induced Protein and Mediates Neuroprotective Effects of RBM3. *Current Biology* 27, 638–650. doi: 10.1016/j.cub.2017.01.047
- Baxter, P. S., Dando, O., Emelianova, K., He, X., McKay, S., Hardingham, G. E., et al. (2021). Microglial identity and inflammatory responses are controlled by the combined effects of neurons and astrocytes. *Cell Rep* 34. doi: 10.1016/j.celrep.2021.108882
- Bazargani, N., and Attwell, D. (2016). Astrocyte calcium signaling: The third wave. *Nat Neurosci* 19, 182–189. doi: 10.1038/nn.4201

- Bellaver, B., Povala, G., Ferreira, P. C. L., Ferrari-Souza, J. P., Leffa, D. T., Lussier, F. Z., et al. (2023). Astrocyte reactivity influences amyloid- β effects on tau pathology in preclinical Alzheimer's disease. *Nat Med*. doi: 10.1038/s41591-023-02380-x
- Bellot-Saez, A., Kékesi, O., Morley, J. W., and Buskila, Y. (2017). Astrocytic modulation of neuronal excitability through K⁺ spatial buffering. *Neurosci Biobehav Rev* 77, 87–97. doi: 10.1016/j.neubiorev.2017.03.002
- Benedikter, B. J., Bouwman, F. G., Vajen, T., Heinzmann, A. C. A., Grauls, G., Mariman, E. C., et al. (2017). Ultrafiltration combined with size exclusion chromatography efficiently isolates extracellular vesicles from cell culture media for compositional and functional studies. *Sci Rep* 7. doi: 10.1038/s41598-017-15717-7
- Benjamini, Y., Krieger, A. M., and Yekutieli, D. (2006). Adaptive linear step-up procedures that control the false discovery rate.
- Benninger, F., Glat, M. J., Offen, D., and Steiner, I. (2016). Glial fibrillary acidic protein as a marker of astrocytic activation in the cerebrospinal fluid of patients with amyotrophic lateral sclerosis. *Journal of Clinical Neuroscience* 26, 75–78. doi: 10.1016/j.jocn.2015.10.008
- Beretta, C., Nikitidou, E., Streubel-Gallasch, L., Ingelsson, M., Sehlin, D., and Erlandsson, A. (2020). Extracellular vesicles from amyloid- β exposed cell cultures induce severe dysfunction in cortical neurons. *Sci Rep* 10. doi: 10.1038/s41598-020-72355-2
- Bertuchi, F. R., Bourgeon, D. M. G., Landemberger, M. C., Martins, V. R., and Cerchiaro, G. (2012). PrP C displays an essential protective role from oxidative stress in an astrocyte cell line derived from PrP C knockout mice. *Biochem Biophys Res Commun* 418, 27–32. doi: 10.1016/j.bbrc.2011.12.098
- Bianco, F., Pravettoni, E., Colombo, A., Schenk, U., Möller, T., Matteoli, M., et al. (2005). Astrocyte-Derived ATP Induces Vesicle Shedding and IL-1 β Release from Microglia. *The Journal of Immunology* 174, 7268–7277. doi: 10.4049/jimmunol.174.11.7268
- Birger, A., Ben-Dor, I., Ottolenghi, M., Turetsky, T., Gil, Y., Sweetat, S., et al. (2019). Human iPSC-derived astrocytes from ALS patients with mutated C9ORF72 show increased oxidative stress and neurotoxicity. *EBioMedicine* 50, 274–289. doi: 10.1016/j.ebiom.2019.11.026
- Blanc, L., and Vidal, M. (2018). New insights into the function of Rab GTPases in the context of exosomal secretion. *Small GTPases* 9, 95–106. doi: 10.1080/21541248.2016.1264352
- Blandford, S. N., Galloway, D. A., and Moore, C. S. (2018). The roles of extracellular vesicle microRNAs in the central nervous system. *Glia* 66, 2267–2278. doi: 10.1002/glia.23445
- Blokhuis, A. M., Groen, E. J. N., Koppers, M., Van Den Berg, L. H., and Pasterkamp, R. J. (2013). Protein aggregation in amyotrophic lateral sclerosis. *Acta Neuropathol* 125, 777–794. doi: 10.1007/s00401-013-1125-6

- Booth, H. D. E., Hirst, W. D., and Wade-Martins, R. (2017). The Role of Astrocyte Dysfunction in Parkinson's Disease Pathogenesis. *Trends Neurosci* 40, 358–370. doi: 10.1016/j.tins.2017.04.001
- Bradbury, E. J., and Burnside, E. R. (2019). Moving beyond the glial scar for spinal cord repair. *Nat Commun* 10. doi: 10.1038/s41467-019-11707-7
- Brandebura, A. N., Paumier, A., Onur, T. S., and Allen, N. J. (2023). Astrocyte contribution to dysfunction, risk and progression in neurodegenerative disorders. *Nat Rev Neurosci* 24, 23–39. doi: 10.1038/s41583-022-00641-1
- Brenna, S., Altmeppen, H. C., Mohammadi, B., Rissiek, B., Schlink, F., Ludewig, P., et al. (2020). Characterization of brain-derived extracellular vesicles reveals changes in cellular origin after stroke and enrichment of the prion protein with a potential role in cellular uptake. *J Extracell Vesicles* 9. doi: 10.1080/20013078.2020.1809065
- Brennan, K., Martin, K., FitzGerald, S. P., O'Sullivan, J., Wu, Y., Blanco, A., et al. (2020). A comparison of methods for the isolation and separation of extracellular vesicles from protein and lipid particles in human serum. *Sci Rep* 10. doi: 10.1038/s41598-020-57497-7
- Brown, A. M., and Ransom, B. R. (2007). Astrocyte glycogen and brain energy metabolism. *Glia* 55, 1263–1271. doi: 10.1002/glia.20557
- Buratta, S., Tancini, B., Sagini, K., Delo, F., Chiaradia, E., Urbanelli, L., et al. (2020). Lysosomal exocytosis, exosome release and secretory autophagy: The autophagic- and endo-lysosomal systems go extracellular. *Int J Mol Sci* 21. doi: 10.3390/ijms21072576
- Bushong, E. A., Martone, M. E., Jones, Y. Z., and Ellisman, M. H. (2002). Protoplasmic astrocytes in CA1 stratum radiatum occupy separate anatomical domains. *Journal of Neuroscience* 22, 183–192. doi: 10.1523/jneurosci.22-01-00183.2002
- Cahoy, J. D., Emery, B., Kaushal, A., Foo, L. C., Zamanian, J. L., Christopherson, K. S., et al. (2008). A transcriptome database for astrocytes, neurons, and oligodendrocytes: A new resource for understanding brain development and function. *Journal of Neuroscience* 28, 264–278. doi: 10.1523/JNEUROSCI.4178-07.2008
- Cali, C., Tauffenberger, A., and Magistretti, P. (2019). The strategic location of glycogen and lactate: From body energy reserve to brain plasticity. *Front Cell Neurosci* 13. doi: 10.3389/fncel.2019.00082
- Casper, K. B., and McCarthy, K. D. (2006). GFAP-positive progenitor cells produce neurons and oligodendrocytes throughout the CNS. *Molecular and Cellular Neuroscience* 31, 676–684. doi: 10.1016/j.mcn.2005.12.006
- Charles, A. C., Merrill, J. E., Dirksen, E. R., and Sandersont, M. J. (1991). Intercellular signaling in glial cells: Calcium waves and oscillations in response to mechanical stimulation and glutamate. *Neuron* 6, 983–992. doi: 10.1016/0896-6273(91)90238-U

- Chatterjee, P., Pedrini, S., Stoops, E., Goozee, K., Villemagne, V. L., Asih, P. R., et al. (2021). Plasma glial fibrillary acidic protein is elevated in cognitively normal older adults at risk of Alzheimer's disease. *Transl Psychiatry* 11. doi: 10.1038/s41398-020-01137-1
- Chaudhuri, A. D., Dasgheyb, R. M., DeVine, L. R., Bi, H., Cole, R. N., and Haughey, N. J. (2020). Stimulus-dependent modifications in astrocyte-derived extracellular vesicle cargo regulate neuronal excitability. *Glia* 68, 128–144. doi: 10.1002/glia.23708
- Chaudhuri, A. D., Dastgheyb, R. M., Yoo, S. W., Trout, A., Talbot, C. C., Hao, H., et al. (2018). TNF α and IL-1 β modify the miRNA cargo of astrocyte shed extracellular vesicles to regulate neurotrophic signaling in neurons. *Cell Death Dis* 9, 1–18. doi: 10.1038/s41419-018-0369-4
- Chen, C., and Dong, X. P. (2016). Epidemiological characteristics of human prion diseases. *Infect Dis Poverty* 5, 1–10. doi: 10.1186/s40249-016-0143-8
- Chen, C., Sun, M., Wang, J., Su, L., Lin, J., and Yan, X. (2021a). Active cargo loading into extracellular vesicles: Highlights the heterogeneous encapsulation behaviour. *J Extracell Vesicles* 10, e12163. doi: 10.1002/JEV2.12163
- Chen, L., Yang, R., Kwan, T., Tang, C., Watt, S., Zhang, Y., et al. (2020). Paired rRNA-depleted and polyA-selected RNA sequencing data and supporting multi-omics data from human T cells. *Sci Data* 7. doi: 10.1038/s41597-020-00719-4
- Chen, X., Sun, G., Tian, E., Zhang, M., Davtyan, H., Beach, T. G., et al. (2021b). Modeling Sporadic Alzheimer's Disease in Human Brain Organoids under Serum Exposure. *Advanced Science* 8, 2101462. doi: 10.1002/ADVS.202101462
- Chen, Y., Zhao, Y., Yin, Y., Jia, X., and Mao, L. (2021c). Mechanism of cargo sorting into small extracellular vesicles. *Bioengineered* 12, 8186–8201. doi: 10.1080/21655979.2021.1977767
- Cherry, J. D., Olschowka, J. A., and O'Banion, M. K. (2014). Are "resting" microglia more "M2"? *Front Immunol* 5, 594. doi: 10.3389/fimmu.2014.00594
- Chevillet, J. R., Kang, Q., Ruf, I. K., Briggs, H. A., Vojtech, L. N., Hughes, S. M., et al. (2014). Quantitative and stoichiometric analysis of the microRNA content of exosomes. *Proc Natl Acad Sci U S A* 111, 14888–14893. doi: 10.1073/pnas.1408301111
- Choi, D. S., Kim, D. K., Kim, Y. K., and Gho, Y. S. (2015). Proteomics of extracellular vesicles: Exosomes and ectosomes. *Mass Spectrom Rev* 34, 474–490. doi: 10.1002/mas.21420
- Chulpanova, D. S., Kitaeva, K. V., James, V., Rizvanov, A. A., and Solovyeva, V. V. (2018). Therapeutic prospects of extracellular vesicles in cancer treatment. *Front Immunol* 9, 1534. doi: 10.3389/fimmu.2018.01534
- Chun, C., Smith, A. S. T., Kim, H., Kamenz, D. S., Lee, J. H., Lee, J. B., et al. (2021). Astrocyte-derived extracellular vesicles enhance the survival and

electrophysiological function of human cortical neurons in vitro. *Biomaterials* 271. doi: 10.1016/j.biomaterials.2021.120700

- Chun, H., and Lee, C. J. (2018). Reactive astrocytes in Alzheimer's disease: A double-edged sword. *Neurosci Res* 126, 44–52. doi: 10.1016/j.neures.2017.11.012
- Clancy, J. W., Schmidtman, M., and D'Souza-Schorey, C. (2021). The ins and outs of microvesicles. *FASEB Bioadv* 3, 399–406. doi: 10.1096/fba.2020-00127
- Clarke, L. E., Liddelow, S. A., Chakraborty, C., Münch, A. E., Heiman, M., and Barres, B. A. (2018). Normal aging induces A1-like astrocyte reactivity. *Proc Natl Acad Sci U S A* 115. doi: 10.1073/pnas.1800165115
- Cocucci, E., and Meldolesi, J. (2015). Ectosomes and exosomes: Shedding the confusion between extracellular vesicles. *Trends Cell Biol* 25, 364–372. doi: 10.1016/j.tcb.2015.01.004
- Cocucci, E., Racchetti, G., Podini, P., and Meldolesi, J. (2007). Enlargeosome traffic: Exocytosis triggered by various signals is followed by endocytosis, membrane shedding or both. *Traffic* 8, 742–757. doi: 10.1111/j.1600-0854.2007.00566.x
- Colodner, K. J., Montana, R. A., Anthony, D. C., Folkner, R. D., De Girolami, U., and Feany, M. B. (2005). Proliferative Potential of Human Astrocytes. Available at: <https://academic.oup.com/jnen/article/64/2/163/2916715>
- Colombo, J. A., and Reisin, H. D. (2004). Interlaminar astroglia of the cerebral cortex: A marker of the primate brain. *Brain Res* 1006, 126–131. doi: 10.1016/j.brainres.2004.02.003
- Colombo, J. A., Yáñez, A., Puissant, V., and Lipina, S. (1995). Long, interlaminar astroglial cell processes in the cortex of adult monkeys. *J Neurosci Res* 40, 551–556. doi: 10.1002/jnr.490400414
- Colombo, M., Moita, C., Van Niel, G., Kowal, J., Vigneron, J., Benaroch, P., et al. (2013). Analysis of ESCRT functions in exosome biogenesis, composition and secretion highlights the heterogeneity of extracellular vesicles. *J Cell Sci* 126, 5553–5565. doi: 10.1242/jcs.128868
- Connolly, K., Lehoux, M., O'Rourke, R., Assetta, B., Erdemir, G. A., Elias, J. A., et al. (2023). Potential Role of Chitinase-3-like Protein 1 (CHI3L1/YKL-40) in Neurodegeneration and Alzheimer's Disease. *Alzheimers Dement* 19, 9. doi: 10.1002/ALZ.12612
- Cook, K. B., Kazan, H., Zuberi, K., Morris, Q., and Hughes, T. R. (2011). RBPDB: A database of RNA-binding specificities. *Nucleic Acids Res* 39. doi: 10.1093/nar/gkq1069
- Corcoran, C. C., Grady, C. R., Pisitkun, T., Parulekar, J., and Knepper, M. A. (2017). From 20th century metabolic wall charts to 21st century systems biology: database of mammalian metabolic enzymes. *Am J Physiol Renal Physiol* 312, 533–542. doi: 10.1152/ajprenal.00601.2016.-The

- Cornell-Bell, A. H., Finkbeiner, S. M., Cooper, M. S., and Smith, S. J. (1990). Glutamate induces calcium waves in cultured astrocytes: Long-range glial signaling. *Science (1979)* 247, 470–473. doi: 10.1126/science.1967852
- Couch, Y., Di, D., Yong, V. 卐, Gho, S., Harrison, P., Hill, A. F., et al. (2021). A brief history of nearly EV-erything – The rise and rise of extracellular vesicles. *J Extracell Vesicles* 10, e12144. doi: 10.1002/JEV2.12144
- Crivelli, S. M., Giovagnoni, C., Zhu, Z., Tripathi, P., Elsherbini, A., Quadri, Z., et al. (2022). Function of ceramide transfer protein for biogenesis and sphingolipid composition of extracellular vesicles. *J Extracell Vesicles* 11, e12233. doi: 10.1002/JEV2.12233
- D’Acunzo, P., Kim, Y., Ungania, J. M., Pérez-González, R., Goulbourne, C. N., and Levy, E. (2022). Isolation of mitochondria-derived mitovesicles and subpopulations of microvesicles and exosomes from brain tissues. *Nat Protoc* 17, 2517–2549. doi: 10.1038/s41596-022-00719-1
- D’Acunzo, P., Pérez-González, R., Kim, Y., Hargash, T., Miller, C., Alldred, M. J., et al. (2021). Mitovesicles are a novel population of extracellular vesicles of mitochondrial origin altered in Down syndrome. Available at: <https://www.science.org>
- Dadsetan, S., Kukolj, E., Bak, L. K., Sørensen, M., Ott, P., Vilstrup, H., et al. (2013). Brain alanine formation as an ammonia-scavenging pathway during hyperammonemia: Effects of glutamine synthetase inhibition in rats and astrocyte-neuron co-cultures. *Journal of Cerebral Blood Flow and Metabolism* 33, 1235–1241. doi: 10.1038/JCBFM.2013.73/FORMAT/EPUB
- Daneman, R., and Prat, A. (2015). The blood–brain barrier. *Cold Spring Harb Perspect Biol* 7. doi: 10.1101/cshperspect.a020412
- Danzer, K. M., Kranich, L. R., Ruf, W. P., Cagsal-Getkin, O., Winslow, A. R., Zhu, L., et al. (2012). Exosomal cell-to-cell transmission of alpha synuclein oligomers. *Mol Neurodegener* 7, 42. doi: 10.1186/1750-1326-7-42
- D’Arrigo, G., Gabrielli, M., Scaroni, F., Swuec, P., Amin, L., Pegoraro, A., et al. (2021). Astrocytes-derived extracellular vesicles in motion at the neuron surface: Involvement of the prion protein. *J Extracell Vesicles* 10, e12114. doi: 10.1002/JEV2.12114
- de Jong, O. G., Verhaar, M. C., Chen, Y., Vader, P., Gremmels, H., Posthuma, G., et al. (2012). Cellular stress conditions are reflected in the protein and RNA content of endothelial cell-derived exosomes. *J Extracell Vesicles* 1. doi: 10.3402/jev.v1i0.18396
- Deczkowska, A., Keren-Shaul, H., Weiner, A., Colonna, M., Schwartz, M., and Amit, I. (2018). Disease-Associated Microglia: A Universal Immune Sensor of Neurodegeneration. *Cell* 173, 1073–1081. doi: 10.1016/j.cell.2018.05.003
- Deitmer, J. W., Theparambil, S. M., Ruminot, I., and Becker, H. M. (2017). Our hungry brain: Which role do glial cells play for the energy supply? *Neuroforum* 23, 1–8. doi: 10.1515/nf-2016-A102

- DeJesus-Hernandez, M., Mackenzie, I. R., Boeve, B. F., Boxer, A. L., Baker, M., Rutherford, N. J., et al. (2011). Expanded GGGGCC Hexanucleotide Repeat in Noncoding Region of C9ORF72 Causes Chromosome 9p-Linked FTD and ALS. *Neuron* 72, 245–256. doi: 10.1016/j.neuron.2011.09.011
- Del Conde, I., Shrimpton, C. N., Thiagarajan, P., and López, J. A. (2005). Tissue-factor-bearing microvesicles arise from lipid rafts and fuse with activated platelets to initiate coagulation. *Blood* 106, 1604–1611. doi: 10.1182/blood-2004-03-1095
- Delepine, C., Shih, J., Li, K., Gaudeaux, P., and Sur, M. (2023). Differential effects of astrocyte manipulations on learned motor behavior and neuronal ensembles in the motor cortex. *Journal of Neuroscience*, JN-RM-1982-22. doi: 10.1523/JNEUROSCI.1982-22.2023
- Dickens, A. M., Tovar-Y-Romo, L. B., Yoo, S. W., Trout, A. L., Bae, M., Kanmogne, M., et al. (2017). Astrocyte-shed extracellular vesicles regulate the peripheral leukocyte response to inflammatory brain lesions. *Sci Signal* 10. doi: 10.1126/scisignal.aai7696
- Dimos, J. T., Rodolfa, K. T., Niakan, K. K., Weisenthal, L. M., Mitsumoto, H., Chung, W., et al. (2008). Induced pluripotent stem cells generated from patients with ALS can be differentiated into motor neurons. *Science (1979)* 321, 1218–1221. doi: 10.1126/science.1158799
- Ding, X., Ma, M., Teng, J., Teng, R. K. F., Zhou, S., Yin, J., et al. (2015). Exposure to ALS-FTD-CSF generates TDP-43 aggregates in glioblastoma cells through exosomes and TNTs-like structure. *Oncotarget* 6, 24178–24191. doi: 10.18632/oncotarget.4680
- Dinkins, M. B., Dasgupta, S., Wang, G., Zhu, G., and Bieberich, E. (2014). Exosome reduction invivo is associated with lower amyloid plaque load in the 5XFAD mouse model of Alzheimer’s disease. *Neurobiol Aging* 35, 1792–1800. doi: 10.1016/j.neurobiolaging.2014.02.012
- Dixson, A. C., Dawson, T. R., Di Vizio, D., and Weaver, A. M. (2023). Context-specific regulation of extracellular vesicle biogenesis and cargo selection. *Nat Rev Mol Cell Biol*. doi: 10.1038/s41580-023-00576-0
- Doss, M. X., and Sachinidis, A. (2019). Current challenges of iPSC-based disease modeling and therapeutic implications. *Cells* 8. doi: 10.3390/cells8050403
- Dringen, R., Brandmann, M., Hohnholt, M. C., and Blumrich, E. M. (2015). Glutathione-Dependent Detoxification Processes in Astrocytes. *Neurochem Res* 40, 2570–2582. doi: 10.1007/s11064-014-1481-1
- Droppelmann, C. A., Campos-Melo, D., Ishtiaq, M., Volkening, K., and Strong, M. J. (2014). RNA metabolism in ALS: When normal processes become pathological. *Amyotroph Lateral Scler Frontotemporal Degener* 15, 321–336. doi: 10.3109/21678421.2014.881377
- Dudzik, D., Macioszek, S., Struck-Lewicka, W., Kordalewska, M., Buszewska-Forajta, M., Waszczuk-Jankowska, M., et al. (2021). Perspectives and challenges in

extracellular vesicles untargeted metabolomics analysis. *TrAC Trends in Analytical Chemistry* 143, 116382. doi: 10.1016/J.TRAC.2021.116382

- Duong, A., Parmar, G., Kirkham, A. M., Burger, D., and Allan, D. S. (2023). Registered clinical trials investigating treatment with cell-derived extracellular vesicles: a scoping review. *Cytotherapy*. doi: 10.1016/j.jcyt.2023.04.007
- Ebert, A. D., Yu, J., Rose, F. F., Mattis, V. B., Lorson, C. L., Thomson, J. A., et al. (2009). Induced pluripotent stem cells from a spinal muscular atrophy patient. *Nature* 457, 277–280. doi: 10.1038/nature07677
- Elsherbini, A., Qin, H., Zhu, Z., Tripathi, P., Wang, G., Crivelli, S. M., et al. (2021). “Extracellular vesicles containing ceramide-rich platforms: ‘mobile raft’ isolation and analysis,” in *Methods in Molecular Biology*, (Humana Press Inc.), 87–98. doi: 10.1007/978-1-0716-0814-2_5
- Emelyanov, A., Shtam, T., Kamyshinsky, R., Garaeva, L., Verlov, N., Miliukhina, I., et al. (2020). Cryo-electron microscopy of extracellular vesicles from cerebrospinal fluid. *PLoS One* 15. doi: 10.1371/journal.pone.0227949
- Emmanouilidou, E., Melachroinou, K., Roumeliotis, T., Garbis, S. D., Ntzouni, M., Margaritis, L. H., et al. (2010). Cell-produced α -synuclein is secreted in a calcium-dependent manner by exosomes and impacts neuronal survival. *Journal of Neuroscience* 30, 6838–6851. doi: 10.1523/JNEUROSCI.5699-09.2010
- Eren, E., Leoutsakos, J. M., Troncoso, J., Lyketsos, C. G., Oh, E. S., and Kapogiannis, D. (2022). Neuronal-Derived EV Biomarkers Track Cognitive Decline in Alzheimer’s Disease. *Cells* 11. doi: 10.3390/cells11030436
- Escartin, C., Brouillet, E., Gubellini, P., Trioulier, Y., Jacquard, C., Smadja, C., et al. (2006). Ciliary neurotrophic factor activates astrocytes, redistributes their glutamate transporters GLAST and GLT-1 to raft microdomains, and improves glutamate handling in vivo. *Journal of Neuroscience* 26, 5978–5989. doi: 10.1523/JNEUROSCI.0302-06.2006
- Escartin, C., Galea, E., Lakatos, A., O’Callaghan, J. P., Petzold, G. C., Serrano-Pozo, A., et al. (2021). Reactive astrocyte nomenclature, definitions, and future directions. *Nat Neurosci* 24, 312–325. doi: 10.1038/s41593-020-00783-4
- Escartin, C., Guillemaud, O., and Carrillo-de Sauvage, M. A. (2019). Questions and (some) answers on reactive astrocytes. *Glia* 67, 2221–2247. doi: 10.1002/glia.23687
- Escartin, C., Pierre, K., Colin, A., Brouillet, E., Delzescaux, T., Guillemier, M., et al. (2007). Activation of astrocytes by CNTF induces metabolic plasticity and increases resistance to metabolic insults. *Journal of Neuroscience* 27, 7094–7104. doi: 10.1523/JNEUROSCI.0174-07.2007
- Fader, C. M., Sánchez, D., Furlán, M., and Colombo, M. I. (2008). Induction of autophagy promotes fusion of multivesicular bodies with autophagic vacuoles in K562 cells. *Traffic* 9, 230–250. doi: 10.1111/j.1600-0854.2007.00677.x

- Fan, J., Liu, J., Liu, J., Chen, C., Koutalos, Y., and Crosson, C. E. (2021). Evidence for ceramide induced cytotoxicity in retinal ganglion cells. *Exp Eye Res* 211. doi: 10.1016/j.exer.2021.108762
- Fevrier, B., Vilette, D., Archer, F., Loew, D., Faigle, W., Vidal, M., et al. (2004). Cells release prions in association with exosomes. *Proc Natl Acad Sci U S A* 101, 9683–9688. doi: 10.1073/pnas.0308413101
- Flügge, G., Araya-Callis, C., Garea-Rodriguez, E., Stadelmann-Nessler, C., and Fuchs, E. (2014). NDRG2 as a marker protein for brain astrocytes. *Cell Tissue Res* 357, 31–41. doi: 10.1007/s00441-014-1837-5
- Fonseca-Ferrer, W., Suárez-Gomez, C., Sambolin-Escobales, L., Santos-Avilés, K., Colón-Romero, M., Hernández-López, A., et al. (2022). Infusion of C20 ceramide induces depressive-like behavior, increases microglia but not astrocyte expression. *The FASEB Journal* 36. doi: 10.1096/FASEBJ.2022.36.S1.L7410
- Foo, L. C., Allen, N. J., Bushong, E. A., Ventura, P. B., Chung, W. S., Zhou, L., et al. (2011a). Development of a method for the purification and culture of rodent astrocytes. *Neuron* 71, 799–811. doi: 10.1016/j.neuron.2011.07.022
- Forostyak, S., Forostyak, O., Kwok, J. C. F., Romanyuk, N., Rehorova, M., Kriska, J., et al. (2020). Transplantation of Neural Precursors Derived from Induced Pluripotent Cells Preserve Perineuronal Nets and Stimulate Neural Plasticity in ALS Rats. *Int J Mol Sci* 21, 9593. doi: 10.3390/ijms21249593
- Forró, T., Manu, D. R., Băjenaru, O.-L., and Bălașa, R. (2024). GFAP as Astrocyte-Derived Extracellular Vesicle Cargo in Acute Ischemic Stroke Patients—A Pilot Study. *Int J Mol Sci* 25, 5726. doi: 10.3390/ijms25115726
- Fortunato, D., Giannoukakos, S., Giménez-Capitán, A., Hackenberg, M., Molina-Vila, M. A., and Zarovni, N. (2022). Selective isolation of extracellular vesicles from minimally processed human plasma as a translational strategy for liquid biopsies. *Biomark Res* 10, 1–24. doi: 10.1186/S40364-022-00404-1/FIGURES/7
- Fowler, S. L., Behr, T. S., Turkes, E., Maglio Cauhy, P., Foiani, M. S., Schaler, A., et al. (2023). Tau filaments are tethered within brain extracellular vesicles in Alzheimer’s disease. *bioRxiv*. doi: 10.1101/2023.04.30.537820
- Fritz, E., Izaurieta, P., Weiss, A., Mir, F. R., Rojas, P., Gonzalez, D., et al. (2013). Mutant SOD1-expressing astrocytes release toxic factors that trigger motoneuron death by inducing hyperexcitability. *J Neurophysiol* 109, 2803–2814. doi: 10.1152/jn.00500.2012
- Fujita, T., Tozaki-Saitoh, H., and Inoue, K. (2009). P2Y1 receptor signaling enhances neuroprotection by astrocytes against oxidative stress via IL-6 release in hippocampal cultures. *Glia* 57, 244–257. doi: 10.1002/glia.20749
- Galland, F., Seady, M., Taday, J., Smaili, S. S., Gonçalves, C. A., and Leite, M. C. (2019). Astrocyte culture models: Molecular and function characterization of primary culture, immortalized astrocytes and C6 glioma cells. *Neurochem Int* 131. doi: 10.1016/j.neuint.2019.104538

- Garcia-Contreras, M., and Thakor, A. S. (2021). Human adipose tissue-derived mesenchymal stem cells and their extracellular vesicles modulate lipopolysaccharide activated human microglia. *Cell Death Discov* 7, 98. doi: 10.1038/s41420-021-00471-7
- Garcia-Martin, R., Wang, G., Brandão, B. B., Zanotto, T. M., Shah, S., Kumar Patel, S., et al. (2021). MicroRNA sequence codes for small extracellular vesicle release and cellular retention. *Nature* 2021, 1–6. doi: 10.1038/s41586-021-04234-3
- Garwood, C. J., Ratcliffe, L. E., Simpson, J. E., Heath, P. R., Ince, P. G., and Wharton, S. B. (2017). Astrocytes in Alzheimer’s disease and other age-associated dementias: a supporting player with a central role. *Neuropathol Appl Neurobiol* 43, 281–298. doi: 10.1111/nan.12338
- Gelibter, S., Marostica, G., Mandelli, A., Siciliani, S., Podini, P., Finardi, A., et al. (2022). The impact of storage on extracellular vesicles: A systematic study. *J Extracell Vesicles* 11, e12162. doi: 10.1002/JEV2.12162
- Giaume, C., and Venance, L. (1998). Intercellular calcium signaling and gap junctional communication in astrocytes. *Glia* 24, 50–64. doi: 10.1002/(SICI)1098-1136(199809)24:1<50::AID-GLIA6>3.0.CO;2-4
- Goetzl, E. J., Elahi, F. M., Mustapic, M., Kapogiannis, D., Pryhoda, M., Gilmore, A., et al. (2019). Altered levels of plasma neuron-derived exosomes and their cargo proteins characterize acute and chronic mild traumatic brain injury. *FASEB Journal* 33, 5082–5088. doi: 10.1096/fj.201802319R
- Goetzl, E. J., Mustapic, M., Kapogiannis, D., Eitan, E., Lobach, I. V., Goetzl, L., et al. (2016). Cargo proteins of plasma astrocyte-derived exosomes in Alzheimer’s disease. *FASEB Journal* 30, 3853–3859. doi: 10.1096/fj.201600756R
- Goetzl, E. J., Schwartz, J. B., Abner, E. L., Jicha, G. A., and Kapogiannis, D. (2018). High complement levels in astrocyte-derived exosomes of Alzheimer disease. *Ann Neurol* 83, 544–552. doi: 10.1002/ana.25172
- Goetzl, E. J., Yaffe, K., Peltz, C. B., Ledreux, A., Gorgens, K., Davidson, B., et al. (2020). Traumatic brain injury increases plasma astrocyte-derived exosome levels of neurotoxic complement proteins. *The FASEB Journal* 34, 3359–3366. doi: 10.1096/fj.201902842R
- Goldberg, M., de Pittà, M., Volman, V., Berry, H., and Ben-Jacob, E. (2010). Nonlinear gap junctions enable long-distance propagation of pulsating calcium waves in astrocyte networks. *PLoS Comput Biol* 6, 1–14. doi: 10.1371/journal.pcbi.1000909
- Goldman, S. A., and Kuypers, N. J. (2015). How to make an oligodendrocyte. *Development* 142, 3983–3995. doi: 10.1242/dev.126409
- Gomes, D. E., and Witwer, K. W. (2022). L1CAM-associated extracellular vesicles: A systematic review of nomenclature, sources, separation, and characterization. *Journal of Extracellular Biology* 1, e35. doi: 10.1002/JEX2.35

- Goodall, E. F., Heath, P. R., Bandmann, O., Kirby, J., and Shaw, P. J. (2013). Neuronal dark matter: The emerging role of microRNAs in neurodegeneration. *Front Cell Neurosci*. doi: 10.3389/fncel.2013.00178
- Goode, A., Butler, K., Long, J., Cavey, J., Scott, D., Shaw, B., et al. (2016). Defective recognition of LC3B by mutant SQSTM1/p62 implicates impairment of autophagy as a pathogenic mechanism in ALS-FTLD. *Autophagy* 12, 1094–1104. doi: 10.1080/15548627.2016.1170257
- Göran Ronquist, K., and Ronquist, K. G. (2019). Extracellular vesicles and energy metabolism. *Clinica Chimica Acta* 488, 116–121. doi: 10.1016/j.cca.2018.10.044
- Görgens, A., Corso, G., Hagey, D. W., Jawad Wiklander, R., Gustafsson, M. O., Felldin, U., et al. (2022). Identification of storage conditions stabilizing extracellular vesicles preparations. *J Extracell Vesicles* 11, e12238. doi: 10.1002/JEV2.12238
- Gosselin, R.-D., Meylan, P., and Decosterd, I. (2013). Extracellular microvesicles from astrocytes contain functional glutamate transporters: regulation by protein kinase C and cell activation. *Front Cell Neurosci* 7, 251. doi: 10.3389/fncel.2013.00251
- Gosset, P., Camu, W., Raoul, C., and Mezghrani, A. (2022). Prionoids in amyotrophic lateral sclerosis. *Brain Commun* 4. doi: 10.1093/BRAINCOMMS/FCAC145
- Grad, L. I., Pokrishevsky, E., Silverman, J. M., and Cashman, N. R. (2014). Exosome-dependent and independent mechanisms are involved in prion-like transmission of propagated Cu/Zn superoxide dismutase misfolding. *Prion* 8, 331–335. doi: 10.4161/19336896.2014.983398
- Gray, M. T., and Woulfe, J. M. (2015). Striatal blood-brain barrier permeability in Parkinson's disease. *Journal of Cerebral Blood Flow and Metabolism* 35, 747–750. doi: 10.1038/jcbfm.2015.32
- Greenbaum, D., Colangelo, C., Williams, K., and Gerstein, M. (2003). Comparing protein abundance and mRNA expression levels on a genomic scale. Available at: <http://genomebiology.com/2003/4/9/117>
- Gstraunthaler, G., Lindl, T., and Van Der Valk, J. (2013). A plea to reduce or replace fetal bovine serum in cell culture media. *Cytotechnology* 65, 791–793. doi: 10.1007/s10616-013-9633-8
- Gu, X. L., Long, C. X., Sun, L., Xie, C., Lin, X., and Cai, H. (2010). Astrocytic expression of Parkinson's disease-related A53T -synuclein causes neurodegeneration in mice. *Mol Brain* 3, 12. doi: 10.1186/1756-6606-3-12
- Guitart, K., Loers, G., Buck, F., Bork, U., Schachner, M., and Kleene, R. (2016). Improvement of neuronal cell survival by astrocyte-derived exosomes under hypoxic and ischemic conditions depends on prion protein. *Glia* 64, 896–910. doi: 10.1002/glia.22963
- Guitart, K., Loers, G., Schachner, M., and Kleene, R. (2015). Prion protein regulates glutathione metabolism and neural glutamate and cysteine uptake via

excitatory amino acid transporter 3. *J Neurochem* 133, 558–571. doi: 10.1111/jnc.13071

- Guix, F. X., Corbett, G. T., Cha, D. J., Mustapic, M., Liu, W., Mengel, D., et al. (2018). Detection of aggregation-competent tau in neuron-derived extracellular vesicles. *Int J Mol Sci* 19, 1–23. doi: 10.3390/ijms19030663
- Guo, M., Wang, J., Zhao, Y., Feng, Y., Han, S., Dong, Q., et al. (2020). Microglial exosomes facilitate α -synuclein transmission in Parkinson's disease. *Brain* 143, 1476–1497. doi: 10.1093/brain/awaa090
- Guo, Y., You, J., Zhang, Y., Liu, W. S., Huang, Y. Y., Zhang, Y. R., et al. (2024). Plasma proteomic profiles predict future dementia in healthy adults. *Nat Aging* 4, 247–260. doi: 10.1038/s43587-023-00565-0
- Gustafsson, G., Lööv, C., Persson, E., Lázaro, D. F., Takeda, S., Bergström, J., et al. (2018). Secretion and Uptake of α -Synuclein Via Extracellular Vesicles in Cultured Cells. *Cell Mol Neurobiol* 38, 1539–1550. doi: 10.1007/S10571-018-0622-5
- Guttenplan, K. A., Stafford, B. K., El-, R. N., Weigel, M. K., Huberman, A. D., Liddelow, S. A., et al. (2020a). Neurotoxic Reactive Astrocytes Drive Neuronal Death after Retinal Injury. *Cell Rep* 31, 107776. doi: 10.1016/j.celrep.2020.107776
- Guttenplan, K. A., Weigel, M. K., Adler, D. I., Couthouis, J., Liddelow, S. A., Gitler, A. D., et al. (2020b). Knockout of reactive astrocyte activating factors slows disease progression in an ALS mouse model. *Nat Commun* 11, 3753. doi: 10.1038/s41467-020-17514-9
- Guttenplan, K. A., Weigel, M. K., Prakash, P., Wijewardhane, P. R., Hasel, P., Rufen-Blanchette, U., et al. (2021). Neurotoxic reactive astrocytes induce cell death via saturated lipids. *Nature*, 1–6. doi: 10.1038/s41586-021-03960-y
- Habib, N., McCabe, C., Medina, S., Varshavsky, M., Kitsberg, D., Dvir-szternfeld, R., et al. (2020). Disease-associated astrocytes in Alzheimer's disease and aging. *Nat Neurosci*. doi: 10.1038/s41593-020-0624-8
- Haidet-Phillips, A. M., Hester, M. E., Miranda, C. J., Meyer, K., Braun, L., Frakes, A., et al. (2011). Astrocytes from familial and sporadic ALS patients are toxic to motor neurons. *Nat Biotechnol* 29, 824–828. doi: 10.1038/nbt.1957
- Halassa, M. M., Fellin, T., and Haydon, P. G. (2007). The tripartite synapse: roles for gliotransmission in health and disease. *Trends Mol Med* 13, 54–63. doi: 10.1016/j.molmed.2006.12.005
- Han, X., Chen, M., Wang, F., Windrem, M., Wang, S., Shanz, S., et al. (2013). Forebrain Engraftment by Human Glial Progenitor Cells Enhances Synaptic Plasticity and Learning in Adult Mice. *Cell Stem Cell* 12, 342–353. doi: 10.1016/J.STEM.2012.12.015
- Harmati, M., Bukva, M., Böröczky, T., Buzás, K., and Gyukity-Sebestyén, E. (2021). The role of the metabolite cargo of extracellular vesicles in tumor progression.

Cancer and Metastasis Reviews 40, 1203–1221. doi: 10.1007/s10555-021-10014-2

- Hart, T., Komori, K., Lamere, S., Podshivalova, K., and Salomon, D. R. (2013). Finding the active genes in deep RNA-seq gene expression studies. Available at: <http://www.biomedcentral.com/1471-2164/14/778>
- Hasel, P., Rose, I. V. L., Sadick, J. S., Kim, R. D., and Liddel, S. A. (2021). Neuroinflammatory astrocyte subtypes in the mouse brain. *Nature Neuroscience* 2021, 1–13. doi: 10.1038/s41593-021-00905-6
- Heckenbach, I., Mkrtchyan, G. V., Ezra, M. Ben, Bakula, D., Madsen, J. S., Nielsen, M. H., et al. (2022). Nuclear morphology is a deep learning biomarker of cellular senescence. *Nat Aging* 2, 742–755. doi: 10.1038/s43587-022-00263-3
- Heithoff, B. P., George, K. K., Shandra, O., and Robel, S. (2021). Mild traumatic brain injury/ concussion initiates an atypical astrocyte response caused by blood-brain barrier dysfunction. *bioRxiv*, 2021.05.28.446153. doi: 10.1101/2021.05.28.446153
- Hergenreder, E., Minotti, A. P., Zorina, Y., Oberst, P., Zhao, Z., Munguba, H., et al. (2024). Combined small-molecule treatment accelerates maturation of human pluripotent stem cell-derived neurons. *Nat Biotechnol.* doi: 10.1038/s41587-023-02031-z
- Hill, A. F. (2019). Extracellular vesicles and neurodegenerative diseases. *Journal of Neuroscience* 39, 9269–9273. doi: 10.1523/JNEUROSCI.0147-18.2019
- Hinckelmann, M. V., Virlogeux, A., Niehage, C., Poujol, C., Choquet, D., Hoflack, B., et al. (2016). Self-propelling vesicles define glycolysis as the minimal energy machinery for neuronal transport. *Nat Commun* 7, 1–13. doi: 10.1038/ncomms13233
- Hol, E. M., and Pekny, M. (2015). Glial fibrillary acidic protein (GFAP) and the astrocyte intermediate filament system in diseases of the central nervous system. *Curr Opin Cell Biol* 32, 121–130. doi: 10.1016/j.ceb.2015.02.004
- Holley, C. L., and Topkara, V. K. (2011). An introduction to small non-coding RNAs: miRNA and snoRNA. *Cardiovasc Drugs Ther* 25, 151–159. doi: 10.1007/s10557-011-6290-z
- Hou, Y., Dan, X., Babbar, M., Wei, Y., Hasselbalch, S. G., Croteau, D. L., et al. (2019). Ageing as a risk factor for neurodegenerative disease. *Nature Reviews Neurology* 2019 15:10 15, 565–581. doi: 10.1038/s41582-019-0244-7
- Hou, Y., Li, J., Guan, S., and Witte, F. (2021). The therapeutic potential of MSC-EVs as a bioactive material for wound healing. *Engineered Regeneration* 2, 182–194. doi: 10.1016/j.engreg.2021.11.003
- Hu, G., Liao, K., Niu, F., Yang, L., Dallon, B. W., Callen, S., et al. (2018). Astrocyte EV-Induced lincRNA-Cox2 Regulates Microglial Phagocytosis: Implications for Morphine-Mediated Neurodegeneration. *Mol Ther Nucleic Acids* 13, 450–463. doi: 10.1016/j.omtn.2018.09.019

- Hu, Y. S., Xin, J., Hu, Y., Zhang, L., and Wang, J. (2017). Analyzing the genes related to Alzheimer's disease via a network and pathway-based approach. *Alzheimers Res Ther* 9, 29. doi: 10.1186/s13195-017-0252-z
- Huang, W., Hickson, L. T. J., Eirin, A., Kirkland, J. L., and Lerman, L. O. (2022). Cellular senescence: the good, the bad and the unknown. *Nat Rev Nephrol* 18, 611–627. doi: 10.1038/s41581-022-00601-z
- Huang, Y., Cheng, L., Turchinovich, A., Mahairaki, V., Troncoso, J. C., Pletniková, O., et al. (2020). Influence of species and processing parameters on recovery and content of brain tissue-derived extracellular vesicles. *J Extracell Vesicles* 9. doi: 10.1080/20013078.2020.1785746
- Huang-Doran, I., Zhang, C. Y., and Vidal-Puig, A. (2017). Extracellular Vesicles: Novel Mediators of Cell Communication In Metabolic Disease. *Trends in Endocrinology and Metabolism* 28, 3–18. doi: 10.1016/j.tem.2016.10.003
- Huntzinger, E., and Izaurralde, E. (2011). Gene silencing by microRNAs: Contributions of translational repression and mRNA decay. *Nat Rev Genet* 12, 99–110. doi: 10.1038/nrg2936
- Iguchi, Y., Eid, L., Parent, M., Soucy, G., Bareil, C., Riku, Y., et al. (2016). Exosome secretion is a key pathway for clearance of pathological TDP-43. *Brain* 139, 3187–3201. doi: 10.1093/brain/aww237
- Ingelsson, M. (2016). Alpha-synuclein oligomers-neurotoxic molecules in Parkinson's disease and other lewy body disorders. *Front Neurosci* 10, 408. doi: 10.3389/fnins.2016.00408
- Iraci, nunzio, Gaude, E., Leonardi, T., Costa, A. S. H., Cossetti, C., Peruzzotti-Jametti, L., et al. (2017). Extracellular vesicles are independent metabolic units with asparaginase activity. *Nat Chem Biol* 13, 951–955. doi: 10.1038/nchembio.2422
- Ittner, L. M., and Götz, J. (2011). Amyloid- β and tau - A toxic pas de deux in Alzheimer's disease. *Nat Rev Neurosci* 12, 67–72. doi: 10.1038/nrn2967
- Jaisa-aad, M., Muñoz-Castro, C., Healey, M. A., Hyman, B. T., and Serrano-Pozo, A. (2024). Characterization of monoamine oxidase-B (MAO-B) as a biomarker of reactive astrogliosis in Alzheimer's disease and related dementias. *Acta Neuropathol* 147, 1–21. doi: 10.1007/S00401-024-02712-2/FIGURES/9
- Jamadar, S. D., Ward, P. G. D., Close, T. G., Fornito, A., Premaratne, M., O'Brien, K., et al. (2020). Simultaneous BOLD-fMRI and constant infusion FDG-PET data of the resting human brain. *Sci Data* 7. doi: 10.1038/s41597-020-00699-5
- Janas, T., Janas, M. M., Sapoń, K., and Janas, T. (2015). Mechanisms of RNA loading into exosomes. *FEBS Lett* 589, 1391–1398. doi: 10.1016/j.febslet.2015.04.036
- Jankovska, N., and Matej, R. (2021). Molecular Pathology of ALS: What We Currently Know and What Important Information Is Still Missing. *Diagnostics* 2021, Vol. 11, Page 1365 11, 1365. doi: 10.3390/DIAGNOSTICS11081365
- Jia, M., Shi, Z., Yan, X., Xu, L., Dong, L., Li, J., et al. (2018). Insulin and heparin-binding epidermal growth factor-like growth factor synergistically promote astrocyte

survival and proliferation in serum-free medium. *J Neurosci Methods* 307, 240–247. doi: 10.1016/j.jneumeth.2018.06.002

- Joshi, A. U., Minhas, P. S., Liddelow, S. A., Haileselassie, B., Andreasson, K. I., Dorn, G. W., et al. (2019). Fragmented mitochondria released from microglia trigger A1 astrocytic response and propagate inflammatory neurodegeneration. *Nat Neurosci* 22, 1635–1648. doi: 10.1038/s41593-019-0486-0
- Jovičić, A., and Gitler, A. D. (2017). Distinct repertoires of microRNAs present in mouse astrocytes compared to astrocytesecreted exosomes. *PLoS One* 12. doi: 10.1371/journal.pone.0171418
- Joy Shepard, C., Cline, S. G., Hinds, D., Jahanbakhsh, S., and Prokop, J. W. (2019). Genome-wide Association Studies and Function: Breakdown of multiple sclerosis genetics to identify an integrated disease network and potential variant mechanisms. *Physiol Genomics* 51, 562. doi: 10.1152/PHYSIOLGENOMICS.00120.2018
- Juopperi, T. A., Kim, W. R., Chiang, C. H., Yu, H., Margolis, R. L., Ross, C. A., et al. (2012). Astrocytes generated from patient induced pluripotent stem cells recapitulate features of Huntingtons disease patient cells. *Mol Brain* 5, 17. doi: 10.1186/1756-6606-5-17
- Jurga, A. M., Paleczna, M., Kadluczka, J., and Kuter, K. Z. (2021). Beyond the GFAP-Astrocyte Protein Markers in the Brain. *Biomolecules* 2021, Vol. 11, Page 1361 11, 1361. doi: 10.3390/BIOM11091361
- Kabani, M., Pilard, M., and Melki, R. (2020). Glucose availability dictates the export of the soluble and prion forms of Sup35p via periplasmic or extracellular vesicles. *Mol Microbiol* 114, 322–332. doi: 10.1111/mmi.14515
- Kaddour, H., Tranquille, M., and Okeoma, C. M. (2021). The Past, the Present, and the Future of the Size Exclusion Chromatography in Extracellular Vesicles Separation. *Viruses* 2021, Vol. 13, Page 2272 13, 2272. doi: 10.3390/V13112272
- Kalluri, R., and LeBleu, V. S. (2020). The biology, function, and biomedical applications of exosomes. *Science* (1979) 367. doi: 10.1126/science.aau6977
- Kalra, H., Simpson, R. J., Ji, H., Aikawa, E., Altevogt, P., Askenase, P., et al. (2012). Vesiclepedia: A Compendium for Extracellular Vesicles with Continuous Community Annotation. *PLoS Biol* 10. doi: 10.1371/journal.pbio.1001450
- Karabiyik, C., Lee, M. J., and Rubinsztein, D. C. (2017). Autophagy impairment in Parkinson's disease. *Essays Biochem* 61, 711–720. doi: 10.1042/EBC20170023
- Kargapolova, Y., Geißen, S., Zheng, R., Baldus, S., Winkels, H., and Adam, M. (2021). The enzymatic and non-enzymatic function of myeloperoxidase (Mpo) in inflammatory communication. *Antioxidants* 10. doi: 10.3390/antiox10040562
- Karumbayaram, S., Novitch, B. G., Patterson, M., Umbach, J. A., Richter, L., Lindgren, A., et al. (2009). Directed differentiation of human-induced pluripotent stem cells generates active motor neurons. *Stem Cells* 27, 806–811. doi: 10.1002/stem.31

- Katsouri, L., Birch, A. M., Renziehausen, A. W. J., Zach, C., Aman, Y., Steeds, H., et al. (2020). Ablation of reactive astrocytes exacerbates disease pathology in a model of Alzheimer's disease. *Glia* 68, 1017–1030. doi: 10.1002/glia.23759
- Kenific, C. M., Zhang, H., and Lyden, D. (2021). An exosome pathway without an ESCRT. *Cell Res* 31, 105–106. doi: 10.1038/s41422-020-00418-0
- Keren-Shaul, H., Spinrad, A., Weiner, A., Matcovitch-Natan, O., Dvir-Szternfeld, R., Ulland, T. K., et al. (2017). A Unique Microglia Type Associated with Restricting Development of Alzheimer's Disease. *Cell* 169, 1276–1290. doi: 10.1016/j.cell.2017.05.018
- Khakh, B. S., and Sofroniew, M. V. (2015). Diversity of astrocyte functions and phenotypes in neural circuits. *Nat Neurosci* 18, 942–952. doi: 10.1038/nn.4043
- Kia, A., McAvoy, K., Krishnamurthy, K., Trotti, D., and Pasinelli, P. (2018). Astrocytes expressing ALS-linked mutant FUS induce motor neuron death through release of tumor necrosis factor-alpha. *Glia* 66, 1016–1033. doi: 10.1002/glia.23298
- Kim, H., Leng, K., Park, J., Sorets, A. G., Kim, S., Shostak, A., et al. (2022). Reactive astrocytes transduce blood-brain barrier dysfunction through a TNF α -STAT3 signaling axis and secretion of alpha 1-antichymotrypsin. *bioRxiv*, 2022.02.21.481336. doi: 10.1101/2022.02.21.481336
- Kim, J. M., Cha, S. H., Choi, Y. R., Jou, I., Joe, E. H., and Park, S. M. (2016). DJ-1 deficiency impairs glutamate uptake into astrocytes via the regulation of flotillin-1 and caveolin-1 expression. *Sci Rep* 6, 1–12. doi: 10.1038/srep28823
- Kim, K. M., Abdelmohsen, K., Mustapic, M., Kapogiannis, D., and Gorospe, M. (2017). RNA in extracellular vesicles. *Wiley Interdiscip Rev RNA* 8, 1–14. doi: 10.1002/wrna.1413
- Kim, K. Y., Shin, K. Y., and Chang, K. A. (2023). GFAP as a Potential Biomarker for Alzheimer's Disease: A Systematic Review and Meta-Analysis. *Cells* 12. doi: 10.3390/cells12091309
- Kimelberg, H. K. (2010). Functions of mature mammalian astrocytes: a current view. *The Neuroscientist* 16, 79–106. doi: 10.1177/1073858409342593
- Kirikae, T., Tamura, H., Hashizume, M., Kirikae, F., Uemura, Y., Tanaka, S., et al. (1997). ENDOTOXIN CONTAMINATION IN FETAL BOVINE SERUM AND ITS INFLUENCE ON TUMOR NECROSIS FACTOR PRODUCTION BY MACROPHAGE-LIKE CELLS J774.1 CULTURED IN THE PRESENCE OF THE SERUM.
- Koprach, J. B., Reske-Nielsen, C., Mithal, P., and Isacson, O. (2008). Neuroinflammation mediated by IL-1 β increases susceptibility of dopamine neurons to degeneration in an animal model of Parkinson's disease. *J Neuroinflammation* 5, 8. doi: 10.1186/1742-2094-5-8
- Kordower, J. H., Chu, Y., Hauser, R. A., Freeman, T. B., and Olanow, C. W. (2008). Lewy body-like pathology in long-term embryonic nigral transplants in Parkinson's disease. *Nat Med* 14, 504–506. doi: 10.1038/nm1747

- Kornilov, R., Puhka, M., Mannerström, B., Hiidenmaa, H., Peltoniemi, H., Siljander, P., et al. (2018). Efficient ultrafiltration-based protocol to deplete extracellular vesicles from fetal bovine serum. *J Extracell Vesicles* 7. doi: 10.1080/20013078.2017.1422674
- Krylova, S. V., and Feng, D. (2023). The Machinery of Exosomes: Biogenesis, Release, and Uptake. *Int J Mol Sci* 24. doi: 10.3390/ijms24021337
- Kukurba, K. R., and Montgomery, S. B. (2015). RNA sequencing and analysis. *Cold Spring Harb Protoc* 2015, 951–969. doi: 10.1101/pdb.top084970
- Kurzawa-Akanbi, M., Tammireddy, S., Fabrik, I., Gliudelytė, L., Doherty, M., Heap, R., et al. (2021). Altered ceramide metabolism is a feature in the extracellular vesicle-mediated spread of alpha-synuclein in Lewy body disorders. *Acta Neuropathol*. doi: 10.1007/S00401-021-02367-3
- Kushwaha, R., Sinha, A., Makarava, N., Molesworth, K., and Baskakov, I. V. (2021). Non-cell autonomous astrocyte-mediated neuronal toxicity in prion diseases. *Acta Neuropathol Commun* 9, 22. doi: 10.1186/s40478-021-01123-8
- Kvamme, E., Torgner, I. A., and Roberg, B. (2001). Kinetics and localization of brain phosphate activated glutaminase., in *Journal of Neuroscience Research*, (John Wiley & Sons, Ltd), 951–958. doi: 10.1002/jnr.10041
- Kvamme, Elling., Nissen-Meyer, L. S. H., Roberg, B. Å., and Torgner, I. A. (2008). Novel form of phosphate activated glutaminase in cultured astrocytes and human neuroblastoma cells, PAG in brain pathology and localization in the mitochondria. *Neurochem Res* 33, 1341–1345. doi: 10.1007/s11064-008-9589-9
- Lafourcade, C., Ramírez, J. P., Luarte, A., Fernández, A., and Wyneken, U. (2016). MiRNAs in astrocyte-derived exosomes as possible mediators of neuronal plasticity. *J Exp Neurosci* 2016, 1–9. doi: 10.4137/JEN.S39916
- Lai, H., Li, Y., Zhang, H., Hu, J., Liao, J., Su, Y., et al. (2022). exoRBase 2.0: an atlas of mRNA, lncRNA and circRNA in extracellular vesicles from human biofluids. *Nucleic Acids Res* 50, D118–D128. doi: 10.1093/NAR/GKAB1085
- Lamark, T., Kirkin, V., Dikic, I., and Johansen, T. (2009). NBR1 and p62 as cargo receptors for selective autophagy of ubiquitinated targets. *Cell Cycle* 8, 1986–1990. doi: 10.4161/cc.8.13.8892
- Larsen, B. R., Stoica, A., and MacAulay, N. (2016). Managing brain extracellular K⁺ during neuronal activity: The physiological role of the Na⁺/K⁺-ATPase subunit isoforms. *Front Physiol* 7. doi: 10.3389/fphys.2016.00141
- Lee, H. G., Wheeler, M. A., and Quintana, F. J. (2022). Function and therapeutic value of astrocytes in neurological diseases. *Nat Rev Drug Discov* 21, 339–358. doi: 10.1038/s41573-022-00390-x
- Lee, H., Lee, J. J., Park, N. Y., Dubey, S. K., Kim, T., Ruan, K., et al. (2021). Multi-omic analysis of selectively vulnerable motor neuron subtypes implicates altered lipid metabolism in ALS. *Nature Neuroscience* 2021, 1–13. doi: 10.1038/s41593-021-00944-z

- Lee, S. S., Won, J. H., Lim, G. J., Han, J., Lee, J. Y., Cho, K. O., et al. (2019). A novel population of extracellular vesicles smaller than exosomes promotes cell proliferation. *Cell Communication and Signaling* 17. doi: 10.1186/s12964-019-0401-z
- Leggio, L., L'Episcopo, F., Magrì, A., Ulloa-Navas, M. J., Paternò, G., Vivarelli, S., et al. (2022). Small Extracellular Vesicles Secreted by Nigrostriatal Astrocytes Rescue Cell Death and Preserve Mitochondrial Function in Parkinson's Disease. *Adv Healthc Mater* 11. doi: 10.1002/adhm.202201203
- Lehre, K. P., and Danbolt, N. C. (1998). The Number of Glutamate Transporter Subtype Molecules at Glutamatergic Synapses: Chemical and Stereological Quantification in Young Adult Rat Brain. *Journal of Neuroscience* 18, 8751–8757.
- Lehrich, B. M., Liang, Y., and Fiandaca, M. S. (2021). Foetal bovine serum influence on in vitro extracellular vesicle analyses. *J Extracell Vesicles* 10, e12061. doi: 10.1002/jev2.12061
- Lehrich, B. M., Liang, Y., Khosravi, P., Federoff, H. J., and Fiandaca, M. S. (2018). Fetal bovine serum-derived extracellular vesicles persist within vesicle-depleted culture media. *Int J Mol Sci* 19, 3538. doi: 10.3390/ijms19113538
- Leidal, A. M., and Debnath, J. (2021). Emerging roles for the autophagy machinery in extracellular vesicle biogenesis and secretion. *FASEB Bioadv* 3, 377–386. doi: 10.1096/fba.2020-00138
- Leidal, A. M., Huang, H. H., Marsh, T., Solvik, T., Zhang, D., Ye, J., et al. (2020). The LC3-conjugation machinery specifies the loading of RNA-binding proteins into extracellular vesicles. *Nat Cell Biol*. doi: 10.1038/s41556-019-0450-y
- Leng, K., Rose, I. V. L., Kim, H., Xia, W., Romero-Fernandez, W., Rooney, B., et al. (2022). CRISPRi screens in human iPSC-derived astrocytes elucidate regulators of distinct inflammatory reactive states. *Nature Neuroscience* 2022 11, 1–15. doi: 10.1038/s41593-022-01180-9
- Li, B., Antonyak, M. A., Zhang, J., and Cerione, R. A. (2012). RhoA triggers a specific signaling pathway that generates transforming microvesicles in cancer cells. *Oncogene* 31, 4740–4749. doi: 10.1038/onc.2011.636
- Li, J. Y., Englund, E., Holton, J. L., Soulet, D., Hagell, P., Lees, A. J., et al. (2008). Lewy bodies in grafted neurons in subjects with Parkinson's disease suggest host-to-graft disease propagation. *Nat Med* 14, 501–503. doi: 10.1038/nm1746
- Li, M., Zeringer, E., Barta, T., Schageman, J., Cheng, A., and Vlassov, A. V (2014). Analysis of the RNA content of the exosomes derived from blood serum and urine and its potential as biomarkers. *Philosophical Transactions of the Royal Society B: Biological Sciences* 369. doi: 10.1098/rstb.2013.0502
- Li, Z., Moniruzzaman, M., Dastgheyb, R. M., Yoo, S., Wang, M., Hao, H., et al. (2020). Astrocytes deliver CK1 to neurons via extracellular vesicles in response to inflammation promoting the translation and amyloidogenic processing of APP. *J Extracell Vesicles* 10. doi: 10.1002/jev2.12035

- Lia, A., Di Spiezio, A., Speggiorin, M., and Zonta, M. (2023). Two decades of astrocytes in neurovascular coupling. *Frontiers in Network Physiology* 3. doi: 10.3389/fnetp.2023.1162757
- Liang, W., Sagar, S., Ravindran, R., Najor, R. H., Quiles, J. M., Chi, L., et al. (2023). Mitochondria are secreted in extracellular vesicles when lysosomal function is impaired. *Nat Commun* 14, 5031. doi: 10.1038/s41467-023-40680-5
- Liddelow, S. A., and Barres, B. A. (2017). Reactive Astrocytes: Production, Function, and Therapeutic Potential. *Immunity* 46, 957–967. doi: 10.1016/j.immuni.2017.06.006
- Liddelow, S. A., Guttenplan, K. A., Clarke, L. E., Bennett, F. C., Bohlen, C. J., Schirmer, L., et al. (2017). Neurotoxic reactive astrocytes are induced by activated microglia. *Nature* 541, 481–487. doi: 10.1038/nature21029
- Liddelow, S. A., and Sofroniew, M. V. (2019). Astrocytes usurp neurons as a disease focus. *Nat Neurosci* 22, 512–513. doi: 10.1038/s41593-019-0367-6
- Linnerbauer, M., and Rothhammer, V. (2020). Protective Functions of Reactive Astrocytes Following Central Nervous System Insult. *Front Immunol* 11. doi: 10.3389/fimmu.2020.573256
- Liu, S., Hossinger, A., Göbbels, S., and Vorberg, I. M. (2017). Prions on the run: How extracellular vesicles serve as delivery vehicles for self-templating protein aggregates. *Prion* 11, 98–112. doi: 10.1080/19336896.2017.1306162
- Liu, S., Yang, W., Li, Y., and Sun, C. (2023). Fetal bovine serum, an important factor affecting the reproducibility of cell experiments. *Sci Rep* 13. doi: 10.1038/s41598-023-29060-7
- Liu, Y., Qu, H. Q., Chang, X., Tian, L., Glessner, J., Sleiman, P. A. M., et al. (2022). Expansion of Schizophrenia Gene Network Knowledge Using Machine Learning Selected Signals From Dorsolateral Prefrontal Cortex and Amygdala RNA-seq Data. *Front Psychiatry* 13. doi: 10.3389/fpsy.2022.797329
- Livak, K. J., and Schmittgen, T. D. (2001). Analysis of relative gene expression data using real-time quantitative PCR and the 2- $\Delta\Delta$ CT method. *Methods* 25, 402–408. doi: 10.1006/meth.2001.1262
- Lobb, R., and Möller, A. (2017). Size Exclusion Chromatography: A Simple and Reliable Method for Exosome Purification. *Methods in molecular biology* 1660, 105–110. doi: 10.1007/978-1-4939-7253-1_9
- Locher, H., Frijns, J. H. M., Huisman, M. A., and Chuva de Sousa Lopes, S. M. (2014). TUBB3: Neuronal marker or Melanocyte Mimic? Cognizant Communication Corporation. doi: 10.3727/096368913X674099
- Lööv, C., Scherzer, C. R., Hyman, B. T., Breakefield, X. O., and Ingelsson, M. (2016). α -Synuclein in Extracellular Vesicles: Functional Implications and Diagnostic Opportunities. *Cell Mol Neurobiol* 36, 437–448. doi: 10.1007/s10571-015-0317-0

- Lötvall, J., Hill, A. F., Hochberg, F., Buzás, E. I., Vizio, D. Di, Gardiner, C., et al. (2014). Minimal experimental requirements for definition of extracellular vesicles and their functions: A position statement from the International Society for Extracellular Vesicles. *J Extracell Vesicles* 3. doi: 10.3402/JEV.V3.26913
- Luarte, A., Cisternas, P., Caviedes, A., Batiz, L. F., Lafourcade, C., Wyneken, U., et al. (2017). Astrocytes at the Hub of the Stress Response: Potential Modulation of Neurogenesis by miRNAs in Astrocyte-Derived Exosomes. *Stem Cells Int* 2017. doi: 10.1155/2017/1719050
- Ma, B., Buckalew, R., Du, Y., Kiyoshi, C. M., Alford, C. C., Wang, W., et al. (2016). Gap junction coupling confers isopotentiality on astrocyte syncytium. *Glia* 64, 214–226. doi: 10.1002/glia.22924
- Mackenzie, I. R. A., Bigio, E. H., Ince, P. G., Geser, F., Neumann, M., Cairns, N. J., et al. (2007). Pathological TDP-43 distinguishes sporadic amyotrophic lateral sclerosis from amyotrophic lateral sclerosis with SOD1 mutations. *Ann Neurol* 61, 427–434. doi: 10.1002/ana.21147
- Macvicar, B. A., and Newman, E. A. (2015). Astrocyte regulation of blood flow in the brain. *Cold Spring Harb Perspect Biol* 7, 1–15. doi: 10.1101/cshperspect.a020388
- Madill, M., McDonagh, K., Ma, J., Vajda, A., McLoughlin, P., O'Brien, T., et al. (2017). Amyotrophic lateral sclerosis patient iPSC-derived astrocytes impair autophagy via non-cell autonomous mechanisms. *Mol Brain* 10, 1–12. doi: 10.1186/s13041-017-0300-4
- Mahdavi-pour, M., Hassanzadeh, G., Seifali, E., Mortezaee, K., Aligholi, H., Shekari, F., et al. (2020). Effects of neural stem cell-derived extracellular vesicles on neuronal protection and functional recovery in the rat model of middle cerebral artery occlusion. *Cell Biochem Funct* 38, 373–383. doi: 10.1002/cbf.3484
- Maher, F. (1995). Immunolocalization of GLUT1 and GLUT3 glucose transporters in primary cultured neurons and glia. *J Neurosci Res* 42, 459–469. doi: 10.1002/jnr.490420404
- Mao, S., Sun, Q., Xiao, H., Zhang, C., and Li, L. (2015). Secreted miR-34a in astrocytic shedding vesicles enhanced the vulnerability of dopaminergic neurons to neurotoxins by targeting Bcl-2. *Protein Cell* 6, 529–540. doi: 10.1007/s13238-015-0168-y
- Marchetto, M. C. N., Muotri, A. R., Mu, Y., Smith, A. M., Cezar, G. G., and Gage, F. H. (2008). Non-Cell-Autonomous Effect of Human SOD1G37R Astrocytes on Motor Neurons Derived from Human Embryonic Stem Cells. *Cell Stem Cell* 3, 649–657. doi: 10.1016/j.stem.2008.10.001
- Marton, S., Miquel, E., Acosta-Rodríguez, J., Fontenla, S., Libisch, G., and Cassina, P. (2023). SOD1G93A Astrocyte-Derived Extracellular Vesicles Induce Motor Neuron Death by a miRNA-155-5p-Mediated Mechanism. *ASN Neuro* 15. doi: 10.1177/17590914231197527

- Mathiisen, T. M., Lehre, K. P., Danbolt, N. C., and Ottersen, O. P. (2010). The perivascular astroglial sheath provides a complete covering of the brain microvessels: An electron microscopic 3D reconstruction. *Glia* 58, 1094–1103. doi: 10.1002/glia.20990
- Matias, I., Diniz, L. P., Araujo, A. P. B., Damico, I. V., de Moura, P., Cabral-Miranda, F., et al. (2023). Age-Associated Upregulation of Glutamate Transporters and Glutamine Synthetase in Senescent Astrocytes In Vitro and in the Mouse and Human Hippocampus. *ASN Neuro* 15. doi: 10.1177/17590914231157974
- Mawuenyega, K. G., Sigurdson, W., Ovod, V., Munsell, L., Kasten, T., Morris, J. C., et al. (2010). Decreased clearance of CNS β -amyloid in Alzheimer's disease. *Science (1979)* 330, 1774. doi: 10.1126/science.1197623
- Memo, C., Parisse, P., Amoriello, R., Pachetti, M., Palandri, A., Casalis, L., et al. (2024). Extracellular vesicles released by LPS-stimulated spinal organotypic slices spread neuroinflammation into naïve slices through connexin43 hemichannel opening and astrocyte aberrant calcium dynamics. *Front Cell Neurosci* 18. doi: 10.3389/fncel.2024.1433309
- Mesquita-Ribeiro, R., Fort, R. S., Rathbone, A., Farias, J., Lucci, C., James, V., et al. (2021). Distinct small non-coding RNA landscape in the axons and released extracellular vesicles of developing primary cortical neurons and the axoplasm of adult nerves. *RNA Biol* 18, 832–855. doi: 10.1080/15476286.2021.2000792
- Michinaga, S., and Koyama, Y. (2019). Dual roles of astrocyte-derived factors in regulation of blood-brain barrier function after brain damage. *Int J Mol Sci* 20. doi: 10.3390/ijms20030571
- Michiorri, S., Gelmetti, V., Giarda, E., Lombardi, F., Romano, F., Marongiu, R., et al. (2010). The Parkinson-associated protein PINK1 interacts with Beclin1 and promotes autophagy. *Cell Death Differ* 17, 962–974. doi: 10.1038/cdd.2009.200
- Minakaki, G., Menges, S., Kittel, A., Emmanouilidou, E., Schaeffner, I., Barkovits, K., et al. (2018). Autophagy inhibition promotes SNCA/alpha-synuclein release and transfer via extracellular vesicles with a hybrid autophagosome-exosome-like phenotype. *Autophagy* 14, 98–119. doi: 10.1080/15548627.2017.1395992
- Mitsui, Y., and Schneider, E. L. (1976). Increased nuclear sizes in senescent human diploid fibroblast cultures. *Exp Cell Res* 100, 147–152. doi: 10.1016/0014-4827(76)90336-0
- Mittelbrunn, M., Gutiérrez-Vázquez, C., Villarroya-Beltri, C., González, S., Sánchez-Cabo, F., González, M. Á., et al. (2011). Unidirectional transfer of microRNA-loaded exosomes from T cells to antigen-presenting cells. *Nat Commun* 2, 1–10. doi: 10.1038/ncomms1285
- Miura, Y., Sato, M., Kuwahara, T., Ebata, T., Tabata, Y., and Sakurai, H. (2022). Transplantation of human iPSC-derived muscle stem cells in the diaphragm of Duchenne muscular dystrophy model mice. *PLoS One* 17. doi: 10.1371/journal.pone.0266391

- Molla, M. D., Akalu, Y., Geto, Z., Dagnew, B., Ayelign, B., and Shibabaw, T. (2020). Role of caspase-1 in the pathogenesis of inflammatory-associated chronic noncommunicable diseases. *J Inflamm Res* 13, 749–764. doi: 10.2147/JIR.S277457
- Mondal, A., Ashiq, K. A., Phulpagar, P., Singh, D. K., and Shiras, A. (2019). Effective Visualization and Easy Tracking of Extracellular Vesicles in Glioma Cells. *Biol Proced Online* 21. doi: 10.1186/s12575-019-0092-2
- Morizawa, Y. M., Hirayama, Y., Ohno, N., Shibata, S., Shigetomi, E., Sui, Y., et al. (2017). Reactive astrocytes function as phagocytes after brain ischemia via ABCA1-mediated pathway. *Nat Commun* 8, 1–15. doi: 10.1038/s41467-017-00037-1
- Morris, K. V., and Mattick, J. S. (2014). The rise of regulatory RNA. *Nat Rev Genet* 15, 423–437. doi: 10.1038/nrg3722
- Müller, M., and Somjen, G. G. (2000). Na⁺ and K⁺ concentrations, extra- and intracellular voltages, and the effect of TTX in hypoxic rat hippocampal slices. *J Neurophysiol* 83, 735–745. doi: 10.1152/jn.2000.83.2.735
- Mullett, S. J., Di Maio, R., Greenamyre, J. T., and Hinkle, D. A. (2013). DJ-1 Expression Modulates Astrocyte-Mediated Protection Against Neuronal Oxidative Stress. *Journal of Molecular Neuroscience* 49, 507–511. doi: 10.1007/s12031-012-9904-4
- Muralidharan-Chari, V., Clancy, J., Plou, C., Romao, M., Chavrier, P., Raposo, G., et al. (2009). ARF6-Regulated Shedding of Tumor Cell-Derived Plasma Membrane Microvesicles. *Current Biology* 19, 1875–1885. doi: 10.1016/j.cub.2009.09.059
- Mustapic, M., Eitan, E., Werner, J. K., Berkowitz, S. T., Lazaropoulos, M. P., Tran, J., et al. (2017). Plasma extracellular vesicles enriched for neuronal origin: A potential window into brain pathologic processes. *Front Neurosci* 11. doi: 10.3389/fnins.2017.00278
- Nagai, M., Re, D. B., Nagata, T., Chalazonitis, A., Jessell, T. M., Wichterle, H., et al. (2007). Astrocytes expressing ALS-linked mutated SOD1 release factors selectively toxic to motor neurons. *Nat Neurosci* 10, 615–622. doi: 10.1038/nn1876
- Nanclares, C., Baraibar, A. M., Araque, A., and Kofuji, P. (2021). Dysregulation of Astrocyte–Neuronal Communication in Alzheimer’s Disease. *International Journal of Molecular Sciences* 2021, Vol. 22, Page 7887 22, 7887. doi: 10.3390/IJMS22157887
- Nichols, N. R., Day, J. R., Laping, N. J., Johnson, S. A., Finch, C. E., Nichols, N. R., et al. (1993). GFAP mRNA Increases With Age in Rat and Human Brain.
- Nigro, A., Finardi, A., Ferraro, M. M., Manno, D. E., Quattrini, A., Furlan, R., et al. (2021). Selective loss of microvesicles is a major issue of the differential centrifugation isolation protocols. *Sci Rep* 11, 3589. doi: 10.1038/s41598-021-83241-w

- Nikitidou, E., Khoonsari, P. E., Shevchenko, G., Ingelsson, M., Kultima, K., and Erlandsson, A. (2017). Increased release of Apolipoprotein E in extracellular vesicles following amyloid- β protofibril exposure of neuroglial co-cultures. *Journal of Alzheimer's Disease* 60, 305–321. doi: 10.3233/JAD-170278
- Nissen, J. D., Lykke, K., Bryk, J., Stridh, M. H., Zaganas, I., Skytt, D. M., et al. (2017). Expression of the human isoform of glutamate dehydrogenase, hGDH2, augments TCA cycle capacity and oxidative metabolism of glutamate during glucose deprivation in astrocytes. *Glia* 65, 474–488. doi: 10.1002/glia.23105
- Niu, H., Álvarez-Álvarez, I., Guillén-Grima, F., and Aguinaga-Ontoso, I. (2017). Prevalence and incidence of Alzheimer's disease in Europe: A meta-analysis. *Neurología* 32, 523–532. doi: 10.1016/j.nrleng.2016.02.009
- Nizamudeen, Z., Markus, R., Lodge, R., Parmenter, C., Platt, M., Chakrabarti, L., et al. (2018). Rapid and accurate analysis of stem cell-derived extracellular vesicles with super resolution microscopy and live imaging. *Biochim Biophys Acta Mol Cell Res* 1865, 1891–1900. doi: 10.1016/j.bbamcr.2018.09.008
- Nogueras-Ortiz, C. J., Mahairaki, V., Delgado-Peraza, F., Das, D., Avgerinos, K., Eren, E., et al. (2020). Astrocyte- and Neuron-Derived Extracellular Vesicles from Alzheimer's Disease Patients Effect Complement-Mediated Neurotoxicity. *Cells* 9, 1618. doi: 10.3390/cells9071618
- Nolte 'T Hoen, E. N. M., Buermans, H. P. J., Waasdorp, M., Stoorvogel, W., Wauben, M. H. M., and 'T Hoen, P. A. C. (2012). Deep sequencing of RNA from immune cell-derived vesicles uncovers the selective incorporation of small non-coding RNA biotypes with potential regulatory functions. *Nucleic Acids Res* 40, 9272–9285. doi: 10.1093/nar/gks658
- Norenberg, M. D., and Martinez-Hernandez, A. (1979). Fine structural localization of glutamine synthetase in astrocytes of rat brain. *Brain Res* 161, 303–310. doi: 10.1016/0006-8993(79)90071-4
- Norman, M., Ter-Ovanesyan, D., Trieu, W., Lazarovits, R., Kowal, E. J. K., Lee, J. H., et al. (2021). L1CAM is not associated with extracellular vesicles in human cerebrospinal fluid or plasma. *Nat Methods* 18, 631–634. doi: 10.1038/s41592-021-01174-8
- Nortley, R., and Attwell, D. (2017). Control of brain energy supply by astrocytes. *Curr Opin Neurobiol* 47, 80–85. doi: 10.1016/j.conb.2017.09.012
- Oakes, J. A., Davies, M. C., and Collins, M. O. (2017). TBK1: a new player in ALS linking autophagy and neuroinflammation. *Mol Brain* 10, 1–10. doi: 10.1186/s13041-017-0287-x
- Oberheim, N. A., Takano, T., Han, X., He, W., Lin, J. H. C., Wang, F., et al. (2009). Uniquely hominid features of adult human astrocytes. *Journal of Neuroscience* 29, 3276–3287. doi: 10.1523/JNEUROSCI.4707-08.2009
- Oberheim, N. A., Wang, X., Goldman, S., and Nedergaard, M. (2006). Astrocytic complexity distinguishes the human brain. *Trends Neurosci* 29, 547–553. doi: 10.1016/j.tins.2006.08.004

- O'Brien, E. R., Kersemans, V., Tredwell, M., Checa, B., Serres, S., Soto, M. S., et al. (2014). Glial activation in the early stages of brain metastasis: TSPO as a diagnostic biomarker. *Journal of Nuclear Medicine* 55, 275–280. doi: 10.2967/jnumed.113.127449
- Oeckl, P., Anderl-Straub, S., Von Arnim, C. A. F., Baldeiras, I., Diehl-Schmid, J., Grimmer, T., et al. (2022). Serum GFAP differentiates Alzheimer's disease from frontotemporal dementia and predicts MCI-to-dementia conversion. *J Neurol Neurosurg Psychiatry* 93, 659–667. doi: 10.1136/jnnp-2021-328547
- Oki, K., Tatarishvili, J., Wood, J., Koch, P., Wattananit, S., Mine, Y., et al. (2012). Human-induced pluripotent stem cells form functional neurons and improve recovery after grafting in stroke-damaged brain. *Stem Cells* 30, 1120–1133. doi: 10.1002/stem.1104
- Orkand, R. K., Nicholls, J. G., and Kuffler, S. W. (1966). Effect of nerve impulses on the membrane potential of glial cells in the central nervous system of amphibia. *J Neurophysiol* 29, 788–806. doi: 10.1152/jn.1966.29.4.788
- Ostrowski, M., Carmo, N. B., Krumeich, S., Fanget, I., Raposo, G., Savina, A., et al. (2010). Rab27a and Rab27b control different steps of the exosome secretion pathway. *Nat Cell Biol* 12, 19–30. doi: 10.1038/ncb2000
- Pajarillo, E., Rizor, A., Lee, J., Aschner, M., and Lee, E. (2019). The role of astrocytic glutamate transporters GLT-1 and GLAST in neurological disorders: Potential targets for neurotherapeutics. *Neuropharmacology* 161. doi: 10.1016/j.neuropharm.2019.03.002
- Palviainen, M., Saari, H., Kärkkäinen, O., Pekkinen, J., Auriola, S., Yliperttula, M., et al. (2019). Metabolic signature of extracellular vesicles depends on the cell culture conditions. *J Extracell Vesicles* 8. doi: 10.1080/20013078.2019.1596669
- Pan, K. M., Baldwin, M., Nguyen, J., Gasset, M., Serban, A., Groth, D., et al. (1993). Conversion of α -helices into β -sheets features in the formation of the scrapie prion proteins. *Proc Natl Acad Sci U S A* 90, 10962–10966. doi: 10.1073/pnas.90.23.10962
- Pankiv, S., Clausen, T. H., Lamark, T., Brech, A., Bruun, J. A., Outzen, H., et al. (2007). p62/SQSTM1 binds directly to Atg8/LC3 to facilitate degradation of ubiquitinated protein aggregates by autophagy. *Journal of Biological Chemistry* 282, 24131–24145. doi: 10.1074/jbc.M702824200
- Pannell, M., Economopoulos, V., Wilson, T. C., Kersemans, V., Isenegger, P. G., Larkin, J. R., et al. (2020). Imaging of translocator protein upregulation is selective for pro-inflammatory polarized astrocytes and microglia. *Glia* 68, 280–297. doi: 10.1002/glia.23716
- Park, I. H., Arora, N., Huo, H., Maherali, N., Ahfeldt, T., Shimamura, A., et al. (2008). Disease-Specific Induced Pluripotent Stem Cells. *Cell* 134, 877–886. doi: 10.1016/j.cell.2008.07.041
- Park, J. H., Ju, Y. H., Choi, J. W., Song, H. J., Jang, B. K., Woo, J., et al. (2019). Newly developed reversible MAO-B inhibitor circumvents the shortcomings of

irreversible inhibitors in Alzheimer's disease. *Sci Adv* 5. doi:
10.1126/SCIADV.AAV0316/SUPPL_FILE/AAV0316_SM.PDF

- Pascual, O., Achour, S. Ben, Rostaing, P., Triller, A., and Bessis, A. (2012). Microglia activation triggers astrocyte-mediated modulation of excitatory neurotransmission. *Proc Natl Acad Sci U S A* 109. doi: 10.1073/pnas.1111098109
- Pascua-Maestro, R., González, E., Lillo, C., Ganfornina, M. D., Falcón-Pérez, J. M., and Sanchez, D. (2019). Extracellular vesicles secreted by astroglial cells transport apolipoprotein D to neurons and mediate neuronal survival upon oxidative stress. *Front Cell Neurosci* 12. doi: 10.3389/fncel.2018.00526
- Patel, M. R., and Weaver, A. M. (2021). Astrocyte-derived small extracellular vesicles promote synapse formation via fibulin-2-mediated TGF- β signaling. *Cell Rep* 34. doi: 10.1016/j.celrep.2021.108829
- Pathan, M., Fonseka, P., Chitti, S. V., Kang, T., Sanwlani, R., Van Deun, J., et al. (2019). Vesiclepedia 2019: A compendium of RNA, proteins, lipids and metabolites in extracellular vesicles. *Nucleic Acids Res* 47, D516–D519. doi: 10.1093/nar/gky1029
- Pavia, F. C., Di Bella, M. A., Brucato, V., Blanda, V., Zummo, F., Vitrano, I., et al. (2019). A 3D-scaffold of PLLA induces the morphological differentiation and migration of primary astrocytes and promotes the production of extracellular vesicles. *Mol Med Rep* 20, 1288–1296. doi: 10.3892/mmr.2019.10351
- Pegtel, D. M., and Gould, S. J. (2019). Exosomes. *Annu Rev Biochem* 88, 487–514. doi: 10.1146/annurev-biochem-013118-111902
- Pei, X., Li, Y., Zhu, L., and Zhou, Z. (2020). Astrocyte-derived exosomes transfer miR-190b to inhibit oxygen and glucose deprivation-induced autophagy and neuronal apoptosis. *Cell Cycle* 19, 906–917. doi: 10.1080/15384101.2020.1731649
- Pekny, M., and Pekna, M. (2014). Astrocyte reactivity and reactive astrogliosis: Costs and benefits. *Physiol Rev* 94, 1077–1098. doi: 10.1152/physrev.00041.2013
- Pekny, M., Pekna, M., Messing, A., Steinhäuser, C., Lee, J. M., Parpura, V., et al. (2016). Astrocytes: a central element in neurological diseases. *Acta Neuropathol* 131, 323–345. doi: 10.1007/s00401-015-1513-1
- Pellerin, L., Bouzier-Sore, A. K., Aubert, A., Serres, S., Merle, M., Costalat, R., et al. (2007). Activity-dependent regulation of energy metabolism by astrocytes: An update. *Glia* 55, 1251–1262. doi: 10.1002/glia.20528
- Pellerin, L., and Magistretti, P. J. (1994). Glutamate uptake into astrocytes stimulates aerobic glycolysis: A mechanism coupling neuronal activity to glucose utilization. *Proc Natl Acad Sci U S A* 91, 10625–10629. doi: 10.1073/pnas.91.22.10625

- Peng, J., Pan, J., Mo, J., and Peng, Y. (2022). MPO/HOCl Facilitates Apoptosis and Ferroptosis in the SOD1G93A Motor Neuron of Amyotrophic Lateral Sclerosis. *Oxid Med Cell Longev* 2022. doi: 10.1155/2022/8217663
- Pereira, J. B., Janelidze, S., Smith, R., Mattsson-Carlsson, N., Palmqvist, S., Teunissen, C. E., et al. (2021). Plasma GFAP is an early marker of amyloid- β but not tau pathology in Alzheimer's disease. *Brain* 144, 3505–3516. doi: 10.1093/brain/awab223
- Pérez-González, R., Kim, Y., Miller, C., Pacheco-Quinto, J., Eckman, E. A., and Levy, E. (2020). Extracellular vesicles: where the amyloid precursor protein carboxyl-terminal fragments accumulate and amyloid- β oligomerizes. *The FASEB Journal* 34, 12922–12931. doi: 10.1096/fj.202000823R
- Pestana, F., Edwards-Faret, G., Belgard, T. G., Martirosyan, A., and Holt, M. G. (2020). No longer underappreciated: The emerging concept of astrocyte heterogeneity in neuroscience. *Brain Sci* 10. doi: 10.3390/brainsci10030168
- Pitcairn, C., Wani, W. Y., and Mazzulli, J. R. (2019). Dysregulation of the autophagic-lysosomal pathway in Gaucher and Parkinson's disease. *Neurobiol Dis* 122, 72–82. doi: 10.1016/j.nbd.2018.03.008
- Pitt, J., Wilcox, K. C., Tortelli, V., Diniz, L. P., Oliveira, M. S., Dobbins, C., et al. (2017). Neuroprotective astrocyte-derived insulin/insulin-like growth factor 1 stimulates endocytic processing and extracellular release of neuron-bound A β oligomers. *Mol Biol Cell* 28, 2623–2636. doi: 10.1091/mbc.E17-06-0416
- Pivoriūnas, A., and Verkhratsky, A. (2021). Astrocyte-derived extracellular vesicles mediate intercellular communications of the neurogliovascular unit. *Neural Regen Res* 16, 1421–1422. doi: 10.4103/1673-5374.300994
- Poehler, A. M., Xiang, W., Spitzer, P., May, V. E. L., Meixner, H., Rockenstein, E., et al. (2014). Autophagy modulates SNCA/ α -synuclein release, thereby generating a hostile microenvironment. *Autophagy* 10, 2171–2192. doi: 10.4161/auto.36436
- Ponath, G., Park, C., and Pitt, D. (2018). The role of astrocytes in multiple sclerosis. *Front Immunol* 9, 217. doi: 10.3389/fimmu.2018.00217
- Ponpuak, M., Mandell, M. A., Kimura, T., Chauhan, S., Cleyrat, C., and Deretic, V. (2015). Secretory autophagy. *Curr Opin Cell Biol* 35, 106–116. doi: 10.1016/j.ceb.2015.04.016
- Pound, P., and Ritskes-Hoitinga, M. (2018). Is it possible to overcome issues of external validity in preclinical animal research? Why most animal models are bound to fail. *J Transl Med* 16. doi: 10.1186/s12967-018-1678-1
- Prah, J., Winters, A., Chaudhari, K., Hersh, J., Liu, R., and Yang, S. H. (2019). A novel serum free primary astrocyte culture method that mimic quiescent astrocyte phenotype. *J Neurosci Methods* 320, 50–63. doi: 10.1016/j.jneumeth.2019.03.013

- Preston, A. N., Cervasio, D. A., and Laughlin, S. T. (2019). "Visualizing the brain's astrocytes," in *Methods in Enzymology*, (Academic Press Inc.), 129–151. doi: 10.1016/bs.mie.2019.02.006
- Prusiner, S. B. (1982). Novel proteinaceous infectious particles cause scrapie. *Science (1979)* 216, 136–144. doi: 10.1126/science.6801762
- Puhka, M., Takatalo, M., Nordberg, M. E., Valkonen, S., Nandania, J., Aatonen, M., et al. (2017). Metabolomic profiling of extracellular vesicles and alternative normalization methods reveal enriched metabolites and strategies to study prostate cancer-related changes. *Theranostics* 7, 3824–3841. doi: 10.7150/thno.19890
- Puschmann, T. B., Zandén, C., Lebkuechner, I., Philippot, C., De Pablo, Y., Liu, J., et al. (2014). HB-EGF affects astrocyte morphology, proliferation, differentiation, and the expression of intermediate filament proteins. *J Neurochem* 128, 878–889. doi: 10.1111/jnc.12519
- Rabinowitz, J. D., and White, E. (2010). Autophagy and metabolism. *Science (1979)* 330, 1344–1348. doi: 10.1126/science.1193497
- Rae, C., Hare, N., Bubb, W. A., McEwan, S. R., Bröer, A., McQuillan, J. A., et al. (2003). Inhibition of glutamine transport depletes glutamate and GABA neurotransmitter pools: Further evidence for metabolic compartmentation. *J Neurochem* 85, 503–514. doi: 10.1046/j.1471-4159.2003.01713.x
- Rajendran, L., Honsho, M., Zahn, T. R., Keller, P., Geiger, K. D., Verkade, P., et al. (2006). Alzheimer's disease β -amyloid peptides are released in association with exosomes. *Proc Natl Acad Sci U S A* 103, 11172–11177. doi: 10.1073.0603838103
- Ramos-Zaldívar, H. M., Polakovicova, I., Salas-Huenuleo, E., Corvalán, A. H., Kogan, M. J., Yefi, C. P., et al. (2022). Extracellular vesicles through the blood–brain barrier: a review. *Fluids and Barriers of the CNS* 2022 19:1 19, 1–15. doi: 10.1186/S12987-022-00359-3
- Ranjit, S., Patters, B. J., Gerth, K. A., Haque, S., Choudhary, S., and Kumar, S. (2018). Potential neuroprotective role of astroglial exosomes against smoking-induced oxidative stress and HIV-1 replication in the central nervous system. *Expert Opin Ther Targets* 22, 703–714. doi: 10.1080/14728222.2018.1501473
- Renton, A. E., Majounie, E., Waite, A., Simón-Sánchez, J., Rollinson, S., Gibbs, J. R., et al. (2011). A hexanucleotide repeat expansion in C9ORF72 is the cause of chromosome 9p21-linked ALS-FTD. *Neuron* 72, 257–268. doi: 10.1016/j.neuron.2011.09.010
- Rikkert, L. G., Nieuwland, R., Terstappen, L. W. M. M., and Coumans, F. A. W. (2019). Quality of extracellular vesicle images by transmission electron microscopy is operator and protocol dependent. *J Extracell Vesicles* 8, 1555419. doi: 10.1080/20013078.2018.1555419

- Ritchie, M. E., Phipson, B., Wu, D., Hu, Y., Law, C. W., Shi, W., et al. (2015). Limma powers differential expression analyses for RNA-sequencing and microarray studies. *Nucleic Acids Res* 43, e47. doi: 10.1093/nar/gkv007
- Rojas, F., Cortes, N., Abarzua, S., Dyrda, A., and van Zundert, B. (2014). Astrocytes expressing mutant SOD1 and TDP43 trigger motoneuron death that is mediated via sodium channels and nitroxidative stress. *Front Cell Neurosci* 8, 24. doi: 10.3389/fncel.2014.00024
- Rosen, D. R., Siddique, T., Patterson, D., Figlewicz, D. A., Sapp, P., Hentati, A., et al. (1993). Mutations in Cu/Zn superoxide dismutase gene are associated with familial amyotrophic lateral sclerosis. *Nature* 362, 59–62. doi: 10.1038/362059a0
- Rothermundt, M., Peters, M., Prehn, J. H. M., and Arolt, V. (2003). S100B in brain damage and neurodegeneration. *Microsc Res Tech* 60, 614–632. doi: 10.1002/jemt.10303
- Roybon, L., Lamas, N. J., Garcia-Diaz, A., Yang, E. J., Sattler, R., Jackson-Lewis, V., et al. (2013). Human stem cell-derived spinal cord astrocytes with defined mature or reactive phenotypes. *Cell Rep* 4, 1035–1048. doi: 10.1016/j.celrep.2013.06.021
- Ruan, Z., Pathak, D., Venkatesan Kalavai, S., Yoshii-Kitahara, A., Muraoka, S., Bhatt, N., et al. (2021). Alzheimer’s disease brain-derived extracellular vesicles spread tau pathology in interneurons. *Brain* 144, 288. doi: 10.1093/BRAIN/AWAA376
- Rudnick, N. D., Griffey, C. J., Guarnieri, P., Gerbino, V., Wang, X., Piersaint, J. A., et al. (2017). Distinct roles for motor neuron autophagy early and late in the SOD1G93A mouse model of ALS. *Proc Natl Acad Sci U S A* 114, 8294–8303. doi: 10.1073/pnas.1704294114
- Saá, P., Yakovleva, O., De Castro, J., Vasilyeva, I., De Paoli, S. H., Simak, J., et al. (2014). First demonstration of transmissible spongiform encephalopathy-associated prion protein (PrPTSE) in extracellular vesicles from plasma of mice infected with mouse-adapted variant creutzfeldt-jakob disease by in vitro amplification. *Journal of Biological Chemistry* 289, 29247–29260. doi: 10.1074/jbc.M114.589564
- Saman, S., Kim, W. H., Raya, M., Visnick, Y., Miro, S., Saman, S., et al. (2012). Exosome-associated tau is secreted in tauopathy models and is selectively phosphorylated in cerebrospinal fluid in early Alzheimer disease. *Journal of Biological Chemistry* 287, 3842–3849. doi: 10.1074/jbc.M111.277061
- Sancho, L., Deng, J., Bosworth, A. ✉, Caldwell, A. L. M., Bosworth, A., Miglietta, A., et al. (2022). Aberrant astrocyte protein secretion contributes to altered neuronal development in multiple models of neurodevelopmental disorders. *Nature Neuroscience* 2022, 1–16. doi: 10.1038/s41593-022-01150-1
- Sándor, G. O., Soós, A. Á., Lörincz, P., Rojkó, L., Harkó, T., Bogyó, L., et al. (2021). Wnt Activity and Cell Proliferation Are Coupled to Extracellular Vesicle Release in Multiple Organoid Models. *Front Cell Dev Biol* 9. doi: 10.3389/fcell.2021.670825

- Santangelo, L., Giurato, G., Cicchini, C., Montaldo, C., Mancone, C., Tarallo, R., et al. (2016). The RNA-Binding Protein SYNCRIP Is a Component of the Hepatocyte Exosomal Machinery Controlling MicroRNA Sorting. *Cell Rep* 17, 799–808. doi: 10.1016/j.celrep.2016.09.031
- Sardar Sinha, M., Ansell-Schultz, A., Civitelli, L., Hildesjö, C., Larsson, M., Lannfelt, L., et al. (2018). Alzheimer's disease pathology propagation by exosomes containing toxic amyloid-beta oligomers. *Acta Neuropathol* 136, 41–56. doi: 10.1007/s00401-018-1868-1
- Sathe, G., Albert, M., Darrow, J., Saito, A., Troncoso, J., Pandey, A., et al. (2021). Quantitative proteomic analysis of the frontal cortex in Alzheimer's disease. *J Neurochem* 156, 988–1002. doi: 10.1111/JNC.15116
- Savchenko, E., Teku, G. N., Boza-Serrano, A., Russ, K., Berns, M., Deierborg, T., et al. (2019). FGF family members differentially regulate maturation and proliferation of stem cell-derived astrocytes. *Sci Rep* 9, 1–13. doi: 10.1038/s41598-019-46110-1
- Schedin-Weiss, S., Inoue, M., Hromadkova, L., Teranishi, Y., Yamamoto, N. G., Wiehager, B., et al. (2017). Monoamine oxidase B is elevated in Alzheimer disease neurons, is associated with γ -secretase and regulates neuronal amyloid β -peptide levels. *Alzheimers Res Ther* 9, 1–19. doi: 10.1186/S13195-017-0279-1/FIGURES/9
- Scheltens, P., De Strooper, B., Kivipelto, M., Holstege, H., Chételat, G., Teunissen, C. E., et al. (2021). Alzheimer's disease. *The Lancet* 397, 1577–1590. doi: 10.1016/S0140-6736(20)32205-4
- Schöndorf, D. C., Aureli, M., McAllister, F. E., Hindley, C. J., Mayer, F., Schmid, B., et al. (2014). iPSC-derived neurons from GBA1-associated Parkinson's disease patients show autophagic defects and impaired calcium homeostasis. *Nat Commun* 5. doi: 10.1038/ncomms5028
- Schousboe, A. (2019). Metabolic signaling in the brain and the role of astrocytes in control of glutamate and GABA neurotransmission. *Neurosci Lett* 689, 11–13. doi: 10.1016/j.neulet.2018.01.038
- Schousboe, A., Sarup, A., Bak, L. K., Waagepetersen, H. S., and Larsson, O. M. (2004). Role of astrocytic transport processes in glutamatergic and GABAergic neurotransmission. *Neurochem Int* 45, 521–527. doi: 10.1016/j.neuint.2003.11.001
- Sedgwick, A. E., and D'Souza-Schorey, C. (2018). The biology of extracellular microvesicles. *Traffic* 19, 319–327. doi: 10.1111/tra.12558
- Selkoe, D. J., and Hardy, J. (2016). The amyloid hypothesis of Alzheimer's disease at 25 years. *EMBO Mol Med* 8, 595–608. doi: 10.15252/emmm.201606210
- Shank, R. P., Bennett, G. S., Freytag, S. O., and Campbell, G. L. M. (1985). Pyruvate carboxylase: an astrocyte-specific enzyme implicated in the replenishment of amino acid neurotransmitter pools. *Brain Res* 329, 364–367. doi: 10.1016/0006-8993(85)90552-9

- Shi, M., Sheng, L., Stewart, T., Zabetian, C. P., and Zhang, J. (2019). New windows into the brain: Central nervous system-derived extracellular vesicles in blood. *Prog Neurobiol* 175, 96–106. doi: 10.1016/j.pneurobio.2019.01.005
- Shi, Y., Inoue, H., Wu, J. C., and Yamanaka, S. (2017). Induced pluripotent stem cell technology: A decade of progress. *Nat Rev Drug Discov* 16, 115–130. doi: 10.1038/nrd.2016.245
- Shinozaki, Y., Shibata, K., Yoshida, K., Shigetomi, E., Gachet, C., Ikenaka, K., et al. (2017). Transformation of Astrocytes to a Neuroprotective Phenotype by Microglia via P2Y1 Receptor Downregulation. *Cell Rep* 19, 1151–1164. doi: 10.1016/J.CELREP.2017.04.047
- Silverman, J. M., Christy, D., Shyu, C. C., Moon, K. M., Fernando, S., Gidden, Z., et al. (2019). CNS-derived extracellular vesicles from superoxide dismutase 1 (SOD1)G93A ALS mice originate from astrocytes and neurons and carry misfolded SOD1. *Journal of Biological Chemistry* 294, 3744–3759. doi: 10.1074/jbc.RA118.004825
- Silverman, J. M., Fernando, S. M., Grad, L. I., Hill, A. F., Turner, B. J., Yerbury, J. J., et al. (2016). Disease Mechanisms in ALS: Misfolded SOD1 Transferred Through Exosome-Dependent and Exosome-Independent Pathways. *Cell Mol Neurobiol* 36, 377–381. doi: 10.1007/s10571-015-0294-3
- Simpson, R. J., Kalra, H., and Mathivanan, S. (2012). Exocarta as a resource for exosomal research. *J Extracell Vesicles* 1. doi: 10.3402/jev.v1i0.18374
- Sims, J. R., Zimmer, J. A., Evans, C. D., Lu, M., Ardayfio, P., Sparks, J., et al. (2023). Donanemab in Early Symptomatic Alzheimer Disease: The TRAILBLAZER-ALZ 2 Randomized Clinical Trial. *JAMA*. doi: 10.1001/jama.2023.13239
- Singh, S., Anshita, D., and Ravichandiran, V. (2021). MCP-1: Function, regulation, and involvement in disease. *Int Immunopharmacol* 101. doi: 10.1016/j.intimp.2021.107598
- Soares Martins, T., Trindade, D., Vaz, M., Campelo, I., Almeida, M., Trigo, G., et al. (2021). Diagnostic and therapeutic potential of exosomes in Alzheimer's disease. *J Neurochem* 156, 162–181. doi: 10.1111/jnc.15112
- Sofroniew, M. V., and Vinters, H. V. (2010). Astrocytes: Biology and pathology. *Acta Neuropathol* 119, 7–35. doi: 10.1007/s00401-009-0619-8
- Söllvander, S., Nikitidou, E., Brolin, R., Söderberg, L., Sehlin, D., Lannfelt, L., et al. (2016). Accumulation of amyloid- β by astrocytes result in enlarged endosomes and microvesicle-induced apoptosis of neurons. *Mol Neurodegener* 11, 38. doi: 10.1186/s13024-016-0098-z
- Solomon, E., Davis-Anderson, K., Hovde, B., Micheva-Viteva, S., Harris, J. F., Twary, S., et al. (2021). Global transcriptome profile of the developmental principles of in vitro iPSC-to-motor neuron differentiation. *BMC Mol Cell Biol* 22, 13. doi: 10.1186/s12860-021-00343-z

- Solvik, T. A., Nguyen, T. A., Lin, Y. H. T., Marsh, T., Huang, E. J., Wiita, A. P., et al. (2022). Secretory autophagy maintains proteostasis upon lysosome inhibition. *Journal of Cell Biology* 221. doi: 10.1083/jcb.202110151
- Somjen, G. G. (1979). Extracellular Potassium in the Mammalian Central Nervous System. *Annu Rev Physiol* 41, 159–177. doi: 10.1146/annurev.ph.41.030179.001111
- Sonntag, K. C., Song, B., Lee, N., Jung, J. H., Cha, Y., Leblanc, P., et al. (2018). Pluripotent stem cell-based therapy for Parkinson's disease: Current status and future prospects. *Prog Neurobiol* 168, 1–20. doi: 10.1016/j.pneurobio.2018.04.005
- Soubannier, V., Maussion, G., Chaineau, M., Sigutova, V., Rouleau, G., Durcan, T. M., et al. (2020). Characterization of human iPSC-derived astrocytes with potential for disease modeling and drug discovery. *Neurosci Lett* 731. doi: 10.1016/j.neulet.2020.135028
- Sproviero, D., La Salvia, S., Giannini, M., Crippa, V., Gagliardi, S., Bernuzzi, S., et al. (2018). Pathological proteins are transported by extracellular vesicles of sporadic amyotrophic lateral sclerosis patients. *Front Neurosci* 12. doi: 10.3389/fnins.2018.00487
- Steiner, J., Bernstein, H. G., Biela, H., Berndt, A., Brisch, R., Mawrin, C., et al. (2007). Evidence for a wide extra-astrocytic distribution of S100B in human brain. *BMC Neurosci* 8. doi: 10.1186/1471-2202-8-2
- Stoklund Dittlau, K., Terrie, L., Baatsen, P., Kerstens, A., De Swert, L., Janky, R., et al. (2023). FUS-ALS hiPSC-derived astrocytes impair human motor units through both gain-of-toxicity and loss-of-support mechanisms. *Mol Neurodegener* 18, 5. doi: 10.1186/S13024-022-00591-3
- Stopschinski, B. E., and Diamond, M. I. (2017). The prion model for progression and diversity of neurodegenerative diseases. *Lancet Neurol* 16, 323–332. doi: 10.1016/S1474-4422(17)30037-6
- Streubel-Gallasch, L., Giusti, V., Sandre, M., Tessari, I., Plotegher, N., Giusto, E., et al. (2021). Parkinson's Disease–Associated LRRK2 Interferes with Astrocyte-Mediated Alpha-Synuclein Clearance. *Molecular Neurobiology* 2021 58:7 58, 3119–3140. doi: 10.1007/S12035-021-02327-8
- Stuendl, A., Kraus, T., Chatterjee, M., Zapke, B., Sadowski, B., Moebius, W., et al. (2021). α -Synuclein in Plasma-Derived Extracellular Vesicles Is a Potential Biomarker of Parkinson's Disease. *Movement Disorders* 36, 2508–2518. doi: 10.1002/MDS.28639
- Stuffers, S., Sem Wegner, C., Stenmark, H., and Brech, A. (2009). Multivesicular endosome biogenesis in the absence of ESCRTs. *Traffic* 10, 925–937. doi: 10.1111/j.1600-0854.2009.00920.x
- Sugai, K., Sumida, M., Shofuda, T., Yamaguchi, R., Tamura, T., Kohzaki, T., et al. (2021). First-in-human clinical trial of transplantation of iPSC-derived NS/PCs in

subacute complete spinal cord injury: Study protocol. *Regen Ther* 18, 321–333. doi: 10.1016/j.reth.2021.08.005

- Sullivan, P. M., Zhou, X., Robins, A. M., Paushter, D. H., Kim, D., Smolka, M. B., et al. (2016). The ALS/FTLD associated protein C9orf72 associates with SMCR8 and WDR41 to regulate the autophagy-lysosome pathway. *Acta Neuropathol Commun* 4, 51. doi: 10.1186/s40478-016-0324-5
- Sun, D., Gao, W., Hu, H., and Zhou, S. (2022a). Why 90% of clinical drug development fails and how to improve it? *Acta Pharm Sin B* 12, 3049–3062. doi: 10.1016/j.apsb.2022.02.002
- Sun, H., Cao, X., Gong, A., Huang, Y., Xu, Y., Zhang, J., et al. (2022b). Extracellular vesicles derived from astrocytes facilitated neurite elongation by activating the Hippo pathway. *Exp Cell Res* 411, 112937. doi: 10.1016/J.YEXCR.2021.112937
- Szebényi, K., Wenger, L. M. D., Sun, Y., Dunn, A. W. E., Limegrover, C. A., Gibbons, G. M., et al. (2021). Human ALS/FTD brain organoid slice cultures display distinct early astrocyte and targetable neuronal pathology. *Nature Neuroscience* 2021, 1–13. doi: 10.1038/s41593-021-00923-4
- Takahashi, K., Tanabe, K., Ohnuki, M., Narita, M., Ichisaka, T., Tomoda, K., et al. (2007). Induction of Pluripotent Stem Cells from Adult Human Fibroblasts by Defined Factors. *Cell* 131, 861–872. doi: 10.1016/j.cell.2007.11.019
- Takahashi, K., and Yamanaka, S. (2006). Induction of Pluripotent Stem Cells from Mouse Embryonic and Adult Fibroblast Cultures by Defined Factors. *Cell* 126, 663–676. doi: 10.1016/j.cell.2006.07.024
- Takashima, C., Kosuge, Y., Inoue, M., Ono, S.-I., and Tokuda, E. (2021). A Metal-Free, Disulfide Oxidized Form of Superoxide Dismutase 1 as a Primary Misfolded Species with Prion-Like Properties in the Extracellular Environments Surrounding Motor Neuron-Like Cells. *Int J Mol Sci* 22, 4155. doi: 10.3390/ijms22084155
- Tan, C. F., Eguchi, H., Tagawa, A., Onodera, O., Iwasaki, T., Tsujino, A., et al. (2007). TDP-43 immunoreactivity in neuronal inclusions in familial amyotrophic lateral sclerosis with or without SOD1 gene mutation. *Acta Neuropathol* 113, 535–542. doi: 10.1007/s00401-007-0206-9
- Tang, B. L. (2018). Brain activity-induced neuronal glucose uptake/glycolysis: Is the lactate shuttle not required? *Brain Res Bull* 137, 225–228. doi: 10.1016/j.brainresbull.2017.12.010
- Tang, Y., and Le, W. (2016). Differential Roles of M1 and M2 Microglia in Neurodegenerative Diseases. *Mol Neurobiol* 53, 1181–1194. doi: 10.1007/s12035-014-9070-5
- Tavares, G., Martins, M., Correia, J. S., Sardinha, V. M., Guerra-Gomes, S., das Neves, S. P., et al. (2017). Employing an open-source tool to assess astrocyte tridimensional structure. *Brain Struct Funct* 222, 1989–1999. doi: 10.1007/s00429-016-1316-8

- TCW, J., Wang, M., Pimenova, A. A., Bowles, K. R., Hartley, B. J., Lacin, E., et al. (2017). An Efficient Platform for Astrocyte Differentiation from Human Induced Pluripotent Stem Cells. *Stem Cell Reports* 9, 600–614. doi: 10.1016/j.stemcr.2017.06.018
- Teh, D. B. L., Prasad, A., Jiang, W., Ariffin, M. Z., Khanna, S., Belorkar, A., et al. (2017). Transcriptome Analysis Reveals Neuroprotective aspects of Human Reactive Astrocytes induced by Interleukin 1 β . *Sci Rep* 7, 1–12. doi: 10.1038/s41598-017-13174-w
- Théry, C., Witwer, K. W., Aikawa, E., Alcaraz, M. J., Anderson, J. D., Andriantsitohaina, R., et al. (2018). Minimal information for studies of extracellular vesicles 2018 (MISEV2018): a position statement of the International Society for Extracellular Vesicles and update of the MISEV2014 guidelines. *J Extracell Vesicles* 7, 1–47. doi: 10.1080/20013078.2018.1535750
- Trajkovic, K., Hsu, C., Chiantia, S., Rajendran, L., Wenzel, D., Wieland, F., et al. (2008). Ceramide triggers budding of exosome vesicles into multivesicular endosomes. *Science (1979)* 319, 1244–1247. doi: 10.1126/science.1153124
- Tripathi, P., Rodriguez-Muela, N., Klim, J. R., de Boer, A. S., Agrawal, S., Sandoe, J., et al. (2017). Reactive Astrocytes Promote ALS-like Degeneration and Intracellular Protein Aggregation in Human Motor Neurons by Disrupting Autophagy through TGF- β 1. *Stem Cell Reports* 9, 667–680. doi: 10.1016/j.stemcr.2017.06.008
- Turola, E., Furlan, R., Bianco, F., Matteoli, M., and Verderio, C. (2012). Microglial microvesicle secretion and intercellular signaling. *Front Physiol* 3 MAY, 149. doi: 10.3389/fphys.2012.00149
- Ueno, H. (2000). Enzymatic and structural aspects on glutamate decarboxylase. *J Mol Catal B Enzym* 10, 67–79. doi: 10.1016/S1381-1177(00)00114-4
- Urzi, O., Bagge, R. O., and Crescitelli, R. (2022). The dark side of foetal bovine serum in extracellular vesicle studies. *J Extracell Vesicles* 11, e12271. doi: 10.1002/jev2.12271
- Valadi, H., Ekström, K., Bossios, A., Sjöstrand, M., Lee, J. J., and Lötvall, J. O. (2007). Exosome-mediated transfer of mRNAs and microRNAs is a novel mechanism of genetic exchange between cells. *Nat Cell Biol* 9, 654–659. doi: 10.1038/ncb1596
- Valle-Tamayo, N., Pérez-González, R., Chiva-Blanch, G., Belbin, O., Serrano-Requena, S., Sirisi, S., et al. (2022). Enrichment of Astrocyte-Derived Extracellular Vesicles from Human Plasma. *Journal of Visualized Experiments* 2022. doi: 10.3791/64107
- Van Deun, J., Mestdagh, P., Agostinis, P., Akay, Ö., Anand, S., Anckaert, J., et al. (2017). EV-TRACK: Transparent reporting and centralizing knowledge in extracellular vesicle research. *Nat Methods* 14, 228–232. doi: 10.1038/nmeth.4185

- van Dyck, C. H., Swanson, C. J., Aisen, P., Bateman, R. J., Chen, C., Gee, M., et al. (2023). Lecanemab in early Alzheimer's Disease. *N Engl J Med* 388, 9–21. doi: 10.1056/nejmoa2212948
- Vandendriessche, C., Bruggeman, A., Van Cauwenberghe, C., and Vandenbroucke, R. E. (2020). Extracellular Vesicles in Alzheimer's and Parkinson's Disease: Small Entities with Large Consequences. *Cells* 9, 2485. doi: 10.3390/cells9112485
- Vandoorne, T., De Bock, K., and Van Den Bosch, L. (2018). Energy metabolism in ALS: an underappreciated opportunity? *Acta Neuropathol* 135, 489–509. doi: 10.1007/s00401-018-1835-x
- Varcianna, A., Myszczyńska, M. A., Castelli, L. M., O'Neill, B., Kim, Y., Talbot, J., et al. (2019). Micro-RNAs secreted through astrocyte-derived extracellular vesicles cause neuronal network degeneration in C9orf72 ALS. *EBioMedicine* 40, 626–635. doi: 10.1016/j.ebiom.2018.11.067
- Vasile, F., Dossi, E., and Rouach, N. (2017). Human astrocytes: structure and functions in the healthy brain. *Brain Struct Funct* 222, 2017–2029. doi: 10.1007/s00429-017-1383-5
- Verde, F., Milone, I., Maranzano, A., Colombo, E., Torre, S., Solca, F., et al. (2023). Serum levels of glial fibrillary acidic protein in patients with amyotrophic lateral sclerosis. *Ann Clin Transl Neurol* 10, 118–129. doi: 10.1002/acn3.51708
- Villarroya-Beltri, C., Baixauli, F., Gutiérrez-Vázquez, C., Sánchez-Madrid, F., and Mittelbrunn, M. (2014). Sorting it out: Regulation of exosome loading. *Semin Cancer Biol* 28, 3–13. doi: 10.1016/j.semcancer.2014.04.009
- Villarroya-Beltri, C., Gutiérrez-Vázquez, C., Sánchez-Cabo, F., Pérez-Hernández, D., Vázquez, J., Martín-Cofreces, N., et al. (2013). Sumoylated hnRNPA2B1 controls the sorting of miRNAs into exosomes through binding to specific motifs. *Nat Commun* 4. doi: 10.1038/ncomms3980
- von Bartheld, C. S., Bahney, J., anderculano-Houzel, S. (2016). The search for true numbers of neurons and glial cells in the human brain: A review of 150 years of cell counting. *Journal of Comparative Neurology* 524, 3865–3895. doi: 10.1002/cne.24040
- Voss, C. M., Arildsen, L., Nissen, J. D., Waagepetersen, H. S., Schousboe, A., Maechler, P., et al. (2021). Glutamate Dehydrogenase Is Important for Ammonia Fixation and Amino Acid Homeostasis in Brain During Hyperammonemia. *Front Neurosci* 15. doi: 10.3389/fnins.2021.646291
- Waagepetersen, H. S., Sonnewald, U., Larsson, O. M., and Schousboe, A. (2002). A Possible Role of Alanine for Ammonia Transfer Between Astrocytes and Glutamatergic Neurons. *J Neurochem* 75, 471–479. doi: 10.1046/j.1471-4159.2000.0750471.x
- Wallis, R., Josipovic, N., Mizen, H., Robles-Tenorio, A., Tyler, E. J., Papantonis, A., et al. (2021). Isolation methodology is essential to the evaluation of the extracellular vesicle component of the senescence-associated secretory phenotype. *J Extracell Vesicles* 10, e12041. doi: 10.1002/jev2.12041

- Walz, W., and Lang, M. K. (1998). Immunocytochemical evidence for a distinct GFAP-negative subpopulation of astrocytes in the adult rat hippocampus. *Neurosci Lett*, 127–130.
- Wang, X., Liu, Q., and Zhang, B. (2014). Leveraging the complementary nature of RNA-Seq and shotgun proteomics data. *Proteomics* 14, 2676–2687. doi: 10.1002/pmic.201400184
- Wang, Y., Balaji, V., Kaniyappan, S., Krüger, L., Irsen, S., Tepper, K., et al. (2017). The release and trans-synaptic transmission of Tau via exosomes. *Mol Neurodegener* 12, 5. doi: 10.1186/s13024-016-0143-y
- Wei, D., Zhan, W., Gao, Y., Huang, L., Gong, R., Wang, W., et al. (2021). RAB31 marks and controls an ESCRT-independent exosome pathway. *Cell Res* 31, 157–177. doi: 10.1038/s41422-020-00409-1
- Wei, Z.-Y. D., and Shetty, A. K. (2021). Treating Parkinson’s disease by astrocyte reprogramming: Progress and challenges. *Sci Adv* 7, eabg3198. doi: 10.1126/SCIADV.ABG3198
- Welsh, J. A., Goberdhan, D. C. I., O’Driscoll, L., Buzas, E. I., Blenkiron, C., Bussolati, B., et al. (2024). Minimal information for studies of extracellular vesicles (MISEV2023): From basic to advanced approaches. *J Extracell Vesicles* 13. doi: 10.1002/jev2.12404
- Wernig, M., Zhao, J. P., Pruszak, J., Hedlund, E., Fu, D., Soldner, F., et al. (2008). Neurons derived from reprogrammed fibroblasts functionally integrate into the fetal brain and improve symptoms of rats with Parkinson’s disease. *Proc Natl Acad Sci U S A* 105, 5856–5861. doi: 10.1073/pnas.0801677105
- Westergard, T., Jensen, B. K., Wen, X., Cai, J., Kropf, E., Iacovitti, L., et al. (2016). Cell-to-Cell Transmission of Dipeptide Repeat Proteins Linked to C9orf72-ALS/FTD. *Cell Rep* 17, 645–652. doi: 10.1016/j.celrep.2016.09.032
- Wildsmith, K. R., Holley, M., Savage, J. C., Skerrett, R., and Landreth, G. E. (2013). Evidence for impaired amyloid β clearance in Alzheimer’s disease. *Alzheimers Res Ther* 5, 33. doi: 10.1186/alzrt187
- Willis, C. M., Ménoret, A., Jellison, E. R., Nicaise, A. M., Vella, A. T., and Crocker, S. J. (2017). A refined bead-free method to identify astrocytic exosomes in primary glial cultures and blood plasma. *Front Neurosci* 11, 335. doi: 10.3389/fnins.2017.00335
- Willis, C. M., Nicaise, A. M., Bongarzone, E. R., Givogri, M., Reiter, C. R., Heintz, O., et al. (2020). Astrocyte Support for Oligodendrocyte Differentiation can be Conveyed via Extracellular Vesicles but Diminishes with Age. *Sci Rep* 10, 828. doi: 10.1038/s41598-020-57663-x
- Winston, C. N., Goetzl, E. J., Schwartz, J. B., Elahi, F. M., and Rissman, R. A. (2019). Complement protein levels in plasma astrocyte-derived exosomes are abnormal in conversion from mild cognitive impairment to Alzheimer’s disease dementia. *Alzheimer’s and Dementia: Diagnosis, Assessment and Disease Monitoring* 11, 61–66. doi: 10.1016/j.dadm.2018.11.002

- Wong, A. D., Ye, M., Levy, A. F., Rothstein, J. D., Bergles, D. E., and Searson, P. C. (2013). The blood-brain barrier: An engineering perspective. *Front Neuroeng* 6, 7. doi: 10.3389/fneng.2013.00007
- Wong, Y. C., and Holzbaur, E. L. F. (2014). Optineurin is an autophagy receptor for damaged mitochondria in parkin-mediated mitophagy that is disrupted by an ALS-linked mutation. *Proc Natl Acad Sci U S A* 111, 4439–4448. doi: 10.1073/pnas.1405752111
- Wright, A., Snyder, O. L., Christenson, L. K., He, H., and Weiss, M. L. (2022). Effect of Pre-Processing Storage Condition of Cell Culture-Conditioned Medium on Extracellular Vesicles Derived from Human Umbilical Cord-Derived Mesenchymal Stromal Cells. *International Journal of Molecular Sciences* 2022, Vol. 23, Page 7716 23, 7716. doi: 10.3390/IJMS23147716
- Wulf, M. A., Senatore, A., and Aguzzi, A. (2017). The biological function of the cellular prion protein: An update. *BMC Biol* 15. doi: 10.1186/s12915-017-0375-5
- Wyss-Coray, T., Loike, J. D., Brionne, T. C., Lu, E., Anankov, R., Yan, F., et al. (2003). Adult mouse astrocytes degrade amyloid- β in vitro and in situ. *Nat Med* 9, 453–457. doi: 10.1038/nm838
- Xia, L., Qi, J., Tang, M., Liu, J., Zhang, D., Zhu, Y., et al. (2022). Continual Deletion of Spinal Microglia Reforms Astrocyte Scar Favoring Axonal Regeneration. *Front Pharmacol* 0, 2153. doi: 10.3389/FPHAR.2022.881195
- Xie, S., Zhang, Q., and Jiang, L. (2022). Current Knowledge on Exosome Biogenesis, Cargo-Sorting Mechanism and Therapeutic Implications. *Membranes (Basel)* 12. doi: 10.3390/membranes12050498
- Xin, S., Zhang, L., Phan, N. V., Carmichael, S. T., and Segura, T. (2022). Reactive astrocyte derived extracellular vesicles promote functional repair post stroke. *bioRxiv*. doi: 10.1101/2022.09.06.506818
- Xiong, L., McCoy, M., Komuro, H., West, X. Z., Yakubenko, V., Gao, D., et al. (2022). Inflammation-dependent oxidative stress metabolites as a hallmark of amyotrophic lateral sclerosis. *Free Radic Biol Med* 178, 125–133. doi: 10.1016/j.freeradbiomed.2021.11.031
- Yamanaka, K., Chun, S. J., Boillee, S., Fujimori-Tonou, N., Yamashita, H., Gutmann, D. H., et al. (2008). Astrocytes as determinants of disease progression in inherited amyotrophic lateral sclerosis. *Nat Neurosci* 11, 251–253. doi: 10.1038/nn2047
- Yamanaka, K., and Komine, O. (2018). The multi-dimensional roles of astrocytes in ALS. *Neurosci Res* 126, 31–38. doi: 10.1016/j.neures.2017.09.011
- You, Y., Borgmann, K., Edara, V. V., Stacy, S., Ghorpade, A., and Ikezu, T. (2020). Activated human astrocyte-derived extracellular vesicles modulate neuronal uptake, differentiation and firing. *J Extracell Vesicles* 9. doi: 10.1080/20013078.2019.1706801

- Yu, J., Vodyanik, M. A., Smuga-Otto, K., Antosiewicz-Bourget, J., Frane, J. L., Tian, S., et al. (2007). Induced pluripotent stem cell lines derived from human somatic cells. *Science (1979)* 318, 1917–1920. doi: 10.1126/science.1151526
- Yuan, Q., Li, X. dong, Zhang, S. miao, Wang, H. wei, and Wang, Y. liang (2020). Extracellular vesicles in neurodegenerative diseases: Insights and new perspectives. *Genes Dis* 8, 1–9. doi: 10.1016/j.gendis.2019.12.001
- Yun, S. P., Kam, T. I., Panicker, N., Kim, S., Oh, Y., Park, J. S., et al. (2018). Block of A1 astrocyte conversion by microglia is neuroprotective in models of Parkinson's disease. *Nat Med* 24, 931–938. doi: 10.1038/s41591-018-0051-5
- Zamanian, J. L., Xu, L., Foo, L. C., Nouri, N., Zhou, L., Giffard, R. G., et al. (2012). Genomic analysis of reactive astrogliosis. *Journal of Neuroscience* 32, 6391–6410. doi: 10.1523/JNEUROSCI.6221-11.2012
- Zhang, W., Hong, J., Zhang, H., Zheng, W., and Yang, Y. (2021). Astrocyte-derived exosomes protect hippocampal neurons after traumatic brain injury by suppressing mitochondrial oxidative stress and apoptosis. *Ageing* 13, 21642–21658. doi: 10.18632/AGING.203508
- Zhang, Y., and Barres, B. A. (2010). Astrocyte heterogeneity: An underappreciated topic in neurobiology. *Curr Opin Neurobiol* 20, 588–594. doi: 10.1016/j.conb.2010.06.005
- Zhang, Y., Sloan, S. A., Clarke, L. E., Caneda, C., Plaza, C. A., Blumenthal, P. D., et al. (2016). Purification and Characterization of Progenitor and Mature Human Astrocytes Reveals Transcriptional and Functional Differences with Mouse. *Neuron* 89, 37–53. doi: 10.1016/j.neuron.2015.11.013
- Zhao, C., Devlin, A. C., Chouhan, A. K., Selvaraj, B. T., Stavrou, M., Burr, K., et al. (2020). Mutant C9orf72 human iPSC-derived astrocytes cause non-cell autonomous motor neuron pathophysiology. *Glia* 68, 1046–1064. doi: 10.1002/glia.23761
- Zhao, H., and Darzynkiewicz, Z. (2013). Biomarkers of cell senescence assessed by imaging cytometry. *Methods in Molecular Biology* 965, 83–92. doi: 10.1007/978-1-62703-239-1_5
- Zhao, S., Sheng, S., Wang, Y., Ding, L., Xu, X., Xia, X., et al. (2021). Astrocyte-derived extracellular vesicles: A double-edged sword in central nervous system disorders. *Neurosci Biobehav Rev* 125, 148–159. doi: 10.1016/j.neubiorev.2021.02.027
- Zhu, C., Bilousova, T., Focht, S., Jun, M., Elias, C. J., Melnik, M., et al. (2021). Pharmacological inhibition of nSMase2 reduces brain exosome release and α -synuclein pathology in a Parkinson's disease model. *Mol Brain* 14, 70. doi: 10.1186/s13041-021-00776-9
- Ziff, O. J., Clarke, B. E., Taha, D. M., Crerar, H., Luscombe, N. M., and Patani, R. (2022). Meta-analysis of human and mouse ALS astrocytes reveals multi-omic signatures of inflammatory reactive states. *Genome Res* 32, 71–84. doi: 10.1101/gr.275939.121

Chapter 8:Appendix

Supplementary Table 1 - Composition of G5 supplement (ThermoFisher Scientific).

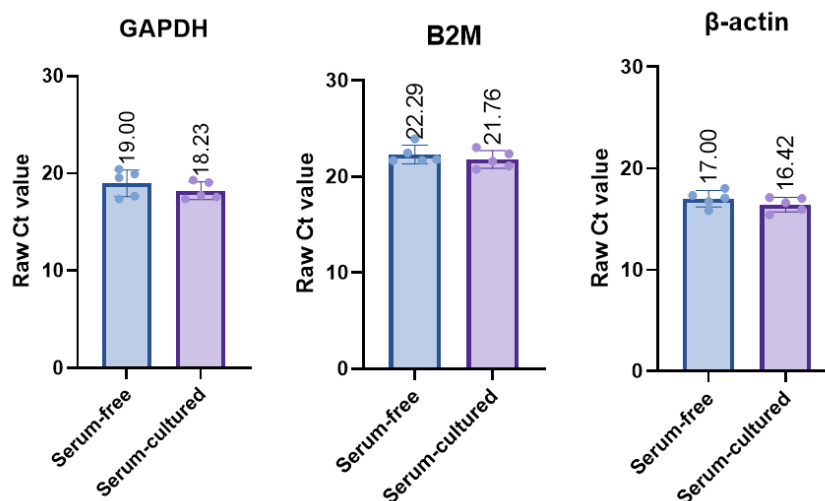
Components	Concentration (mg/L)	Molar (mM)
Biotin	100	0.41
Basic FGF	0.5	Infinity
EGF	1	Infinity
Human transferrin	5000	Infinity
Insulin	500	Infinity
Hydrocortisone	0.36	9.9×10^{-4}
Selenite	0.52	0.003

```

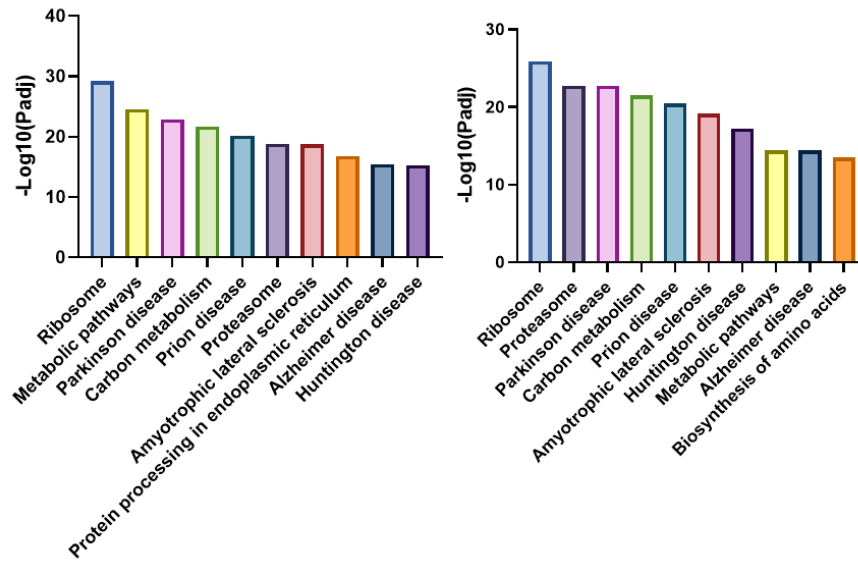
1 run("Auto Threshold", "method=Li white");
2 run("Gaussian Blur...", "sigma=3");
3 run("Unsharp Mask...", "radius=3 mask=0.9");
4 run("Set Scale...", "distance=1 known=5 pixel=1 unit=nm global");
5 run("Auto Threshold", "method=Li white");
6 //run("Invert");
7 run("Set Measurements...", "area mean standard min centroid center perimeter bounding shape median stack display redirect=None decimal=2");
8 run("Analyze Particles...", "size=0-Infinity circularity=0.00-1.00 show=Outlines exclude summarize display");
9 //run("Close ALL");

```

Supplementary figure 1 - ImageJ macro used for EV analysis of dSTORM images



Supplementary figure 2 - Raw Ct values of GAPDH, B2M and β -actin used to determine suitability as housekeeping genes for RT-qPCR of serum-free and serum-cultured human primary astrocytes. Ct values of (A) GAPDH, (B) B2M and (C) β -actin were compared across serum-free and serum-cultured human primary astrocytes to determine whether their expression remain consistent. All three genes had < 2 cycle variation across both serum-free and serum-cultured astrocytes (GAPDH = 0.77, B2M = 0.53, β -actin = 0.58), Error bars represent mean and standard deviation with annotations displaying the mean value (N = 5).



Supplementary figure 3 – The top 10 KEGG pathways upregulated in serum-free and serum-cultured human primary astrocyte whole cell lysates analysed by traditional LC-MS/MS. (A) Serum-free astrocytes and (B) serum-cultured astrocytes have very similar KEGG pathway enrichment suggesting a similar proteome across both conditions.

Supplementary Table 2 -The number of differentially expressed proteins between BDEVs analysed by SWATH-MS identified using Limma analysis after trialling different NA and CV values. To determine the most appropriate criteria for the BDEV proteomic analysis, different NA and CV values were trialled. The NA value is based upon the number of missing values within the condition (0.4 = present in 5/8 samples, 0.2 = 6/8 samples, 0 = found in all samples). The CV value is the threshold for the coefficient of variation. Any proteins above this level of variation between samples were removed from the analysis (E.g. 0.3 = only proteins with <30% variance). Due to the number of proteins analysed, the P-values were adjusted using the Benjamini-Hochberg procedure. Green highlight indicates the thresholds selected for further analysis.

	NA (Missing values)	CV (Variance)	Total Proteins	P<0.05	Padj<0.05
Alz vs Control Alz	0.4	0.3	15	1	0
Alz vs Control Alz	0.4	0.5	318	21	1
Alz vs Control Alz	0.2	0.3	14	2	0
Alz vs Control Alz	0.2	0.5	236	15	2
Alz vs Control Alz	0	0.3	12	5	0
Alz vs Control Alz	0	0.5	167	11	1
ALS vs Control ALS	0.4	0.3	11	0	0
ALS vs Control ALS	0.4	0.5	237	12	1
ALS vs Control ALS	0.2	0.3	12	0	0
ALS vs Control ALS	0.2	0.5	142	7	0
ALS vs Control ALS	0	0.3	14	2	1
ALS vs Control ALS	0	0.5	96	6	0
Alz vs ALS	0.4	0.3	10	3	3
Alz vs ALS	0.4	0.5	225	38	12
Alz vs ALS	0.2	0.3	7	3	1
Alz vs ALS	0.2	0.5	136	26	4
Alz vs ALS	0	0.3	4	2	2
Alz vs ALS	0	0.5	88	19	1

OBB ID	UK BBN ID	Sex	Age	CLINICAL DIAGNOSIS	HISTOLOGY DIAGNOSIS	DIAGNOSIS 1	DIAGNOSIS 2	DIAGNOSIS 3	PM DELAY
12/017	BBN_10312	male	38	MND	The features are those of TDP-43 associated motor neuron disease with upper and lower motor neuron involvement. There is no obvious frontotemporal lobar degeneration (FTLD) component.	MND-TDP			120
12/135	BBN_11068	female	70	MND	Motor Neuron Disease of TDP-43 molecular subtype (MND-TDP), both upper and lower motor neuron involvement. No significant frontotemporal lobar degeneration (FTLD). Characteristic p62 C9orf72 mutation-related immunostaining signature not present	MND-TDP	“low” Alzheimer’s disease (AD) neuropathologic change (ABC score: A:1, B:1, C:0). No alpha-synuclein pathology	Mild to moderate small vessel disease (arteriosclerosis). Mild hypoxic ischaemic damage (hippocampus CA1 region). No cerebral amyloid angiopathy	24
12/092	BBN_11052	female	64	Motor neuron disease (MND). Symptom onset: December 2010 1.5 yrs before death (bulbar). No family history of MND.	Motor Neuron Disease of TDP-43 molecular subtype (MND-TDP). Both upper and lower motor neuron involvement. No evidence of frontotemporal lobar degeneration (FTLD). Characteristic p62 C9orf72 mutation-related immunostaining signature not present	MND-TDP	“low” Alzheimer’s disease (AD) neuropathologic change (ABC score: A:0 or 1, B:1, C:0). No alpha-synuclein pathology	Mild small vessel disease (likely age-related). No significant cerebral amyloid angiopathy (2 vessels only). Incidental focal lesion in parietal block: small collection of subcortical balloon cells	48
12/147	BBN_11084	male	48	MND. Terminal respiratory failure	TDP-43 associated motor neuron disease (MND-TDP). Upper and lower motor neuron involvement (including hypoglossal nucleus). No frontotemporal lobar degeneration (FTLD) component. Characteristic C9orf72 mutation-related immunostaining signature NOT present	MND-TDP	No Alzheimer’s disease neuropathologic change (A score: 0, B score: 1, C score: 0). No alpha-synuclein pathology	Hypoxic ischaemic damage restricted to the hippocampal CA1 region. No significant small vessel disease (SVD). No cerebral amyloid angiopathy	48
18/062	BBN004.33642	female	71	MND	MND-TDP	MND-TDP			72
12/157	BBN_11093	male	62	MND	Motor neuron disease (MND) of TDP-43 molecular subtype with lower motor neuron predominance. No frontotemporal lobar degeneration (FTLD) component	MND-TDP	Early Alzheimer neuropathologic change (Braak/Braak neurofibrillary tangle stage II). Hypoxic ischaemic changes observed in the CA1 region of the hippocampus	Incidental meningioma, WHO grade I	24

13/022	BBN_15235	male	63	MND	Motor neuron disease of TDP-43 molecular subtype (MND-TDP). Both upper and lower motor neuron involvement. No evidence of frontotemporal lobar degeneration (FTLD). Characteristic p62 C9orf72 mutation-related immunostaining signature not present	MND-TDP	No Alzheimer's disease (AD) neuropathologic change (ABC score: A:0, B:1, C:0). No alpha-synuclein pathology	Mild to moderate small vessel disease / arteriosclerosis. Hypoxic ischaemic damage (cerebellum). No cerebral amyloid angiopathy	24
18/030	BBN004.32860	female	59	MND	ALS-TDP	MND-TDP			11

Supplementary table 3 - Human tissue details of ALS frontal lobe tissue used to isolate ALS BDEVs. PM delay = post-mortem delay.

OBB ID	UK BBN ID	Sex	Age	CLINICAL DIAGNOSIS	HISTOLOGY DIAGNOSIS	DIAGNOSIS 1	DIAGNOSIS 2	DIAGNOSIS 3	PM DELAY
05/176	BBN004.2707 1	male	37	multisystem organ failure due to cardiogenic shock after surgical repair of type A aortic dissection	Cerebral oedema which in this case is likely to be due to prolonged cerebral hypoxia secondary to hypotension. Mild hypoxic-ischaemic damage consistent with the clinical history.	Normal brain with regards to neurodegenerative diseases	Global hypoperfusion/ ischaemic damage	Oedema	45
09/041	BBN_2942	female	72	72-year-old woman with no known neurological or psychiatric disease (control brain donation). Found dead by family, post-mortem showed pneumonia. Past medical history of severe chronic obstructive pulmonary disease with several hospital admissions since diagnosis in 1998, ischaemic heart disease, carcinoma of the uterus diagnosed in 2008 for which she was receiving radiotherapy (last session 5 days before death). She was also receiving treatment for indigestion and depression.	Normal aged brain	Normal aged brain	Early Alzheimer pathology affecting predominantly the trans entorhinal cortex (Braak/Braak state I-II). No evidence of alpha-synuclein pathology or other neurodegenerative process	Mild hypertensive changes affecting the basal ganglia	72
18/053	BBN004.3362 3	female	65	Control donation. Acute myocardial infarction, due to atherosclerosis	Control brain (minimal AD pathology)	No abnormality detected	Braak tangle stage I CERAD sparse neuritic plaques Braak LB stage 0 Thal phase 3	No TDP43 pathology accompanying AD/ other disease/ ageing.	26

12/088	BBN_11051	male	51	Control donation. Chronic renal failure since 1985. Failed transplant, hypertension, lumbar and cervical instrumentation, necrotising fasciitis, right enucleation, and multiple ITU admissions. Elective cervical instrumentation. Found collapsed by his family. A cardiac arrest was called, and he was stabilised for cardiac catheterisation which showed 4 vessel coronary artery disease.	Normal brain	Normal brain.			24
12/132	BBN_10609	female	67	Control brain donation	Normal brain	No evidence of neurodegenerative or other significant disease process.	Mild to moderate small vessel disease.		40
12/094	BBN_11053	male	63	Control brain donation. Chronic obstructive pulmonary disease with type 2 respiratory failure. Slowly deteriorated and died.	Normal brain	Normal brain			20
11/073	BBN_2946	male	64	GI bleed/?sepsis. No brain disease known.	no neuropathological findings or normal aging changes, no significant abnormalities	Normal brain			40
13/012	BBN_15230	female	60	End stage metastatic breast cancer - control brain donation	Normal aged brain	No abnormality detected	Braak tangle stage I CERAD no plaques Braak LB stage 0 Thal phase 3		48

Supplementary table 4 - Human tissue details of control frontal lobe tissue used to isolate ALS-Control BDEVs. PM delay = post-mortem delay.

BB NO	BDR NO	MRC ID	Age	Sex	HISTOLOGY DIAGNOSIS	DIAGNOSIS 1	DIAGNOSIS 2	DIAGNOSIS 3	PM DELAY	Braak tangle stage
859	B506	BBN_4238	85	Female	AD definite, moderate arteriosclerotic small vessel disease, moderate to marked CAA	AD	CVD	CAA	14	5
912	B436	BBN_14405	82	Female	AD definite, hippocampal sclerosis	AD	Hippocampal sclerosis	NO	22	5
946	B346	BBN_24309	92	Male	AD definite, moderately severe arteriosclerotic SVD	AD	CVD	NO	30.5	5
968	B548	BBN_24553	57	Female	AD definite	AD	NO	NO	63	6
983	B496	BBN_24899	70	Male	AD definite	AD	NO	NO	32.25	5
989	B441	BBN_25026	63	Male	AD definite	AD	NO	NO	21.25	6
935	B426	BBN_19632	91	Male	AD definite, hippocampal sclerosis, severe CVD with several infarcts	AD	Hippocampal sclerosis	CVD	43	6
994	B410	BBN_26015	90	Female	AD definite, moderate CAA	AD	CAA	NO	21.25	6

Supplementary table 5 - Human tissue details of Alzheimer's disease frontal lobe tissue used to isolate Alz BDEVs. PM delay = post-mortem delay.

BB NO	BDR NO	MRC ID	Age	Sex	HISTOLOGY DIAGNOSIS	DIAGNOSIS 1	DIAGNOSIS 2	DIAGNOSIS 3	PM DELAY	Braak tangle stage
881	BC357	BBN_4240	86	Female	Control, severe arteriosclerotic small vessel disease with microinfarcts	CONTROL	CVD	NO	38.5	1
948	BC1141	BBN_24311	82	Female	Fine to use as control. Mild argyrophilic grain disease	CONTROL	Argyrophilic grain disease	NO	36	2
914	BC536	BBN_19608	96	Male	Control, no significant abnormalities	CONTROL	NO	NO	21	2
930	BC736	BBN_19627	94	Female	Control, moderate CAA	CONTROL	CAA	NO	29.5	2
957	BC1087	BBN_24325	86	Male	No significant abnormalities (control)	CONTROL	NO	NO	44.25	2
927	BC665	BBN_19624	78	Male	Control, mild SVD	CONTROL	NO	NO	51.5	2
941	BC702	BBN_24337	92	Male	Control, moderate CAA	CONTROL	CAA	NO	56.5	1
1028	BC478	BBN006.29018	89	Female	Nil of note	CONTROL	NO	NO	26.5	2

Supplementary table 6 - Human tissue details of control frontal lobe tissue used to isolate Alz-Control BDEVs. PM delay = post-mortem delay.